

WBS: 1.2.1.5  
QA: N/A

**Civilian Radioactive Waste Management System  
Management and Operating Contractor**

**THERMAL LOADING STUDY FOR FY 1995**

**January 31, 1996**

**Revision 00**

**B00000000-01717-5705-00016**

Prepared for:

U. S. Department of Energy  
Yucca Mountain Site Characterization  
Project Office  
P.O. Box 98608  
Las Vegas, Nevada 89193-8608

Prepared by:

TRW Environmental Safety Systems Inc.  
101 Convention Center Drive  
Las Vegas, Nevada 89109

Under Contract Number  
DE-AC01-91RW00134

WBS: 1.2.1.5  
QA: N/A

**Civilian Radioactive Waste Management System  
Management and Operating Contractor**

**THERMAL LOADING STUDY FOR FY 1995**

**January 31, 1996**

**Revision 00**

**B00000000-01717-5705-00016**

Prepared for:

U. S. Department of Energy  
Yucca Mountain Site Characterization  
Project Office  
P.O. Box 98608  
Las Vegas, Nevada 89193-8608

Prepared by:

TRW Environmental Safety Systems Inc.  
101 Convention Center Drive  
Las Vegas, Nevada 89109

Under Contract Number  
DE-AC01-91RW00134

**Civilian Radioactive Waste Management System  
Management and Operating Contractor**

**THERMAL LOADING STUDY FOR FY 1995**

**B00000000-01717-5705-00016 Revision 00**

**January 31, 1996**

*Steven F. Saterlie*

Steven F. Saterlie  
Study Manager and  
Lead Document Preparer

*1/31/96*

Date

*Richard D. Memory*

Richard D. Memory  
Systems Analysis and Modeling  
Department Manager

*1/31/96*

Date

*Thomas C. Geer*

Thomas C. Geer  
Systems Engineering  
Office Manager

*31 JAN 96*

Date

## ACKNOWLEDGEMENT

This report was prepared from work done by the Civilian Radioactive Waste Management System (CRWMS) Management and Operating (M&O) contractor under Contract Number DE-AC01-91RW00134 for the U.S. Department of Energy (DOE) office of Civilian Radioactive Waste Management, Yucca Mountain Site Characterization Project. Contributors to the work were from a variety of organizations including TRW, Lawrence Livermore National Laboratory (LLNL), Lawrence Berkeley Laboratory (LBL), Sandia National Laboratories (SNL), Los Alamos National Laboratory (LANL), Intera Corporation (IN), Morrison Knudsen (MK), and University of Nevada, Reno.

The authors of the study were S. F. Saterlie (TRW), T. A. Buscheck (LLNL), E. E. Ryder (SNL), M. Reeves (IN), S. S. Levy (LANL), C. A. Rautman (SNL), J. W. Carey (LANL), Y. W. Tsang (LBL), G. Danko (UNR), B. H. Thomson (TRW), J. A. Davis (TRW), F. C. Tsai (IN), J. J. Nitao (LLNL), E. Dunn (SNL), R. S. Longenbaugh (SNL), and R. W. Elayer (MK).

Thanks are extended to J. C. de la Garza of the Yucca Mountain Site Characterization Office (YMSCO) for his suggestions and oversight of the effort. Special thanks are also extended to Kathleen Ornella and Maria E. Machicao for document preparation and Terri Rodriguez and Jean Gonzalez for technical editing.

INTENTIONALLY LEFT BLANK

## EXECUTIVE SUMMARY

This report provides the results of sensitivity analyses designed to assist the test planners in focusing their in-situ measurements on parameters that appear to be important to waste isolation. Additionally, the study provides a preliminary assessment of the feasibility of certain thermal management options. The sensitivity analysis, in many cases, provided a significant advance in that data/measurements were used as inputs to the analysis. The study recommendations should help focus the test planning. Additionally, the thermal management evaluations should assist the designers as they consider options for the conceptual designs.

A decision on thermal loading is a critical part of the scientific and engineering basis for evaluating regulatory compliance of the potential repository for waste isolation. To show, with reasonable assurance, that the natural and engineered barriers will perform adequately under expected repository conditions (thermally perturbed) will require an integrated approach based on thermal testing (laboratory, and in-situ), natural analog observations, and analytic modeling. The Office of Civilian Radioactive Waste Management needed input to assist in the planning of the thermal testing program. Additionally, designers required information on the viability of various thermal management concepts. An approximately 18-month Thermal Loading Study was conducted from March, 1994 until September 30, 1995 to address these issues. This report documents the findings of that study.

This Thermal Loading Study had two main objectives. The first objective was to provide input/recommendations to the design of the testing program by performing a limited sensitivity analyses on selected parameters influenced by thermal loading. The analyses identified the range of uncertainty existing in these parameters and whether or not changes in these parameters might potentially affect performance as indicated by significant changes in temperature and hydrology. In the context of evaluating different thermal loading options, the study's second objective was to look at selected thermal management issues which could provide flexibility to achieve alternative loading options. Conclusions and recommendations are therefore provided on (1) *thermal testing recommendations* and (2) *thermal management evaluations*.

The sensitivity calculations in this report are based, in most cases, on state-of-the-art analytic models. However, these models are as yet unverified. Additionally, in many areas, there is little data available (where possible, as much data as available was used) and so many of the parameters have significant uncertainty associated with them. As such, results from in-situ tests may differ from the performance predicted in some of these calculations. Additionally, in many areas, only coupling of thermal and hydrology or thermal and geochemistry were considered. It is possible that more complex coupling could exist and may alter the predicted performance. This is one of the key reasons that conducting the testing program is essential to establish the necessary understanding.

## Thermal Testing Recommendations

The thermal testing program must ensure a well integrated set of laboratory tests, field-scale thermal tests (including in-situ tests), and natural analog studies in concert with appropriate analytic models to be able to develop an adequate understanding of the thermally-driven processes in order to demonstrate with reasonable assurance that the applicable regulatory requirements for a geologic repository will be satisfied. To accomplish this, the thermal test program must rely on a set of complementary tests that are optimized to: (1) provide increased confidence in our numerical models; (2) diagnose the major regimes and processes that will dominate heat and moisture flow; (3) adequately assess the effects of heterogeneity on those regimes and processes; and (4) provide an understanding of the prevalent coupled processes and the scale over which they are important. To assist in focusing the thermal testing necessary, this study performed a number of sensitivity analyses to identify parameters which appeared to potentially influence performance as a function of thermal loading, and the range of uncertainty in these parameters. Evaluation of whether or not changes could impact performance was based on whether or not significant differences in temperature and/or hydrology resulted. The following provides a brief overview of the study conclusions and recommendations. An overview of these is shown in Table 1:

1. Variations in bulk permeability (fracture plus matrix) were determined to influence the amount of water movement as a function of thermal loading, particularly if permeabilities are above  $10^{-12}$  m<sup>2</sup>. The current range of values of the bulk permeability for the welded tuff Topopah Spring Member are from  $10^{-13}$  to  $10^{-11}$  m<sup>2</sup>. In-situ measurements are recommended to measure the value of permeability in the host rock and the degree of spatial variability, if any, in this rock property. Additionally, observations of the existence of and extent of heat pipes in thermal tests might be used to verify permeability measurements.
2. Calculations were conducted spanning a range of rock matrix parameters (developed from laboratory measurements of core samples) to analyze their influence on gas and liquid-phase flow. Results indicate that, within the context of an Effective Continuum Model, the temperature, duration of boiling, and relative humidity of the waste package environment at the end of the boiling period are not very dependent on the choice of liquid saturation, porosity, and van Genuchten parameters. However, calculations of liquid-phase saturation and relative humidity show a sensitivity to the capillary suction pressure curve used as the repository rewets. Thus, the sensitivity of rewetting behavior to actual (heterogeneous) distributions of matrix properties should be further investigated, and it is recommended that measurements be taken to deduce the capillary suction in the rock.

Table 1. Summary of Sensitivity Analyses and Test Recommendations

Feature/Process	Parameter	Current Range of Values	Potential Impact on Performance	Recommendation
Rock Permeability	Bulk permeability	$10^{-13}$ to $10^{-11} \text{m}^2$ (in TSw2)	Moderate; if $> 10^{-11} \text{m}^2$ significant	Measure in in-situ test; look for heat pipes
Rock Properties	Liquid saturation, porosity, suction potential	Unknown	Small	Measure rock properties in-situ
Faults	Spatial variability	Unknown	Moderate to significant	In-situ measurement of properties near fault. 3-D modeling
Binary Gas Phase Diffusion	Tortuosity, porosity, gas saturation	Unknown but estimated tortuosity to be from 0.2 to 4	Small to moderate	In-situ measurements of gas diffusion
Rock Conductivity	Thermal conductivity	Depends on saturation, porosity, and rock type	Moderate	In-situ measurement of temperature; spatial variation
Rock Permeability	Fracture-matrix coupling $K_{fm}$ average permeability $K_m$ matrix permeability	Unknown $K_{fm}/K_m = 0.1$ to 1,000; $\infty$	Moderate	In-situ measurement of permeability and fracture properties; spatial variability
Geochemical	Zeolite dehydration and alteration	----	Moderate to significant	Include amount of water in performance assessment. May need in-situ test in CH for high thermal loads
Overburden Depth	Depth to surface or depth to water table	200 to 400 m (in primary area)	Moderate to significant	Perform 3-D modeling to evaluate, consider in performance assessment
Thermo- mechanical	Stress; strain	Temperature dependent Ambient (SNL, 1987) 5-10 MPa	Moderate	Conduct in-situ test of tunnel segment to $\geq 200^\circ\text{C}$ , measure parameters
Scaling (temporal/ spacial)	All	----	Moderate to significant	Use stochastic approach to testing; assess importance of coupling at various scales

Additionally, three-dimensional site-scale model calculations incorporating heat effects predict that the Ghost Dance and Solitario Canyon Faults may provide major pathways for the transport of heated gas and heat. Orders of magnitude increases in surface heat and gas flux were predicted for high thermal loads with consequences that potential repository temperatures and boiling duration could be reduced (e.g.  $30^\circ\text{C}$  lower temperatures at 1,000 years). It is recommended that in-situ measurements of the rock properties around faults be done and used in a site-scale model to evaluate the way in which these faults transport heat and moisture.

3. Model calculations were conducted to investigate the sensitivity of thermohydrologic behavior to variations in binary gas-phase diffusion in a porous medium. Enhanced binary gas-phase diffusion, enhanced over nominal diffusion, has been observed in soils but not yet directly observed or measured in fractured tuffs at Yucca Mountain. To examine whether or not enhanced diffusion might be important or not a sensitivity study was conducted in which the binary gas-phase diffusion was enhanced by factors of 1 (nominal diffusion) to 20. The calculations showed enhanced vapor diffusion may modestly increase the overall cooling of the repository. The results indicated that at high thermal loads, higher vapor diffusion (a factor of 10) can result in some decrease (10 to 12 percent) in the duration of boiling. Thus, some investigation of binary gas-phase diffusion is warranted at high loadings but it does not appear to have a profound impact on the temperature and liquid saturation.
4. Geostatistical models were used with borehole data to construct estimates of porosity and thermal conductivity representing possible rock mass spatial variability. Moderate changes in rock saturation (40 to 80 percent) can only produce some variation in thermal conductivity which results only in minor (at most 5°C) changes in temperature. However, larger changes in conductivity occurring due to drying (increased temperature and essentially zero saturation) could produce significant increases in predicted repository temperatures by up to 30°C. Additionally, the spatial heterogeneity in material properties could produce temperature differences of 20°C. The issue of conductivity variations due to potential high-porosity (large-cavity) lithophysal zones and the impact this might have on repository temperatures needs to be resolved through subsurface mapping and possibly in-situ testing. Conclusions were based on very limited data (three boreholes) and may change as more data becomes available.
5. The study investigated the effect of fracture-matrix coupling on thermohydrology by using dual permeability calculations. More than four orders of magnitude variations in coupling resulted in predicted waste package and drift temperature of more than 20°C cooler than what predictions would indicate with either an Effective Continuum Model with small bulk permeabilities or a conduction model. Potentially cooler temperatures may not produce the anticipated dry-out at high thermal loads. It is recommended that measurements of matrix permeability, derivations of fracture-matrix interface area, and fracture separations as well as heterogeneity in these parameters should be taken.
6. A preliminary evaluation was made of heat on bound water in zeolitic mineral assemblages and the impact dehydration and/or mineral alteration have on the porosity of the rock. The calculations, based on laboratory data from borehole samples and mineral separates, show that clinoptilolite produces about three times as much water per unit volume of rock upon heating at the Area Mass Loading (AML) of 27.3 kilograms uranium (kgU)/m<sup>2</sup> (111 metric tons uranium [MTU]/acre) than it does at an AML of 8.9 kgU/m<sup>2</sup> (36 MTU/acre). The amount of water lost from the zeolites, the effect this water has on temperature, and where this water goes once mobilized, is critical to understand for waste isolation. The calculations also found appreciable increases in porosity resulting from irreversible crystallization of clinoptilolite to analcime at the higher thermal loads. Examination of zeolitized rock before, during, and after heating to assess this issue and its potential impact on waste isolation should be done and the

results considered in Total System Performance Assessment (TSPA). If the results indicate a potential impact on performance, then in-situ testing in Calico Hills may be warranted for a high thermal loading.

7. The potential repository overburden (200 to 400 m in the Primary Area) may produce significant variations in temperature. For high AMLs, shallower repository areas were calculated to cool significantly faster than the areas with more overburden. Additionally, calculations of a deeper area (in this case, the example was outside the Primary Area in one of the Optional Areas) show the potential repository tends to rewet faster due to proximity to the water table. Calculations at low AMLs found essentially negligible differences. Tests cannot be done in the short term to investigate this behavior but should be considered during performance confirmation. It is suggested however, that multi-dimensional calculations be done to supplement these one-dimensional simulations in order to quantify potential thermohydrologic mixing. As required, the results should be considered in the design analysis and TSPA evaluations.
8. Although in some cases, heat may even stabilize a drift until cooling begins, the thermomechanical analyses found that predicted rock mass strength was exceeded at an AML of 27.4 kgU/m<sup>2</sup> (111 MTU/acre) but was not exceeded, except in localized areas, at 20.5 kgU/m<sup>2</sup> (83 MTU/acre). The vertical fractures around the drift tend to close during heating but the horizontal fractures are predicted to open. Since current strategy focuses design on 19.8 to 24.7 kgU/m<sup>2</sup> (80 to 100 MTU/acre), in-situ testing to establish the rock strength will be needed. A determination of a factor of safety will almost certainly require that an area of tunnel be heated sufficiently above what is expected for peak temperatures. Thus, heating to at least 200°C is recommended.

The study examined the important issue of scaling (time and distance) and the implications on testing. The program must rely on laboratory scale and eventually in-situ drift scale thermal tests combined with analytic modeling and natural analogs for prediction of the behavior of the host rock. At each scale (laboratory, drift scale, etc.), a stochastic approach is recommended by the study. A stochastic approach is needed because the number of samples tested at any particular scale would not be numerous enough to cover the entire test site. The in-situ tests should evaluate the uncertainty associated with using parameters derived from small core samples to extrapolate to larger scale conditions. As the analyses above showed, the spatial variability in properties and the scale of this variability was found to be important. A prime example of the potential effects of spatial variability on performance was the examination of a high thermal load emplaced in two areas separated by the Ghost Dance Fault which indicated faster cooling and potentially faster rewetting than a single area with no faults. Thus, it is recommended that understanding the impact of spatial variability will be important. Additionally, the reliance on numerical modeling to provide performance predictions requires that the verification of such models be a key emphasis in the testing program.

## Thermal Management Evaluations

The study performed preliminary investigations of selected thermal management issues to assess feasibility and advantages/disadvantages. Thermal management could provide enhanced flexibility and/or mitigation of risk for the potential repository. The following are a synopsis of the conclusions obtained in the study:

1. A significant advance was made by coupling a thermohydrologic code (NUFT) with a psychrometric environmental (ventilation) code to provide a three-dimensional, time-dependent method for calculating heat and moisture transport in an emplacement drift and surrounding host rock. Ventilation calculations showed an emplacement drift could be kept at or below 40°C for 100 years by a 10 m<sup>3</sup>/s air flow even for a high thermal load. The coupled code predicted somewhat lower temperatures than a ventilation code which does not include moisture effects. Additionally a significant amount of water can be removed from the surrounding host rock by ventilation. Calculations showed that if natural ventilation were used, it could produce air flows of about 0.8 m<sup>3</sup>/s which would moderate the temperature during preclosure.
2. To maintain viable alternatives of low AMLs as suggested in the Proposed Thermal Strategy will likely require more emplacement area than the Primary Area. This study performed a preliminary assessment of stratigraphic variations and mineral distributions and abundances which could affect repository performance and fluid flow using currently available borehole data on regions outside the Primary Area. Based on these evaluations, both Optional Area D (optional areas are based on proposed subsurface layouts [M&O, 1994a]) and the area south of the Primary Area (at least south as far as drill holes G/GU-3) appear to have stratigraphic features, thicknesses, and mineralogic characteristics which fall within the range of parameters that exists in the Primary Area. As such, it is possible that these areas can be relatively easy to characterize. Optional Area C may be significantly different from the Primary Area and no assessment could be done of Optional Areas A and B at this time.
3. The study evaluated loading the edges of the potential repository with a higher density of waste packages. The calculations showed non-uniform AMLs can be used to increase the duration of boiling at the edges under conditions of a high thermal load, but in doing so, produced significantly higher temperatures. Increasing the AML in the edges results in conditions that exceed some preclosure thermal goals. Potential tradeoffs, however, may be considered, such as loading the outer drifts to higher density just prior to closure or ventilation and/or aging.
4. Calculations of temperature and heat mobilized fluid flow for variations in Lineal Mass Loadings (LMLs) found a relative insensitivity to boiling duration and boiling front propagation for AMLs above about 9.9 kgU/m<sup>2</sup> (40 MTU/acre). At lower AMLs, the choice of LML does make a difference. Thus, above this threshold, a choice of an LML should be based on operational efficiency. The choice of LML at a lower AML should be based on satisfying near-field criteria that are yet to be established.

5. Evaluations of waste stream variability showed the resolution at which the waste stream is modeled is important for thermal predictions. Localized (on the order of 10 m) "hot" and "cooler" areas could occur as a result of the waste stream variations with predicted temperature differences of as much as 100°C for emplacement of the large Multi-Purpose Canister waste packages (based on YFF(10) fuel with no emplacement heat limit). These temperature differences were calculated at locations 5 m above the repository plane and occurred during preclosure. This magnitude of temperature difference could lead to thermomechanical problems in localized areas or transport of water to the cooler regions. It is recommended that the waste stream variability be considered in the design analyses. The need to mitigate variability may provide incentive for other thermal management options.
6. The thermal management option of using aging of the spent nuclear fuel (SNF) in an interim or Centralized Storage Facility (CSF) with heat based Inventory Management to retain MGDS design flexibility was studied. Lower emplacement limits below 14.2 kW on WPs clearly increase the length of CSF and repository operations but does not contribute a significant lower thermal source term unless limits are reduced to 10 kW or below. When considering just the preclosure operations period, this difference is significant during preclosure but not over the long-term. CSF costs were about \$0.1 to \$0.4 billion dollars for any of the 14.2 and 12 kW emplacement heat limit cases, to as much as \$1.8 billion dollars (1995 constant year dollars) for a scenario with an 8 kW emplacement heat limit. Tradeoffs between cost impacts and ability to provide a more uniform heat distribution should be examined further for viability and, if such a facility is found to be needed, to determine a size.

In summary, this Thermal Loading Study focused on two main areas: (1) to perform sensitivity studies on a variety of parameters to make recommendations to support the testing program design and (2) to evaluate selected thermal management issues. Sensitivity studies were done on a variety of parameters using various models to assess whether or not changes in these parameters as a function of thermal loading could affect temperatures, water movement, geochemistry, etc., which might affect performance. This study used whatever measurements/data were available as the basis for the scoping studies. However, in most cases these data points were widely spaced and an obvious recommendation is that more data is needed to reduce uncertainties. Additionally, the study evaluated a number of thermal management issues and concluded there was potential merit in further consideration of some of the issues depending on the objectives. To evaluate whether or not a specific thermal management technique should be employed will require that a systems study be done to evaluate the trades needed and the value to the system. Finally, it is recommended that the results and recommendations of these sensitivity studies be provided to the testing community to help them plan their tests and implement the requisite measurements. Additionally, the thermal management evaluations should be provided to the design organizations.

INTENTIONALLY LEFT BLANK

# CONTENTS

	Page
1. INTRODUCTION .....	1-1
1.1 STUDY OBJECTIVE .....	1-1
1.2 BACKGROUND .....	1-2
1.3 SCOPE .....	1-3
1.4 REPORT ORGANIZATION .....	1-4
2. INPUT AND ASSUMPTIONS .....	2-1
2.1 REFERENCE CASE .....	2-1
2.2 WASTE STREAM ANALYSIS .....	2-1
2.3 WASTE PACKAGE DESIGNS .....	2-11
2.4 REPOSITORY SURFACE DESIGNS .....	2-12
2.5 REPOSITORY SUBSURFACE DESIGNS .....	2-12
2.6 INPUTS AND ASSUMPTIONS PERTINENT TO YUCCA MOUNTAIN ...	2-16
3. PARAMETRIC THERMAL EVALUATIONS .....	3-1
3.1 BULK PERMEABILITY VARIATIONS .....	3-1
3.1.1 VTOUGH Calculations .....	3-1
3.1.2 TOUGH2 Calculations .....	3-4
3.1.3 Results .....	3-4
3.2 EFFECT OF VARIATIONS IN SELECTED ROCK PROPERTIES ON THERMOHYDROLOGY .....	3-10
3.2.1 VTOUGH Calculations .....	3-11
3.2.2 Site-Scale Model Calculations .....	3-15
3.2.3 Summary .....	3-29
3.3 EXAMINATION OF GAS-PHASE DIFFUSION ON THE THERMOHYDROLOGY .....	3-29
3.4 EFFECT OF MODELING ASSUMPTIONS ON THERMAL PROFILES ...	3-35
3.5 EFFECT OF FRACTURE-MATRIX COUPLING ON THERMOHYDROLOGY .....	3-49
3.6 GEOCHEMISTRY ISSUES .....	3-59
3.7 THE EFFECT OF ELEVATION VARIATIONS ON THERMAL PERFORMANCE .....	3-69
3.8 THERMOMECHANICAL EVALUATIONS .....	3-75
4. THERMAL MANAGEMENT EVALUATIONS .....	4-1
4.1 VENTILATION ANALYSIS .....	4-1
4.2 PRELIMINARY ASSESSMENT OF EXPANSION AREAS .....	4-13
4.2.1 Zeolite Distribution .....	4-17
4.2.2 Assessment of Optional Areas C and D .....	4-18
4.2.3 Assessment of Southern Yucca Mountain .....	4-19
4.2.4 Summary .....	4-20
4.3 NONUNIFORM AREAL MASS LOADING .....	4-20

**CONTENTS (continued)**

	<b>Page</b>
4.4 VARIATIONS IN LINE LOADING AS A THERMAL MANAGEMENT TOOL .....	4-30
4.5 REPOSITORY THERMAL RESPONSE DUE TO WASTE STREAM VARIABILITY .....	4-37
4.5.1 Modeling Assumptions .....	4-38
4.5.2 Method and Results .....	4-38
4.5.3 Section Summary .....	4-55
4.6 AGING OF SPENT NUCLEAR FUEL VIA INTERIM STORAGE .....	4-59
5. SCALING ISSUES .....	5-1
6. CONCLUSIONS AND RECOMMENDATIONS .....	6-1
6.1 SENSITIVITY ANALYSIS AND TESTING RECOMMENDATIONS .....	6-1
6.2 THERMAL MANAGEMENT EVALUATIONS .....	6-7
6.3 SUMMARY .....	6-11
7. REFERENCES, STANDARDS, AND REGULATIONS .....	7-1
7.1 REFERENCES .....	7-1
7.2 STANDARDS AND REGULATIONS .....	7-8
8. ACRONYMS .....	8-1

## FIGURES

**Page**

2.2-1.	Instantaneous Power Per MTU Versus Time for the FY 1995 Base Case - Average Characteristics . . . . .	2-4
2.2-2.	Instantaneous Heat Output Versus Time for the FY 1995 Base Case - Average Characteristics . . . . .	2-5
2.2-3.	Instantaneous Heat Output Versus Time for the FY 1995 Base Case - Collapsed Profile . . . . .	2-7
2.2-4.	Actual Total Heat Output Versus Time . . . . .	2-8
2.2-5.	Comparison of Heat Output Profiles . . . . .	2-9
2.5-1.	Potential repository Primary Area and Potential Expansion Areas . . . . .	2-13
3.1-1.	Maximum Equivalent Liquid Column Height Moved from the dry-out Zone (Some Decrease in Liquid Saturation over Ambient) as a Function of Bulk Permeability for Five Thermal Loads . . . . .	3-3
3.1-2.	Vertical Temperature Profile at 100 Years for a Bulk Permeability of $1 \times 10^{-15} \text{ m}^2$ (1 mD) and a Thermal Load of $20.5 \text{ kgU/m}^2$ . . . . .	3-5
3.1-3.	Vertical Temperature Profile at 100 Years for a Bulk Permeability of $1 \times 10^{-14} \text{ m}^2$ (10 mD) and a Thermal Load of $20.5 \text{ kgU/m}^2$ . . . . .	3-6
3.1-4.	Vertical Temperature Profile at 100 Years for a Bulk Permeability of $1 \times 10^{-13} \text{ m}^2$ (100 mD) and a Thermal Load of $20.5 \text{ kgU/m}^2$ . . . . .	3-8
3.1-5.	Vertical Temperature Profile at 100 Years for a Bulk Permeability of $1 \times 10^{-12} \text{ m}^2$ (1 D) and a Thermal Load of $20.5 \text{ kgU/m}^2$ . . . . .	3-9
3.2-1.	Vertical temperature profiles at various radial distances, r, for AML = 110.5 MTU/acre at (a) t = 100 yr, (b) t = 1,000 yr, (c) t = 10,000 yr, and (d) t = 36,000 yr. Note different temperature scales. Vertical liquid saturation profiles are also plotted at (e) t = 100 yr, (f) t = 1,000 yr, (g) t = 10,000 yr, and (h) t = 36,000 yr. . . . .	3-16
3.2-2.	Vertical temperature profiles at various radial distances, r, for AML = 110.5 MTU/acre at (a) t = 100 yr, (b) t = 1,000 yr, (c) t = 10,000 yr, and (d) t = 36,250 yr. Note different temperature scales. Vertical liquid saturation profiles are also plotted at (e) t = 100 yr, (f) t = 1,000 yr, (g) t = 10,000 yr, and (h) t = 36,250 yr. . . . .	3-17
3.2-3.	Vertical temperature profiles at various radial distances, r, for AML = 110.5 MTU/acre at (a) t = 100 yr, (b) t = 1,000 yr, (c) t = 10,000 yr, and (d) t = 35,400 yr. Note different temperature scales. Vertical liquid saturation profiles are also plotted at (e) t = 100 yr, (f) t = 1,000 yr, (g) t = 10,000 yr, and (h) t = 35,400 yr. . . . .	3-18
3.2-4.	Vertical temperature profiles at various radial distances, r, for AML = 110.5 MTU/acre at (a) t = 100 yr, (b) t = 1,000 yr, (c) t = 10,000 yr, and (d) t = 34,630 yr. Note different temperature scales. Vertical liquid saturation profiles are also plotted at (e) t = 100 yr, (f) t = 1,000 yr, (g) t = 10,000 yr, and (h) t = 34,630 yr.. . . .	3-19

**FIGURES (continued)**

	<b>Page</b>
3.2-5. Vertical temperature profiles at various radial distances, r, for AML = 110.5 MTU/acre at (a) t = 100 yr, (b) t = 1,000 yr, (c) t = 10,000 yr, and (d) t = 35,150 yr. Note different temperature scales. Vertical liquid saturation profiles are also plotted at (e) t = 100 yr, (f) t = 1,000 yr, (g) t = 10,000 yr, and (h) t = 35,150 yr. . . . .	3-20
3.2-6. Vertical temperature profiles at various radial distances, r, for AML = 110.5 MTU/acre at (a) t = 100 yr, (b) t = 1,000 yr, (c) t = 10,000 yr, and (d) t = 35,730 yr. Note different temperature scales. Vertical liquid saturation profiles are also plotted at (e) t = 100 yr, (f) t = 1,000 yr, (g) t = 10,000 yr, and (h) t = 35,730 yr. . . . .	3-21
3.2-7. Surface Heat Flux for an APD of 28.2 W/m <sup>2</sup> (114 kW/acre) . . . . .	3-23
3.2-8. Surface Gas Flux for an APD of 28.2 W/m <sup>2</sup> (114 kW/acre) . . . . .	3-24
3.2-9. Calculated Temperature Profiles at 1,000 Years for an APD of 28.2 W/m <sup>2</sup> (114 kW/acre) . . . . .	3-25
3.2-10. Calculated Saturation Profiles at 1,000 Years for an APD of 28.2 W/m <sup>2</sup> (114 kW/acre) . . . . .	3-27
3.4-1. Index map showing the potential Yucca Mountain high-level nuclear-waste repository site in Southern Nevada, and the location of the cross section for which thermal-properties modeling was conducted. . . . .	3-36
3.4-2. Geologic cross-section of the northern portion of the potential repository region at Yucca Mountain corresponding to section C--C' of Brandshaug, 1991 . . . . .	3-37
3.4-3. Temperature differences between thermal models computed using thermal conductivity values converted from porosity at a uniform initial saturation of 60 percent and at saturations of 80 percent for welded and 40 percent for nonwelded materials for an elapsed calculation time of 500 years. . . . .	3-41
3.4-4. Temperature differences between thermal models computed using thermal conductivity values converted from porosity at 50°C and at 110°C for elapsed calculational time of 500 years. . . . .	3-43
3.4-5. Temperature differences between simulated model GC2HL and the equivalent E-type model for an elapsed computational time of 500 years; both material property models use a range of spatial correlation of 1,000 meters. . . . .	3-47
3.5-1. Temperature Response at 100 Years to Changes in Fracture-Matrix Coupling Factor $K_{im}/K_m$ . The depth axis passes through the drift centerline. . . . .	3-52
3.5-2. Temperature Response at 100 Years to Changes in Fracture-Matrix Coupling Factor $K_{im}/K_m$ . Both axes are expanded over previous figure and depth axis passes through the drift centerline. . . . .	3-53
3.5-3. Waste-Package Temperature Response to Changes in Fracture-Matrix Coupling Factor $K_{im}/K_m$ . . . . .	3-54
3.5-4. Temperature Response at 100 Years to Changes in Bulk Permeability $K_b$ . Depth axis passes through the drift centerline. . . . .	3-56
3.5-5. Temperature Response at 100 Years to Changes in Bulk Permeability $K_b$ . Both axes are expanded over the previous figure and the drift axis passes through the drift centerline. . . . .	3-57

## FIGURES (continued)

	Page
3.5-6. Waste-Package Temperature Response to Changes in Bulk Permeability $K_b$ . . . . .	3-58
3.6-1. Temperature of Clinoptilolite With and Without Dehydration as a Function of Heating Time . . . . .	3-67
3.7-1. Ambient Geothermal Gradient . . . . .	3-70
3.7-2. Ambient Liquid Saturation . . . . .	3-71
3.7-3. Vertical Temperature Profiles at Various Radial Distances, $r$ , from Repository Centerline for $k_b = 280$ millidarcy, a 200 m Thick Overburden, and an AML of $27.4 \text{ kgU/m}^2$ at (a) $t = 1,000$ yr; (b) $t = 10,000$ yr; and (c) $t = 32,730$ yr. . . . .	3-73
3.7-4. Vertical Temperature Profiles at Various Radial Distances, $r$ , from Repository Centerline for $k_b = 280$ millidarcy, a 430 m Thick Overburden, and an AML of $27.4 \text{ kgU/m}^2$ at (a) $t = 1,000$ yr; (b) $t = 10,000$ yr; and (c) $t = 31,680$ yr. . . . .	3-74
3.8-1. Temperature Profile for Runs #1 and #2 . . . . .	3-78
3.8-2. Principal Stresses After Excavation for Run #4 . . . . .	3-79
3.8-3. Principal Stresses After Thermal Loading for Run #4 . . . . .	3-81
4.1-1. Container Emplacement With the Thermal Interactions . . . . .	4-3
4.1-2. Air Temperature Profiles at Four Times Over Tunnel Length for a $10 \text{ m}^3/\text{s}$ Ventilation Rate at $20.6 \text{ kgU/m}^2$ . . . . .	4-5
4.1-3. Partial Vapor Pressure Profile Calculated Over Tunnel Length at Four Times for a $10 \text{ m}^3/\text{s}$ Ventilation Rate at $20.6 \text{ kgU/m}^2$ . . . . .	4-6
4.1-4. Maximum Wall Temperatures as a Function of Time at Distances along the Emplacement Drift for a $10 \text{ m}^3/\text{s}$ Ventilation Rate at $20.6 \text{ kgU/m}^2$ . . . . .	4-7
4.1-5. Wall Moisture Flux Density Versus Time . . . . .	4-9
4.1-6. Total Moisture Removed per Unit Length . . . . .	4-10
4.1-7. Cumulative Moisture Removed by Ventilation from a Drift . . . . .	4-11
4.2-1. Existing and Planned Boreholes with Subsurface Layout . . . . .	4-15
4.3-1. Vertical temperature profiles at various radial distances, $r$ , from repository centerline for a nonuniform AML of $64.0 \text{ MTU/acre}$ at (a) $t = 100$ yr, (b) $t = 1,000$ yr, (c) $t = 10,000$ yr, and (d) $t = 33,100$ yr. Note different temperature scales. Vertical liquid saturation profiles are also plotted at (e) $t = 100$ yr, (f) $t = 1,000$ yr, and (g) $t = 10,000$ yr, and (h) $t = 33,100$ yr. . . . .	4-23
4.3-2. Vertical temperature profiles at various radial distances, $r$ , from repository centerline for a nonuniform AML of $81.3 \text{ MTU/acre}$ at (a) $t = 100$ yr, (b) $t = 1,000$ yr, (c) $t = 10,000$ yr, and (d) $t = 32,670$ . Note different temperature scales. Vertical liquid saturation profiles are also plotted at (e) $t = 100$ yr, (f) $t = 1,000$ yr, and (g) $t = 10,000$ yr, and (h) $t = 32,670$ . . . . .	4-24
4.3-3. Vertical temperature profiles at various radial distances, $r$ , from repository centerline for a nonuniform AML of $96.9 \text{ MTU/acre}$ at (a) $t = 100$ yr, (b) $t = 1,000$ yr, (c) $t = 10,000$ yr, and (d) $t = 33,550$ yr. Note different temperature scales. Vertical liquid saturation profiles are also plotted at (e) $t = 100$ yr, (f) $t = 1,000$ yr, and (g) $t = 10,000$ yr, and (h) $t = 33,550$ yr. . . . .	4-25

## FIGURES (continued)

	Page
4.3-4. Vertical temperature profiles at various radial distances, $r$ , from repository centerline for a nonuniform AML of 128.4 MTU/acre at (a) $t = 100$ yr, (b) $t = 1,000$ yr, (c) $t = 10,000$ yr, and (d) $t = 30,920$ yr. Note different temperature scales. Vertical liquid saturation profiles are also plotted at (e) $t = 100$ yr, (f) $t = 1,000$ yr, and (g) $t = 10,000$ yr, and (h) $t = 30,920$ yr. . . . .	4-26
4.3-5. Vertical temperature profiles at various radial distances, $r$ , from repository centerline for a uniform AML of 55.3 MTU/acre at (a) $t=1,000$ yr, (b) $t=10,000$ yr, and (c) $t=36,000$ yr. . . . .	4-27
4.3-6. Vertical temperature profiles at various radial distances, $r$ , from repository centerline for a uniform AML of 83.4 MTU/acre at (a) $t=1,000$ yr, (b) $t=10,000$ yr, and (c) $t=33,000$ yr. . . . .	4-28
4.4-1. A Given Repository-Wide Areal Mass Loading Can Be Achieved by Various Combinations of Drift and Waste Package Spacing. . . . .	4-31
4.4-2a. Peak Waste Package Temperature for Lineal Mass Loading of 0.63 MTU/m (12-m 21-Pressurized Water Reactor Waste Package Spacing) . . . . .	4-34
4.4-2b. Peak Waste Package Temperature for Lineal Mass Loading of 1.25 MTU/m (6-m 21-Pressurized Water Reactor Waste Package Spacing) . . . . .	4-34
4.4-3a. Duration of the Boiling Period on the Drift Wall for Lineal Mass Loading of 0.63 MTU/m (12-m 21-Pressurized Water Reactor Waste Package Spacing) . . . . .	4-35
4.4-3b. Duration of the Boiling Period on the Drift Wall for Lineal Mass Loading of 1.25 MTU/m (6-m 21-Pressurized Water Reactor Waste Package Spacing) . . . . .	4-35
4.4-4a. Maximum vertical extent of the boiling point isotherm above the repository for Mass Loading of 0.63 MTU/m (12-m 21-Pressurized Water Reactor waste package spacing) . . . . .	4-36
4.4-4b. Maximum vertical extent of the boiling point isotherm above the repository for Lineal Mass Loading of 1.25 MTU/m (6-m 21-Pressurized Water Reactor waste package spacing) . . . . .	4-36
4.5-1. Contours of Temperature Change 5 m Above the Repository Plane 50 Years After the Start of Waste Emplacement . . . . .	4-41
4.5-2. Contours of Temperature Change 5 m Above the Repository Plane 1,000 Years After the Start of Waste Emplacement . . . . .	4-43
4.5-3. Location of High Resolution Grid . . . . .	4-45
4.5-4. Temperature Difference History Between the Base Case and the Case I Models . . . . .	4-49
4.5-5. Logical Grouping for Averaging Waste Stream Characteristics for 2029 Pressurized Water Reactor Waste Packages . . . . .	4-53
4.5-6. Integrated Energy Deposition for 2029 Pressurized Water Reactor Waste Packages Calculated Using Both the Yearly Averaged Characteristics and Package-by-Package Characteristics . . . . .	4-54
4.5-7. Temperature Difference History Between the Base Case and the Case II Models . . . . .	4-57
4.6-1. Inventory Management Flow Model . . . . .	4-60
4.6-2. Centralized Storage Facility Cask Inventory . . . . .	4-63
4.6-3. Centralized Storage Facility Total Storage Requirements . . . . .	4-63

## TABLES

Page

2.2-1.	FY 95 Scenario Descriptions (No Monitored Retrieval Storage, Dry Storage Loaded Oldest Fuel First) . . . . .	2-2
2.2-2.	Overall Average Spent Nuclear Fuel Characteristics (Averaged by MTU) . . . . .	2-3
2.2-3.	Comparison of Waste Stream Scenarios For FY 1993, FY 1994, and FY 1995 Thermal Loading System Study . . . . .	2-10
2.2-4.	Comparison of Package Quantities . . . . .	2-11
2.2-5.	Overall Average Spent Nuclear Fuel Characteristics . . . . .	2-11
2.5-1.	Depths and Distances for Selected Locations in the Primary Area and Optional Areas A and B . . . . .	2-14
2.5-2.	Distances to Thermal/Mechanical Features for Selected Repository Locations in Yucca Mountain . . . . .	2-15
3.2-1.	Matrix Hydrological Property Data for the TSw1 and TSw2 units . . . . .	3-12
3.2-2.	Calculations of Duration of Boiling for Reference Case . . . . .	3-13
3.2-3.	Calculations of Duration of Boiling for Variations in Rock Properties . . . . .	3-14
3.2-3a.	Areal Mass Loading = 13.7 kgU/m <sup>2</sup> (55.3 MTU/Acre) . . . . .	3-14
3.2-3b.	Areal Mass Loading = 27.3 kgU/m <sup>2</sup> (110.5 MTU/Acre) . . . . .	3-14
3.2-3c.	Areal Mass Loading = 37.1 kgU/m <sup>2</sup> (150 MTU/Acre) . . . . .	3-14
3.3-1.	Duration of Boiling and Relative Humidity Calculations for TSw1 and TSw2 Matrix Properties from Klavetter and Peters (1986) . . . . .	3-33
3.3-1a.	Gas-Phase Diffusion Tortuosity Factor, $\tau_{\text{eff}} = 0.2$ . . . . .	3-33
3.3-1b.	Gas-Phase Diffusion Tortuosity Factor, $\tau_{\text{eff}} = 2.0$ . . . . .	3-33
3.3-2.	Predicted Time to Achieve a Specified Relative Humidity at an Areal Mass Loading = 110.5 MTU/Acre . . . . .	3-34
3.3-2a.	Gas-Phase Diffusion Tortuosity Factor, $\tau_{\text{eff}} = 0.2$ . . . . .	3-34
3.3-2b.	Gas-Phase Diffusion Tortuosity Factor, $\tau_{\text{eff}} = 1.0$ . . . . .	3-34
3.3-2c.	Gas-Phase Diffusion Tortuosity Factor, $\tau_{\text{eff}} = 2.0$ . . . . .	3-34
3.4-1.	Coefficients from Multiple Regression Relationships Relating Thermal Conductivity and Porosity . . . . .	3-38
3.4-2.	Comparison of Maximum Predicted Temperature Differences for Differing Material-Property Modeling Assumption . . . . .	3-40
3.6-1.	Effects of Hydrus Minerals . . . . .	3-60
3.7-1.	Predicted Peak Temperatures as a Function of Depth of Overburden for three times . . . . .	3-72
3.8-1.	Computer Run Identification . . . . .	3-77
4.1-1.	Areal Mass Load, Waste Package and Drift Spacing . . . . .	4-2
4.5-1.	Maximum and Minimum Temperature Differences Predicted Between the Base Case and Case I ( $T_{\text{Base}} - T_{\text{Case I}}$ ) . . . . .	4-47
4.6-1.	Inventory Management Study Case Description . . . . .	4-61
4.6-2.	Multi-Purpose Canister/Cask Savings Resulting from an Increase to 15.33 kW Transportation Limit . . . . .	4-62
4.6-3.	Inventory Management Summary Statistics . . . . .	4-62
4.6-4.	Inventory Management Emplacement Summary Statistics . . . . .	4-65
4.6-5.	Inventory Management Heat Emplacement Summary Statistics . . . . .	4-66

**TABLES (continued)**

	<b>Page</b>
4.6-6. Summary Cost Deltas, All Scenarios versus Program Approach . . . . .	4-67

## **1. INTRODUCTION**

The thermal loading in the potential repository can impact the waste disposal system in a number of areas (e.g., receipt of waste, repository size and design, engineered barrier design and performance [including waste package size and other issues associated with the current proposed multi-purpose canister (MPC)], and natural barrier performance). The ultimate purpose of a Thermal Loading System Study will be to develop the technical basis for making a thermal loading decision and providing information necessary to support license application, testing, and design. To accomplish this, a Thermal Loading System Study would evaluate a variety of options to rate performance and examine safety issues from the standpoint of both pre- and postclosure performance, operability, cost, and schedule to identify thermal loading options that will meet requirements.

A systems study performs a comparative analysis between options with a recommendation of an option based on performance with respect to the others that will tend to optimize the system, not just a sub-element of the system. The Thermal Loading System Study will ultimately use a combination of "validated" and/or benchmarked analytic models, experimental data, and expert judgment. The effort needed to develop a final recommendation starts as a scoping study and proceeds in an iterative manner as data and analysis capabilities develop. The study will also attempt to synthesize recommendations for testing that can be used to differentiate among thermal loads as well as identify tests that may be insensitive to thermal loading. Through this process, the Thermal Loading System Study will support the requisite technical basis for a final decision on thermal loading.

Evaluations of options in a Thermal Loading System Study will require verified performance calculations and/or criteria established with test data. To be able to establish verified models will also require comparisons against measurements made in thermal tests (laboratory, in-situ, and natural analog). The Program is currently in the process of developing a testing strategy. Thus, while a Thermal Loading Study was not able to perform an evaluation of options at this time, the study did conduct sensitivity analyses to provide information to the test planners. Additionally, selected design options such as ventilation and the use of expansion areas were evaluated to determine feasibility. This report discusses these sensitivity studies and evaluations.

### **1.1 STUDY OBJECTIVE**

As a part of the process discussed above, an 18-month Thermal Loading Study was done with two main objectives designed to support the program goal of ultimately making a thermal loading decision. The first objective was to provide input to the design of the thermal testing program. The approach taken was to perform a limited sensitivity analysis on selected parameters important to waste isolation and thermal loading and to establish their influence on performance. The information gained in this effort will be developed into recommendations that will be factored into the test program. The second objective was to examine selected thermal management issues which could provide flexibility to the designer and evaluate their viability and advantages or disadvantages. The purpose of this report is to provide the details and findings of the effort.

A cursory look was taken at the first objective of the 18-month study during the FY 1993 Thermal Loading Study in which expert judgment and some limited analyses were used to identify parameters important to waste isolation. The present study provided a more detailed examination of these issues and identified parameters and the current anticipated range of values and/or the uncertainties associated with them. Recommendations are made for testing and/or analysis to ensure that the program has an adequate characterization program.

Some of the potential thermal management issues of interest were suggested in the Thermal Management Strategy being developed. This study examined issues dealing with thermal management and some thermomechanical analyses.

## 1.2 BACKGROUND

The ability to meet the overall performance requirements for the potential MGDS at Yucca Mountain, Nevada, requires the two major subsystems (natural barriers and engineered barriers) to positively contribute to waste containment and isolation. In addition to the postclosure performance, the potential repository must meet certain preclosure requirements for safety, retrievability, and operability, and must take into consideration cost and schedule. The thermal loading strategy chosen for a potential repository may significantly affect both its postclosure and preclosure performance. Additionally, Nuclear Regulatory Commission (NRC) NUREG 1466 (NRC, 1992a) specifies that demonstrating the system performance of the potential repository must comply with 10 CFR 60.133(i) (CFR, 1993) and will require that the coupled thermal, mechanical, hydrological, and chemical (T-M-H-C) aspects of the repository performance be considered. To address the thermal loading issues of the repository, systems studies are being conducted by the M&O in addition to design and thermal testing efforts.

Developing an accurate estimate of the effects of thermal loading on the repository will be necessary to ensure that regulatory standards for nuclear waste disposal are satisfied. Essential to obtaining a license to emplace waste is understanding and predicting, with reasonable assurance, the behavior of the host rock and engineered barrier system (EBS) in the potential repository when it is subjected to heat released from the disposed waste. The effectiveness of these barriers for the various alternative thermal loads must be compared and presented in the licensing application [10 CFR 60.21(c)(1)(ii)(D)].

The rate of heat generation by nuclear waste decreases continuously with time. However, heat from the waste will be generated in appreciable quantity for thousands of years after initial nuclear waste emplacement. Temperatures throughout the repository and host rock environment will increase and reach a maximum at different places in the repository at different times. Depending on the thermal strategy selected, waste package size, age of the fuel, emplacement mode, and a number of other factors, the temperatures in the host rock could be above the boiling point of water for a very long period of time (thousands of years). In the near term, high temperatures can have a significant impact on preclosure performance from the standpoint of safety and waste retrievability. Over a longer period of time, the high temperatures could, in some cases, improve performance by drying out the rock or, conversely, contribute to a degradation in waste isolation capabilities. For example, temperatures above boiling will tend to dry-out the rock, resulting in a reduction of the aqueous corrosion of waste canisters for a significant period of time. Conversely, high temperatures and thermal gradients can, under

certain conditions, induce fractures in the rock. This behavior could change the structural integrity of the host rock as water movement may also be driven by heat along pre-existing fractures. High temperatures can also induce chemical and/or phase changes in some minerals which may then produce favorable or unfavorable conditions for adsorption of radionuclides.

At intermediate temperatures, the effects may mobilize water and change the water chemistry which could result in an increase in the corrosion rate of the waste package. When T-M-H-C coupled behavior is considered, the problem is further complicated. From the standpoint of safely emplacing the waste and/or retrieving it, high temperatures can degrade the ability to perform these operations. All these considerations indicate that the ability of the MGDS to isolate waste will be affected by thermal loading. According to NUREG/CR-5428 (NRC, 1992b), "The thermal loading capacity is probably the single most important parameter to determine for a repository."

A number of activities have taken place to investigate thermal loading, and although not all inclusive, the following is a summary of some of those efforts. A Thermal Loading Systems Study (M&O, 1994c) was conducted from December 1, 1992 through December 30, 1993 and, among other things, resulted in a conclusion that the upper limit for thermal loading is about 25 kilograms uranium (kgU)/m<sup>2</sup> (100 MTU/acre) based primarily on re-evaluated thermal goals (M&O, 1993a). This follow-on study was initiated to conduct parametric analyses to provide recommendations to the thermal test program and an interim report was prepared (M&O, 1994d). Work was done to develop a thermal strategy for the program. In the absence of in-situ thermal testing data, a programmatic decision was made to focus current design activities on a reference design thermal load using a working hypothesis of 19.8 to 24.7 kgU/m<sup>2</sup> (80 to 100 MTU/acre) and to maintain prudent levels of flexibility by including viable alternative thermal loads through design options and variations in operational parameters. Additionally, significant effort is underway to develop testing plans for the in-situ thermal tests, which will provide for the majority of the data/information needs while meeting the program constraints of cost and schedule. This present study will provide recommendations to the test planners that should render useful information on parameters to measure and T-M-H-C processes to observe.

### 1.3 SCOPE

This report documents activities related to the MGDS Thermal Loading Study for the potential repository at Yucca Mountain, Nevada. Activities which impact functions external to the "Disposal of Waste" function were coordinated with OCRWM through the M&O Vienna Systems Analysis group.

The scope of this effort encompassed a wide range of activities and involved a number of different organizations within OCRWM. The activities extended over the period from April 1, 1994, through September 30, 1995.

The scope of activities for this report is as follows:

Sensitivity analyses were done involving the following issues to examine the impact of various parameters on performance.

- The sensitivity to waste stream (fuel) variability in heat output and its impact on waste emplacement management were evaluated.
- A number of sensitivities were observed in the calculated hydrothermal behavior. Such things as permeability variations, both in the lateral and vertical stratigraphy, and binary diffusion coefficients were observed to produce significant changes in hydrothermal behavior of the host rock based on predictions of an equivalent continuum model (ECM). The evaluation of these parameters is discussed. Additionally, the elevation of the potential repository and the impact of elevation changes on thermohydrology were examined.
- The effect of thermal conductivity spatial variability on the rock temperatures was evaluated. Additionally, geochemistry spatial variability was also examined.

Some thermal management options were evaluated:

- One of the tasks of the study was to produce a ventilation code that was coupled with a hydrothermal code. The amount of sensible heat and moisture that can be removed from the mountain was estimated using the coupled codes.
- Thermomechanical aspects were evaluated for the various thermal loads and fuel types used.
- The effects of waste stream variability on the potential repository temperatures, and fuel aging/storage were examined.
- Nonuniform AML was examined to determine whether or not the technique should be used to reduce the impact of edge cooling.

The Thermal Loading Study involved assistance and participation from a number of different groups in OCRWM. The Performance Assessment (PA) group played an integral part in the activities. Subsurface design provided preliminary information on layouts and distances to stratigraphic units for various locations in the repository. Near-field thermal calculations were performed by SNL. Hydrothermal predictions were performed by LLNL and the CRWMS M&O PA Group. Geochemistry evaluations were done by LANL, and LBL provided assistance on evaluation of thermohydrologic scaling issues.

#### **1.4 REPORT ORGANIZATION**

This document provides a report of the Thermal Loading Study. The report organization follows the outline in the Technical Document Preparation Plan.

- The Executive Summary provides a top-level description of the study.
- Section 1 provides the study objective, background, scope, and organization of the report.

- Section 2 documents inputs and assumptions.
- Section 3 provides results of the parametric thermal evaluations.
- Section 4 documents the thermal management evaluations.
- Section 5 discusses the issue of scaling.
- Section 6 provides conclusions and recommendations.
- Section 7 contains the Reference List.
- Section 8 contains the Acronym List.

INTENTIONALLY LEFT BLANK

## 2. INPUT AND ASSUMPTIONS

This section identifies the reference case, the major input conditions for the study, and the assumptions used. This section begins with a brief discussion of the changes in the reference system that have occurred over the last year due to the refinement of the Program Approach. The waste stream analysis is presented along with the changes that have occurred in the waste stream assumptions. The design of the MGDS has progressed and a brief discussion includes the major subsystems of the first repository, waste package, repository surface facility, and repository subsurface facility. However, little discussion is provided about the data and assumptions used in the analytic models, since these have not changed (except for the waste stream) over the values described in the FY 1993 Thermal Loading System Study (M&O, 1994c) and last year's Thermal Loading System Study Interim Report (M&O, 1994d). Additional detail is provided in the specific sections when necessary.

### 2.1 REFERENCE CASE

The technical baseline for the MGDS has been changed from a small, thin-walled waste package emplaced in a vertical borehole at a thermal loading of about  $14.1 \text{ W/m}^2$  (57 kW/acre), to in-drift emplacement of large MPC waste packages. The Conceptual Description of the CRWMS (DOE, 1995a) provides a description of the system as envisioned under the Program Approach. The OCRWM Program Change Control Board (PCCB) has approved changing the technical baseline to include MPCs, but these changes to the baseline have not been fully implemented at the MGDS. The thermal loading to be considered as the baseline has not been decided at this time. The final section of thermal loading for the potential repository is still uncertain, but the currently proposed strategy focuses design activities on a reference design thermal load that will permit emplacement of at least the statutory maximum (70,000 MTU) for a single repository within the primary repository area. The current working hypothesis is that an AML of 80-100 MTU per acre ( $19.8\text{-}24.7 \text{ kgU/m}^2$ ) will satisfy this criteria. Given current waste stream assumptions, this corresponds to an initial areal power density ranging from  $19.9\text{-}24.9 \text{ W/m}^2$  (81-101 kW/acre). As a working hypothesis, the strategy will maintain prudent levels of flexibility by including alternate AMLs through design options and variations in operational parameters. The issue of the final thermal loading remains to be resolved, although it does not preclude comparisons of the various options.

No comparison of options will be examined in this report, and thus, a more detailed description of the reference case is not needed. Further, there were changes in the waste stream base case (Section 2.2) during development of the report. There are some instances where calculations were done using the waste characteristics in the FY 1993 study, the FY 1994 study, and other cases where calculations used waste characteristics of the most recently defined base case. When these occur in the report, they will be identified.

### 2.2 WASTE STREAM ANALYSIS

Several refinements of the base set of waste stream scenarios have been made for analysis purposes. A scenario developed this year and documented in the Controlled Design Assumptions (CDA) Document (M&O, 1995a) is now considered the base case waste stream for supporting

the systems studies, systems analysis, and design analyses being done on the program. This base case has a pickup selection which uses oldest fuel first (OFF) from the utilities. This section briefly discusses the base case and one waste stream scenario variant that uses youngest fuel first (YFF) with fuel age 10 years or older (YFF[10]). More details can be found in M&O 1995g.

In last year's Thermal Loading System Study Interim Report (M&O, 1994d), a preliminary analysis was performed to determine bounding waste stream characteristics for various assumptions on the selection and dry storage pickup deferral options. Based on this analysis, two scenarios have been selected as reasonable cases which provide a suitable range of heats and conditions for the thermal loading study. They are: 1) OFF selection with deferred dry storage pickup; and 2) YFF(10) selection without deferred dry storage pickup. These cases were selected to be conservative (hotter) examples OFF and YFF(10). These two scenarios, referred to as the FY 1995 Base Case and FY 1995 Variant, are summarized in Table 2.2-1.

Table 2.2-1. FY 95 Scenario Descriptions (No Monitored Retrieval Storage, Dry Storage Loaded Oldest Fuel First)

Scenario Name and Case Name	Pickup Selection <sup>1</sup>	Defer Dry Storage <sup>2</sup>	Derate <sup>3</sup>	Number Trucks <sup>4</sup>
FY 1995 Base Case - FY 1995 CDAO	OFF	Yes	Yes	4
FY 1995 Variant - FY 1995 Y_ND	YFF(10)	No	Yes	4

<sup>1</sup> "Pickup Selection" refers to the age-based rule used to select fuel from spent fuel pools.

<sup>2</sup> "Defer Dry Storage" means fuel in dry storage is not eligible for pickup, while fuel greater than 10 years old remains in the pool.

<sup>3</sup> "Derate" means a total heat output limit is applied during cask loading, limiting some casks to partial loading.

<sup>4</sup> "Number Trucks" is the number of truck sites. (All others are rail, possibly with barge or heavy haul.)

The variability of the heat output of the fuel (based on variations in enrichment, burnup, and age) was identified as a potentially important parameter, particularly for preclosure performance in the FY 1993 Thermal Loading System Study (M&O, 1994c). The pickup rate and selection strategy OFF versus YFF(10) affect the heat output of the various waste packages. Basic variability data were developed for the four scenarios used in the FY 1994 work reported in the Thermal Loading System Study Interim Report (M&O, 1994d).

The Mined Geologic Disposal System Requirements Document (MGDS-RD) (DOE, 1995b) contains an assumption that the loaded MPCs emplaced for disposal will have a maximum thermal output of 14.2 kW. For the FY 1995 Base Case and FY 1995 Variant scenarios, the transportation limit was set to 14.2 kW to ensure MPCs loaded for direct shipment to the repository would not exceed the disposal limit. The derating limits used were taken primarily from the MPC Subsystem Design Requirements Document (DRD) (DOE, 1995c) with the following exceptions. The ultimate disposal heat limit is 14.2 kW/package for all waste packages. For the large Pressurized Water Reactor (PWR) MPC, the transportation limit was set

to the same value since no monitored retrieval storage (MRS) is assumed (all other transportation limits are already below 14.2 kW). Also, for some large PWR sites, the storage limit was set to a lower value than that specified in the MPC Subsystem DRD following shutdown. This change was made because fuel in the pools in the MPC system is unloaded into dry storage as soon as possible following shutdown. The storage limit was overridden to a lower limit to avoid loading MPCs for storage that are subsequently withdrawn and sent to the MGDS over 14.2 kW.

Overall average SNF characteristics for the first repository are shown in Table 2.2-2 (M&O, 1995i.) The table is separated as to whether the SNF was generated by PWR or boiling water reactor (BWR) since the characteristics can be somewhat different. These characteristics were previously used to develop heat output profiles as input to repository thermal and thermohydrologic models. The fidelity of these thermal models and their capability to accommodate representations of the emplaced waste differ. Each model must represent the heat output from the waste over time in some manner. In the simplest representations of the waste's heat output profile (heat output versus time), three characteristics (age, burnup, and enrichment) and the fuel type have been used as input to heat output routines (M&O, 1995j) to generate the instantaneous heat. Given a waste stream scenario, the time of discharge and year of emplacement of each assembly are known. With this information, an age of the assembly at emplacement is calculated. The average age (shown below in Table 2.2-2) is the average of the ages weighted by the MTU per assembly. It has been recognized, and discussed below, that by utilizing these average characteristics versus calculating the heat for each assembly, the heat output of the waste is underestimated. A comparison of different models and the fidelity of data used in generating heat output profiles is discussed in the following paragraphs.

Table 2.2-2. Overall Average Spent Nuclear Fuel Characteristics (Averaged by MTU)

Scenario Name	BWR			PWR		
	Age (years)	Burnup (MWd/MTU)	Enrichment (% wt. Initial U235)	Age (years)	Burnup (MWd/MTU)	Enrichment (% wt. Initial U235)
FY 1995 Base Case	26.1	31,190	2.97	26.4	39,650	3.68
FY 1995 Variant	21.1	34,430	3.18	20.6	43,100	3.99

By using the average characteristics of the two fuels types (PWR and BWR), the heat output profiles per MTU for the FY 1995 Base Case are provided in Figure 2.2-1. These profiles, when multiplied by the total MTU of PWR and BWR waste, have been used as one representation of the heat output profile of the waste emplaced in the repository. These profiles are provided in Figure 2.2-2 for the FY 1995 Base Case for BWR and PWR SNF, and the total repository. These profiles resemble a decay heat profile of SNF, and by using the average age at emplacement, in one sense, incorporates the emplacement schedule of the waste that occurs over a 24-year time period.

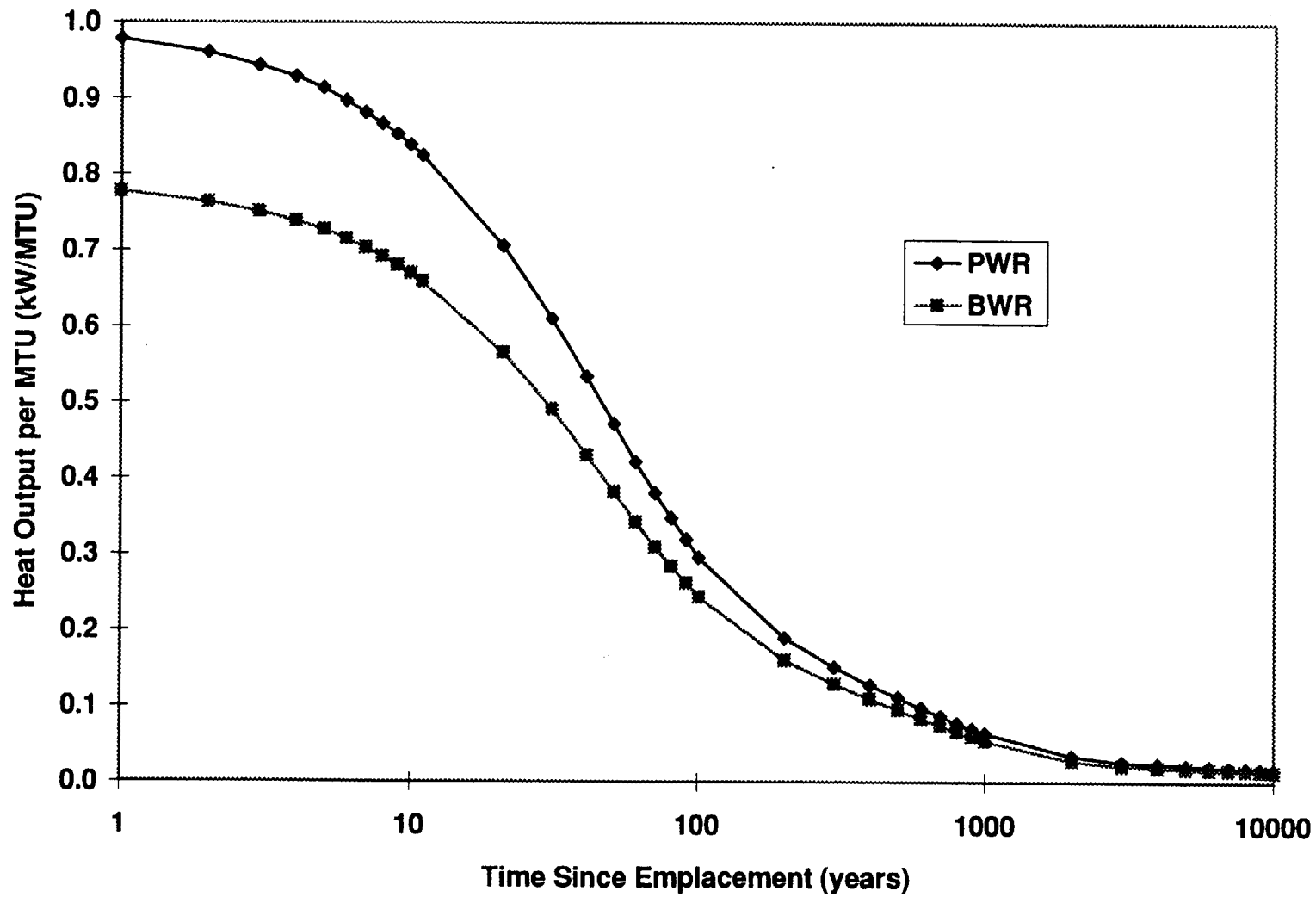


Figure 2.2-1. Instantaneous Power Per MTU Versus Time for the FY 1995 Base Case - Average Characteristics.

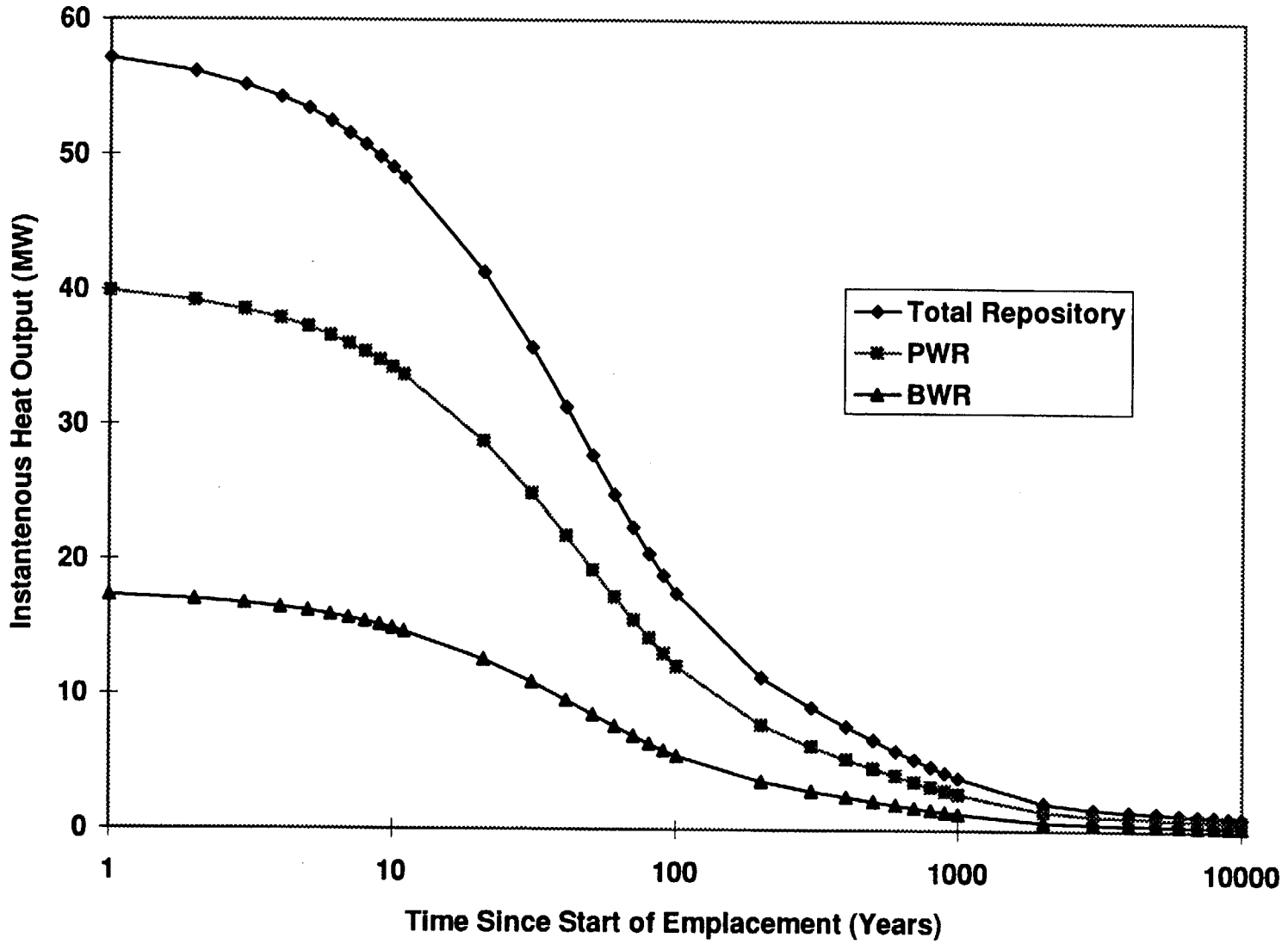


Figure 2.2-2. Instantaneous Heat Output Versus Time for the FY 1995 Base Case - Average Characteristics.

Examples of how these data have been used in thermal models are provided. The Total Repository curve (Figure 2.2-2) has been used in a "repository-scale disk" thermohydrologic model as the heat source for the repository. This model assumes the total amount of waste is emplaced at one time (not spread out over 24 years) and then calculates the thermohydrologic perturbation due to the time varying heat source. A second example of where these data have been used is a "drift-scale" thermohydrologic model where an average waste package's heat output is used as input to the model. This model assumes adiabatic and no-flow boundary conditions and then calculates the thermohydrologic perturbation due to the time varying heat source. The heat outputs using average characteristics of either fuel type or a combination of both have been used as inputs to this model.

As mentioned above, the use of average characteristics may not properly estimate the heat output profile of the waste emplaced in the repository. An analysis was performed that utilized individual assembly characteristics to calculate the heat output profile and then accumulate the data to form waste package heat profiles (M&O, 1995i). This data can then be accumulated in a number of ways. One method of accumulation that provides a similar profile as shown above groups all heats at emplacement (this has also been called a collapsed heat profile). The heat is then decayed a number of years and accumulated again. For the FY 1995 Base Case, this collapsed heat profile is shown in Figure 2.2-3. Another analysis (M&O, 1995h) accumulated the heat output for each year of emplacement and determined the decay heat from previously emplaced waste. The total heat output profile for the first 200 years after emplacement is provided in Figure 2.2-4. The shape of this profile is significantly different from the earlier profiles. This total heat output profile ramps up, as waste is emplaced, to a peak in the final year of emplacement, 2033, and then decays at the rate consistent with the collapsed profile. The peak total heat output is lower than the collapsed profile, as expected, because the waste emplaced in the year 2010 is now 24 years older. This profile, although it represents the total heat output profile of the repository, may not be as useful as the collapsed profile depending upon the thermal model in which it is used. If a waste package or drift-scale thermal model is used, the ramp up does not properly represent the thermal source profile of an individual waste package. Thus, the heat output profile used in a particular thermal model should be selected based on the particular application. A comparison of all three profiles is provided in Figure 2.2-5.

Several significant differences exist between the scenarios used in the FY 1993 Thermal Loading Study, the scenarios used in FY 1994, and the current refinements warranting a brief discussion of the differences and their impacts. Table 2.2-3 summarizes the scenarios used in the Thermal Loading System Study efforts and indicates the scenario selected as the Base Case. Several key differences exist between the respective Base Cases. The FY 1993 Base Case was a bare fuel system with an MRS, YFF(10) selection, and a large waste package. The FY 1994 Base Case is an MPC system with no MRS, OFF selection, and both a large and small size MPC waste package. The FY 1995 Base Case is a refinement of the FY 1994 Base Case due to the following adjustments: 1) the "pipeline" reactors (Bellefonte 1&2, Watts Bar 2) were removed following their cancellation; and 2) the fuel at Shoreham was removed since this fuel has been moved to Limerick where it will be reused (M&O, 1995h). Additionally, an updated and improved configuration of the Waste Stream Model (WSM) was used.

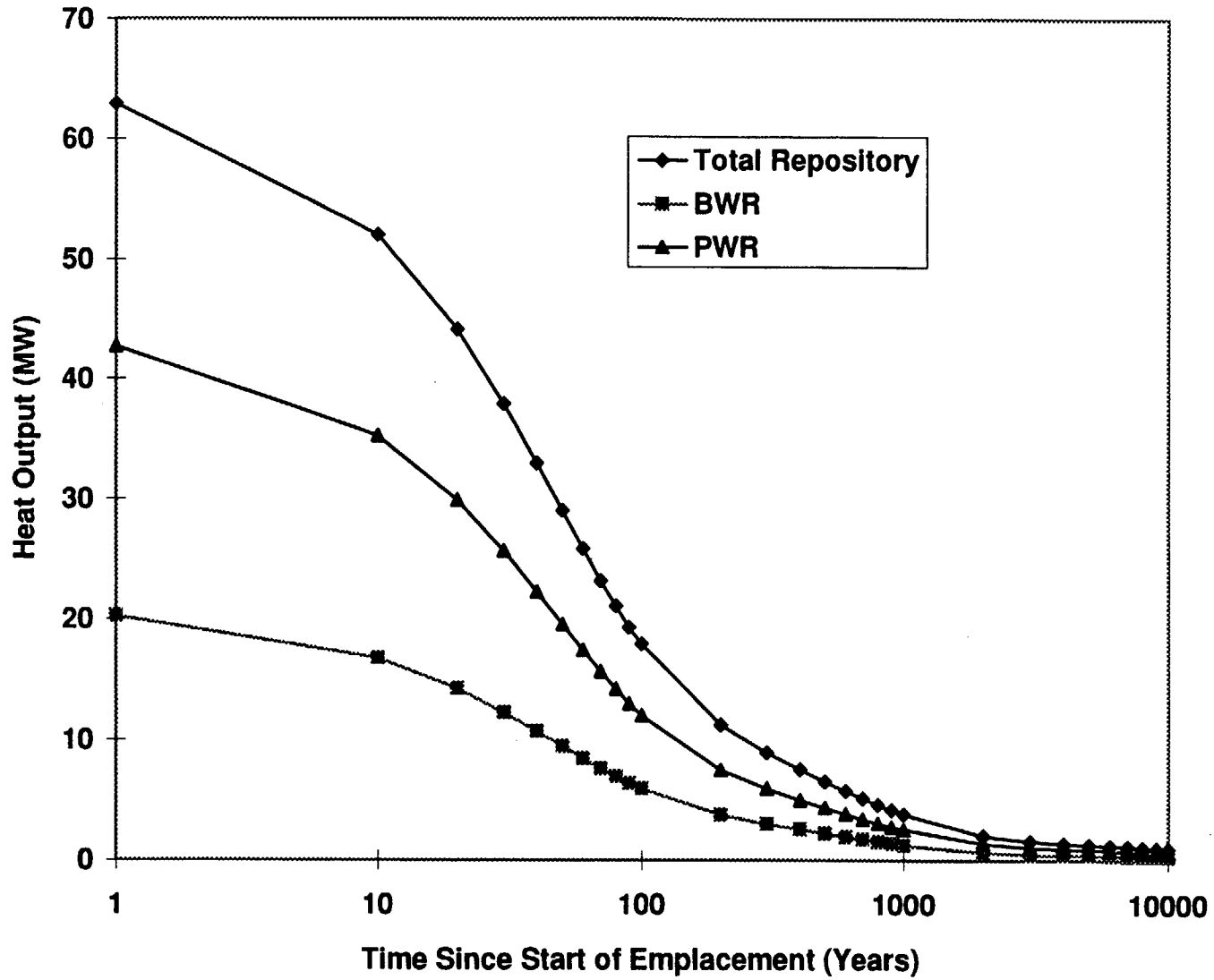


Figure 2.2-3. Instantaneous Heat Output Versus Time for the FY 1995 Base Case - Collapsed Profile.

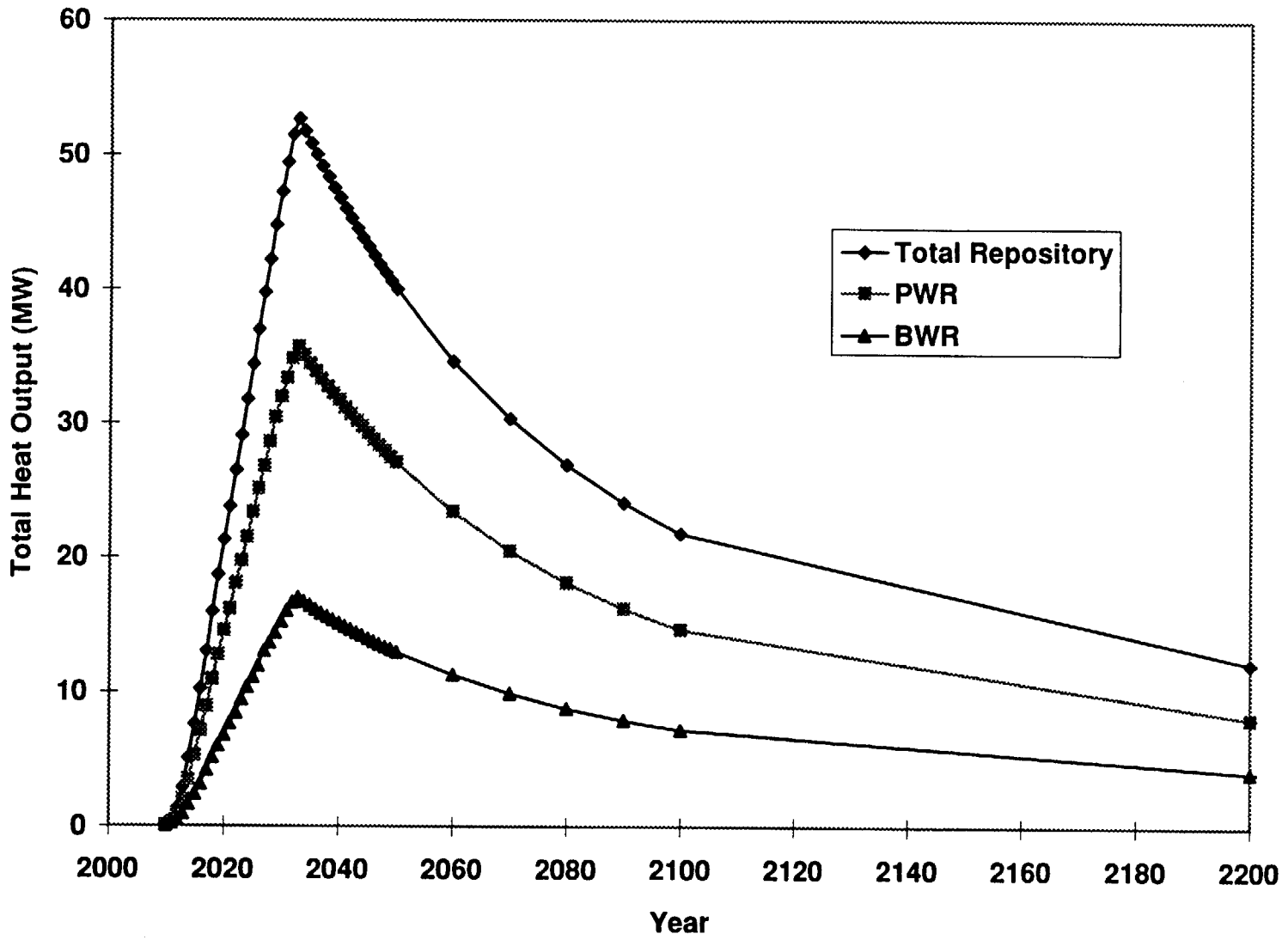


Figure 2.2-4. Actual Total Heat Output Versus Time.

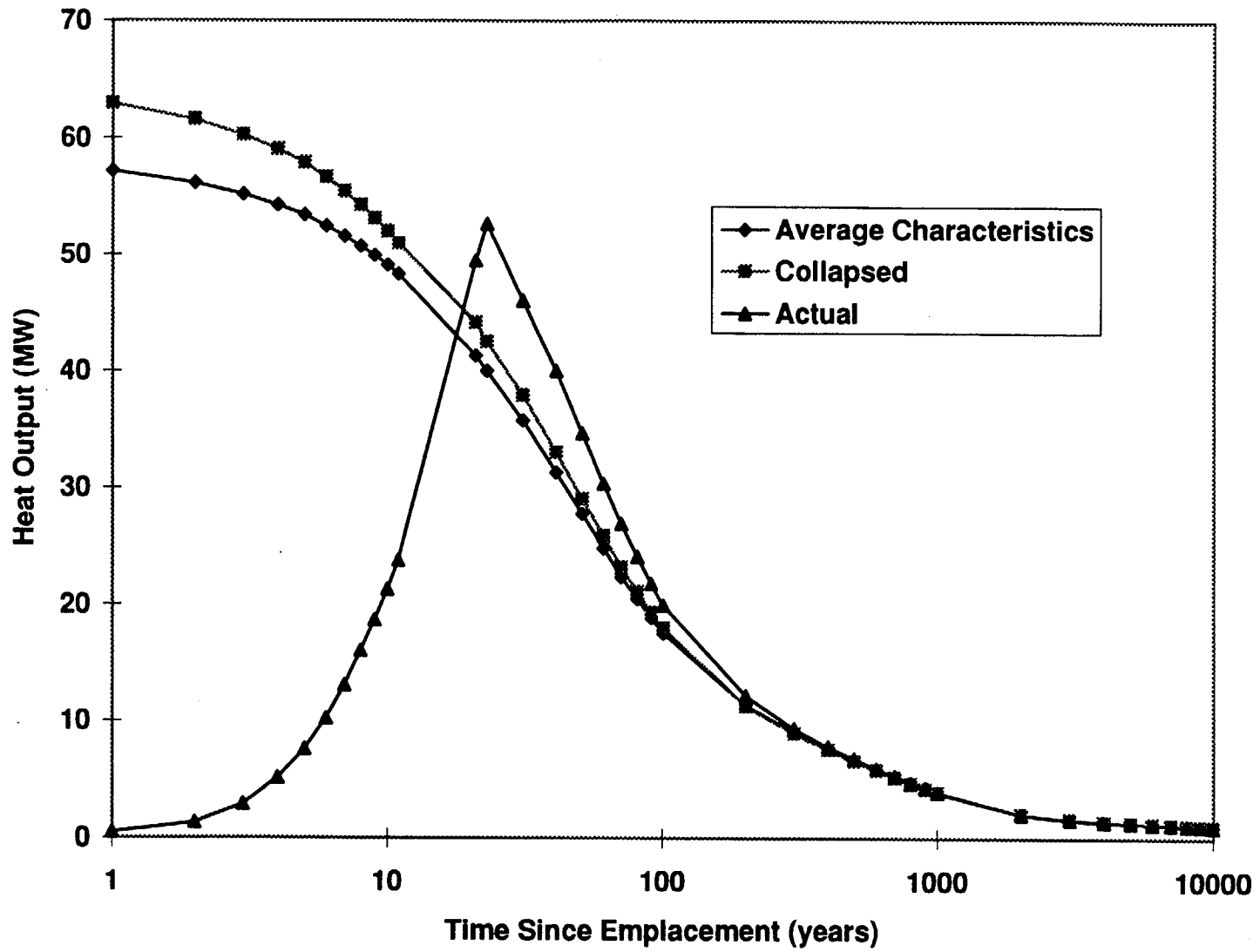


Figure 2.2-5. Comparison of Heat Output Profiles.

Table 2.2-3. Comparison of Waste Stream Scenarios For FY 1993, FY 1994, and FY 1995 Thermal Loading System Study

Year	Predominantly Bare/MPC	Selection	Defer Dry Storage	MRS	Derate	Waste Pkg Capacity	Base Case
FY 1993	Bare	OFF	Yes	Yes	Yes	2P / 4B 4P / 6B 12P / 21B 16P / 32B 21P / 40B	
	Bare	YFF(10)	Yes	Yes	Yes	2P / 4B 4P / 6B 12P / 21B 16P / 32B 21P / 40B	<====
FY 1994	MPC	OFF	Yes	No	Yes	12P / 24B + 21P / 40B	<====
	MPC	OFF	Yes	No	No	12P / 24B + 21P / 40B	
	MPC	YFF(10)	No	No	Yes	12P / 24B + 21P / 40B	
	MPC	YFF(10)	No	No	No	12P / 24B + 21P / 40B	
FY 1995	MPC	OFF	Yes	No	Yes	12P / 24B + 21P / 40B	<====
	MPC	YFF(10)	No	No	Yes	12P / 24B + 21P / 40B	

The waste packages in the FY 1993 Base Case were not derated to a 14.2 kW limit because that limit had not been established during that period. In the FY 1994 and FY 1995 Base Cases, the use of derating and small MPCs, and therefore small waste packages, increases the total number of SNF waste packages to 8,778 in the FY 1995 Base Case versus 7,650 for the FY 1993 bare fuel Base Case with all large and full waste packages. Table 2.2-4 shows the breakdown of package quantities for the Base Cases. The small quantities of bare fuel waste packages in FY 1994 and FY 1995 reflect an optimistic assumption of only four truck sites in the MPC system.

Table 2.2-4. Comparison of Package Quantities

Base Case	Large MPCs		Small MPCs		Bare Fuel Waste Pkgs		Total
	BWR	PWR	BWR	PWR	BWR	PWR	
FY 1993	n/a	n/a	n/a	n/a	3,118	4,532	7,650
FY 1994	2,209	4,102	1,553	759	1	189	8,813
FY 1995	2,242	4,041	1,545	765	3	182	8,778

Table 2.2-5 shows a comparison between the overall average SNF characteristics for the successive years' Base Cases. The differences in characteristics result from the differences in scenario parameters discussed above, most notably OFF (FY 1994 and FY 1995) versus YFF(10) (FY 1993) selection.

Table 2.2-5. Overall Average Spent Nuclear Fuel Characteristics

Base Case	BWR				PWR			
	Age (years)	Burnup (MWd/MTU)	Enrichment (% wt. Initial U235)	Heat Output at Emplacement (kW/MTU)	Age (years)	Burnup (MWd/MTU)	Enrichment (% wt. Initial U235)	Heat Output at Emplacement (kW/MTU)
FY 1993	23.5	32,240	3.10	0.860	22.5	42,210	3.92	1.126
FY 1994	26.0	30,860	2.93	0.765	26.3	39,770	3.70	0.983
FY 1995	26.1	31,190	2.97	0.777	26.4	39,650	3.68	0.978

In summary, the system scenarios used in waste stream analyses for thermal loading studies changed significantly between FY 1993 and FY 1994, with additional minor changes that have occurred in FY 1995. These changes reflect system level changes in the OCRWM Program direction. The primary impact on MGDS studies in general, and thermal loading in particular, is an increase in the number of packages from the implementation of an MPC system and the broadening of waste package heat output distributions, both attributable to introducing the small MPC. The change in average characteristics, and therefore the magnitude of heat output, is caused primarily by different selection assumptions and not the introduction of MPCs.

### 2.3 WASTE PACKAGE DESIGNS

The waste stream defines the waste that will arrive at the first repository including the types, quantities, and arrival rates. The arriving waste will be placed in waste packages. The waste package is the primary subsystem of the Engineered Barrier. For the disposal of 70,000 MTU of waste in the first repository, the majority of waste packages, approximately 8,600 out of 12,000 (which includes high-level waste) are expected to be MPCs with disposal container overpacks. A smaller number of SNF waste packages, approximately 200, will be uncanistered fuel waste packages. The remaining waste packages, approximately 3200, will be for Defense

and Commercial High Level Waste glass canisters. The capacities of the waste packages, their heat outputs and waste package spacings have the greatest influence on the thermal loading and repository temperatures and environment. The specifics of the waste package designs influence the internal and the near-field temperatures. The current disposal container designs are focused on metallic, multi-barrier conceptual designs with an outer corrosion allowance barrier and an inner corrosion resistant barrier. A preliminary selection of materials was made for the disposal containers. For all waste packages, Alloy 825 is the inner barrier material for the conceptual design. The conceptual outer barrier material for SNF waste packages is carbon steel. For the high-level waste glass packages, the conceptual outer barrier material is 70/30 copper-nickel.

## 2.4 REPOSITORY SURFACE DESIGNS

The repository surface designs include the geologic repository operations area and the general support facilities. The surface facilities will be located adjacent to the North Portal of the Exploratory Studies Facility (ESF). These facilities do not have a direct influence on the thermal loading but would have to interface with any of the Interim or CSFs that are described later in the report.

## 2.5 REPOSITORY SUBSURFACE DESIGNS

The repository subsurface designs used in the majority of thermal calculations to date were the generic designs provided previously in support of the FY 1993 Thermal Loading System Study (M&O, 1994c). In last year's Thermal Loading System Study Interim Report (M&O, 1994d), the subsurface design group provided the elevations of the conceptual repository subsurface design with respect to the different thermal/mechanical features as defined by Ortiz, et al. (1985). The potential repository in Yucca Mountain is not at a constant elevation to the various features for different locations in the repository. A sensitivity analysis examined if the thermohydrologic performance of the repository changed as a function of the changing distance to the various features. This would simulate waste being emplaced at different locations in the potential repository.

The conceptual layout of the potential repository with potential expansion areas is depicted in Figure 2.5-1 (M&O, 1994a). This layout is somewhat different than what is contained in the Site Atlas that had been based on the *Site Characterization Plan*, DOE/RW-0199 (SCP). Several locations were identified in the primary and two optional areas (Figure 2.5-1) where the elevation to various thermal/mechanical features (such as the surface, water table, or base of the Paint Brush nonwelded [PTn] unit) changed significantly. For example, the overburden, or distance from the potential repository to the surface varied from a minimum of 200 m to a maximum of 400 m within the Primary Area. Table 2.5-1 shows the various elevations and thicknesses for the different features at the locations selected. The uppermost layer TCw + UO consists of the Tiva Canyon welded unit and the unconsolidated overburden. It should be noted that the elevation of a potential repository layout in a given area may vary by 10 to 20 m, however, distances between layout horizons and various stratigraphic units may vary by 100 m or more, especially when considering both the Primary Area and the Expansion Areas.

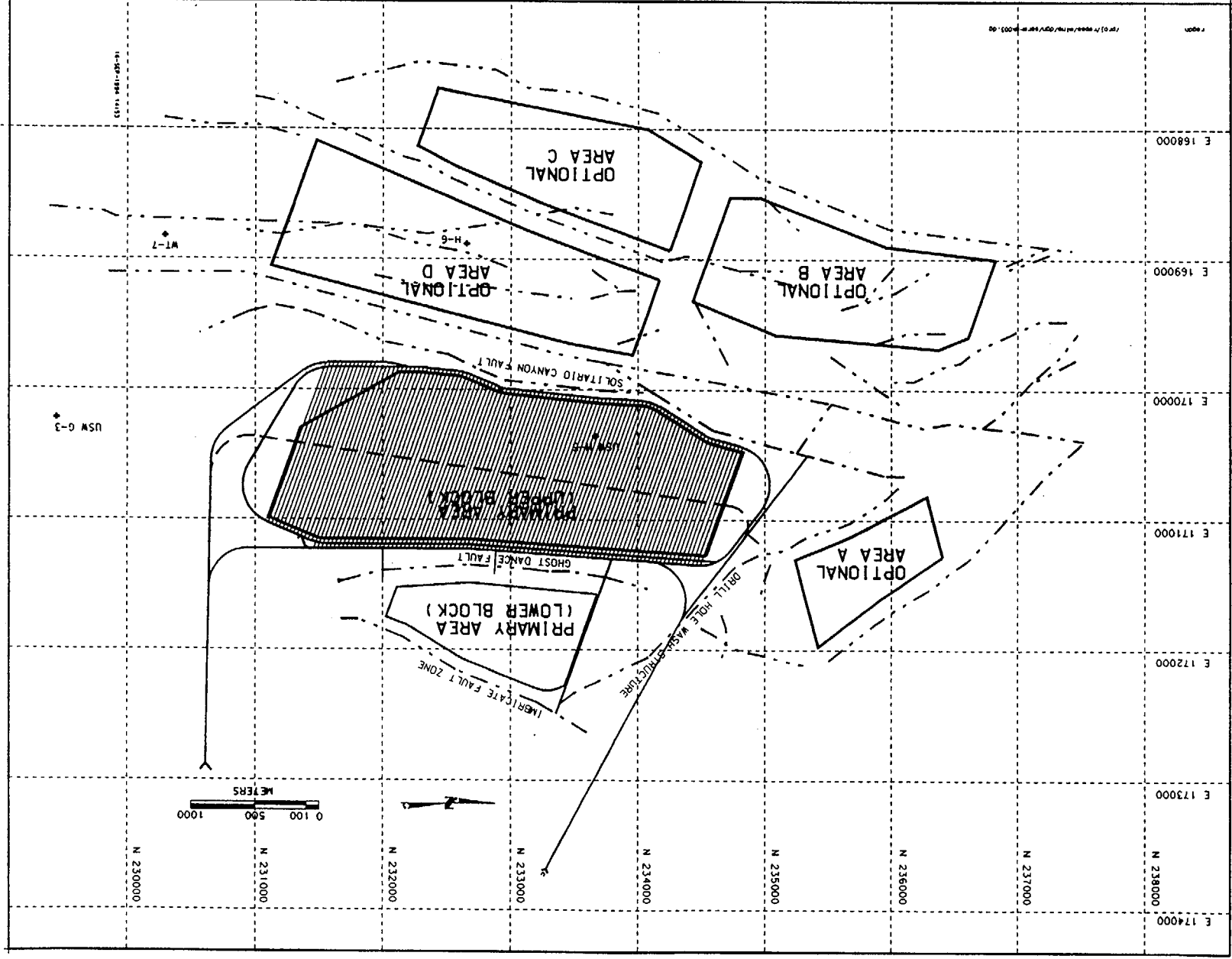


Figure 2.5-1. Potential Repository Primary Area and Potential Expansion Areas.

Table 2.5-1. Depths and Distances for Selected Locations in the Primary Area and Optional Areas A and B

Thermal/ Mechanical Features	Primary Area Thickness (m) <sup>4</sup>			Optional Area A Thickness (m) <sup>4</sup>	Optional Area B Thickness (m) <sup>4</sup>	
	Min. 200 m Overburden	400 m Overburden	Min. to Top CHn <sup>6</sup>	Min. 110 m to Water Table	Min. 135 m to Base PTn	430 m Overburden
General Location (m)	N:232562 E:169865	N:231953 E:170170	N:231648 E:169835	N:236220 E:170840	N:235001 E:169591	N:236525 E:168981
Surface Elevation	1295	1509	1353	1459	1408	1650
TCw+UO Thickness	0	168	0	0	0	7
PTn Thickness <sup>1</sup>	0	24	0	127	79	150
TSw1 Thickness <sup>1</sup>	81	99	89	145	125	125
TSw2 Thickness <sup>1</sup>	178	174	174	167	180	180
Repository Elevation <sup>5</sup>	1095	1109	1113	1038	1194	1220
TSw2 Base Structure Elevation <sup>3</sup>	1036	1044	1090	1020	1024	1188
TSw3 Thickness <sup>1</sup>	38	29	30	26	25	25
CHn Thickness to Groundwater Table <sup>2</sup>	233	265	301	66	107	135
Groundwater Table Elevation <sup>2</sup>	765	750	759	928	892	1029

- 1 PTn, TSw1, TSw2, and TSw3 thicknesses for Primary Area and Optional Area A were as estimated by USGS in Lynx Model YMP.R1.0. For Optional Area B, the following thickness estimates were used: PTn=150 m; TSw1=125 m; TSw2=180 m; and TSw3=25 m.
- 2 Ground-water table as defined by Fridrich et al. (1994).
- 3 Base of TSw2 in Primary Area from Sandia National Laboratories Interactive Graphics Information System Model and in Optional Areas A and B from northward and westward projection of the Interactive Graphics Information System Model.
- 4 Point stratigraphy estimated using cross sections and topographic isopach contour maps.
- 5 Repository elevation measured from cross sections and generally represents the centerline (springline) of the excavation.
- 6 Minimum distance to the top of CHn is corrected to 25 m, not 15 m. The 25 m distance was estimated based on a TSw3 thickness of 15 m in Borehole G-4 and from Ortiz et al. (1985), and an estimated 10 m distance from the base of the TSw2. The USGS TSw3 thickness estimates now show a thickness of 30 m in this area.

In the Primary Area, which supports thermal loadings from 17.3 to 24.7 kgU/m<sup>2</sup> (70 to 100 MTU/acre), if all 70,000 MTU are to be emplaced, three locations were chosen for further study. The first case, shown in column 2 of Table 2.5-1, shows the overburden (distance from the repository to the surface) of a minimum of 200 m. The second case, which occurs at another location in the Primary Area, has the maximum (in the Primary Area) distance of 400 m from the repository to the surface. The next column in Table 2.5-1 shows a case in the Primary Area having the minimum distance of 25 m to the top of the Calico Hills nonwelded (CHn) unit. In the other areas, for example Optional Area A (column 5), a case was found which had a minimum distance from the repository to the water table of 110 m. The use of this area would only be required if AMLs of 13.6 kgU/m<sup>2</sup> (55 MTU/acre) or less are needed to emplace all 70,000 MTU of fuel. In Optional Area B, which might be added if AMLs of 5.9 to 8.9 kgU/m<sup>2</sup> (24 to 36 MTU/acre) would be required, a case was found where there was a minimum distance of 135 m to the base of the nonwelded PTn, as shown in column 6 of Table 2.5-1. In the last data column in Table 2.5-1, a case was found in Area B that had a large overburden of 430 m. Table 2.5-2 translates the various elevations into the depth below the surface of the various thermal/mechanical features. It should be noted that lower AMLs than those shown in Table 2.5-2 could be emplaced in the different areas if capacities less than 70,000 MTU were to be emplaced. Table 2.5-2 provides depths from the surface to the various units in meters.

Table 2.5-2. Distances to Thermal/Mechanical Features for Selected Repository Locations in Yucca Mountain

Thermal/ Mechanical Features	Primary Area				Optional Area A	Optional Area B	
	Base Case	Min. 200 m Overburden	400 m Overburden	Min. to Top CHn	Min. 100 m to Water Table	Min. 135 m to Base PTn	430 m Overburden
TCw+UO	29.3	0	168	0	0	0	7
PTn	67.4	0	192	0	127	79	157
TSw1	197.5	81	291	89	272	204	282
Repository	343	200	400	253	421	214	430
TSw2	387.3	259	465	263	439	384	462
TSw3	403.1	297	494	293	465	409	487
Water Table	568	530	759	594	531	516	622
AML (kgU/m <sup>2</sup> )	5.9-24.7	17.3-24.7	17.3-24.7	17.3-24.7	5.9-13.6	5.9-8.9	5.9-8.9

The features described above and used in the majority of calculations were based on the thermal/mechanical and hydrological stratigraphy defined by Ortiz, et al. (1985). Where other nomenclature is used, as in Section 4.2, the units are defined in those sections.

## 2.6 INPUTS AND ASSUMPTIONS PERTINENT TO YUCCA MOUNTAIN

Much of the input and assumptions pertinent to Yucca Mountain used in development of the FY 1993 Thermal Loading System Study have remained the same for this study. Details of those can be found in Section 2.6 and Appendix C of that report (M&O, 1994c). As stated in that report, much of the input used was taken from the *Reference Information Base* (RIB), YMP/93-02 (YMP, 1995). However, in this study some of the input did change and/or parameters were varied over a range of values. Additional detail on information that differs from the FY 1993 input are provided in each section.

### 3. PARAMETRIC THERMAL EVALUATIONS

The testing strategy currently being developed evolves from the philosophy of the SCP which was basically to conduct comprehensive studies on a wide variety of issues. To better manage the available resources, the philosophy adopted in the Program Approach (DOE, 1994) is to focus characterization activities into essentially three areas: 1) those activities needed for evaluating site suitability (to be completed by 1998); 2) those required for supporting License Application in 2001; and 3) those for confirming postclosure performance. As such, OCRWM is focusing on a few specific in-situ thermal tests to support these activities. The thermal testing program must ensure a well integrated set of laboratory tests, in-situ thermal tests, and natural analog studies in concert with appropriate analytic models be accomplished to develop an adequate understanding of the thermally affected processes. Currently, many of the parameters associated with the processes that may influence performance as a function of thermal loading are not well known or have values of significant uncertainty. Additional significant uncertainty exists as to how some of these parameters scale (from changes in time and distance) as one goes from laboratory to waste package to drift to repository or mountain scale. Thus, the program observed a need to help focus the planning of the testing program by conducting preliminary evaluations to determine where sensitivities might exist. This study performed a number of sensitivity analyses in an attempt to identify parameters and processes which potentially influenced performance as a function of thermal loading and the range of uncertainty in these parameters. From the results of these sensitivity analyses, testing recommendations are provided.

The sensitivity studies conducted and reported in this section were:

- bulk permeability variations,
- the effect of variation in selected rock properties on thermohydrology,
- the examination of gas-phase diffusion on thermohydrology,
- the effect of modeling assumptions on thermal profiles,
- the effect of fracture-matrix coupling on thermohydrology,
- the geochemistry issues (dehydration and mineral alteration of zeolites),
- the effect of elevation variations on thermal performance, and
- thermomechanical evaluations.

#### 3.1 BULK PERMEABILITY VARIATIONS

##### 3.1.1 VTOUGH Calculations

Water movement and the uncertainty in determining the amount of water movement are important issues in selecting a thermal loading. The higher the permeability, the easier it is to move water. A permeability of  $2.8 \times 10^{-13} \text{ m}^2$  (280 millidarcy) has been used for the majority of the mountain-scale calculations, since this is believed to be a representative value for the bulk average at the repository horizon. However, there is uncertainty in this value; it could be higher or lower on the average, and locally some areas of rock could be significantly different. Air permeability measurements in TSw2 and reported by Wilson, et al. (1994) show bulk permeabilities in the range from  $10^{-13}$  to  $10^{-11} \text{ m}^2$  (0.1 to 10 darcy). The  $2.8 \times 10^{-13} \text{ m}^2$  value is at the low end of the range determined by Wilson, et al. Some preliminary investigation was done in the FY 1993

Thermal Loading System Study (M&O, 1994c) to examine the sensitivity to bulk permeability. Additional work was done for this study to establish the impact that bulk permeability has on the hydrologic behavior under the influence of heat. This work was initially reported in M&O, 1994d and in Buscheck, et al. (1994). This section discusses the work done and provides the findings which show implications on bulk water movement.

In general, the modeling work indicates that at high fracture and bulk permeabilities, water movement occurs principally by water vapor movement through fractures. At the lower fracture and bulk permeabilities, the flow of vapor through the rock matrix begins to play a significant role in the movement of water.

LLNL used the VTOUGH code (Nitao, 1989) which is in the TOUGH family of codes (Pruess, 1987) to calculate the amount of liquid moved under the influence of heat in the host rock. Estimates of liquid flux distribution through the repository are needed to estimate performance. However, at this time, only estimates of total volume of liquid moved above the repository have been calculated. From these predictions of volume of liquid moved, estimates of equivalent column of liquid above the repository were determined and these estimates were used as a surrogate for flux. These estimates were obtained by dividing the total volume of water moved at each AML for each bulk permeability by the area over which the heat is distributed (e.g., potential repository area) to determine the equivalent height of the column of water that must be supported by capillary and vapor pressure above the potential repository. This water may also leave the system as vapor, drain through fast paths, or shed around the heated zone. This volume of water per unit area also gives an upper bound of the additional amount of water, excluding episodic flow or linkages with perched water potentially available to contact a waste package upon cool down.

The calculations with VTOUGH used parameters, which were essentially the same as those identified in the FY 1993 Thermal Loading System Study (M&O, 1994c). Details may be found in Section 3.6 and Appendix C of that report. As stated in the report, many of the inputs used were taken from the RIB (YMP, 1995). YFF(10) fuel was used in large MPCs to model the waste streams. Figure 3.1-1 shows a plot of the calculated equivalent column height of water plotted as a function of bulk permeability for each AML considered. This plot was done at the time when the maximum volume of water was perturbed. A line designating the nominal permeability of  $2.8 \times 10^{-13} \text{ m}^2$  (280 millidarcy), used in many previous analyses, is designated on the plot in addition to lines drawn at permeabilities of  $10^{-13}$  and  $10^{-11} \text{ m}^2$  (0.1 to 10 darcy), which describe the most likely range of bulk permeabilities for TSw2 (Wilson, et al., 1994). The calculations in Figure 3.1-1 show the maximum column of liquid water that is removed from a dry-out zone around the repository. This dry-out zone is defined as the region where there is any reduction in liquid saturation levels from ambient. Calculations were performed over a large range of values for a sensitivity study to determine whether significant changes occurred as the thermal load or permeabilities changed.

The results indicate that negligible water movement is predicted at low thermal loads ( $\leq 12.2 \text{ kgU/m}^2$  [49.2 MTU/acre]) with less than 1 m column affected at permeabilities less than or equal to  $1 \times 10^{-12} \text{ m}^2$  (1 darcy). At high thermal loads of  $27.4 \text{ kgU/m}^2$  (111 MTU/acre), the column of water affected is more than a factor of 10 larger. This water, as indicated above, will move until it can drain since the rock matrix pore space is insufficient to support that amount of

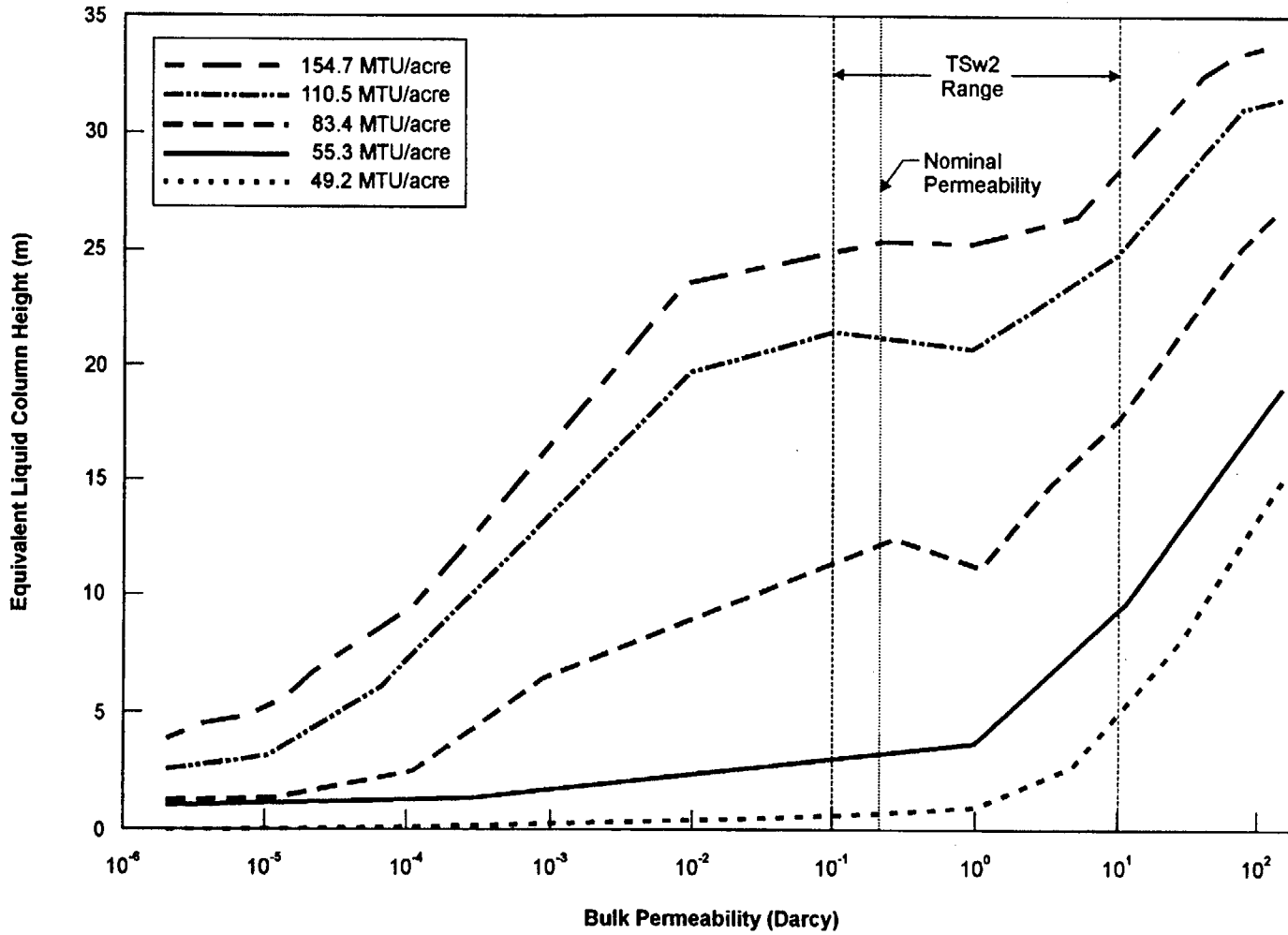


Figure 3.1-1. Maximum Equivalent Liquid Column Height Moved from the dry-out Zone (Some Decrease in Liquid Saturation over Ambient) as a Function of Bulk Permeability for Five Thermal Loads.

water. Below boiling (bulk average) thermal loads are not shown on this figure; these loads produce less equivalent liquid column; and these predictions are reported in a previous document (M&O, 1994d). As a result, the equivalent column of water becomes larger for all thermal loads. The below-boiling thermal loads produce the smallest equivalent column of liquid for any permeability.

### 3.1.2 TOUGH2 Calculations

Some additional thermohydrologic calculations were done to examine the result of changes in bulk permeability in more detail. These hydrothermal calculations were done by the M&O PA Department using the TOUGH2 code (Pruess, 1991). This code is similar in nature to VTOUGH used by LLNL. The TOUGH code (Pruess, 1987) was the basis for both VTOUGH and TOUGH2. TOUGH2 solves up to three governing equations in as many as three dimensions. Mass conservation is determined for the water component, considering both water and gas phases. Mass conservation is calculated for the noncondensing gas component (e.g., air), which is assumed to be present in both the gas phase and, as a soluble constituent, in the water phase. Finally, an energy conservation equation treats heat transport. The model employs the integrated finite-difference technique for space discretization which allows flexibility in specifying the geometry. The time discretization is accomplished by a fully implicit procedure (Pruess, 1991).

The calculations were conducted for an AML of 20.5 kgU/m<sup>2</sup> (83 MTU/acre) using an OFF waste stream. The calculations used large waste packages. The waste package separation was 16 m while the drift spacing was 26.7 m. The surface temperature boundary conditions at the top of Yucca Mountain was taken to be isothermal at 15°C, the annual mean temperature. The calculations were only run during the preclosure period from emplacement to 100 years. Bulk permeabilities were varied from about 1 x 10<sup>-15</sup> to 1 x 10<sup>-12</sup> m<sup>2</sup> (1 millidarcy to 1 darcy) and the vertical temperature profiles calculated at 100 years after emplacement are shown in Figures 3.1-2 through 3.1-5. In these calculations, the surface of Yucca Mountain is at a depth of a 0 m and the potential repository is at 343 meters.

### 3.1.3 Results

The results of the VTOUGH calculations indicate that for bulk permeabilities above about 1 x 10<sup>-12</sup> m<sup>2</sup> (1 darcy), much larger increases in the amount of mobilized liquid water occur with increasing permeabilities than for similar increases in permeabilities for ranges less than 1 x 10<sup>-12</sup> m<sup>2</sup>. Thus, bulk permeability is an important parameter, and is particularly important at permeabilities above 1 x 10<sup>-12</sup> m<sup>2</sup>.

The TOUGH2 calculations found that when the permeabilities reached about 1 x 10<sup>-13</sup> m<sup>2</sup> (100 millidarcy) the formation of heat pipes appears to occur. The extent of the heat pipes was found to increase with increasing permeability. Figure 3.1-2 for a bulk permeability of 1 x 10<sup>-15</sup> m<sup>2</sup> (relatively tight rock with limited pore connectivity or significant fractures) shows that heat is transported primarily by conduction. For the slightly more porous matrix of 1 x 10<sup>-14</sup> m<sup>2</sup> shown in Figure 3.1-3, the change in slopes on either side of the peak is representative of some heat convection taking place. The heat convection provides more efficient transport of heat than conduction; and thus, the calculated peak temperature at the repository horizon is reduced somewhat (about 5°C). There is as yet no relatively constant plateau representative of a heat

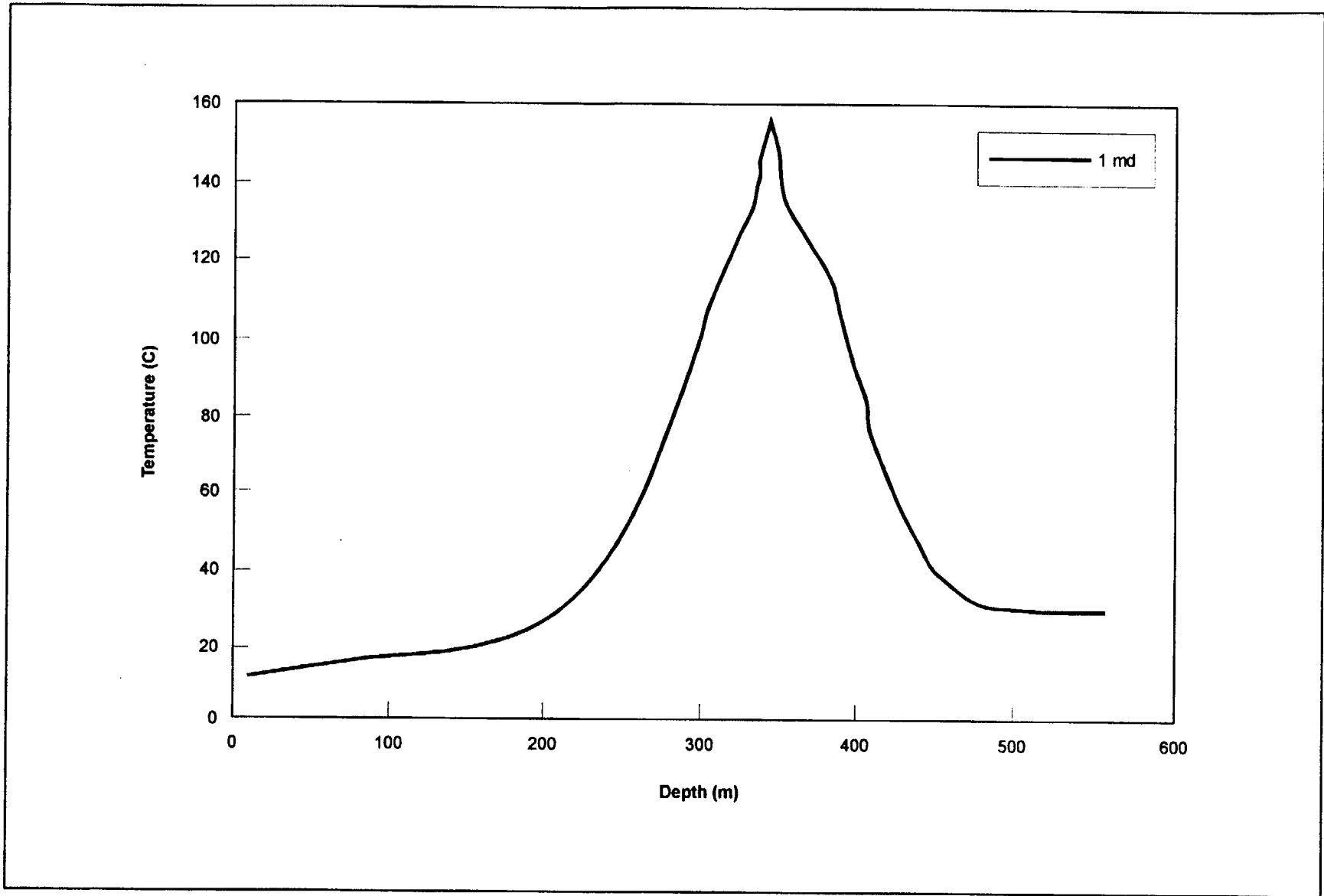


Figure 3.1-2. Vertical Temperature Profile at 100 Years for a Bulk Permeability of  $1 \times 10^{-15} \text{ m}^2$  (1 mD) and a Thermal Load of  $20.5 \text{ kgU/m}^2$ .

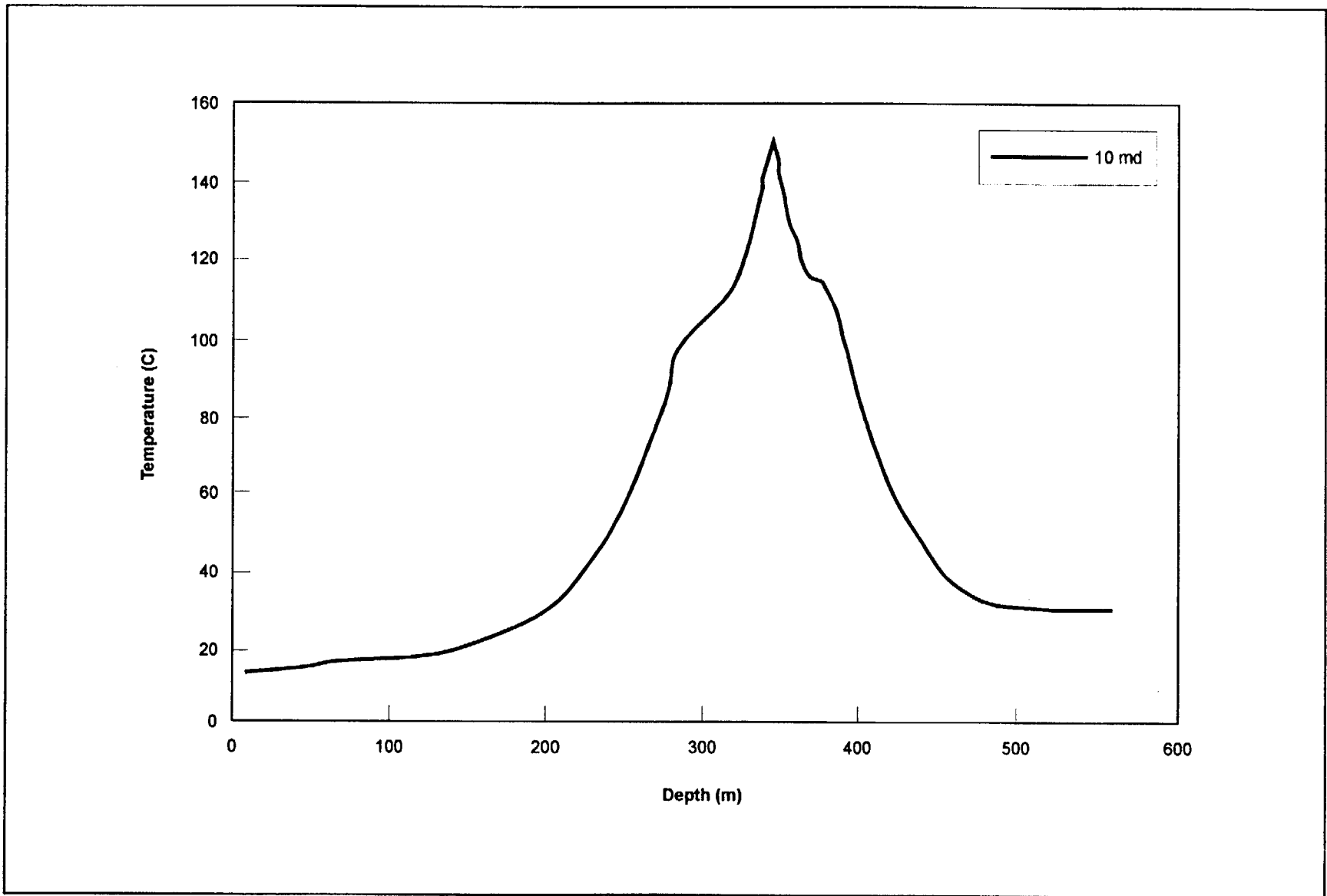


Figure 3.1-3. Vertical Temperature Profile at 100 Years for a Bulk Permeability of  $1 \times 10^{-14} \text{ m}^2$  (10 mD) and a Thermal Load of 20.5 kgU/m<sup>2</sup>.

pipe, because the rock is relatively impermeable resulting in increased pressure and therefore increased boiling point of water. As the bulk permeability is increased to  $1 \times 10^{-13} \text{ m}^2$  (shown in Figure 3.1-4), the formation of a distinct heat pipe occurs above the repository horizon as buoyant gas-phase convection becomes important. Below the repository horizon, the heat pipe is not present because convection and conduction are in opposite directions. That is, the vapor tends to rise above the repository through buoyant convection and condense to liquid near the boiling point producing the heat pipe. As the bulk permeability is further increased to  $1 \times 10^{-12} \text{ m}^2$  (Figure 3.1-5), the heat pipe above the repository horizon continues to strengthen and increase in vertical extent. As the bulk permeability increases, the predicted repository horizon temperatures decrease as a result of more heat being transported away by convection.

The heat-pipe effect is a heat transfer mechanism of high efficiency consisting of a cyclic fluid-thermal system. Latent heat is transported away from a heat source by movement of vaporized gas. The gas is driven away from the heat source by the resulting buildup in gas phase pressure. A continual return flux of condensate replenishing the liquid phase as it boils is usually provided by a capillary wick or nonequilibrium fracture flow. As the calculations show, the heat-pipe effect results in heat transfer that can dominate thermal conduction. Investigations of the possible presence of heat pipes should be a prime objective of the in-situ thermal tests.

If the water mobilized is assumed to be available to contact waste packages, conclusions can be determined with respect to AML and bulk permeability. Above about  $8.9 \text{ kgU/m}^2$  ( $36 \text{ MTU/acre}$ ), locally saturated regions occur (M&O, 1994c), allowing the possibility of liquid flow in fractures which may or may not enter the repository drifts depending on near-field heterogeneities and the extent that liquid may concentrate in fractures. These saturated regions are not predicted to occur, however, if the bulk rock permeabilities are below about  $1 \times 10^{-14} \text{ m}^2$ . Several factors can alter the conclusions of the preceding paragraph. One or more of the following mechanisms can either remove the water before it contacts waste packages or preferentially concentrate water at certain locations:

- matrix imbibition
- boiling
- the capillary barrier effect of potential backfill
- condensate drainage through regions not occupied by waste packages, and
- focused liquid flow driven by spatial heterogeneity in bulk permeability.

These need to be examined further and carefully evaluated in heater tests.

From this analysis, it can be concluded that there are significant increases in buoyant gas-phase convection that occur if the bulk permeabilities are above about  $10^{-13} \text{ m}^2$  (10 darcy). Additionally, between  $10^{-12}$  and  $10^{-11} \text{ m}^2$  (1 and 10 darcy), this increase in convection becomes apparent even for low thermal loads. From this analysis, it can be concluded that if bulk permeabilities are below about  $1 \times 10^{-14} \text{ m}^2$  (10 millidarcy), heat transport is dominated by conduction. Above this bulk permeability, more and more heat transport occurs by convection. The subsequent buoyant gas phase convection that occurs produces heat pipes which are efficient carriers of heat. Thus, the test program must ensure that the bulk permeability measurement is done. The sensitivity range for the measurements should at least span the range from a few tenths of  $10^{-12} \text{ m}^2$  to about  $10^{-11} \text{ m}^2$  or more.

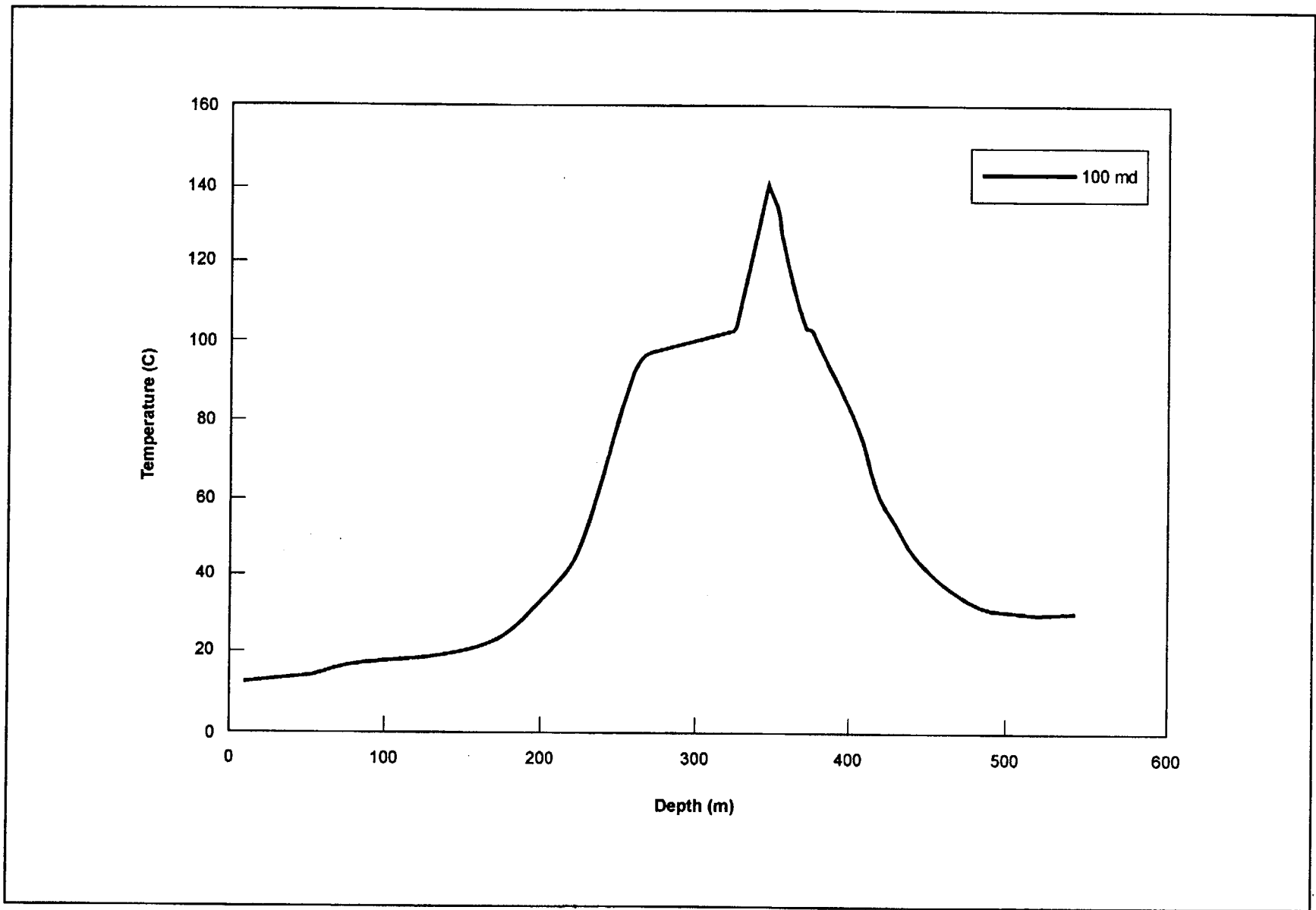


Figure 3.1-4. Vertical Temperature Profile at 100 Years for a Bulk Permeability of  $1 \times 10^{-13} \text{ m}^2$  (100 mD) and a Thermal Load of  $20.5 \text{ kgU/m}^2$ .

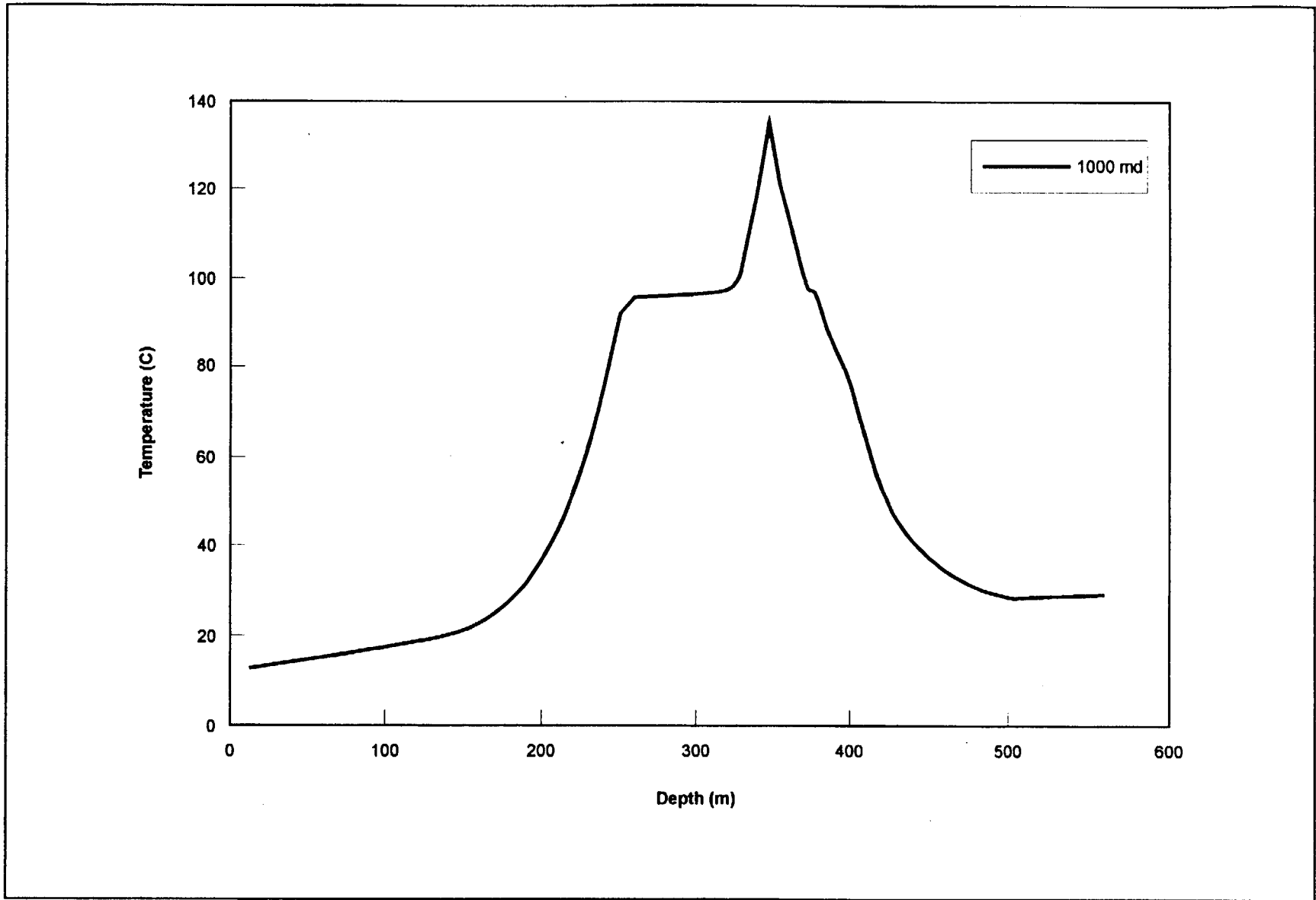


Figure 3.1-5. Vertical Temperature Profile at 100 Years for a Bulk Permeability of  $1 \times 10^{-12} \text{ m}^2$  (1 D) and a Thermal Load of  $20.5 \text{ kgU/m}^2$ .

The above discussion has concentrated primarily on the higher permeability conditions. Some additional low permeability calculations for  $1 \times 10^{-15} \text{ m}^2$  (1 millidarcy) permeabilities have been done. The results show that the lower permeabilities result in substantial increases in gas-phase pressure in the rock. The increased pressure increases the boiling point and suppresses the rate of vaporization and dry-out. Thus, a sufficiently small permeability may produce conditions where high temperatures coincide with high humidity. This issue needs to be addressed in the characterizations by determining whether fracture density and connectivity are sufficient to promote a reduction in relative humidity due to boiling.

The testing efforts should be designed to evaluate whether or not high permeabilities and large gas flow exists, particularly at high thermal loads. Additionally, the tests should establish not only how much water is mobilized but where the water goes. This is important for both high and low thermal loads. The range of uncertainty in bulk permeability for the TSw2 member has been identified by Wilson, et al., (1994) to be from  $10^{-13}$  to  $10^{-11} \text{ m}^2$  (0.1 to about 10 darcy). Since this range was based on air permeability measurements, establishing what the bulk permeability is through in-situ tests and the degree of heterogeneity that exists will be critical in understanding the hydrothermal performance of the natural barrier and the waste package performance. The measurement of bulk permeability is very dependent on the scale over which the measurements are made and care needs to be taken to ensure that representative values are obtained. Field tests are perhaps the most appropriate method of measuring bulk permeability at a scale of importance to the predictions. Some additional discussion of rock permeability is provided later in the report when dual permeability calculations are discussed in which the rock matrix and fracture permeabilities are treated separately.

The calculations in this section were based on a highly idealized homogeneous system and hence the effects of heterogeneity on these calculations could not be addressed. The importance of spatial variations in permeability is addressed to some extent in Sections 3.2, 3.5, and 5. These sections will investigate some of the implications of stratigraphic, hydrologic property, fracture, and fault heterogeneity on the temperature and hydrology predictions.

Based on the analyses conducted during this study, it would appear that the formation and extent of heat pipes can be used to verify some of the aspects of the predictions and can be used to establish estimates of the bulk permeability values used. The thermal tests should be designed to measure the presence and extent of heat pipes. Temperature sensors can provide much of the information needed to determine if heat pipes exist as long as sufficient density of instruments is used.

### **3.2 EFFECT OF VARIATIONS IN SELECTED ROCK PROPERTIES ON THERMOHYDROLOGY**

Estimates of rock properties that may affect water and gas flow are uncertain because the measurements made to date rely on information from a limited number of samples taken from only a few boreholes and are at a scale that is considerably smaller than the repository scale. A parametric study was conducted and is reported in this section to determine if variations in some of the derived rock parameters that affect capillary suction and liquid relative permeability could significantly impact thermohydrologic performance. The parametric study was conducted using the VTOUGH code described in Nitao (1989) and Pruess (1987). The majority of the

parameters and inputs used in the calculations were those reported earlier in M&O, 1994c and in the previous section. The calculation uses a smeared heat source, repository scale model. This VTOUGH model is a simplified model that relies on radially symmetric geometry. The differences in inputs between those earlier calculations and these parametric calculations are discussed below.

### 3.2.1 VTOUGH Calculations

In addition to the VTOUGH calculations, which addressed spatial variability in rock properties, some calculations of the influence on heat, fluid, and vapor of fracture zones are provided. Some preliminary calculations of hydrothermal behavior have been done by LBL using a site-scale model (Wu, Chen, and Bodvarsson, 1995). An overview of some of these calculations showing the potential influence of such features is the Ghost Dance Fault and the Solitario Canyon Fault and is presented in the second part of this section.

The parametric calculations in this section were done for a set of matrix properties for the Topopah Spring (TSw) welded unit that have been derived primarily from USGS measurements. Specifically, the effect on thermohydrologic predictions as a result of changes in the capillary suction,  $P_{suc}$ , and the liquid relative permeability,  $k_{rl}$ , due to different rock matrix properties was examined. The capillary suction and liquid relative permeability are written in terms of a set of curve fitting parameters based on van Genuchten (1978) according to:

$$P_{suc} = (1/\alpha)[S_{EF}^{(-1/m)} - 1]^{(1-m)} \quad (3.2-1)$$

$$k_{rl} = (S_{EF})^{1/2} [1 - (1 - S_{EF}^{1/m})^m]^2 \quad (3.2-2)$$

Here  $S_{EF} = (S_l - S_r) / (1 - S_r)$  is scaled (effective) liquid saturation with  $S_l$  and  $S_r$  the liquid and residual saturations respectively. The matrix hydrological property data used to estimate these parameters is discussed in Pruess and Tsang (1994) and was based on work done by Flint, et al. (1993) of the USGS. Five different cases were developed by LBL (Pruess and Tsang, 1994) based on different combinations of USGS measurements (Flint, et al., 1993) and the resultant matrix hydrologic parameters are provided in Table 3.2-1. It should be noted that Table 3.2-1 only provides  $k_{m,sat}$ , the saturated matrix permeability, and the actual matrix saturation is found by multiplying this value times  $k_{rl}$  in Equation (3.2-2). Yucca Mountain has been divided into a number of different sublayers (see Flint, et al., 1993) and thus the set of parameters labeled LBL-USGS-3.2 in Table 3.2-1, for example, used the properties from the sublayer 3.2 of the TSw unit. All of the -3. designations of sublayers were for the various sublayers within the TSw unit.

It should be noted that the range of these hydrologic parameters represent averages determined by LBL developers. Other efforts (Wilson, et al., 1994) have suggested that a wider range for some of the parameters may exist.

Table 3.2-1. Matrix Hydrological Property Data for the TSw1 and TSw2 units<sup>1</sup>

Sample Name	$S_r$	$\phi_m$	$k_{m,sat}(m^2)$	$\alpha (10^{-5} Pa^{-1})$	$m$
Reference Case	0.08	0.11	$1.9 \times 10^{-18}$	0.058	0.4438
LBL-USGS-3.2	0.0	0.10	$4.0 \times 10^{-16}$	0.125	0.18
LBL-USGS-3.5	0.0	0.10	$5.0 \times 10^{-18}$	0.133	0.25
LBL-USGS-3.1/3.6	0.0	0.10	$1.0 \times 10^{-18}$	0.067	0.29
LBL-USGS-3.4	0.0	0.11	$5.0 \times 10^{-18}$	0.067	0.25
LBL-USGS-3.3	0.0	0.11	$4.0 \times 10^{-18}$	0.2	0.22

<sup>1</sup> The properties listed are  $S_r$ ,  $\alpha$ , and  $m$  (the three van Genuchten characteristic curve fitting parameters), the matrix porosity ( $\phi_m$ ), and the saturated matrix permeability ( $k_{m,sat}$ ).

The reference case used for the comparisons and listed in Table 3.2-1 is the case that was run previously in support of the systems studies. The input parameters are discussed in Nitao (1989) and M&O, 1994c and are based primarily on the work done by Klavetter and Peters (1986). Zero net recharge flux was assumed and the initial liquid saturation at the repository horizon was calculated to be 68, 76, 78, 74, 66, and 64 percent for the six cases reported in Table 3.2-1 respectively. It should be noted that zero net recharge flux may underestimate the water saturation conditions at the repository. Under nonzero recharge flux the duration of boiling and rewetting times may be different than those predicted here. In all of the calculations, YFF(10) fuel characteristics are used (see M&O, 1994d) and a bulk permeability of  $2.8 \times 10^{-13} m^2$  (280 millidarcy) with a binary gas-phase tortuosity factor,  $\tau_{eff}=0.2$ , were used in the Effective Continuum Model.

Cases are run and reported for three different AMLs of 13.7, 27.3, and 37.1 kgU/m<sup>2</sup> (55.3, 110.5, and 150 MTU/acre). The highest AML is outside the range that was considered appropriate for emplacement (M&O, 1994c), but was used to overdrive the system to determine if the rock matrix parameters would make a difference. Table 3.2-2 provides VTOUGH calculations of duration of the boiling period at various repository locations and the bulk average relative humidity attained in the repository horizon at this same time for the reference property case. The calculations are done at four different locations on the disk representing the emplaced area (e.g. radial locations where 50, 75, 90, and 97 percent of the area enclosed). Values of duration of boiling and relative humidity are reported here as a convenient method of determining differences resulting from parameter changes since the duration of boiling and relative humidity are important from the standpoint of waste package corrosion for the high thermal loading AMLs. Similar calculations were done for the five LBL-USGS cases identified in Table 3.2-1 and the results of these calculations are provided in the three-paneled Table 3.2-3.

Table 3.2-2. Calculations of Duration of Boiling for Reference Case<sup>1</sup>

Fraction of repository area enclosed (%)	Duration of the boiling period (yr) and the relative humidity (%) at the end of the boiling period for indicated AMLs		
	55.3 MTU/Acre	110.5 MTU/Acre	150 MTU/Acre
50	1760 yr 81%	6130 yr 44%	9590 yr 47%
75	1160 yr 84%	4290 yr 51%	7210 yr 45%
90	440 yr 93%	2870 yr 68%	5010 yr 54%
97	80 yr 98.5%	2150 yr 87%	3960 yr 67%

Comparisons of the duration of boiling and the relative humidities at that time for the five LBL-USGS cases with the reference case show that the duration of boiling at the repository horizon is generally insensitive to the matrix properties considered. In terms of the relative humidity that is predicted to exist at the end of the boiling period, the comparison of Table 3.2-2 and Table 3.2-3 indicates that, except for LBL-USGS-3.2, similar relative humidities to the reference case are predicted. LBL-USGS-3.2 has a substantially larger value of  $k_{m,sat}$  which produces faster liquid-phase rewetting rates, in turn producing more humid conditions at the end of the boiling period.

<sup>1</sup> Duration of the boiling period at various repository locations and the relative humidity attained at the end of the boiling period for 22.5-year-old SNF, various AMLs,  $K_p = 280$  millidarcy, and assuming the matrix properties from Klavetter and Peters (1986) for the TSw1 and TSw2 units. The locations are identified as the fraction of the repository area enclosed, with 0 percent corresponding to the repository center, and 100 percent corresponding to the outer perimeter.

Table 3.2-3. Calculations of Duration of Boiling for Variations in Rock Properties<sup>2</sup>

Table 3.2-3a. Areal Mass Loading = 13.7 kgU/m<sup>2</sup> (55.3 MTU/Acre)

Fraction of repository area enclosed (%)	Duration of the boiling period (yr) and the relative humidity (%) at the end of the boiling period for the indicated sources of TSw1 and TSw2 matrix properties				
	LBL-USGS-3.2	LBL-USGS-3.5	LBL-USGS-3.1/3.6	LBL-USGS-3.4	LBL-USGS-3.3
50	1660 yr 97.5%	1730 yr 82%	1770 yr 78%	1760 yr 77%	1780 yr 76%
75	1100 yr 98.2%	1140 yr 85%	1190 yr 79%	1180 yr 79%	1180 yr 76%
90	430 yr 98.8%	420 yr 95.8%	430 yr 89%	440 yr 86%	440 yr 83%
97	90 yr 98.9%	80 yr 98.8%	80 yr 98.7%	90 yr 97.6%	90 yr 95.7%

Table 3.2-3b. Areal Mass Loading = 27.3 kgU/m<sup>2</sup> (110.5 MTU/Acre)<sup>2</sup>

Fraction of repository area enclosed (%)	Duration of the boiling period (yr) and the relative humidity (%) at the end of the boiling period for the indicated sources of TSw1 and TSw2 matrix properties				
	LBL-USGS-3.2	LBL-USGS-3.5	LBL-USGS-3.1/3.6	LBL-USGS-3.4	LBL-USGS-3.3
50	5850 yr 68%	6110 yr 36%	6050 yr 38%	5930 yr 35%	6130 yr 36%
75	4020 yr 86%	4250 yr 48%	4200 yr 49%	4200 yr 46%	4280 yr 46%
90	2690 yr 95.3%	2800 yr 71%	2810 yr 67%	2850 yr 65%	2870 yr 63%
97	2070 yr 98.0%	2080 yr 93%	2110 yr 88%	2140 yr 85%	2170 yr 81%

Table 3.2-3c. Areal Mass Loading = 37.1 kgU/m<sup>2</sup> (150 MTU/Acre)<sup>2</sup>

Fraction of repository area enclosed (%)	Duration of the boiling period (yr) and the relative humidity (%) at the end of the boiling period for the indicated sources of TSw1 and TSw2 matrix properties				
	LBL-USGS-3.2	LBL-USGS-3.5	LBL-USGS-3.1/3.6	LBL-USGS-3.4	LBL-USGS-3.3
50	9320 yr 76%	9520 yr 36%	9370 yr 38%	9380 yr 37%	9360 yr 36%
75	6720 yr 89%	7030 yr 38%	6970 yr 39%	6980 yr 37%	7020 yr 36%
90	4420 yr 95.1%	4820 yr 55%	4860 yr 52%	4880 yr 50%	4920 yr 49%
97	3290 yr 96.5%	3720 yr 73%	3780 yr 66%	3810 yr 64%	3840 yr 62%

<sup>2</sup> Duration of the boiling period at various repository locations and the relative humidity attained at the end of the boiling period for 22.5-year-old SNF, various AMLs,  $K_b = 280$  millidarcy, and matrix properties for the TSw1 and TSw2 units obtained from the indicated sources. The locations are identified as the fraction of the repository area enclosed, with 0 percent corresponding to the repository center, and 100 percent corresponding to the outer perimeter.

Some additional investigation of the differences noted was done. Plots of vertical temperature profiles and liquid saturation changes at various times were examined for the AML of 27.3 kgU/m<sup>2</sup> (110.5 MTU/acre). The reference case is plotted in Figure 3.2-1 for times of 100, 1000, 10,000, and 36,000 years. Similarly, the five LBL-USGS cases are plotted in Figures 3.2-2 through 3.2-6. A comparison of the reference case with all of the LBL-USGS cases, except LBL-USGS-3.2, shows close agreement in both temperature and liquid saturations at all times. However, when a comparison is made between the reference case and LBL-USGS-3.2, marked differences are noted. The predicted temperatures of the LBL-USGS-3.2 case are 10°C to 20°C cooler than the reference case at 1000 years. Additionally the reduction in liquid saturation (drying) does not extend vertically as far above the repository horizon as occurs in the reference case. As a result, the calculations for this case do not produce regions of essentially 100 percent saturation above the repository as are predicted in the reference case. The plots of liquid saturation also show that the repository horizon tends to return to near ambient saturation much more quickly than the reference case with near ambient conditions by 10,000 years.

The  $k_{m, sat}$  value used for the LBL-USGS-3.2 case is much larger than the other cases and may be indicative of a more highly fractured medium. While most of the TSw unit is welded tuff, this measurement may represent a region of nonwelded, fractured tuff. It should be noted that in measurements of a sample, particularly a highly fractured one, it is not possible to separate matrix permeabilities. Thus the values quoted in Table 3.2-1 for  $K_{m, sat}$ , could reflect contributions from fractures in some cases. Most of the drying depends on gas permeability, which would not change in the model with changes in the parameters provided in Table 3.2-1. The changes in  $k_{m, sat}$  with no corresponding changes in the suction potential, would influence the liquid flux with the results that are seen in the calculations. However, in actual fact the capillary pressure of the rock would likely change as well and such a scaling of the suction potential could not be evaluated with the parameters used.

### 3.2.2 Site-Scale Model Calculations

Yucca Mountain has spatial variability in rock and fracture properties at various scales. Of concern to performance is the presence of such fault zones as the Ghost Dance and Solitario Canyon faults. The extent of these faults and the degree to which they serve as fast paths for liquid and gas flow is not well known. In an effort to evaluate some of the sensitivities associated with having such faults in the mountain, some calculations were done by LBL that incorporate the effect of thermal loading into a three-dimensional site-scale model (Wu, Chen, and Bodvarsson; 1995).

The calculations were based on the three-dimensional LBL/USGS site-scale model, although only results for two-dimensional vertical cross sections will be shown. The section discussed in this report is a West-East section along the Nevada coordinates N233000. The thermal sources are located in two zones separated by the Ghost Dance Fault along the lower middle portions of Topopah Spring with 6 m thickness, 1200 m long for the west zone (upper block of the Primary Area) and 800 m long for the east zone (lower block of the Primary Area). The dimensions and placement are chosen from Figure 9-1 in the Recommended Layout and Concepts Report (M&O, 1995b). The properties of the Ghost Dance and Solitario Canyon fault zones were assumed since no data exists on those areas. The faults were assumed to have a high absolute

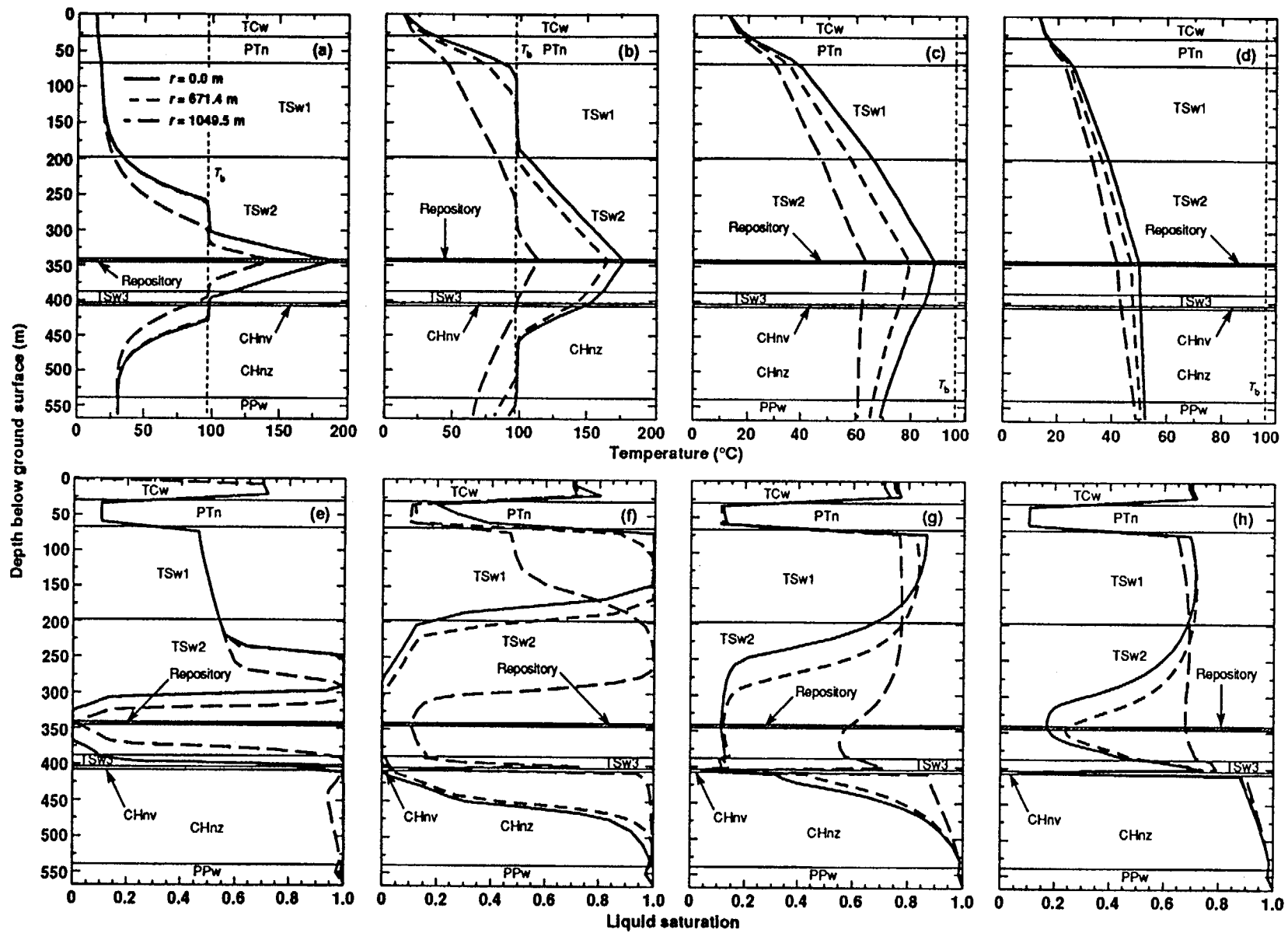


Figure 3.2-1. Vertical temperature profiles at various radial distances,  $r$ , for AML = 110.5 MTU/acre at (a)  $t = 100$  yr, (b)  $t = 1,000$  yr, (c)  $t = 10,000$  yr, and (d)  $t = 36,000$  yr. Note different temperature scales. Vertical liquid saturation profiles also are plotted at (e)  $t = 100$  yr, (f)  $t = 1,000$  yr, (g)  $t = 10,000$  yr, and (h)  $t = 36,000$  yr. Matrix properties for the TSw1 and TSw2 are based on Klavetter and Peters (1986). Binary gas-phase tortuosity factor  $\tau_{\text{eff}} = 0.2$  for all units.

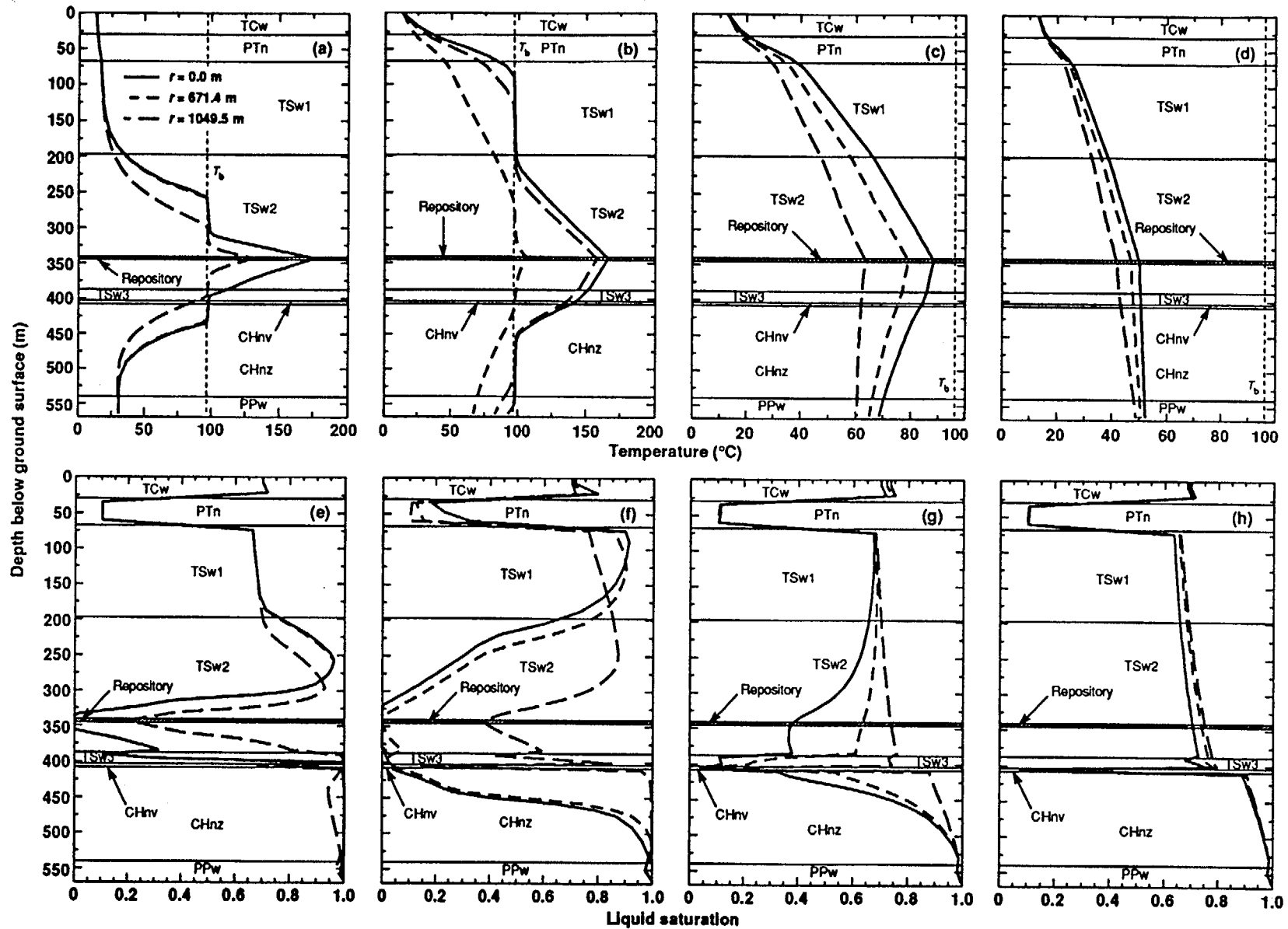


Figure 3.2-2. Vertical temperature profiles at various radial distances,  $r$ , for AML = 110.5 MTU/acre at (a)  $t = 100$  yr, (b)  $t = 1,000$  yr, (c)  $t = 10,000$  yr, and (d)  $t = 36,250$  yr. Note different temperature scales. Vertical liquid saturation profiles also are plotted at (e)  $t = 100$  yr, (f)  $t = 1,000$  yr, (g)  $t = 10,000$  yr, and (h)  $t = 36,250$  yr. Matrix properties for the TSw1 and TSw2 are based on LBL-USGS-3.2 properties. Binary gas-phase tortuosity factor  $\tau_{\text{eff}} = 0.2$  for all units.

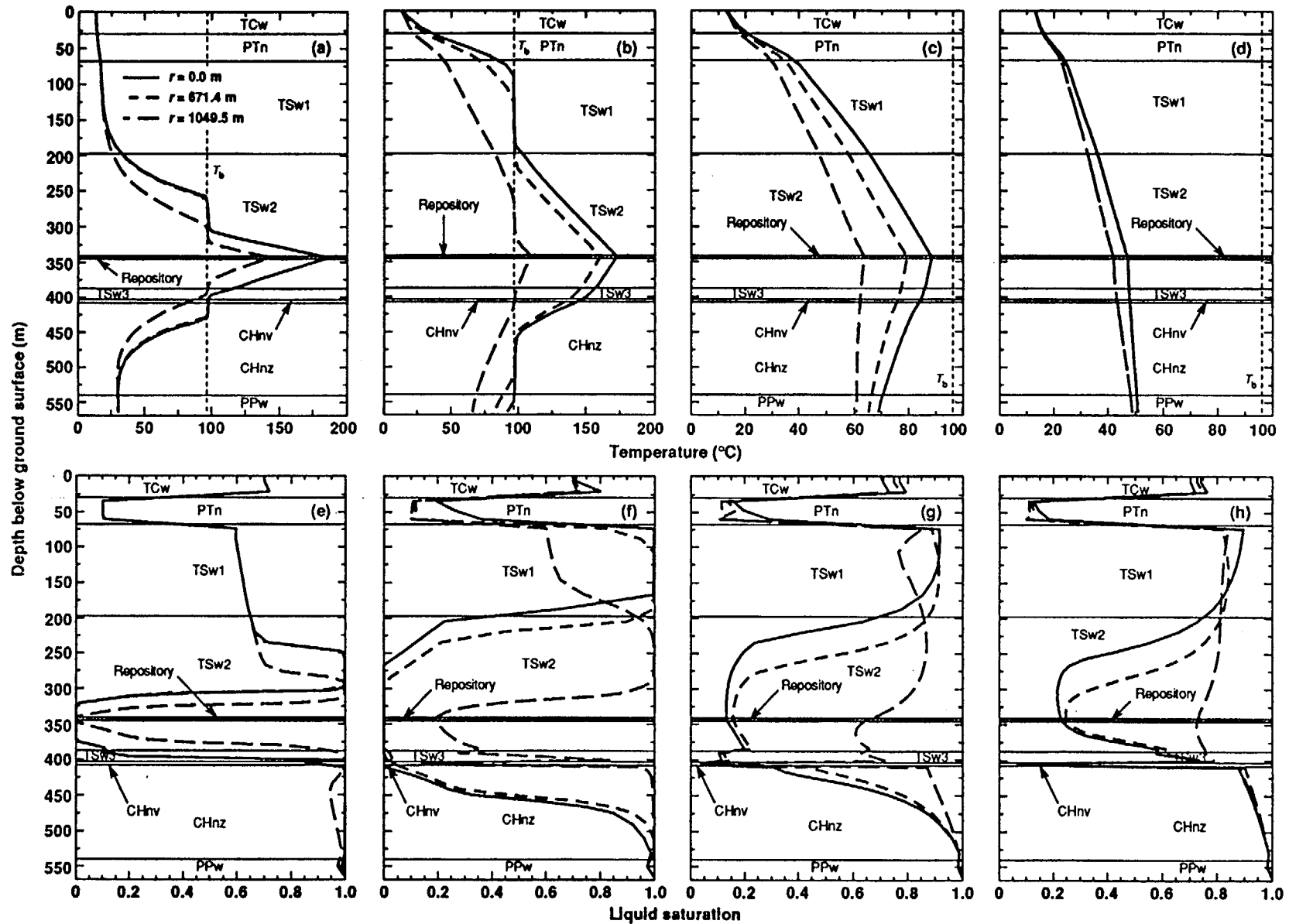


Figure 3.2-3. Vertical temperature profiles at various radial distances,  $r$ , for AML = 110.5 MTU/acre at (a)  $t = 100$  yr, (b)  $t = 1,000$  yr, (c)  $t = 10,000$  yr, and (d)  $t = 35,400$  yr. Note different temperature scales. Vertical liquid saturation profiles also are plotted at (e)  $t = 100$  yr, (f)  $t = 1,000$  yr, (g)  $t = 10,000$  yr, and (h)  $t = 35,400$  yr. Matrix properties for the TSw1 and TSw2 are based on LBL-USGS-<sup>2</sup> 1/3.6 properties. Binary gas-phase tortuosity factor  $\tau_{eff} = 0.2$  for all units.

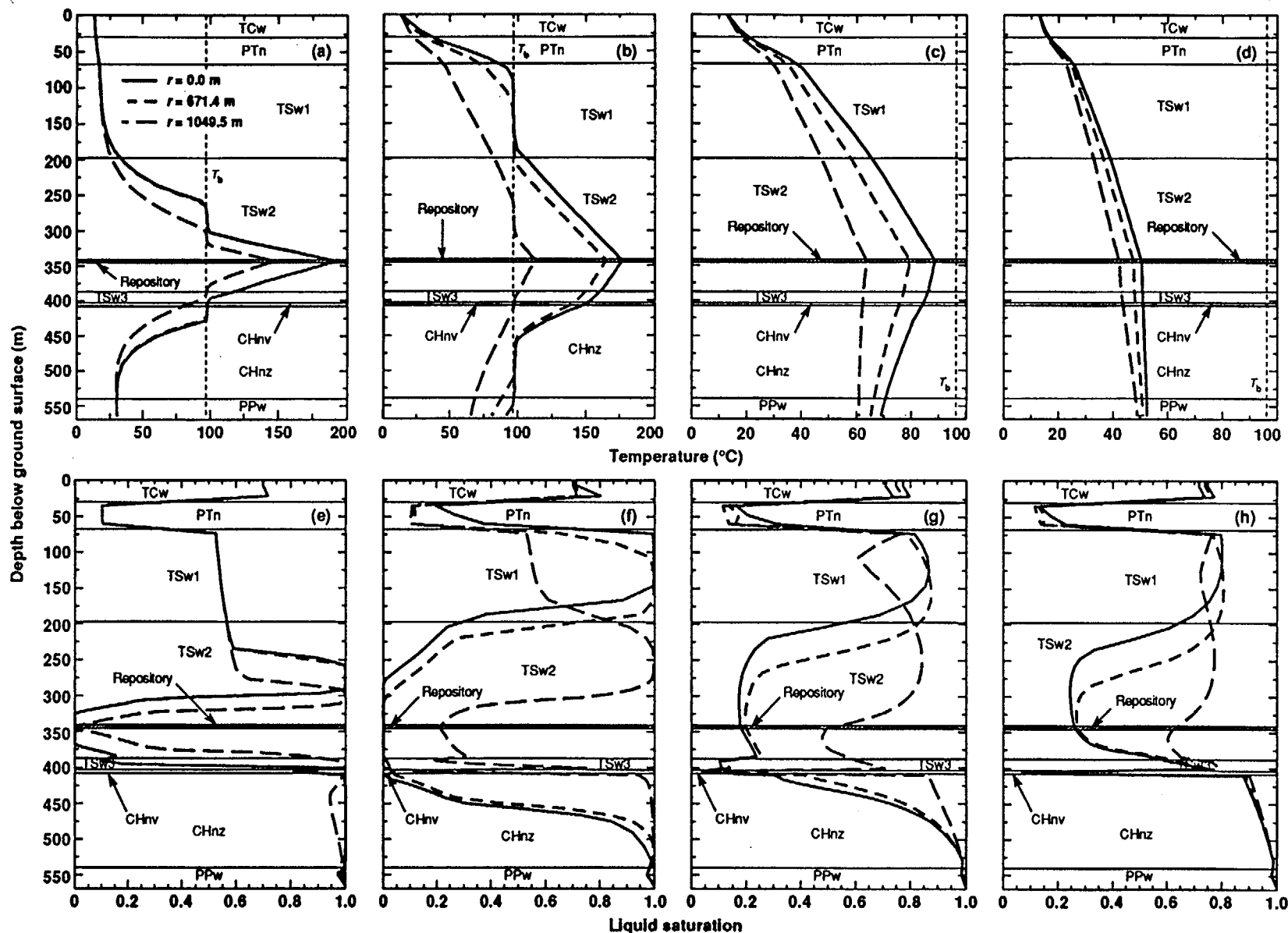


Figure 3.2-4. Vertical temperature profiles at various radial distances,  $r$ , for AML = 110.5 MTU/acre at (a)  $t = 100$  yr, (b)  $t = 1,000$  yr, (c)  $t = 10,000$  yr, and (d)  $t = 34,630$  yr. Note different temperature scales. Vertical liquid saturation profiles also are plotted at (e)  $t = 100$  yr, (f)  $t = 1,000$  yr, (g)  $t = 10,000$  yr, and (h)  $t = 34,630$  yr. Matrix properties for the TSw1 and TSw2 are based on LBL-USGS-3.3 properties. Binary gas-phase tortuosity factor  $\tau_{eff} = 0.2$  for all units.

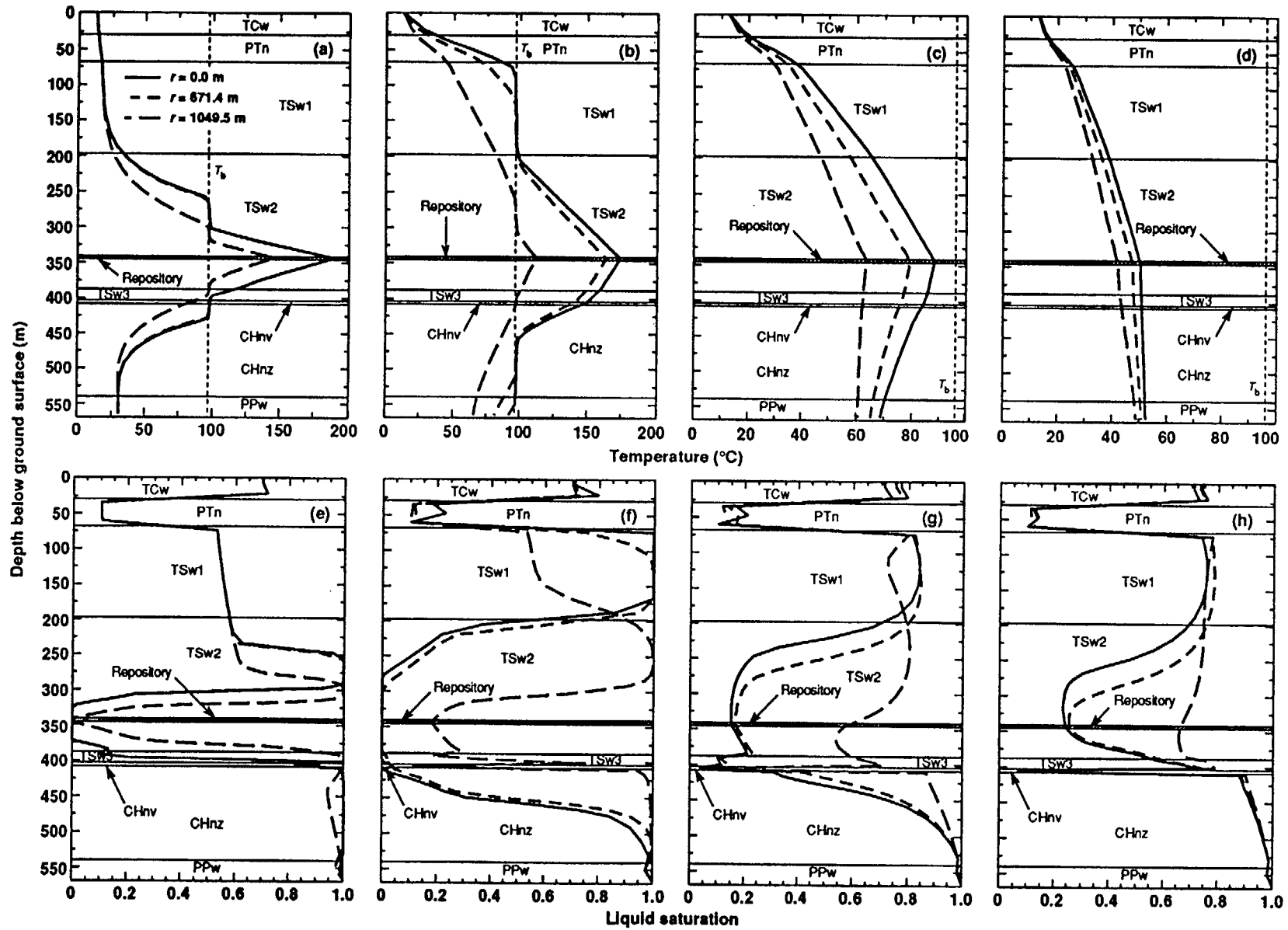


Figure 3.2-5. Vertical temperature profiles at various radial distances,  $r$ , for AML = 110.5 MTU/acre at (a)  $t = 100$  yr, (b)  $t = 1,000$  yr, (c)  $t = 10,000$  yr, and (d)  $t = 35,150$  yr. Note different temperature scales. Vertical liquid saturation profiles also are plotted at (e)  $t = 100$  yr, (f)  $t = 1,000$  yr, (g)  $t = 10,000$  yr, and (h)  $t = 35,150$  yr. Matrix properties for the TSw1 and TSw2 are based on LBL-USGS <sup>2</sup> 4 properties. Binary gas-phase tortuosity factor  $\tau_{eff} = 0.2$  for all units.

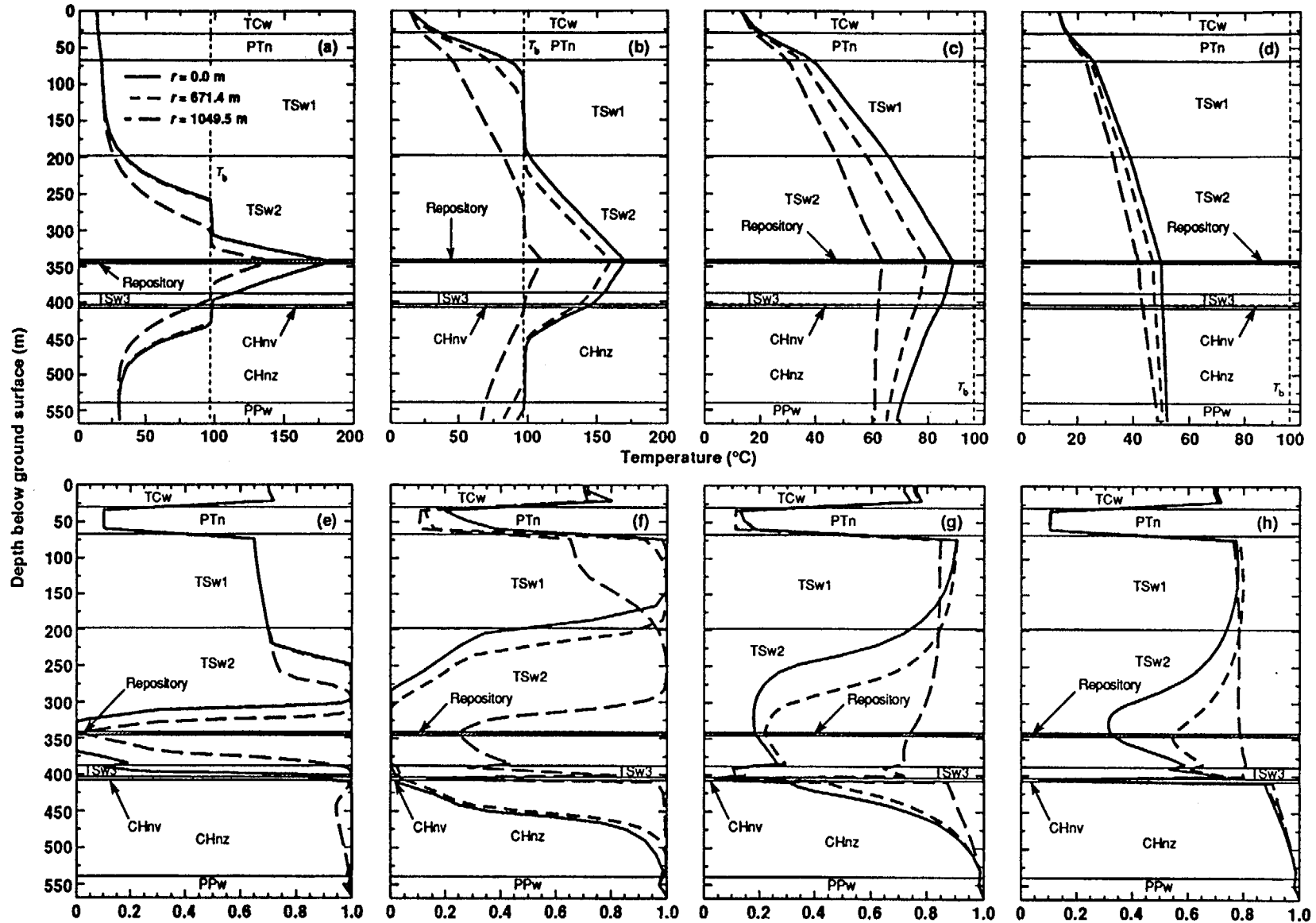


Figure 3.2-6. Vertical temperature profiles at various radial distances,  $r$ , for  $AML = 110.5$  MTU/acre at (a)  $t = 100$  yr, (b)  $t = 1,000$  yr, (c)  $t = 10,000$  yr, and (d)  $t = 35,730$  yr. Note different temperature scales. Vertical liquid saturation profiles also are plotted at (e)  $t = 100$  yr, (f)  $t = 1,000$  yr, (g)  $t = 10,000$  yr, and (h)  $t = 35,730$  yr. Matrix properties for the TSw1 and TSw2 are based on LBL-USGS-3.5 properties. Binary gas-phase tortuosity factor  $\tau_{eff} = 0.2$  for all units.

permeability and weak capillary suction. The faults therefore tend to be fast pathways for gas, but barriers for liquid until the liquid saturation in the matrix adjacent to the fault becomes high enough. Additional details of the assumptions and the data inputs for the calculations can be found in Wittwer, et al. (1995).

The calculations shown in this section were done for an AML of 27.3 kgU/m<sup>2</sup> (111 MTU/acre) which, for the YFF(10) waste stream used, was an area power density (APD) of 28.2 W/m<sup>2</sup> (114 kW/acre). The surface heat flux was calculated and shown in Figure 3.2-7 while the gas flux at the surface is shown in Figure 3.2-8. These calculations were done at three different times of 1000, 10,000, and 100,000 years. It takes between 200 to 500 years for the heat to travel to the surface from the repository. The calculations show that for a high thermal loading both the heat and gas flux at the surface are increased many orders of magnitude over the ambient as a result of the thermal load and that the faults serve as major pathways for heated gas and heat. There may be environmental implications in these high heat and gas fluxes that need to be considered.

Figures 3.2-9 and 3.2-10 show the temperature contours and liquid saturation contours respectively in the mountain at 1000 years for the case considered. The results show that the temperatures in the repository horizon are significantly cooler than those calculated with a two-dimensional model without fault zones. Specifically, the site-scale model calculates temperatures in the center of the repository to be about 150°C with substantially cooler temperatures at the edges at 100 years. For comparison purposes, a two-dimensional model calculates temperatures at the center of the repository of about 180°C at 1000 years as shown in Figure 3.2-1b. The fact that these calculations show the repository is about 30°C cooler and tends to drop below boiling sooner than predicted with a two-dimensional model without faults is due to the significant heat flow through the two faults. A comparison of the saturation profiles with those calculated by the two-dimensional model and shown in Figure 3.2-1f are similar in the repository horizon (produces predicted dry-out) but the dry-out does not extend as far as in the three-dimensional case. The consequences of this need to be determined.

This sensitivity study has shown the potential of significant differences in predicted temperature with time due to the presence of faults. As such, what the properties (permeability, porosity, etc.) of these faults actually are and how they will respond to heat needs to be determined. The properties of these faults need to be measured in-situ and some monitoring of the moisture content in the rock around the fault is needed. The measured rock parameters should then be used in the three-dimensional site-scale model to provide a better calculation of the response of the mountain to heat and water movement in the presence of the Ghost Dance and Solitario Canyon faults.

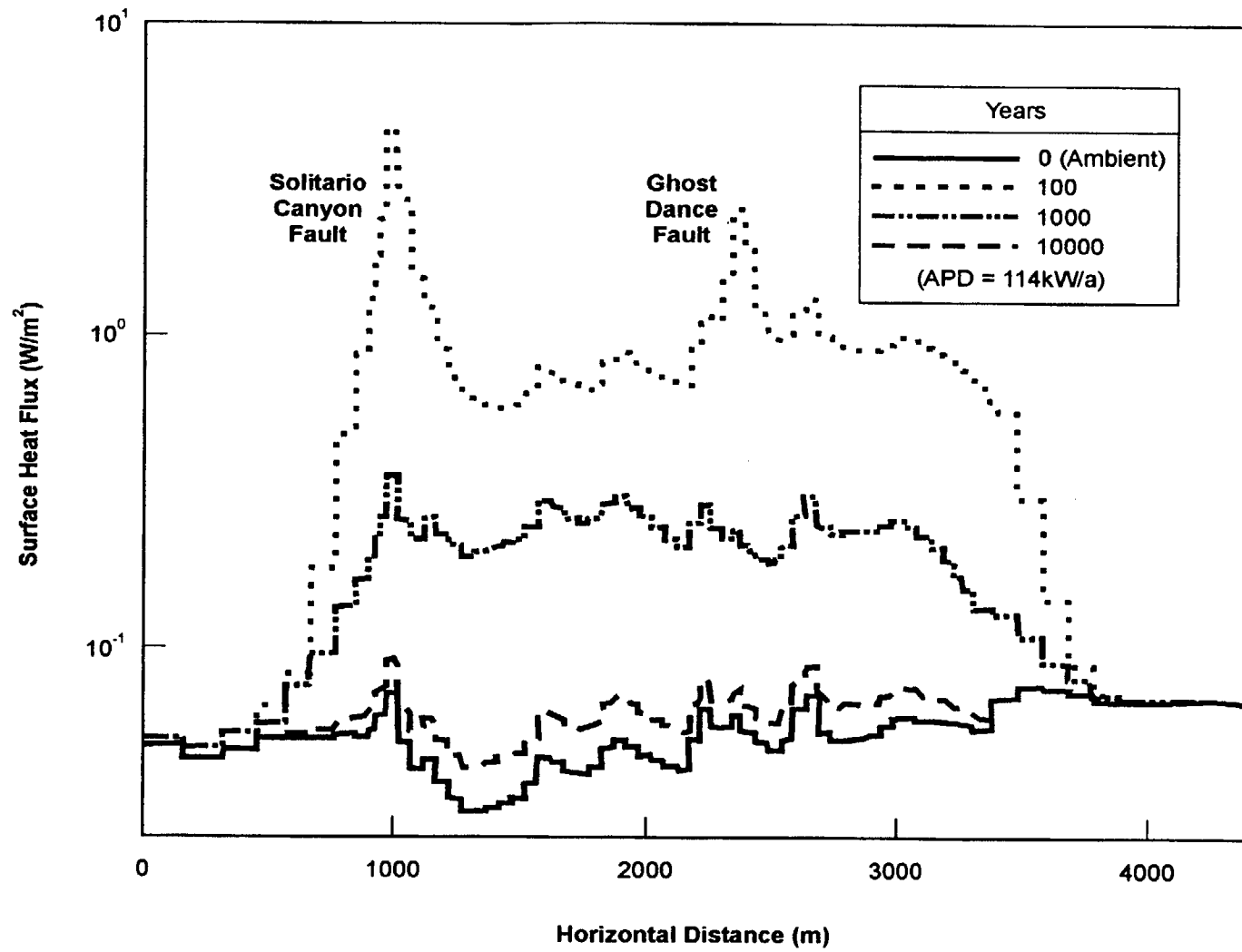


Figure 3.2-7. Surface Heat Flux for an APD of 28.2 W/m<sup>2</sup> (114 kW/acre).

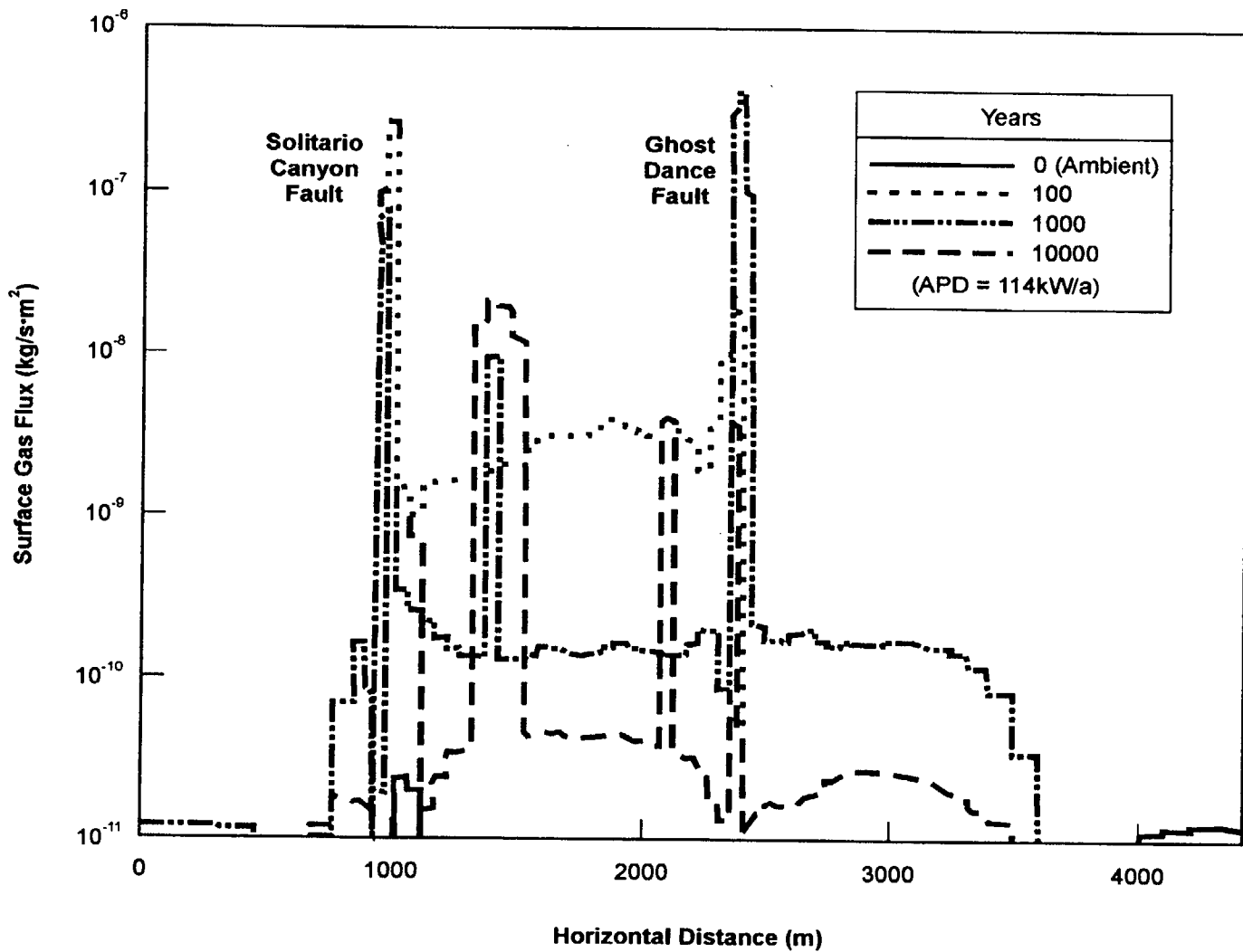


Figure 3.2-8. Surface Gas Flux for an APD of 28.2 W/m<sup>2</sup> (114 kW/acre).

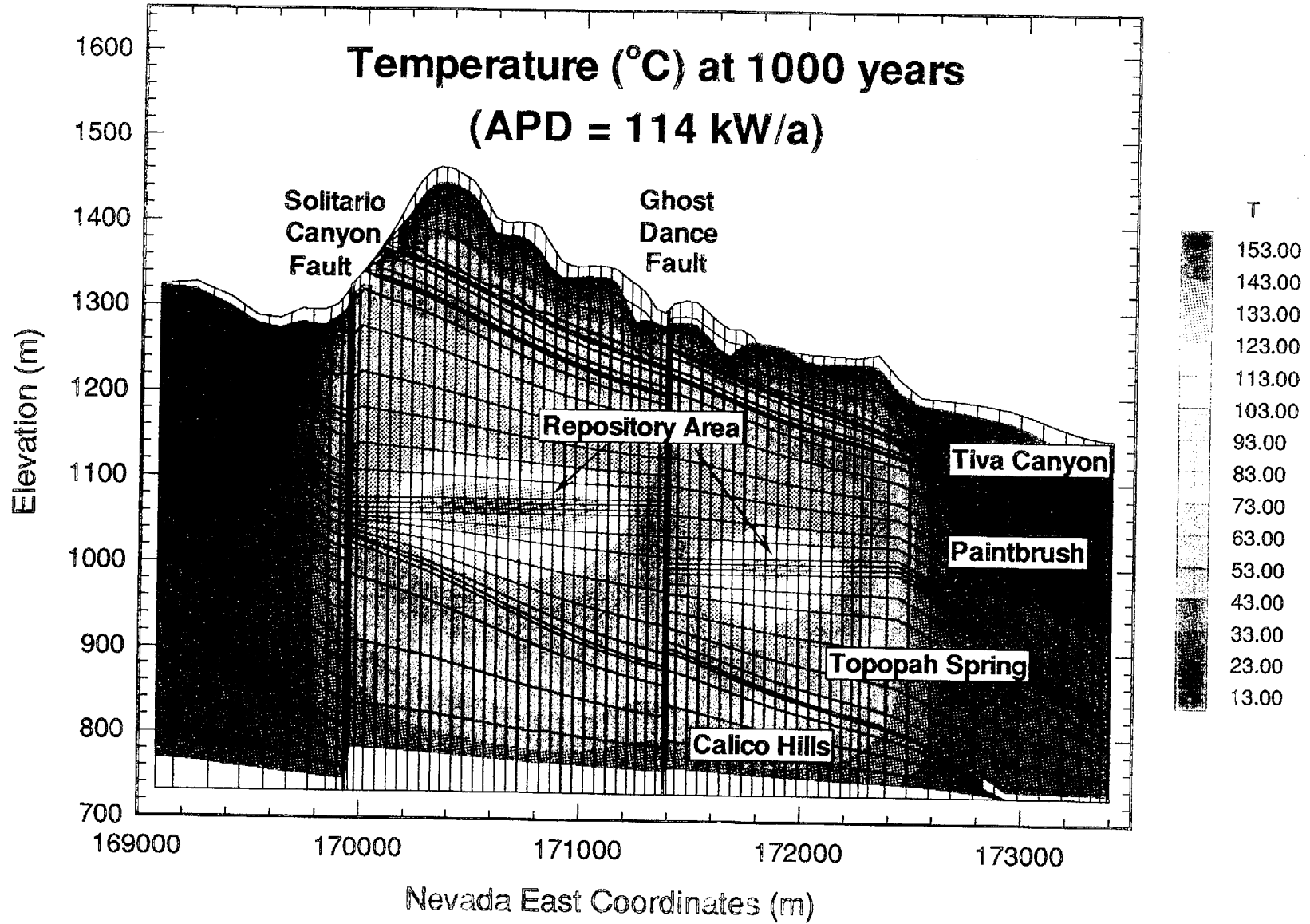


Figure 3.2-9. Calculated Temperature Profiles at 1000 Years for an APD of 28.2 W/m<sup>2</sup> (114 kW/acre).

INTENTIONALLY LEFT BLANK

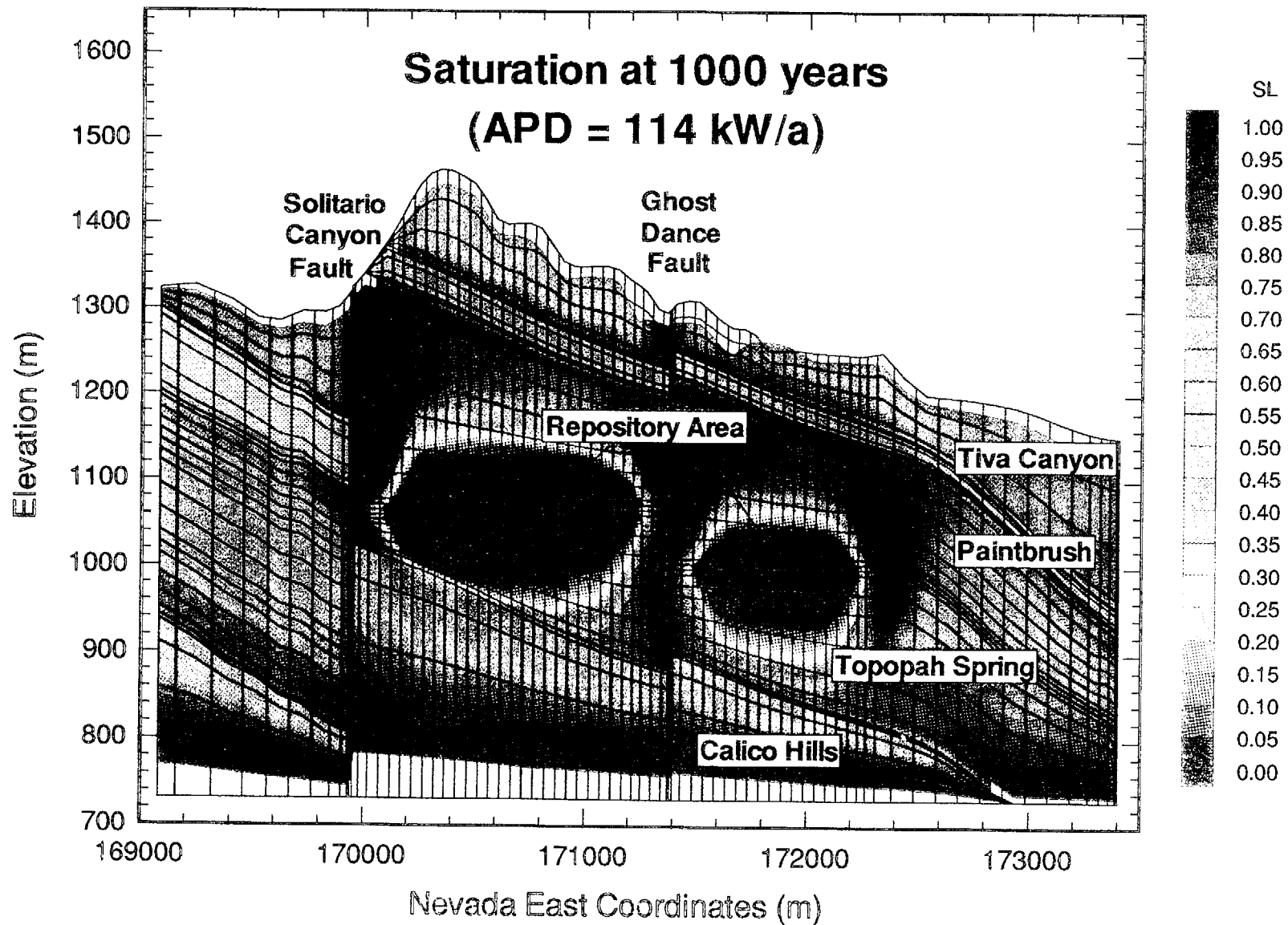


Figure 3.2-10. Calculated Saturation Profiles at 1000 Years for an APD of 28.2 W/m<sup>2</sup> (114 kW/acre).

INTENTIONALLY LEFT BLANK

### 3.2.3 Summary

In summary, a parametric set of calculations was done in which the effect of changes in a variety of rock matrix properties were evaluated. The suction potential and liquid permeability of the rock were functions of these matrix properties. The results indicate that for most cases the temperature, duration of boiling, and relative humidity at the end of the boiling period are not very dependent on the choice of matrix properties selected from the range of values determined in borehole measurements at least within the context of using an Effective Continuum model. However, the results showed that the liquid saturation and consequently relative humidity do depend on the capillary suction pressure curve that is used. There may be some rock that exists in the TS member that could have properties sufficiently different to produce liquid saturations different than the reference case. However, using the measurements from these regions to determine what the liquid permeability is without commensurate scaling of the capillary suction curve may produce errors in the predictions. Thus, some emphasis needs to be placed on determining how the capillary suction curve might change in different types of rock in the mountain and how heterogeneous these areas are in the mountain. Some sensitivity analyses with nonzero infiltration and a dual permeability simulation probably are warranted.

Results based on a three-dimensional site-scale model were evaluated to determine what effect the presence of the Ghost Dance and Solitario Canyon faults may have on the thermal and hydrologic response of the potential repository. Based on the predictions, the faults could serve as major pathways for transport of heated gas and heat away from the potential repository. Such pathways could produce substantially cooler repository conditions than what is calculated with a two-dimensional model without such pathways. As such, it is recommended that in-situ measurements of the fracture and surrounding rock properties such as permeability, saturation, and porosity be measured. Additionally, the moisture content near the fault should be monitored. These measured parameters should then be used in a site-scale model to evaluate the environment as a function of time to establish duration of boiling, extent of dry-out, relative humidity in the drift, and rewetting time. Additionally, the implications on the environmental impact of high thermal loads should be considered as a result of the faults serving as major pathways for heat and gas.

### 3.3 EXAMINATION OF GAS-PHASE DIFFUSION ON THE THERMOHYDROLOGY

In the previous two sections the report explored the effect that changes in bulk permeability and some selected rock matrix properties might have on the thermohydrologic behavior of the host rock. For the most part, the above evaluations concentrated on parameters that primarily affected the transport of the liquid in the rock matrix. In the analysis given in this section, the sensitivity of the hydrothermal predictions to variations in the gas diffusion parameter was examined.

The movement of water vapor away from the potential repository occurs by:

1. Advective transport of water vapor to regions of condensation, driven by gas-phase pressure buildup from the generation of steam;
2. Advective vapor transport driven by buoyant, gas-phase convection; and

3. Molecular diffusion of water vapor from regions of high to low mole fractions of water vapor.

Buoyant, gas-phase convection is predicted to cause vapor flow to be driven upward where it can condense above the zone where dry-out (a reduction in liquid saturation) occurs. If the bulk permeability is sufficiently large, large-scale buoyant convection cells can develop that also could transport water vapor from regions below the repository to regions above. This process can contribute to redistribution of moisture so that the rock in the repository horizon becomes drier while regions above the repository may become wetter (Buscheck and Nitao, 1994). In all cases, the term rock dry-out is defined to imply that the liquid saturation is less than the ambient liquid saturation. The calculation of this dry-out is based on idealized, as yet unverified analytic models.

The mole fraction,  $n_v$ , of water vapor under conditions of local thermodynamic equilibrium within the rock is a function of liquid saturation  $S_l$ , absolute temperature  $T$ , and gas-phase pressure  $P_g$  and is given by the equation:

$$n_v = [P_{sat}(T)/P_g] \exp[-\psi M_w / (\rho_l RT)] \quad (3.3-1)$$

which is a generalization of Kelvin's law for porous media. In this equation,  $P_{sat}(T)$  is the saturation pressure,  $\psi = \psi(S_l, T)$  is the matrix potential,  $M_w$  is the molecular weight of water,  $\rho_l$  is the density of liquid water, and  $R$  is the universal gas constant. The matrix potential, for ambient conditions with a saturation of more than 60 to 80 percent, is sufficiently small that the exponential term is essentially unity. It is not until the saturation becomes low as a result of heating that the exponential factor has a significant effect on  $n_v$ .

When the temperature rises in the rock,  $P_{sat}(T)$  increases and as a result the equilibrium amount of water vapor in the gas phase increases. As temperatures reach the boiling point of water,  $P_{sat}$  approaches  $P_g$  and the mole fraction of water vapor approaches unity (i.e. the gas phase becomes 100 percent water vapor). The water in the rock near the fractures also starts to boil, causing the gas-phase pressure in the fractures and the rock matrix to rise, which leads to the advective transport of water vapor and a reduction in the water vapor mole fraction in the rock based on Equation 3.3-1. Gas-phase advection is likely to be the dominant mechanism carrying water vapor from the boiling zone to the condensation zone except for a condition where low permeabilities throttle gas-phase advection and the rate of boiling. Beyond the condensation zone, vapor diffusion is the dominant mechanism of vapor movement except where the permeabilities are large enough that buoyant gas-phase convection occurs. Temperatures near the condensation zone are close to the boiling point, which means that the water vapor mole fraction in Equation 3.3-1 is nearly unity, while further away the temperatures are cooler and the mole fraction is much less (approximately 0.02 at ambient conditions). This gradient in mole fraction leads to diffusive fluxes that carry water away from the condensation zone.

The transport of the water vapor gas phase is governed by the gas diffusion properties of the rock and fracture matrix. The diffusive gas flux is related to the mass fraction of the various gas-phase components by the diffusion coefficient for the vapor-air mixture in a porous medium,  $D_{va}$ . Water vapor, which is a condensable gas, is effectively transported through "islands" of liquid

water by virtue of condensation and evaporation when driven by a temperature gradient. The diffusion coefficient for this vapor-air mixture is given by Vargaftik (1975) as:

$$D_{va} = \beta D_{va}^0 \left( \frac{P_0}{P} \right) \left( \frac{T}{T_0} \right)^\theta \quad (3.3-2)$$

In this equation, the  $D_{va}^0$  at standard conditions is  $2.14 \times 10^{-5} \text{ m}^2 \text{ s}^{-1}$ ,  $P_0$  is 1 bar,  $T_0$  is 273.15 degrees Kelvin,  $\theta$  is 1.8,  $T$  is the temperature, and  $P$  the pressure based on the work done by Tsang and Pruess (1990) using the work of Bird, et al. (1960) and Langkopf (1987). The parameter  $\beta$  specifies properties relevant to binary diffusion in a porous medium, as governed by Fick's law, and is given as:

$$\beta = \tau \phi S_g \quad (3.3-3)$$

where  $\phi$  is the porosity,  $\tau$  is a tortuosity factor dependent on the pore geometry, and  $S_g$  is the gas saturation (see discussion in Buscheck and Nitao, 1994). In most of the calculations, the tortuosity factor was set equal to 0.2. For relevant values of porosity (about 0.1) and gas saturation (a variable which in this case was chosen to be about 50 percent), Equation 3.3-3 yields  $\beta \sim 10^{-2}$ . This is the same nominal value used in most of the previous calculations. To evaluate the significance of changes in this parameter, the binary gas-phase tortuosity factor was increased to values of 1, 2, and 4. Because of the uncertainty in the value of tortuosity to use the values 0.2 to 4 were considered as effective values of tortuosity and are labeled as  $\tau_{\text{eff}}$  in the tables. Considerable uncertainty exists in the gas phase diffusion parameters since these parameters are derived from a number of other measured parameters and some estimates of the validity of these derivations should be done.

Based on the above, water vapor continues to diffuse away from the repository because of the higher temperatures there. As the temperature declines in the repository, due to decay of the SNF and latent heat transport, the mole fraction of water vapor,  $n_v$ , becomes smaller than that in the wetter rock away from the repository. Thus, vapor diffusion can occur from cooler to hotter regions which have lower  $S_1$ . Water vapor diffuses away from the repository until repository temperatures have decreased enough so that the temperature effect, which drives water vapor away from the repository, can no longer compensate for the vapor pressure lowering effect (that drives water back toward the repository). The "vapor pressure lowering" effect on  $n_v$  is significant only at lower  $S_1$  (less than about 20 to 30 percent). For  $S_1$  greater than 20 to 30 percent, re-wetting of the dry-out zone will be dominated by liquid-phase advection driven by matrix potential gradients and gravity.

The evaluations were conducted using the VTOUGH code which is described in Nitao (1989) and Pruess (1987). The majority of the parameters and inputs used in the calculations were those reported earlier in M&O, 1994c and in the previous sections. The calculation used a smeared heat source, repository scale model. The calculations used YFF(10) fuel selection. The binary gas-phase tortuosity factor, referred to as  $\tau$  or  $\tau_{\text{eff}}$ , was selected to be a value of 0.2, 1, 2, or 4 in the calculations. Like the previous sections, changes in the duration of boiling and the relative humidity at the end of the boiling period were examined as appropriate measures potentially important to waste isolation.

Calculations showing duration of boiling and the relative humidity at the time that boiling ceases in the repository horizon are presented in Table 3.3-1 for binary gas-phase diffusion tortuosity factors of 0.2 and 2.0. These calculations were done for AMLs of 17.3, 20.6, 27.3, and 37.1 kgU/m<sup>2</sup> (70, 83.4, 110.5, and 150 MTU/acre). It should be noted that a higher AML case than currently considered for emplacement was calculated to attempt to determine any sensitivities that might exist. The table shows that, because increased vapor diffusion enhances the rate of heat loss from the repository, the duration of boiling is decreased somewhat over the case with a smaller tortuosity factor. This is particularly true for the center 75 percent of the repository disk. Less cooling due to enhanced gas-phase diffusion is observed at the outer edges of the potential repository. Approximately a 10- to 12-percent decrease in duration of boiling is produced by a factor of 10 increase in gas-phase diffusion coefficient. The relative humidity (this is a bulk average for the repository horizon and lower values would be predicted in the vicinity of a drift) at the end of boiling shows, for the most part, small changes for different gas-phase diffusion factors. There are some indications that the edges of the repository may have minor changes in relative humidity at the end of boiling but they do not appear to be significant. Although not presented here, calculations also were done for different gas-phase diffusion factors for each of the cases presented in the previous section with different rock matrix properties. That is, the rock matrix parameters did not make an appreciable difference to the boiling duration and relative humidity, except for LBL-USGS 3.2, but similar decreases in duration of boiling were noted for increases in the diffusion factor.

Another examination of the calculations involved looking at the predicted time that a specific relative humidity (bulk average) was attained in the repository horizon. These times and the corresponding predicted temperatures (bulk average) are provided in Table 3.3-2 for the case of an AML of 27.3 kgU/m<sup>2</sup> as an illustration of the results. An examination of the table indicates that an increase in gas-phase diffusion is predicted to have some effect on the time that it takes to return to a particular relative humidity. For the inner areas of the repository and humidities to about 80 percent, the increased diffusion appears to decrease the time to rewet. In the outer edges of the repository and for the relative humidities above 80 percent, the increased diffusion appears to increase the time required to rewet.

It would appear that changes in vapor diffusion do modestly affect the duration of boiling and/or the time required to rewet to a particular relative humidity. In areas such as the center of the repository disk, where rewetting tends to be slower than the edges, enhanced diffusion tends to somewhat decrease the time to rewet. In the repository's outer edges, which tend to rewet more rapidly, the enhanced diffusion tends to retard this rewetting. These are only preliminary results based on calculations with an idealized model. The results, however, do indicate that gas-phase diffusion is likely an important parameter and should be investigated as part of the in-situ testing effort. Techniques are needed to measure the binary gas-phase diffusion, and the degree of heterogeneity that might exist also needs to be determined.

Table 3.3-1. Duration of Boiling and Relative Humidity Calculations for TSw1 and TSw2 Matrix Properties from Klavetter and Peters (1986)<sup>3</sup>

Table 3.3-1a. Gas-Phase Diffusion Tortuosity Factor,  $\tau_{\text{eff}} = 0.2$

Fraction of repository area enclosed (%)	Duration of the boiling period (yr) and the relative humidity (%) at the end of the boiling period for the indicated AMLs							
	70 MTU/acre		83.4 MTU/acre		110.5 MTU/acre		150 MTU/acre	
50	2610 yr	68%	3870 yr	57%	6130 yr	44%	9590 yr	47%
75	2000 yr	72%	2740 yr	73%	4290 yr	51%	7210 yr	45%
90	1090 yr	81%	1700 yr	77%	2870 yr	68%	5010 yr	54%
97	410 yr	96%	990 yr	93%	2150 yr	87%	3960 yr	67%

Table 3.3-1b. Gas-Phase Diffusion Tortuosity Factor,  $\tau_{\text{eff}} = 2.0^4$

Fraction of repository area enclosed (%)	Duration of the boiling period (yr) and the relative humidity (%) at the end of the boiling period for the indicated AMLs							
	70 MTU/acre		83.4 MTU/acre		110.5 MTU/acre		150 MTU/acre	
50	2650 yr	67%	3430 yr	55%	5400 yr	45%	8780 yr %	44%
75	1940 yr	70%	2550 yr	63%	3960 yr	50%	6530 yr	45%
90	1040 yr	77%	1680 yr	73%	2710 yr	64%	4510 yr	52%
97	360 yr	87%	930 yr	85%	2030 yr	78%	3550 yr	61%

<sup>3</sup> Duration of the boiling period at various repository locations and the relative humidity attained at the end of the boiling period for 22.5-year-old SNF, various AMLs,  $K_b = 280$  millidarcy. The locations are identified as the percentage of the repository area enclosed, with 0 percent corresponding to the repository center, and 100 percent corresponding to the outer perimeter.

<sup>4</sup> Duration of the boiling period at various repository locations and the relative humidity attained at the end of the boiling period for 22.5-year-old SNF, various AMLs,  $K_b = 280$  millidarcy. The locations are identified as the percentage of the repository area enclosed, with 0 percent corresponding to the repository center, and 100 percent corresponding to the outer perimeter.

Table 3.3-2. Predicted Time to Achieve a Specified Relative Humidity at an Areal Mass Loading = 110.5 MTU/Acre<sup>5</sup>

Table 3.3-2a. Gas-Phase Diffusion Tortuosity Factor,  $\tau_{eff} = 0.2$

Fraction of repository area enclosed (%)	Time required to attain the indicated relative humidity (yr.)				Temperature at which the indicated relative humidity is attained (°C)			
	70%	80%	90%	95%	70%	80%	90%	95%
50	15,960	27,910	40,990	49,980	68	54	45	42
75	9540	15,520	24,950	32,590	76	64	53	48
90	3190	4890	7460	9890	93	82	73	68
97	1410	1810	2360	2890	106	101	93	88

Table 3.3-2b. Gas-Phase Diffusion Tortuosity Factor,  $\tau_{eff} = 1.0^6$

Fraction of repository area enclosed (%)	Time required to attain the indicated relative humidity (yr.)				Temperature at which the indicated relative humidity is attained (°C)			
	70%	80%	90%	95%	70%	80%	90%	95%
50	13,490	22,790	39,960	54,040	72	58	46	40
75	9160	15,570	27,210	37,890	76	63	51	45
90	3480	6170	11,400	16,740	90	77	64	57
97	1410	1970	3170	4760	106	98	85	76

Table 3.3-2c. Gas-Phase Diffusion Tortuosity Factor,  $\tau_{eff} = 2.0$

Fraction of repository area enclosed (%)	Time required to attain the indicated relative humidity (yr.)				Temperature at which the indicated relative humidity is attained (°C)			
	70%	80%	90%	95%	70%	80%	90%	95%
50	14,260	23,850	42,270	59,750	70	57	44	38
75	10,180	17,870	33,350	47,150	72	59	46	41
90	3920	7730	16,040	26,640	85	71	57	48
97	1490	2240	4490	8130	104	93	76	65

<sup>5</sup> Time required to attain the indicated relative humidity at various repository locations and the temperature at which that value of relative humidity is attained for 22.5-years-old SNF,  $k_b = 280$  millidarcy, and three gas-phase diffusion tortuosity factors,  $\tau_{eff}$ . The locations are identified as the fraction of the repository area enclosed, with 0 percent corresponding to the repository center, and 100 percent corresponding to the outer perimeter.

<sup>6</sup> Time required to attain the indicated relative humidity at various repository locations and the temperature at which that value of relative humidity is attained for 22.5-years-old SNF,  $k_b = 280$  millidarcy, and three gas-phase diffusion tortuosity factors,  $\tau_{eff}$ . The locations are identified as the fraction of the repository area enclosed, with 0 percent corresponding to the repository center, and 100 percent corresponding to the outer perimeter.

### 3.4 EFFECT OF MODELING ASSUMPTIONS ON THERMAL PROFILES

The issue of heterogeneity in the rock properties and any subsequent effect on temperatures as a result of heating is a concern that needs to be resolved by testing. High-porosity (large-cavity) lithophysal zones in the TS Member have been hypothesized and some variations have been observed to date in boreholes and in the initial excavations completed by the Tunnel Boring Machine. In question is whether such variations in porosity might affect the temperatures and hydrology in the rock as a function of thermal loading. If it is determined that there may be some impact on repository host rock temperatures, then it would be useful to ensure that the subsurface investigations (mapping and possibly in-situ thermal testing) examine this issue. SNL, in support of the thermal loading study, assisted in addressing the question of whether or not porosity heterogeneities may affect the temperatures in the host rock (Rautman and Longenbaugh, 1995). This section provides a discussion of the results of that analysis.

Lithophysal-cavity zones within the welded tuff in the potential repository at Yucca Mountain have been recognized to exist for some time (for example Spengler, et al, 1979). These lithophysal cavities are a result of vapor phase alteration phenomena caused by hot magmatic gasses escaping from the consolidating and welding pile of volcanic glass shards. The vapor phase alterations can result in generally higher porosity regions. These lithophysae, which consist of a granular, vapor-phase altered region, with or without an actual void or cavity, have been found from borehole investigations to vary widely in size from less than 5 millimeters (mm) to areas as large as several tens of centimeters (cm) (Rautman and Longenbaugh, 1995). Larger size cavities also may exist or can be inferred based on the existence of cores from which only rubble has been recovered.

The presence of high-porosity lithophysal zones will have a different thermal conductivity in those regions than regions of more competent rock. These differences will, in turn, influence the temperatures in the host rock. The degree that these temperatures would be influenced and the locations where this would occur is the subject that was investigated in this effort using borehole data from several different boreholes, a geostatistical model, and a thermal conduction model.

Thermal conductivity has been found to be correlated with rock porosity and temperature. Geostatistical models were used to construct estimates of porosity which were then used as a surrogate to represent spatial variability in the undersampled thermal conductivity of the rock mass. Two-dimensional profiles were created along an east-west cross-section of Yucca Mountain. The location and stratigraphic units around this cross-section are shown in Figures 3.4-1 and 3.4-2. A more detailed description of the geostatistical model can be found in Rautman (1995) but in general, the values of porosity for a vertical slice were selected based on borehole measurements from USW G-4 and USW G-3/GU-3. The G-3 data was used primarily to provide information for the Tiva Canyon Member and beneath CH since G-4 did not provide information in those units. This data was replicated at three locations (composite "drill holes") across the calculational cross-section. This conditioning data was used to develop simulated porosity values away from the composite "drill holes" using Gaussian simulations after Deutsche and Journel (1992) as a function of spatial correlation length. The spatial correlation length, or length at which the variance is equal to that obtained for uncorrelated measurements, was chosen to be 5000 m for the base case model used in the study which GC1HL. Another set of porosity

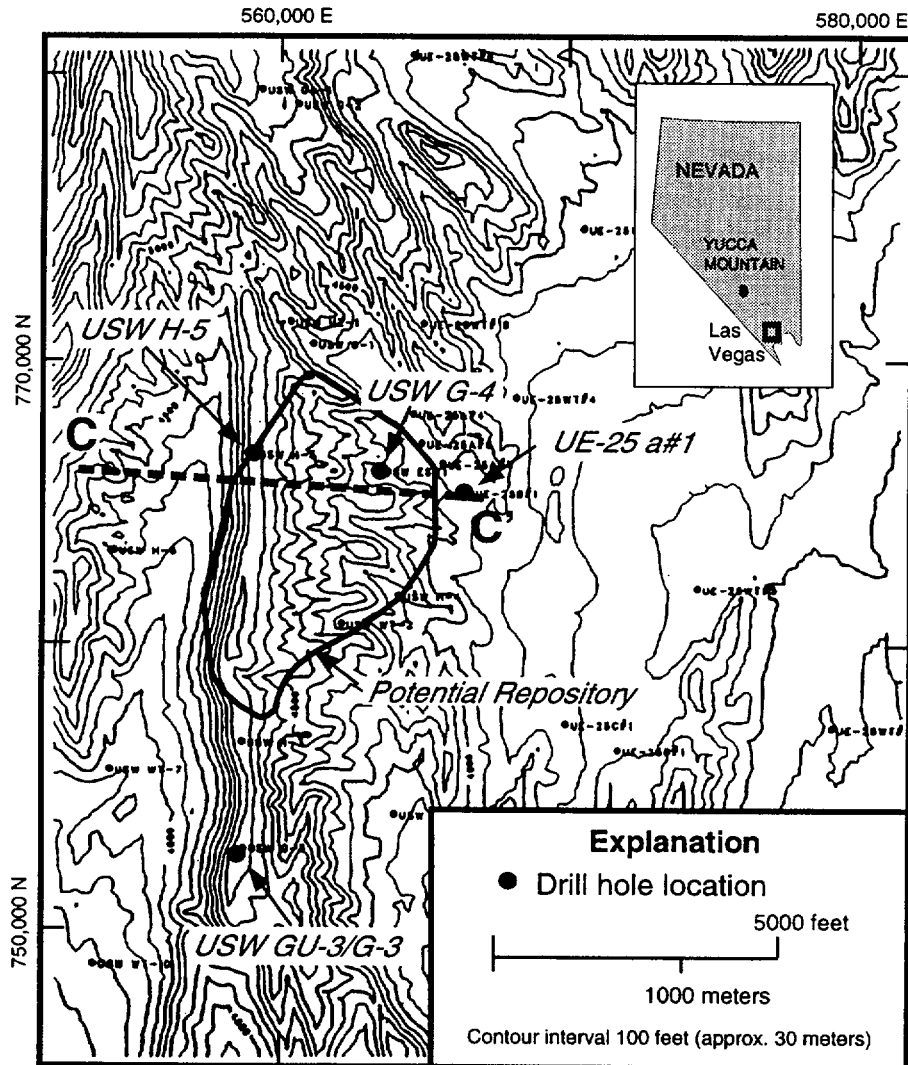


Figure 3.4-1. Index map showing the potential Yucca Mountain high-level nuclear-waste repository site in Southern Nevada, and the location of the cross-section for which thermal-properties modeling was conducted. (Note: The index map shows the layout from the SCP-CDR. Figure 2.5-1 shows the current potential repository and expansion areas.)

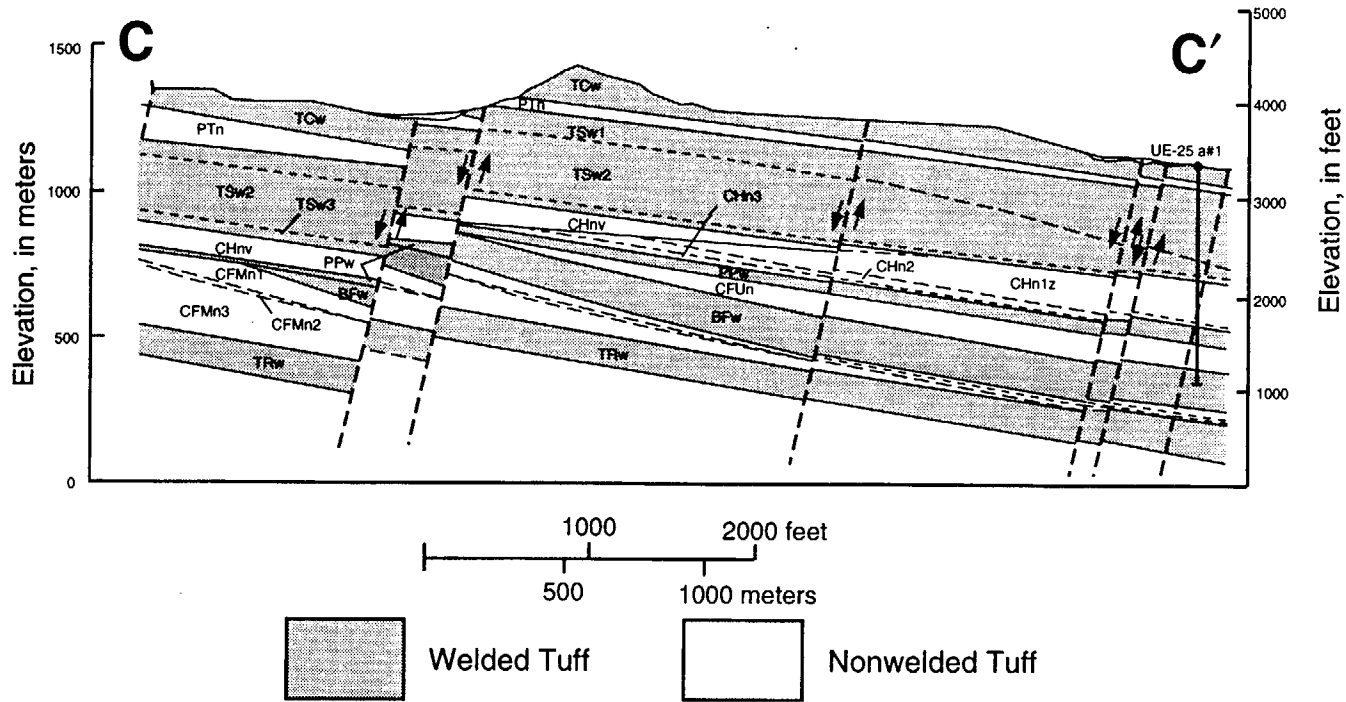


Figure 3.4-2. Geologic cross-section of the northern portion of the potential repository region at Yucca Mountain corresponding to section C--C' of Brandshaug, 1991 (see Figure 3.4-1, this report). Stratigraphic units are thermal/mechanical units (Ortiz et al., 1985). Welded intervals are shaded.

values was generated using a 1000 m correlation length and these values are labeled the GC2HL model.

The porosity estimates at various grid locations were then translated into thermal conductivities,  $k_t$ , using the following relationship developed from laboratory data taken on USW NRG-6 borehole data samples (Rautman, in review):

$$k_t = C_0 + C_1 T + C_2 S + C_3 \Phi \quad (3.4-1)$$

where  $T$  is temperature,  $S$  saturation, and  $\Phi$  is porosity.  $C_0$ ,  $C_1$ ,  $C_2$ , and  $C_3$  are coefficients derived from multiple-regression analyses and are given in Table 3.4-1. These coefficients were reported for welded and nonwelded tuff but the results would have been similar had they used a single set for both rock types. However, the coefficients also are a function of temperature since dry rock will have a significantly lower conductivity (e.g.,  $S$  in equation above becomes zero or very small and so the  $C_2$  term is negligible.). Additionally, the calculations required density and the bulk density,  $\rho_b$  in  $\text{gm/cm}^3$ , was estimated from the porosity values using the relationship (Rautman, et al., 1995):

$$\rho_b = 2.35 - 2.40 \Phi \quad (3.4-2)$$

Table 3.4-1. Coefficients from Multiple Regression Relationships Relating Thermal Conductivity and Porosity

Coefficient	Low Temperature, $T < 100^\circ\text{C}$		High Temperature, $T > 100^\circ\text{C}$	
	Welded	Nonwelded	Welded	Nonwelded
$C_0$	1.75	1.25	1.92	1.04
$C_1$	$3.53 \times 10^{-4}$	$2.10 \times 10^{-3}$	$-1.56 \times 10^{-4}$	$3.37 \times 10^{-4}$
$C_2$	0.43	0.58	0	0
$C_3$	-3.2	-2.24	-4.06	-1.53
No. of Analyses	78	204	135	29
Multiple $r^2$	0.58	0.95	0.47	0.99

Thermal calculations were done with this array of thermal conductivity and density values to establish the temperatures at various locations in the host rock as a function of time. The thermal calculations presented here were done using the multi-dimensional, nonlinear, heat-conduction code, COYOTE-II. The calculations used a YFF(10) waste stream, which yielded about  $24.7 \text{ W/m}^2$  (100 kW/acre) for emplacing the spent nuclear fuel in the upper block of the primary area ( $3.47 \times 10^6 \text{ m}^2$  or 857 acre) at about  $19.3 \text{ kgU/m}^2$  (78 MTU/acre).

Sensitivity studies were conducted to evaluate the impact of changes in rock saturation, conductivity changes, and the choice of spatial correlation length used in estimating the porosity values. The differences in predicted temperatures, by location in the rock and at various times, were used to estimate the impact that these heterogeneities might produce. The temperature predictions for a given case were compared with the base case GC1HL for most of the runs. The temperature difference at a given location is the difference between the new model and the GC1HL base case according to the following:

$$\Delta T_i = T_i(\text{base model}) - T_i(\text{new model}) \quad (3.4-3)$$

The effect of saturation variations was the first sensitivity case that was run and the details are described in Rautman and Longenbaugh (1995). In general, the base case GC1HL assumed an initial saturation of the rock of 60 percent for converting porosity to thermal conductivity in Equation (3.4-1) above. Additionally, the base case used the parameters in Table 3.4-1 for temperatures less than 100°C since it was assumed that rock of about 50°C would be representative of the early stages of heating. In actual fact, the saturation profiles encountered in Yucca Mountain drill holes are quite complex (Rautman, 1995). The saturation appears to not only be a function of rock type but also of location. To roughly estimate how changes in saturation might affect the temperatures, the thermal conductivities were recalculated from the base case using values of 80 percent saturation in the welded tuff materials and 40 percent for the nonwelded. Based on these revised thermal conductivities, the temperature calculations were redone and the temperature predictions compared to those for GC1HL. The results indicate that in the revised model, the nonwelded Paintbrush Tuff (PTn) and CH formation had somewhat lower thermal conductivities of at most 0.25 W/m-K. This results in somewhat higher temperatures in those layers but the repository itself appears to have somewhat lower temperatures, about 5°C, as shown in Figure 3.4-3 (recall that based on Equation (3.4-3), red or positive values of  $\Delta T$  indicate the model with revised saturations predicts lower temperatures than the base case). In this case, more of the heat seems to be conducted laterally than vertically, although this level of temperature change is probably not significant. Figure 3.4-3 reflects a period of 500 years. Other times show similar results and the maximum temperature differences noted between the base case and the new model for several times are shown in Table 3.4-2. This seems to indicate that accurate representations of in-situ moisture content are not a particularly important factor in conduction modeling (Rautman and Longenbaugh, 1995).

Table 3.4-2. Comparison of Maximum Predicted Temperature Differences for Differing Material-Property Modeling Assumption

Model	Temperature Maximum Predicted Difference			
	50 years	100 years	500 years	1000 years
Saturation: 60/60 - 80/40	5.1	5.5	5.6	4.8
Temperature: 50°C - 110°C	29.0	31.2	31.0	31.6
Algorithm: GC2HL-E-type	17.69	20.6	18.8	15.7
Algorithm: GC1HL-E-type	14.3	12.6	8.8	8.0
Lithophysae: continuous	3.0	3.4	12.7	12.8
Lithophysae: discontinuous	1.4	2.3	7.4	8.8

As mentioned above, the thermal conductivity estimates used in the base case were converted from spatially correlated porosity fields using an initial temperature of 50°C, which was believed to be a reasonable in-situ rock mass temperature during the early stages of heating. Since the coefficients of Equation (3.4-1) depend on temperature, the influence of temperature on the estimates of thermal conductivity were examined. This analysis simulates the changes in thermal conductivity in the rock that might occur due to dry-out of the host rock as a result of heating. The results (Rautman and Longenbaugh, 1995) indicate a marked decrease of 0.25 to 0.5 W/m-K in thermal conductivity in the drier rock in the near field. Temperature predictions at 500 years shown in Figure 3.4-4 indicate that, using these temperature-dependent thermal conductivities, the near field is predicted to be significantly hotter than the base case predicts. Up to 30°C temperature differences are noted between the maximum and minimum temperatures and, as shown in Table 3.4-2, this is similar to what is calculated at other times.

A few degrees temperature difference is not likely to make much difference to performance since there probably are existing uncertainties in the model that could produce those temperature differences. However, 10° to 30°C temperature differences could, for example, mean the difference between exceeding a thermal goal or not, or having a waste package in a corrosive environment or not.

Such a magnitude of temperature change as predicted above indicates that the temperature-dependent nature of thermal conductivity cannot be neglected in modeling the thermal impact of the spent nuclear fuel. As the temperature increases, rock dry-out also can change the saturation conditions. Based on these issues, information needs to be obtained on the changes in thermal conductivity as a function of temperature and this parameter should be measured in the in-situ tests as well as determining the degree of saturation change as a function of heating.

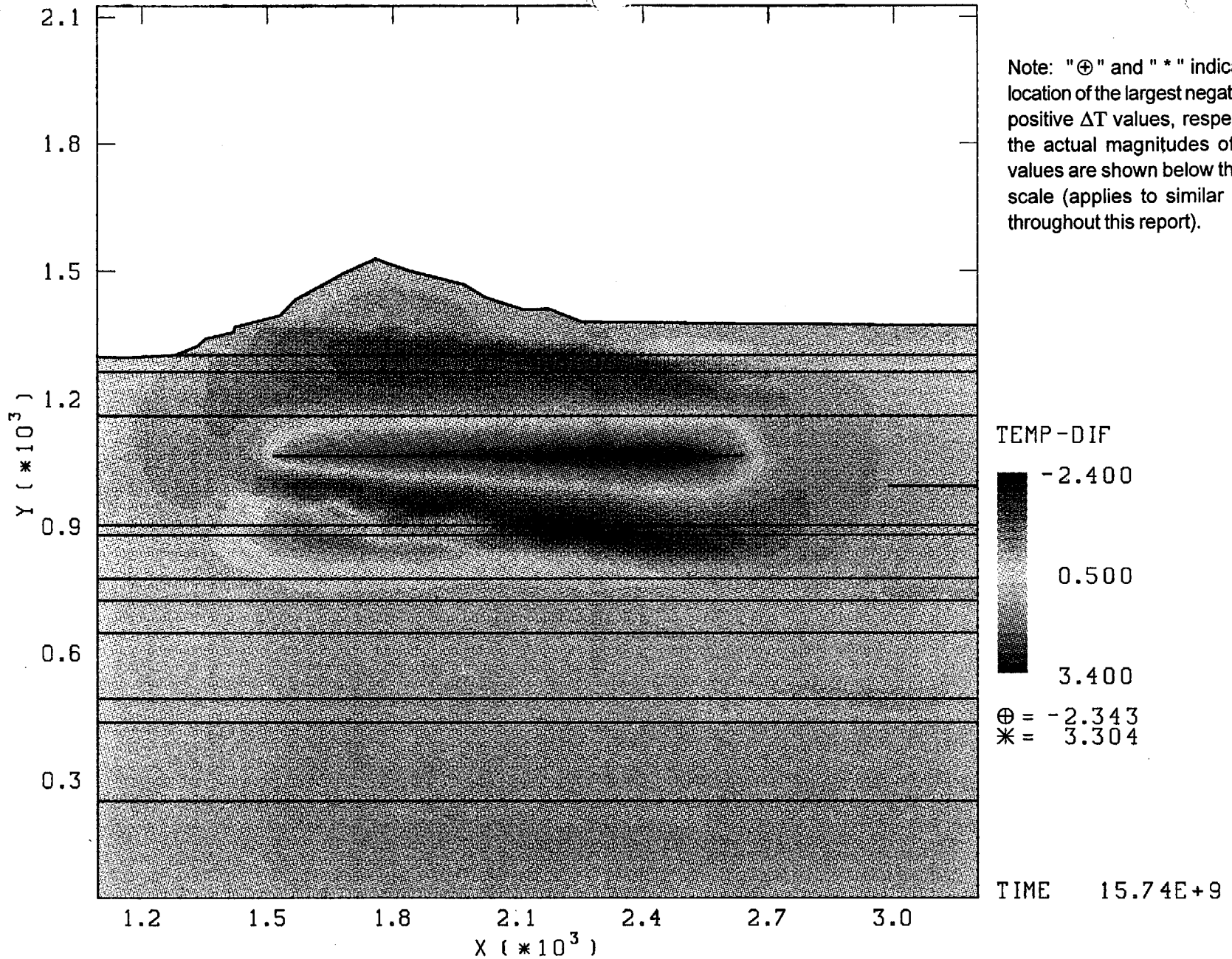


Figure 3.4-3. Temperature differences between thermal models computed using thermal conductivity values converted from porosity at a uniform initial saturation of 60 percent and at saturations of 80 percent for welded and 40 percent for nonwelded materials for an elapsed calculation time of 500 years. Distances in meters; temperature scale in °C.

INTENTIONALLY LEFT BLANK

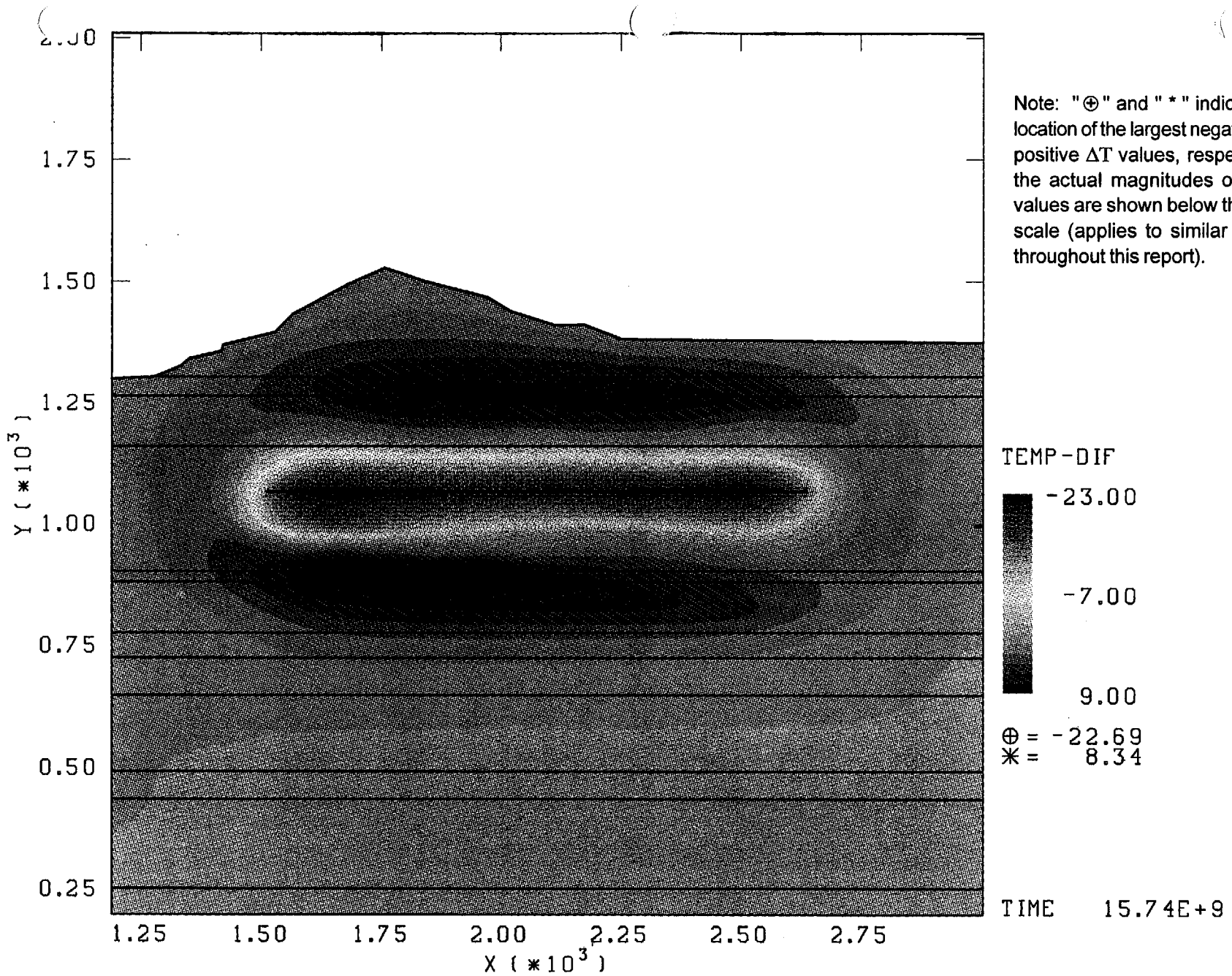


Figure 3.4-4. Temperature differences between thermal models computed using thermal conductivity values converted from porosity at 50°C and at 110°C for elapsed calculational time of 500 years. Distances in meters; temperature scale in °C.

INTENTIONALLY LEFT BLANK

Two principal geostatistical approaches to modeling material properties from sparse data were considered in this investigation. To see what effect the estimation technique might have on the results, the simulation technique discussed previously was compared with an estimation technique. The estimation technique, developed earlier and discussed by Journel and Huijbregts (1978), places emphasis on producing values that represent the most likely material property expected at any location and is referred to as producing a "E-type" estimate (Journel, 1983). On the other hand, the geostatistical simulation attempts to reproduce the statistical character of the phenomenon being modeled, including potential short-scale heterogeneity allowed under the representation of spatial continuity. Additional details can be found in Rautman and Longenbaugh (1995). To evaluate the impact of the choice of geostatistical algorithm, the thermal profiles produced with the E-type, estimation model were compared with the geostatistical simulation models. The first algorithm comparison summarized in Table 3.4-2 used the GC2HL geostatistical model, which had a 1000 m spatial correlation length in the horizontal although the vertical-to-horizontal anisotropy ratio remained at 20:1. The magnitude of the thermal conductivity values between the simulation model with 1000 m correlation length and the estimation model with the same correlation length are relatively large with maximum differences of about 1.9 W/m-K. These conductivity differences generally form lenticular regions of relatively limited lateral extent (Rautman and Longenbaugh, 1995), which are estimates of the statistical variability of the material property data being modeled. The maximum temperature differences between these two models were found to average 20°C. At early times (the first 100 years or so), the temperature predictions in the potential repository region are hotter for the estimation models than for the simulation models. At later times, the thermal pulse expands outward in a somewhat irregular fashion consistent with the material property differences and, as demonstrated in Figure 3.4-5 for 500 years, the estimation technique predicts cooler temperatures in regions of the potential repository vicinity of about 20°C. As a point of comparison, the simulation model GC1HL, which used a 5000 m spatial correlation distance, was compared with the E-type model and these comparisons indicated that the factor of 5 difference in the range of spatial correlation produces less of a difference in the resulting material properties and subsequently in the thermal profile predictions. In this case, the difference is at most 14°C, and the potential repository region is always hotter under the estimation model. Developing an understanding of the appropriate correlation lengths to use through modeling and data analyses will be important. This will require data from more densely spaced boreholes.

The potential impact of heterogeneity in material properties caused by the presence of zones of lithophysal-cavity development also was investigated in this effort. There is some indication based on large intervals of rubble from portions of boreholes, such as drill hole USW SD-9, that potential zones of lithophysal cavities may exist that could produce bulk rock porosity values that are a factor of two larger than the rock in adjacent zones (Rautman and Longenbaugh, 1995). To examine the impact this may have on predicted temperatures, the estimated core porosities in the upper lithophysal interval of TS (in stratigraphic coordinates this is -92 m to -147.7 m) were doubled. The results of comparing predicted temperatures for this continuous lithophysae region with the base case GC1HL model indicate, as shown in Table 3.4-2, that the lower conductivity upper portion of the TS Member initially results in little difference in temperature. However, at later times, as the thermal pulse reaches this region, the insulating nature of the lithophysal region produces rock temperatures above the repository that could be as much as 13°C more than the base case (Rautman and Longenbaugh, 1995). The lateral extent of the high-porosity, large lithophysal zone at Yucca Mountain is not well known, and in another evaluation



INTENTIONALLY LEFT BLANK



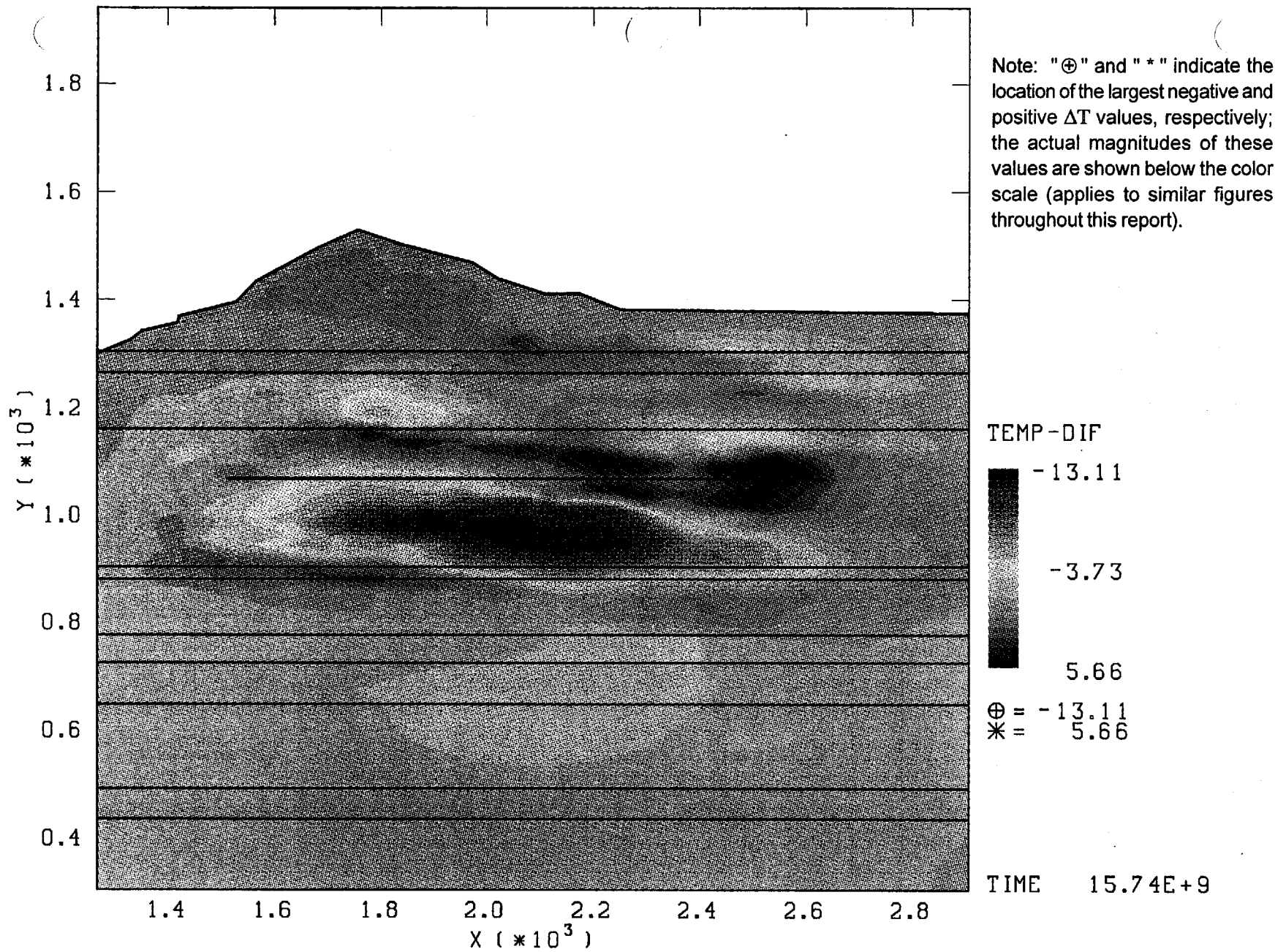


Figure 3.4-5. Temperature differences between simulated model GC2HL and the equivalent E-type model for an elapsed computational time of 500 years; both material property models use a range of spatial correlation of 1,000 meters. Distances in meters; temperature scale in °C.

INTENTIONALLY LEFT BLANK

the lithophysal cavity was considered to be discontinuous and only extend over a portion of the potential repository region. The temperature difference profiles between this hypothetical model and the base case model indicate little difference at early times, but at 500 years or later (see Table 3.4-2), temperature differences of about 9°C are observed above the potential repository where the lithophysal region exists. In this case, some of the heat buildup is allowed to escape through the higher-conductivity, low-lithophysal interval.

The above sensitivity studies provide information that needs to be factored into the testing and subsurface investigation program. Understanding the specific values of the liquid saturation in the rock was found not to be of critical importance in the prediction of temperatures using heat conduction. However, the dependence of thermal conductivity on temperature was found to be significant. Predicted temperature differences of as much as 30°C were noted because of the impact of changes in thermal conductivity in the rock caused by drying of the rock during heating. The fact that the repository could be substantially hotter than anticipated, if constant values of thermal conductivity are used for the predictions, may have an effect on such things as tunnel stability, retrieval, and postclosure performance. Additionally, the type of estimation model used also was found to be important. Heterogeneities in rock porosities in the vicinity of the repository could result in temperature differences of tens of degrees. Thus, this important effect needs to be investigated by determining the degree of heterogeneity that exists in the rock properties, specifically porosity and hence thermal conductivity in the potential repository vicinity. Potential high-porosity (large-cavity) lithophysal zones also could affect the temperatures depending on their location and extent. Work is needed to identify these lithophysal zones.

### **3.5 EFFECT OF FRACTURE-MATRIX COUPLING ON THERMOHYDROLOGY**

A variety of parameters can influence the thermal response of the host rock geologic system, the engineered barrier, and the waste packages because of the heat generated by the decay of the spent nuclear fuel. In other sections of the report, a conduction model was used to examine the effect of variations in spent nuclear fuel properties (Section 4.5) and changes in the rock thermal conductivity as a result of heterogeneity (Section 3.4) on temperature predictions. The thermohydrologic response has been calculated using an Effective Continuum Model to evaluate the effect of changes in bulk permeability (Section 3.1), changes in rock properties (porosity, liquid permeability, etc.) (Section 3.2), and sensitivity to variations in gas phase diffusion (Section 3.3). The Effective Continuum Model treats the rock matrix and fracture as the same (the conductance between fractures and matrix is infinite) so that the transport of liquid and vapor is governed by average permeabilities. However, the conductance between fractures and rock matrix is not infinite and it may not be justified to determine the liquid and vapor transport with averages of fracture and matrix permeabilities (the bulk permeability). This section investigates the effect that the fracture-matrix coupling has on thermohydrology by using dual permeability calculations.

The bulk intrinsic permeability can be expressed in terms of the matrix permeability,  $K_m$ , the fracture permeability,  $K_f$ , and the fracture porosity,  $\phi_f$  (the portion of the total porosity in fractures), according to:

$$K_b = (1 - \phi_f) K_m + \phi_f K_f \quad (3.5-1)$$

Fractures of welded tuffs are more permeable than the matrix by many orders of magnitude, and thus, bulk permeabilities are predominately governed by the fracture permeabilities. In a dual permeability model, the fractures and matrix can be modeled as two separate blocks, each with its own permeability. Communication between these two blocks depends on a number of factors, but, in particular, the area of the fracture-matrix interface,  $A_{fm}$ , the average distance between fractures and matrix blocks (fracture half spacing),  $L_{fm}$ , and also an average permeability,  $K_{fm}$ . This communication between fractures and matrix is generally expressed as the fracture-matrix transmissibility:

$$T_{fm} \sim \frac{K_{fm} A_{fm}}{L_{fm}} \quad (3.5-2)$$

The transmissibility represents, in electrical circuitry terms, a conductance between fracture and matrix. Thus the inverse of the permeability  $K_{fm}$  is related to the sum of the inverses of the fracture and matrix permeabilities weighted by appropriate length factors. If the matrix permeability is much smaller than the fracture permeability, then  $k_{fm}$  is primarily governed by the matrix permeability.

The proportionality sign is used in Equation (3.5-2) since there are other factors such as phase densities and viscosities that can affect the transmissibility. The permeability  $K_{fm}$  in Equation (3.5-2) is written as:

$$K_{fm} = F_{fm} K_m \quad (3.5-3)$$

The matrix potential governs the transmissibility since, for a gas or liquid to get into the fractures it must first travel through low permeability matrix rock. As an expression of uncertainty in the fracture-matrix coupling, the factor  $F_{fm}$  was varied over four orders of magnitude in the evaluation. This factor can be used to characterize uncertainties not only in the matrix permeability but also in the area and fracture spacing. The purpose of this sensitivity study is to assess the uncertainty in the geometric factors that govern fracture and matrix interactions.

In examining the sensitivity of thermal response to changes in the fracture-matrix coupling and changes in the bulk permeability, the TOUGH2 code developed by Pruess (1991) was run using a dual permeability grid. This code has been used in previous system study calculations and the description of many of the inputs can be found in a previous study (M&O, 1994d). Changes of inputs over those described in the previous work are discussed below, including inputs specifically used in the dual permeability calculations. For comparison purposes, some runs also were done running the code as an ECM in which the conductance between fractures and matrix is infinite and the liquid/vapor transport is governed by bulk permeabilities.

The matrix permeability used in the calculations was chosen to be  $1.9 \times 10^{-18} \text{ m}^2$  ( $1.9 \times 10^{-6}$  darcy) and fracture permeabilities on the order of  $10^{-10} \text{ m}^2$  (100 darcy) were used for the repository horizon. With fracture porosities in the range of about  $10^{-3}$ , Equation (3.5-1) yields a bulk permeability of 100 millidarcy, which is consistent with the range of bulk permeability values given by Wilson, et al (1994). This bulk permeability was used in all of the dual permeability calculations. The matrix permeability identified above was multiplied by the factor  $F_{fm}$  which had values from 0.1 to 1000 and also infinity to determine the transmissibility factor. A coupling factor of infinity represents the ECM case in which there is perfect coupling between the fractures and matrix. For simplicity, values for the interface area were set at  $A_{fm}=1 \text{ m}^2/\text{m}^3$  with a half spacing of  $L_{fm}=1 \text{ m}$ , which is representative of 1 fracture in a cubic meter of rock. Other values have been suggested such as three fractures per cubic meter (Buscheck and Nitao, 1993). In this study, the fracture-matrix coupling factor  $F_{fm}$  was used to allow variations in matrix permeability which can compensate for area or length variability.

The thermohydrologic calculations were done for a large, 21 PWR capacity (8.75 MTU) waste package. PWR fuel was used with a YFF(10) waste selection criteria. TOUGH2 was run as a two-dimensional model and thus the waste packages were treated as a line source. The calculations were done for a thermal loading of  $20.6 \text{ kgU}/\text{m}^2$  (83 MTU/acre), which was established with a drift spacing of 26.7 m and a WP spacing of 16 m. The waste package had uniform distribution of heat inside a cylinder, which had a radius of 0.90 m. The waste packages were emplaced in air-filled, closed (no ventilation) drifts, which had a radius of 3.81 m. Although this is a larger drift than used in the other calculations it should not significantly impact the results nor change the conclusions.

Dual permeability calculations were done for the various coupling factors ( $F_{fm} = K_{fr}/K_m$ ) to a time after emplacement of 100 years at an AML of  $20.6 \text{ kgU}/\text{m}^2$ . Figure 3.5-1 shows the vertical temperature profiles at 100 years for the bounding cases where the coupling factor is 0.1 and infinity. In the case where the coupling is very small, the temperature profile approaches the temperature which would be calculated with a pure conduction model. This condition produces the highest temperature predictions at the repository horizon. As the fracture-matrix transmissibility factor increases, the temperature at the repository decreases as vapor movement more effectively carries the heat away. Additionally, the figure shows the development of heat pipes above the repository where two-phase conditions persist at the boiling point. The maximum temperature difference between the two extremes is predicted to be about  $25^\circ\text{C}$ .

Figure 3.5-2 shows plots of five coupling factor calculations done at 100 years on an expanded vertical distance scale around the repository for a location at approximately the drift centerline. The predicted temperatures internal to the waste packages (in the calculation grid block which is 0.28 m from the center of the waste package) are shown as a function of time after emplacement for six cases in Figure 3.5-3. It should be noted that these temperatures in Figure 3.5-3 are substantially lower than would be encountered in an actual waste package since these calculations used a smeared line source.

Fracture permeability was kept constant in the previous calculations. A set of ECM calculations also was done to determine the impact of varying bulk permeability, which is controlled by fracture permeability, over a range from  $10^{-15}$  to  $10^{-12} \text{ m}^2$  (1 to 1000 millidarcy). The results of predictions of vertical temperature profiles at 100 years for the ECM calculations for the two

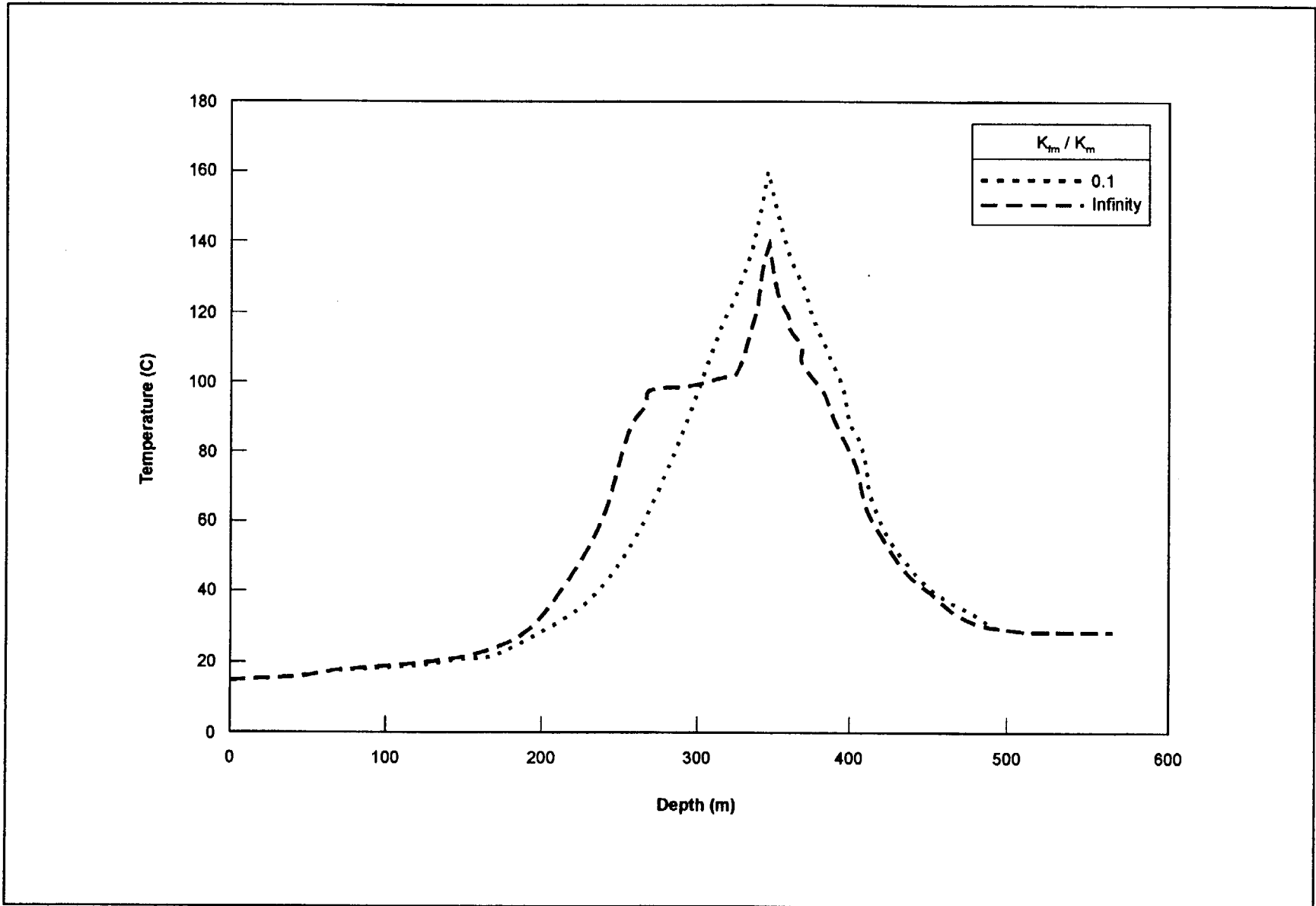


Figure 3.5-1. Temperature Response at 100 Years to Changes in Fracture-Matrix Coupling Factor  $K_{fm}/K_m$ . The depth axis passes through the drift centerline.

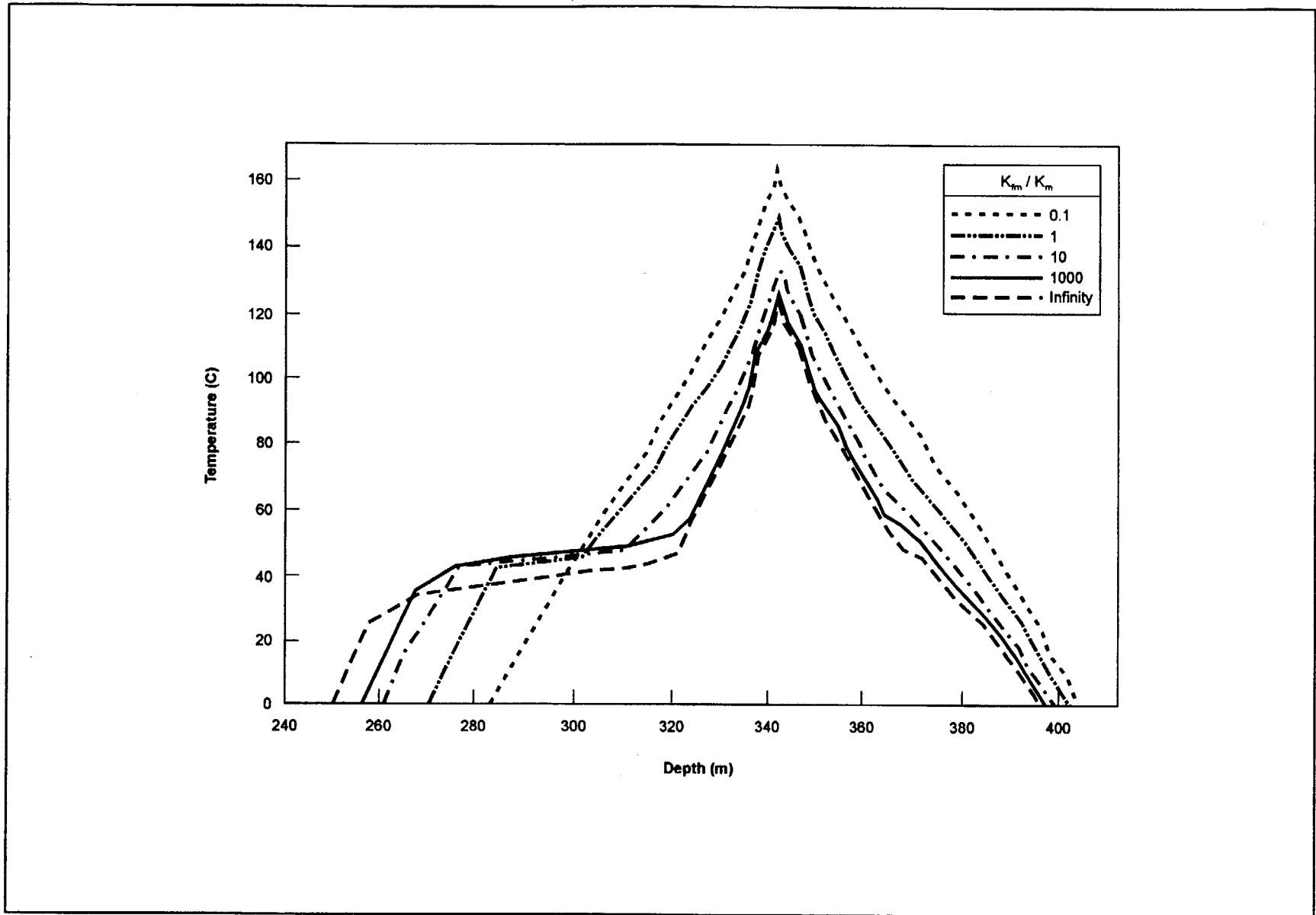


Figure 3.5-2. Temperature Response at 100 Years to Changes in Fracture-Matrix Coupling Factor  $K_{fm}/K_m$ . Both axes are expanded over previous figure and the depth axis passes through the drift centerline.

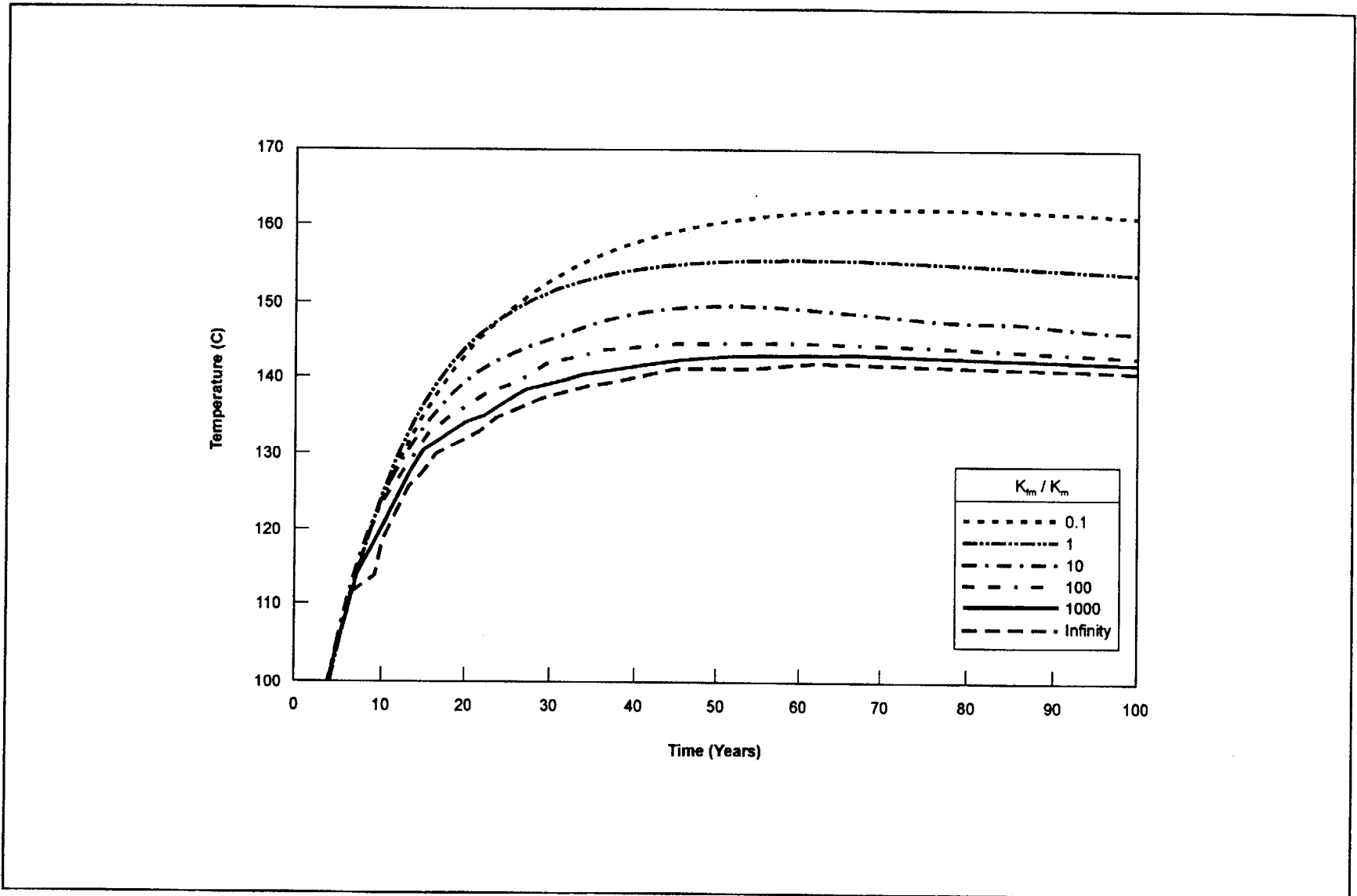


Figure 3.5-3. Waste-Package Temperature Response to Changes in Fracture-Matrix Coupling Factor  $K_{fm}/K_m$ .

extremes in the above range in bulk permeabilities are plotted in Figure 3.5-4. An expanded vertical scale is used in Figure 3.5-5 and the four different bulk permeability cases run are plotted for comparison. It should be noted that the ECM case for  $10^{-13} \text{ m}^2$  (100 millidarcy) is the same case as done for the dual permeability calculations with a coupling factor of infinity. A difference of about  $20^\circ\text{C}$  in peak temperature is predicted over this range of bulk permeability. Predictions of waste package internal temperatures as a function of time are shown in Figure 3.5-6 for these four cases, and the figure shows that in the case of the largest bulk permeability the temperatures are somewhat lower than those predicted in the dual permeability case with a bulk permeability of  $10^{-13} \text{ m}^2$  (100 millidarcy). That is, the sensitivity of temperature response to fracture permeability is higher than to fracture-matrix transmissibility.

The results of this investigation into the effects of the fracture-matrix coupling in the host rock and changes in permeabilities have shown a sensitivity to variations in these parameters. The predictions show that the temperatures of the drifts and waste packages could be more than  $20^\circ\text{C}$  cooler than predictions using an ECM with small bulk permeabilities. Fracture permeability was kept constant in the previous calculations. A set of ECM calculations also were done to determine the impact of varying fracture permeability, actually bulk permeability, over a fairly wide range from  $10^{-15}$  to  $10^{-12} \text{ m}^2$  (1 to 1000 millidarcy). The results of predictions of vertical temperature profiles at 100 years for the ECM calculations for the two extremes in bulk permeability are plotted in Figure 3.5-4. An expanded vertical scale is used in Figure 3.5-5 and the four different bulk permeability cases run are plotted for comparison. It should be noted that the ECM case for  $10^{-13} \text{ m}^2$  (100 millidarcy) is the same case as done for the dual permeability calculations with a coupling factor of infinity. As in the previous calculations, a difference of about  $20^\circ\text{C}$  is predicted between the two extremes in bulk permeability. Predictions of waste package internal temperatures as a function of time are shown in Figure 3.5-6 for these four cases, and the figure shows that in the case of the largest bulk permeability the temperatures are somewhat lower than those predicted in the dual permeability case with a bulk permeability of  $10^{-13} \text{ m}^2$  (100 millidarcy). These sets of calculations were only meant to show that variations in bulk permeability can affect the temperatures predicted and even for a given bulk permeability the degree of coupling between fractures and matrix also can affect the temperatures with similar magnitude changes.

The results of this investigation into the effects of the fracture-matrix coupling in the host rock and changes in permeabilities have shown a sensitivity to variations in these parameters. The predictions show that the temperatures of the drifts and waste packages could be more than  $20^\circ\text{C}$  cooler than predictions using an ECM with small bulk permeabilities or a conduction model would indicate. These results show that not only are variations in the host rock permeability important but the communication between fractures and matrix is also critical to understand. A large range chosen for the coupling factor and the sensitivities predicted over that range indicate the need for test information. Such information would include measurements of matrix permeability, area of the fracture-matrix interface, and fracture separations. Additionally, the heterogeneity in these parameters is important, as well, since variations in temperature could occur across the repository, resulting in hotter or cooler spots forming in some areas.

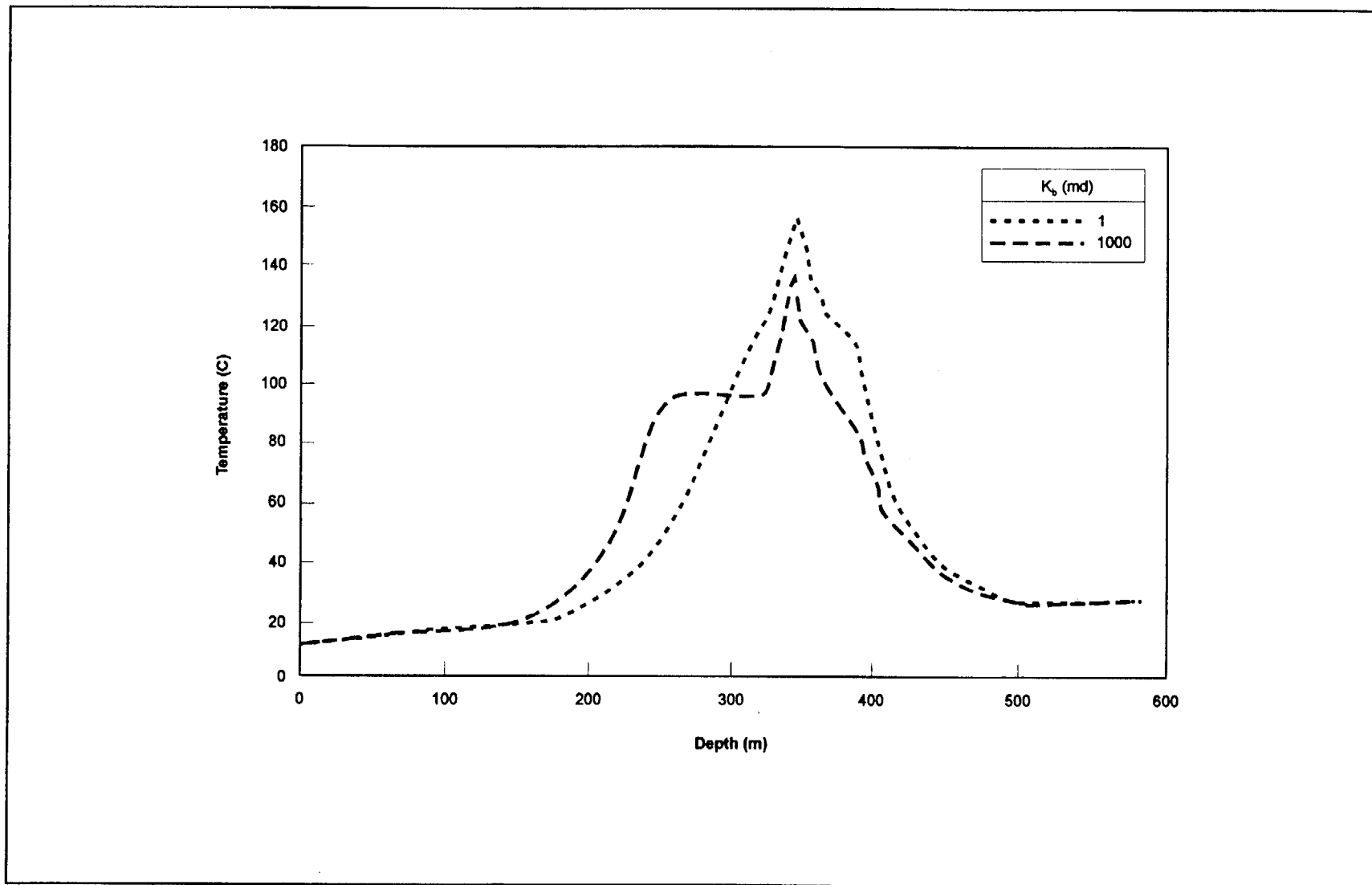


Figure 3.5-4. Temperature Response at 100 Years to Changes in Bulk Permeability  $K_b$ . Depth axis passes through the drift centerline.



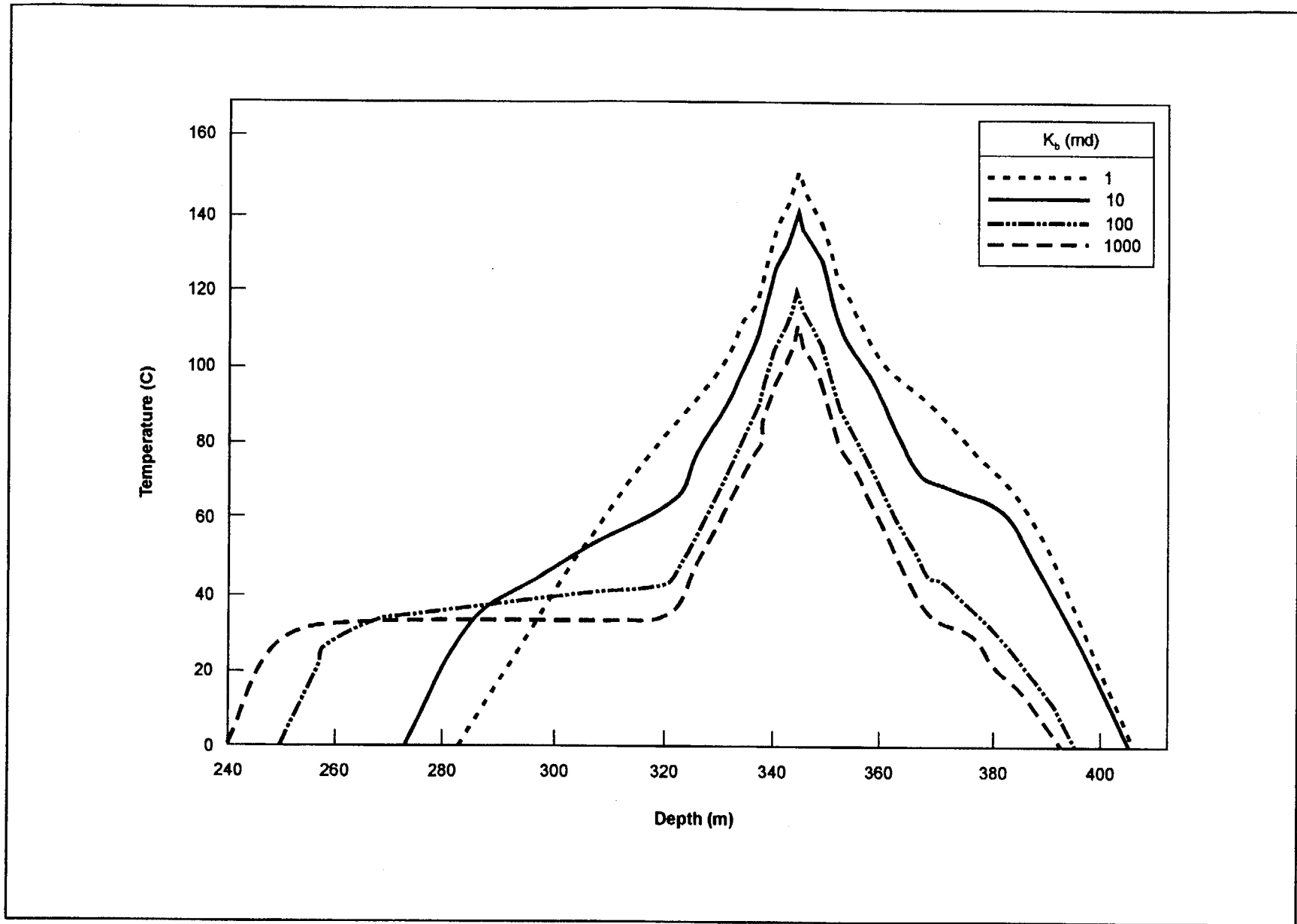


Figure 3.5-5. Temperature Response at 100 Years to Changes in Bulk Permeability  $K_b$ . Both axes are expanded over the previous figure and the drift axis passes through the drift centerline.

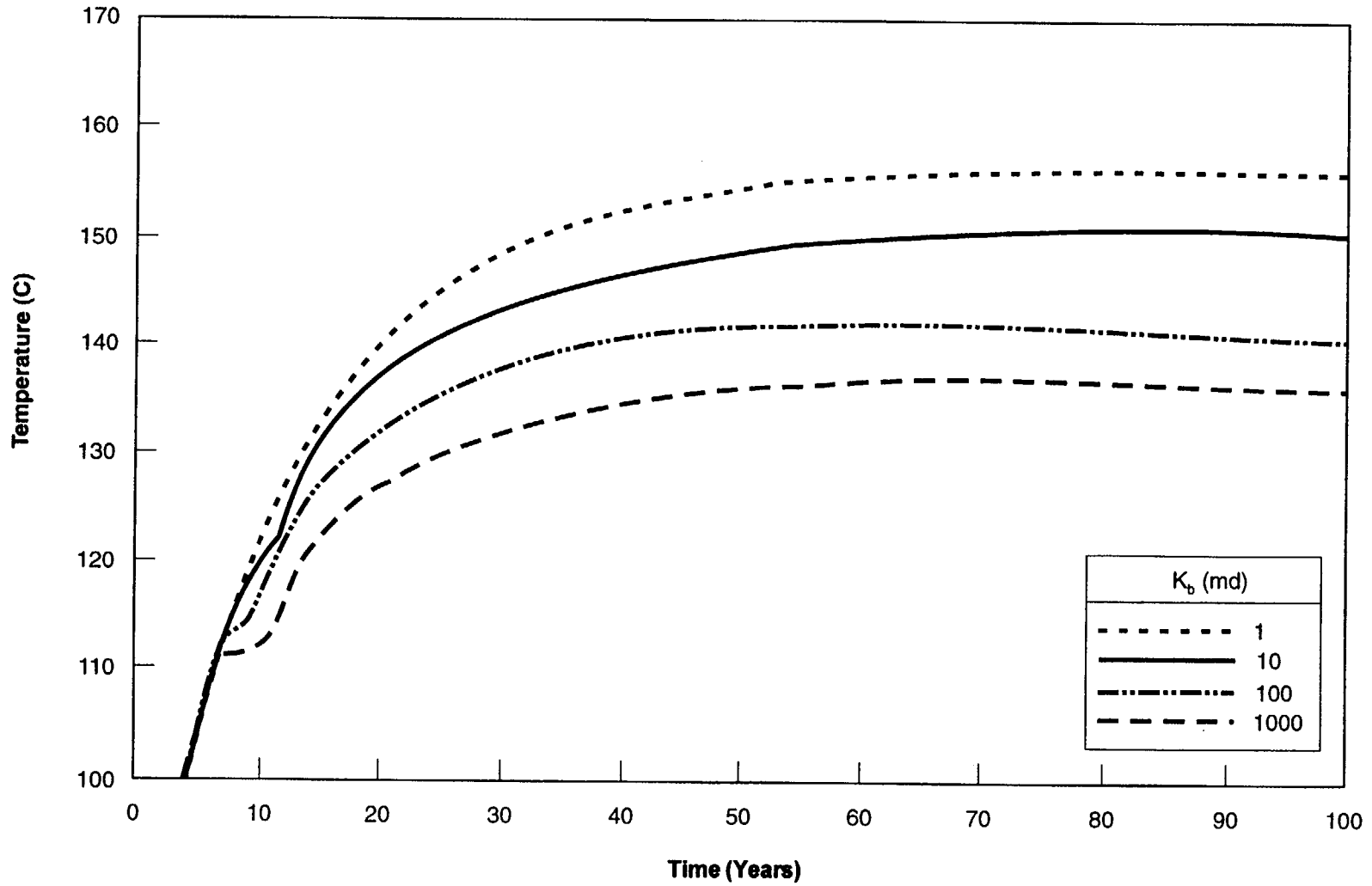


Figure 3.5-6. Waste-Package Temperature Response to Changes in Bulk Permeability  $K_b$ .

### 3.6 GEOCHEMISTRY ISSUES

Geochemical processes will play an important part in waste isolation in Yucca Mountain. These geochemical processes can be affected by the heat introduced into the host rock as a result of the decay of the SNF. The preceding sections have focused on the influence of heat on the liquid water resident in the pores of the rock and the mobilization of that water. This section will provide a preliminary evaluation of the effect that heat may have on the water that is bound in the zeolitic mineral assemblages and the impact that dehydration and/or mineral alteration might have on the porosity of the rock and hence the permeability of that rock. These are preliminary calculations that are based on currently available measurements taken in the laboratory using samples from borehole and mineral separates.

Three important geochemical processes considered in previous system studies were: 1) mineral dehydration of zeolites, clays, and volcanic glass; 2) crystallization of volcanic glass to a secondary mineral assemblage ("zeolitization"); and 3) recrystallization of clinoptilolite-opal cristobalite-tridymite mineral assemblages to analcime-quartz assemblages. This section will concentrate on the first and third processes. In the first process, dehydration of minerals, the concern is that heating will result in a loss of water from the zeolites which can be mobilized by the heat. How much water is involved and where this water goes is dependent on the thermal loading. Additionally the loss of water from zeolites may cause structural changes. Contraction of the crystal lattices of the minerals may cause irreversible changes in bulk hydraulic properties, but for the most part if temperatures remain below 100°C these processes are reversible. The third process of recrystallization also may have an impact since analcime, the final product, has less sorptive capacity for some radionuclides than does clinoptilolite and is a part of a denser mineral assemblage that can change the porosity and/or result in microfractures which could change the permeability of the host rock. This process is irreversible. The dehydration of clinoptilolite is reversible once the temperatures drop but if the clinoptilolite has been converted to analcime it cannot reabsorb as much water as was originally released.

A set of calculations was made to provide an estimate of the magnitude of the effect of hydrous minerals on the thermal and hydrologic evolution of Yucca Mountain. The calculations are based upon the mineral abundance reported by Bish and Chipera (1989); the measured properties of Na-clinoptilolite reported by Bish (1984; volumetric data) and Carey and Bish (1995s; water content and energy data); the thermal evolution models for Yucca Mountain by Buscheck, Nitao, and Saterlie (1994); and inferences on the thermal stability of clinoptilolite with respect to analcime by Smyth (1982). The calculations were made for mineral abundance taken from three drill holes, USW G-1, USW G-3, and USW G-4 and thermal loads of 27.3, 20.6, 13.7, and 8.9 kgU/m<sup>2</sup> (110.5, 83.4, 55.3, and 35.9 MTU/acre). The results of the calculations are summarized in the Table 3.6-1.

Using only three boreholes that are widely separated will only provide indications of what geochemistry issues exist. Each borehole had numerous samples taken but the information given in Table 3.6-1 at each 50 m interval was based on a representative sample from that depth interval.

Table 3.6-1. Effects of Hydrus Minerals

27.3 kgU/m <sup>2</sup> (110.5 MTU/Acre) Case										
Calculation based on USW G1										
				Clinoptilolite Only			Clinoptilolite + Mordenite			
Depth	mordenite	clinoptilolite	Temp.	H <sub>2</sub> O released	Δ porosity	Extra Energy	H <sub>2</sub> O released	Δ porosity	Extra Energy	Δ porosity
(m)	wt%	wt%	(°C)	cm <sup>3</sup> /m <sup>3</sup>	%	Consumed %	cm <sup>3</sup> /m <sup>3</sup>	%	Consumed %	Clinoptilolite ⇒ Analcime %
100		3	96	785	+0.23	1.35	785	+0.23	1.35	+0.65
150			96							
200			105							
250			127							
300			155							
350			175							
400		5	150	4493	+0.42	4.28	4493	+0.42	4.28	+1.08
450	11	63	100	17456	+5.32	28.16	20504	+6.25	33.08	+13.55
500	12	60	96	15701	+5.07	26.99	18842	+6.08	32.39	+12.90
550	5	50	96	13084	+4.22	22.49	14393	+4.65	24.74	+10.75
Calculation based on USW G3										
				Clinoptilolite Only			Clinoptilolite + Mordenite			
Depth	mordenite	clinoptilolite	Temp.	H <sub>2</sub> O released	Δ porosity	Extra Energy	H <sub>2</sub> O released	Δ porosity	Extra Energy	Δ porosity
(m)	wt%	wt%	(°C)	cm <sup>3</sup> /m <sup>3</sup>	%	Consumed %	cm <sup>3</sup> /m <sup>3</sup>	%	Consumed %	Clinoptilolite ⇒ Analcime %
100			96							
150			96							
200			105							
250			127							
300			155							
350			175							
400			150							
450		1	100	277	+0.08	0.45	277	+0.08	0.45	+0.22
500			96							
550		30	96	7851	+2.53	13.49	7851	+2.53	13.49	+6.45

Notes:

1) Calculations on the consequences of heating clinoptilolite-bearing rocks at Yucca Mountain as a function of thermal loading. 2) Clinoptilolite abundances taken from USW G1, USW G3, and USW G4 and are in weight percent. In all calculations, the magnitude of the effect of dehydration on the unit volume of rock was determined by assuming zero porosity. Inclusion of the effect of initial porosity would decrease the values given for H<sub>2</sub>O released and Δ porosity. 3) The calculations are based upon the thermal response of Na-clinoptilolite as reported by Carey and Bish (1995a, b) and Bish (1984). 4) Temperatures are taken from the thermal log calculations at 1,000 years (Buscheck et al., 1994). 5) H<sub>2</sub>O released is calculated assuming that the maximum allowable vapor pressure is 1 bar. 6) Δ porosity is calculated for the most significant volumetric change reported by Bish (1994) and represents an increase in porosity. 7) Extra energy consumed is calculated by considering the extra energy required to dehydrate clinoptilolite and implies a cooling effect. 8) A second calculation assumes that mordenite's behavior is similar to that of clinoptilolite to obtain a net effect of all zeolites. 9) The conversion of clinoptilolite to analcime was considered possible at T>96°C.

B00000000-01717-5705-00016 REV 00

3-60

01/31/96

Table 3.6-1. Effects of Hydrated Minerals (Continued)

Calculation based on USW G4										
				Clinoptilolite Only			Clinoptilolite + Mordenite			
Depth	mordenite	clinoptilolite	Temp.	H <sub>2</sub> O released	Δ porosity	Extra Energy	H <sub>2</sub> O released	Δ porosity	Extra Energy	Δ porosity
(m)	wt%	wt%	(°C)	cm <sup>3</sup> /m <sup>3</sup>	%	Consumed %	cm <sup>3</sup> /m <sup>3</sup>	%	Consumed %	Clinoptilolite ⇒ Analcime %
100			96							
150			96							
200			105							
250			127							
300			155							
350			175							
400		28	150	25162	+2.37	23.97	25162	+2.37	23.97	+6.02
450		77	100	21335	+6.50	34.42	21335	+6.50	34.42	+16.56
500		45	96	11776	+3.80	20.24	11776	+3.80	20.24	+9.68
550		10	96	2617	+0.84	4.50	2617	+0.84	4.50	+2.15
20.6 kgU/m <sup>2</sup> (83.4 MTU/acre) Case										
Calculation based on USW G1										
				Clinoptilolite Only			Clinoptilolite + Mordenite			
Depth	mordenite	clinoptilolite	Temp.	H <sub>2</sub> O released	Δ porosity	Extra Energy	H <sub>2</sub> O released	Δ porosity	Extra Energy	Δ porosity
(m)	wt%	wt%	(°C)	cm <sup>3</sup> /m <sup>3</sup>	%	Consumed %	cm <sup>3</sup> /m <sup>3</sup>	%	Consumed %	Clinoptilolite ⇒ Analcime %
100		3	81	611	+0.18	1.36	611	+0.18	1.36	0
150			96							
200			96							
250			106							
300			123							
350			140							
400		5	122	2798	+0.42	3.49	2798	+0.42	3.49	+1.08
450	11	63	96	16486	+5.32	28.34	19365	+6.25	33.29	+13.55
500	12	60	95	15481	+4.63	27.18	18577	+5.55	32.62	0
550	5	50	77	9443	+2.85	22.78	10387	+3.14	25.06	0

Notes:

1) Calculations on the consequences of heating clinoptilolite-bearing rocks at Yucca Mountain as a function of thermal loading. 2) Clinoptilolite abundances taken from USW G1, USW G3, and USW G4 and are in weight percent. In all calculations, the magnitude of the effect of dehydration on the unit volume of rock was determined by assuming zero porosity. Inclusion of the effect of initial porosity would decrease the values given for H<sub>2</sub>O released and Δ porosity. 3) The calculations are based upon the thermal response of Na-clinoptilolite as reported by Carey and Bish (1995a, b) and Bish (1984). 4) Temperatures are taken from the thermal load calculations at 1,000 years (Buscheck et al., 1994). 5) H<sub>2</sub>O released is calculated assuming that the maximum sustainable vapor pressure is 1 bar. 6) Δ porosity is calculated for the most significant volumetric change reported by Bish (1994) and represents an increase in porosity. 7) Extra energy consumed is calculated by considering the extra energy required to dehydrate clinoptilolite and implies a cooling effect. 8) A second calculation assumes that mordenite's behavior is similar to that of clinoptilolite to obtain a net effect of all zeolites. 9) The conversion of clinoptilolite to analcime was considered possible at T>96°C.

Table 3.6-1. Effects of Hydrous Minerals (Continued)

Calculation based on USW G3										
				Clinoptilolite Only			Clinoptilolite + Mordenite			
Depth	mordenite	clinoptilolite	Temp.	H <sub>2</sub> O released	Δ porosity	Extra Energy	H <sub>2</sub> O released	Δ porosity	Extra Energy	Δ porosity
(m)	wt%	wt%	(°C)	cm <sup>3</sup> /m <sup>3</sup>	%	Consumed %	cm <sup>3</sup> /m <sup>3</sup>	%	Consumed %	Clinoptilolite ⇒ Analcime %
100			81							
150			96							
200			96							
250			106							
300			123							
350			140							
400			122							
450		1	96	262	+0.08	0.45	262	+0.08	0.45	+0.22
500			95							
550		30	77	5666	+1.71	13.67	5666	+1.71	13.67	0
Calculation based on USW G4										
				Clinoptilolite Only			Clinoptilolite + Mordenite			
Depth	mordenite	clinoptilolite	Temp.	H <sub>2</sub> O released	Δ porosity	Extra Energy	H <sub>2</sub> O released	Δ porosity	Extra Energy	Δ porosity
(m)	wt%	wt%	(°C)	cm <sup>3</sup> /m <sup>3</sup>	%	Consumed %	cm <sup>3</sup> /m <sup>3</sup>	%	Consumed %	Clinoptilolite ⇒ Analcime %
100			81							
150			96							
200			96							
250			106							
300			123							
350			140							
400		28	122	15669	+2.37	19.56	15669	+2.37	19.56	+6.02
450		77	96	20150	+6.50	34.63	20150	+6.50	34.63	+16.56
500		45	95	11611	+3.47	20.39	11611	+3.47	20.39	0
550		10	77	1889	+0.57	4.56	1889	+0.57	4.56	0

Notes:

1) Calculations on the consequences of heating clinoptilolite-bearing rocks at Yucca Mountain as a function of thermal loading. 2) Clinoptilolite abundances taken from USW G1, USW G3, and USW G4 and are in weight percent. In all calculations, the magnitude of the effect of dehydration on the unit volume of rock was determined by assuming zero porosity. Inclusion of the effect of initial porosity would decrease the values given for H<sub>2</sub>O released and Δ porosity. 3) The calculations are based upon the thermal response of Na-clinoptilolite as reported by Carey and Bish (1995a, b) and Bish (1984). 4) Temperatures are taken from the thermal log calculation at 1,000 years (Buscheck et al., 1994). 5) H<sub>2</sub>O released is calculated assuming that the maximum allowable vapor pressure is 1 bar. 6) Δ porosity is calculated for the most significant volumetric change resulting from the extra energy required to dehydrate clinoptilolite and implies a cooling effect. 7) Extra energy consumed is calculated by assuming the extra energy required to dehydrate clinoptilolite and implies a cooling effect. 8) A second calculation assumes that mordenite's behavior is similar to that of clinoptilolite to obtain a net effect of all zeolites. 9) The conversion of clinoptilolite to analcime was considered possible at T>96°C.

Table 3.6-1. Effects of Hydrus Minerals (Continued)

13.7 kgU/m <sup>2</sup> (55.3 MTU/acre) Case										
Calculation based on USW G1										
Depth	mordenite	clinoptilolite	Temp.	Clinoptilolite Only			Clinoptilolite + Mordenite			
				H <sub>2</sub> O released	Δ porosity	Extra Energy	H <sub>2</sub> O released	Δ porosity	Extra Energy	Δ porosity
(m)	wt%	wt%	(°C)	cm <sup>3</sup> /m <sup>3</sup>	%	Consumed %	cm <sup>3</sup> /m <sup>3</sup>	%	Consumed %	Clinoptilolite ⇒ Analcime %
100		3	51	275	+0.08	1.35	275	+0.08	1.35	0
150			65							
200			79							
250			92							
300			96							
350			106							
400		5	92	1231	+0.37	2.26	1231	0.37	2.26	0
450	11	63	79	12362	+3.73	28.64	14520	+4.39	33.64	0
500	12	60	65	8598	+2.62	27.59	10317	+3.15	33.11	0
550	5	50	55	5305	+1.63	23.04	5835	+1.79	25.34	0
Calculation based on USW G3										
Depth	mordenite	clinoptilolite	Temp.	Clinoptilolite Only			Clinoptilolite + Mordenite			
				H <sub>2</sub> O released	Δ porosity	Extra Energy	H <sub>2</sub> O released	Δ porosity	Extra Energy	Δ porosity
(m)	wt%	wt%	(°C)	cm <sup>3</sup> /m <sup>3</sup>	%	Consumed %	cm <sup>3</sup> /m <sup>3</sup>	%	Consumed %	Clinoptilolite ⇒ Analcime %
100			51							
150			65							
200			79							
250			92							
300			96							
350			106							
400			92							
450		1	79	196	+0.06	0.45	196	+0.06	0.45	0
500			65							
550		30	55	3183	+0.98	13.82	3183	+0.98	13.82	0

Notes:

1) Calculations on the consequences of heating clinoptilolite-bearing rocks at Yucca Mountain as a function of thermal loading. 2) Clinoptilolite abundances taken from USW G1, USW G3, and USW G4 and are in weight percent. In all calculations, the magnitude of the effect of dehydration on the unit volume of rock was determined by assuming zero porosity. Inclusion of the effect of initial porosity would decrease the values given for H<sub>2</sub>O released and Δ porosity. 3) The calculations are based upon the thermal response of Na-clinoptilolite as reported by Carey and Bish (1995a, b) and Bish (1984). 4) Temperatures are taken from the thermal load calculations at 1,000 years (Buscheck et al., 1994). 5) H<sub>2</sub>O released is calculated assuming that the maximum sustainable vapor pressure is 1 bar. 6) Δ porosity is calculated for the most significant volumetric change reported by Bish (1994) and represents an increase in porosity. 7) Extra energy consumed is calculated by considering the extra energy required to dehydrate clinoptilolite and implies a cooling effect. 8) A second calculation assumes that mordenite's behavior is similar to that of clinoptilolite to obtain a net effect of all zeolites. 9) The conversion of clinoptilolite to analcime was considered possible at T>96°C.

B00000000-01717-5705-00016 REV 00

3-63

01/31/96

Table 3.6-1. Effects of Hydrous Minerals (Continued)

				Clinoptilolite Only			Clinoptilolite + Mordenite			
Depth	mordenite	clinoptilolite	Temp.	H <sub>2</sub> O released	Δ porosity	Extra Energy	H <sub>2</sub> O released	Δ porosity	Extra Energy	Δ porosity
(m)	wt%	wt%	(°C)	cm <sup>3</sup> /m <sup>3</sup>	%	Consumed %	cm <sup>3</sup> /m <sup>3</sup>	%	Consumed %	Clinoptilolite ⇒ Analcime %
100			51							
150			65							
200			79							
250			92							
300			96							
350			106							
400		28	92	6896	+2.07	12.68	6896	2.07	12.68	0
450		77	79	15109	+4.56	35.00				0
500		45	65	6448	+1.97	20.69				0
550		10	55	1061	+0.33	4.61				0
<b>8.9 kgUm<sup>2</sup> (35.9 MTU/Acre) Case</b>										
				Clinoptilolite Only			Clinoptilolite + Mordenite			
Depth	mordenite	clinoptilolite	Temp.	H <sub>2</sub> O released	Δ porosity	Extra Energy	H <sub>2</sub> O released	Δ porosity	Extra Energy	Δ porosity
(m)	wt%	wt%	(°C)	cm <sup>3</sup> /m <sup>3</sup>	%	Consumed %	cm <sup>3</sup> /m <sup>3</sup>	%	Consumed %	Clinoptilolite ⇒ Analcime %
100		3	51	125	0.04	1.32	125	0.04	1.32	0
150			65							
200			79							
250			92							
300			96							
350			106							
400		5	92	849	0.26	2.24	849	+0.26	2.24	0
450	11	63	79	8291	2.54	28.28	9739	+2.99	33.21	0
500	12	60	65	5932	1.82	27.79	7118	+2.18	33.35	0
550	5	50	55	3825	1.18	22.00	4208	+1.30	24.20	0

Notes:

1) Calculations on the consequences of heating clinoptilolite-bearing rocks at Yucca Mountain as a function of thermal loading. 2) Clinoptilolite abundances taken from USW G1, USW G3, and USW G4 and are in weight percent. In all calculations, the magnitude of the effect of dehydration on the unit volume of rock was determined by assuming zero porosity. Inclusion of the effect of initial porosity would decrease the values given for H<sub>2</sub>O released and Δ porosity. 3) The calculations are based upon the thermal response of Na-clinoptilolite as reported by Carey and Bish (1995a, b) and Bish (1984). 4) Temperatures are taken from the thermal log calculated at 1,000 years (Buscheck et al., 1994). 5) H<sub>2</sub>O released is calculated assuming that the maximum sustainable vapor pressure is 1 bar. 6) Δ porosity is calculated for the most significant volumetric change reported by Bish (1994) and represents an increase in porosity. 7) Extra energy consumed is calculated by considering the extra energy required to dehydrate clinoptilolite and implies a cooling effect. 8) A second calculation assumes that mordenite's behavior is similar to that of clinoptilolite to obtain a net effect of all zeolites. 9) The conversion of clinoptilolite to analcime was considered possible at T>96°C.

B00000000-01717-5705-00016 REV 00

3-64

01/31/96

Table 3.6-1. Effects of Hydrated Minerals (Continued)

Calculation based on USW G3										
Depth	mordenite	clinoptilolite	Temp.	Clinoptilolite Only			Clinoptilolite + Mordenite			
				H <sub>2</sub> O released	Δ porosity	Extra Energy	H <sub>2</sub> O released	Δ porosity	Extra Energy	Δ porosity
(m)	wt%	wt%	(°C)	cm <sup>3</sup> /m <sup>3</sup>	%	Consumed %	cm <sup>3</sup> /m <sup>3</sup>	%	Consumed %	Clinoptilolite ⇒ Analcime %
100			37							
150			46							
200			55							
250			65							
300			74							
350			82							
400			72							
450		1	62	132	0.04	0.45	132	+0.04	0.45	0
500			53							
550		30	47	2295	0.71	13.20	2295	+0.71	13.20	0
Calculation based on USW G4										
Depth	mordenite	clinoptilolite	Temp.	Clinoptilolite Only			Clinoptilolite + Mordenite			
				H <sub>2</sub> O released	Δ porosity	Extra Energy	H <sub>2</sub> O released	Δ porosity	Extra Energy	Δ porosity
(m)	wt%	wt%	(°C)	cm <sup>3</sup> /m <sup>3</sup>	%	Consumed %	cm <sup>3</sup> /m <sup>3</sup>	%	Consumed %	Clinoptilolite ⇒ Analcime %
100			37							
150			46							
200			55							
250			65							
300			74							
350			82							
400		28	72	4752	1.44	12.54	4752	1.44	12.54	0
450		77	62	10134	3.11	34.56	10134	3.11	34.56	0
500		45	53	4449	1.36	20.84	4449	1.36	20.84	0
550		10	47	765	0.24	4.40	765	0.24	4.40	0

Notes:

1) Calculations on the consequences of heating clinoptilolite-bearing rocks at Yucca Mountain as a function of thermal loading. 2) Clinoptilolite abundances taken from USW G1, USW G3, and USW G4 and are in weight percent. In all calculations, the magnitude of the effect of dehydration on the unit volume of rock was determined by assuming zero porosity. Inclusion of the effect of initial porosity would decrease the values given for H<sub>2</sub>O released and Δ porosity. 3) The calculations are based upon the thermal response of Na-clinoptilolite as reported by Carey and Bish (1995a, b) and Bish (1984). 4) Temperatures are taken from the thermal load calculations at 1,000 years (Buscheck et al., 1994). 5) H<sub>2</sub>O released is calculated assuming that the maximum sustainable vapor pressure is 1 bar. 6) Δ porosity is calculated for the most significant volumetric change reported by Bish (1994) and represents an increase in porosity. 7) Extra energy consumed is calculated by considering the extra energy required to dehydrate clinoptilolite and implies a cooling effect. 8) A second calculation assumes that mordenite's behavior is similar to that of clinoptilolite to obtain a net effect of all zeolites. 9) The conversion of clinoptilolite to analcime was considered possible at T>96°C.

The calculations are based upon the achievement of equilibrium at the temperature-depth relations given by Buscheck, Nitao, and Saterlie (1994) at 1000 years. In other words, the calculations predict what will have happened in the rocks if the model predicted temperatures are achieved. However, it should be noted that the geochemistry calculations are in fact not truly coupled. For example, rising temperature dehydrates zeolites and/or results in recrystallization, with a certain amount of heat being consumed as a result. The fact that this heat is consumed decreases the rates of temperature rise and possibly the final temperature achieved in the affected rock layers. This coupling was not considered in the calculations and the estimates are conservative in that they overestimate the amount of geochemical changes as one proceeds farther away from the potential repository horizon. The following list describes the parameters that have been calculated:

1. **H<sub>2</sub>O Released.** The amount of H<sub>2</sub>O (as liquid water) released from clinoptilolite in cm<sup>3</sup> of water per m<sup>3</sup> of rock. The calculation is based upon Carey and Bish (1995) and is based upon the difference in water content between clinoptilolite at 25°C and the temperature of interest assuming that the rocks are water saturated to 100°C and that water-vapor pressures remain at 1 atmosphere at higher temperatures.
2. **ΔPorosity.** As clinoptilolite dehydrates, its volume decreases. The increase in porosity of the rock mass caused by this change in volume is calculated from the data on Na-clinoptilolite given by Bish (1984). This is a bounding calculation, in that the volume change used is the most significant observed by Bish (1984) under anhydrous conditions. The results were obtained by calculating the percent change in volume of clinoptilolite between 25°C and the temperature of interest.
3. **Excess Energy Consumed.** Dehydration of clinoptilolite consumes thermal energy. This parameter is calculated as the additional energy required to dehydrate clinoptilolite compared to simply raising the temperature of rocks lacking hydrous minerals expressed as a percent. The calculation is derived from Bish and Carey (1995). As a further illustration of the effect of dehydration energy on thermal evolution, Figure 3.6-1 describing the thermohydrologic evolution of clinoptilolite is provided (Carey and Bish, 1995). This is a simplified model of thermal and hydrologic evolution in which a thermally insulated block of pure clinoptilolite receives a constant source of thermal energy. It is not a good model for the thermal evolution of zeolitic layers at Yucca Mountain (since these are not thermally insulated), but illustrates the effect of dehydration processes. In the model, a block or box has 10 percent porosity, is initially at 25°C, 100 percent relative humidity, and receives a thermal power of 14 watts (the value of the thermal flux is representative of those considered for Yucca Mountain). The thermal flux is consumed by the heat capacity of clinoptilolite and by dehydration processes. It is assumed that the box is porous to water vapor and a maximum pressure of 1 bar is maintained. The figure shows the results of these calculations comparing the thermal evolution of a box of clinoptilolite that does not dehydrate with one that does. There is a dramatic difference in the temperature evolution, because dehydration absorbs energy, thereby decreasing temperature rise. The box without dehydration reaches 395°C after 844 days, while the one with dehydration reaches only 250°C. The kink in the temperature evolution at 100°C is the point at which the pores attain the maximum water-vapor pressure of 1 bar.

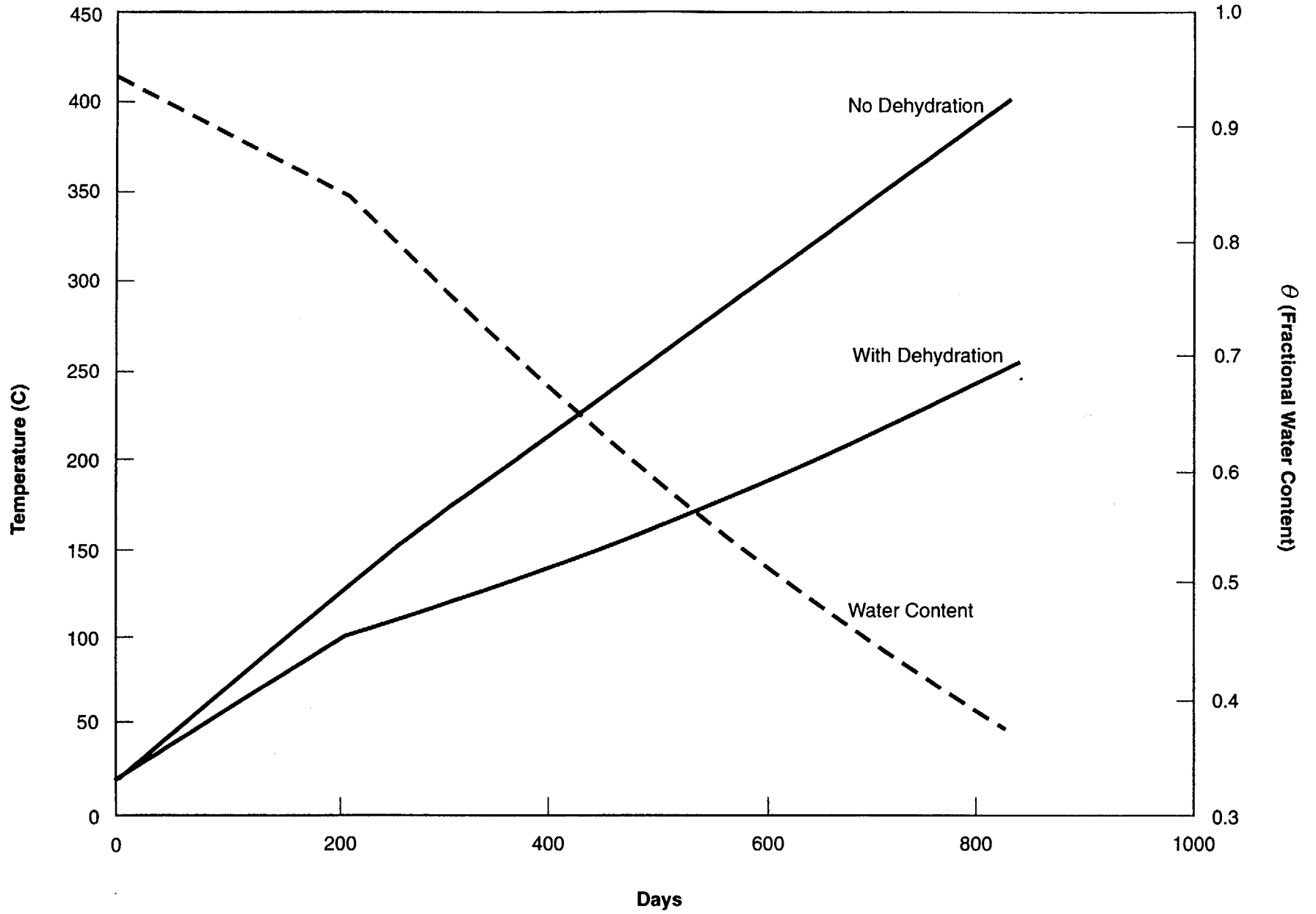


Figure 3.6-1. Temperature of Clinoptilolite With and Without Dehydration as a Function of Heating Time.

4. **Clinoptilolite⇒Analcime.** The breakdown of clinoptilolite to analcime would result in a significant increase in porosity. An estimate of the upper thermal stability of clinoptilolite under equilibrium conditions of approximately 95°C to 100°C (Smyth 1982) was used in the calculation.

There are other important hydrous minerals of Yucca Mountain that may have an impact on thermohydrologic evolution similar to that of clinoptilolite. These include mordenite and smectite. Mordenite may behave similarly to clinoptilolite and as a way of incorporating its effect, the table of calculations presents values in which the amount of mordenite and clinoptilolite are added together and the properties of clinoptilolite are used to calculate the effect on the thermohydrologic evolution. There is much more uncertainty concerning the properties of smectite, particularly the amount of water as a function of pressure and temperature and the energy associated with dehydration processes. At this time, it is not possible to make a reasonable estimate of the effect of smectite. Thus smectite was not considered in this evaluation.

An examination of Table 3.6-1 shows factors that may be important to waste isolation. Specifically, the concentrations of the zeolites are significantly different between the different boreholes. Borehole G-1 is just north of the block, G-4 is in the Lower Level of the Primary Block, and G-3 is south of the Primary Area. The measurements from G-3 are clearly the most different with lower concentrations of clinoptilolite and mordenite. Thus heterogeneity is an issue that must be resolved.

The estimates of the amount of water released show, as expected, a strong dependence on thermal loading. Significant amounts of water are lost from the zeolites at the higher thermal loads. Specifically, the maximum amount of water released from a cubic meter of rock containing clinoptilolite and mordenite is the range of  $1.6$  to  $2.5 \times 10^4$  cm<sup>3</sup> at the highest AMLs. This is an increase of 20 to 30 percent in the amount of water available to be released from the rock pores (assuming 10 percent porosity and 80 percent saturation) if all of the water in the rock pores is mobilized. Thus, the presence of zeolites could increase the amount of water available. An examination of the estimates of the amount of water released from the clinoptilolite based on USW G-1 core measurements show that the total water released per unit volume of rock at the AML of 27.3 kgU/m<sup>2</sup> is approximately a factor of three larger than the amount released at the AML of 8.9 kgU/m<sup>2</sup>. Estimates from other boreholes show similar results as a function of AML. The amount of water lost from the zeolites, the effect this water loss has on temperature, and where this water goes once mobilized could be significant to understanding waste isolation.

The ambient porosities in the zeolitized regions of host rock vary from about 5 to around 20 percent. Examination of Table 3.6-1 shows that the increase in porosity as a result of the water loss can be appreciable at the higher thermal loads. On the positive side this increase in porosity may provide some volume for storage of the water that is released from the zeolites. However, a concern is that the rock shrinkage could produce a network of microfractures which may increase permeability and thus enhance water transport. The recrystallization of clinoptilolite to analcime produces a significant increase in porosity (about 10 to 15 percent at the higher thermal loads). This could exacerbate the production of fractures. Investigation of this issue needs to be done to examine the behavior of zeolitized rock before, during, and after heating to assess its potential impact on waste isolation.

Full, numerical calculations of the interaction between repository heat and hydrous minerals in a realistic model of Yucca Mountain should be done. In-situ and laboratory tests should examine the issues discussed above and develop data necessary to validate such realistic models.

This analysis found that potentially important geochemical changes occur as a result of thermal loading which may produce significant impacts on the hydrology and mechanical properties. For example, a potential 20 to 30 percent increase in the amount of water available for transport from zeolitized regimes results due to dehydration of the zeolites at the highest thermal loads.

Additionally, porosity changes of up to 10 to 15 percent occur in the rock at the highest thermal loadings as a result of the irreversible change from clinoptilolite to analcime. These changes absorb energy as well. For the most part these effects are occurring in the CH stratigraphic layers. As a consequence, understanding these effects are likely to require in-situ thermal tests in CH if a high thermal loading is to be implemented.

### **3.7 THE EFFECT OF ELEVATION VARIATIONS ON THERMAL PERFORMANCE**

Section 2 discussed the fact that the potential repository horizon is not at a constant depth in the mountain with respect to the distance to the surface or the water table, and this could potentially affect the thermal performance. The distance to the surface, and the distance to various stratigraphic units and the water table, varies from place to place in the Primary Area of the potential repository and in some of the alternate areas under consideration for waste disposal. The nominal overburden, which was considered in the FY 1993 study, was 343 m. However, the overburden can be as little as 200 m to as much as 430 m within the Primary Area (Section 2). The predicted hydrothermal behavior of the host rock for various thermal loads can change under conditions where the overburden or distance to the water table differs from the nominal case. The performance of the potential repository could change under these conditions. An evaluation of this was done during the reporting period, and a brief summary of the results are presented in this section. The complete analysis and a more detailed discussion of the methodology can be found in the interim report (M&O, 1994d).

This evaluation utilized the VTOUGH hydrothermal model to make predictions of the behavior as a function of time. The code did not model the dipping of the repository drifts and the stratigraphic units in a three-dimensional sense. Instead, the simulations were done assuming that all the waste was emplaced at that depth with a constant overburden and distance to the water table. These simplified estimates should provide only an indication as to whether or not there is some sensitivity in the hydrothermal behavior to a change in location in the potential repository and hence depth to various units. Analysis of the thermohydrologic response of an actual three-dimensional repository with variable topography will require a three-dimensional model.

The calculations shown in this section were all made with a bulk permeability of  $2.80 \times 10^{-13} \text{ m}^2$  (280 millidarcy) in TSW2 as was used in the FY 1993 study. For the different depths, the corresponding ambient temperatures and liquid saturations for those depths were selected from the values shown in Figures 3.7-1 and 3.7-2 as the initial input to the calculations. However, if the stratigraphy changes, the ambient values also could change in a more complex manner as a function of depth. For these initial calculations, no reinitialization was attempted to account for differences in stratigraphy with location in the Primary Area since this was a scoping calculation

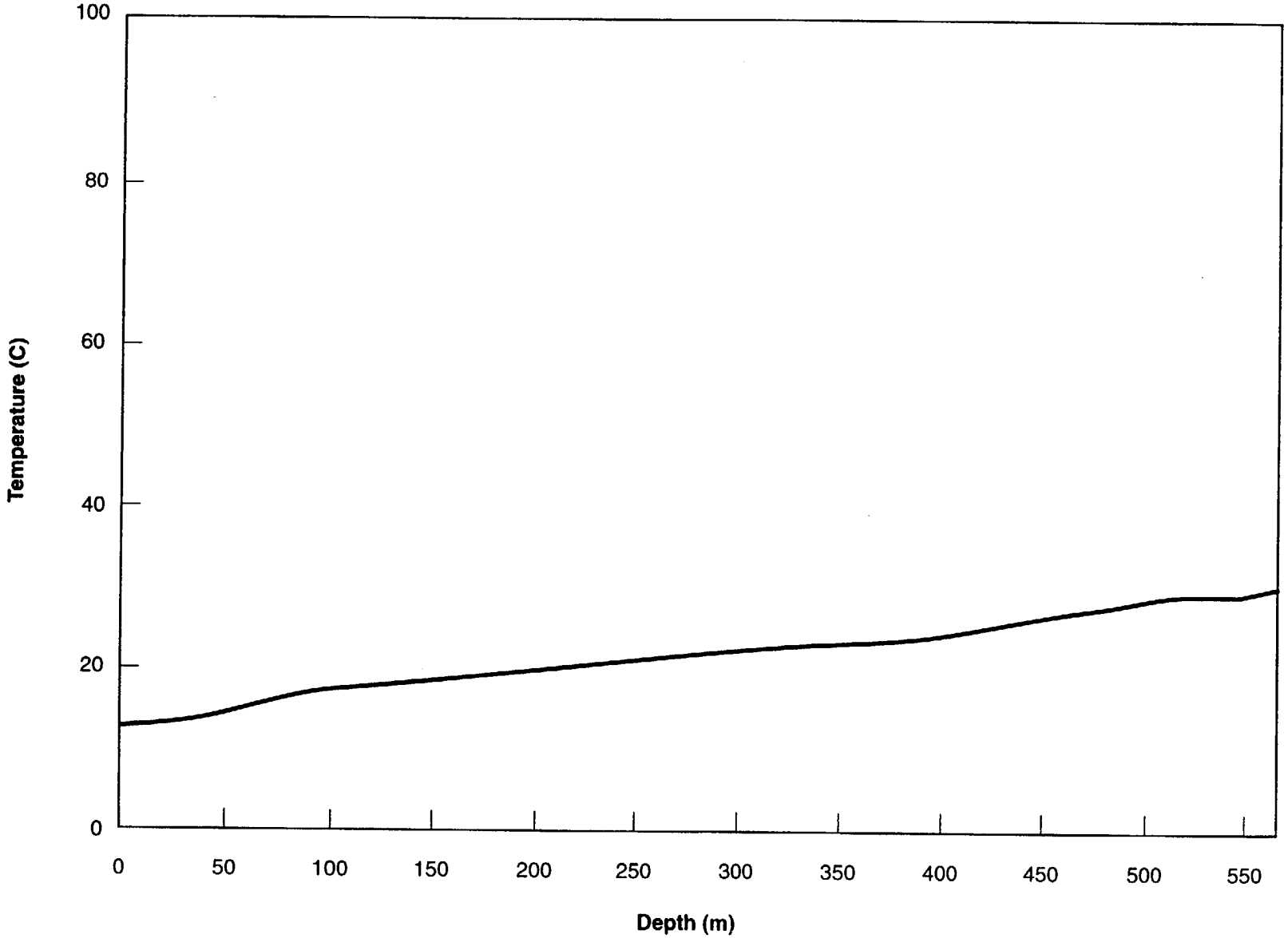


Figure 3.7-1. Ambient Geothermal Gradient.

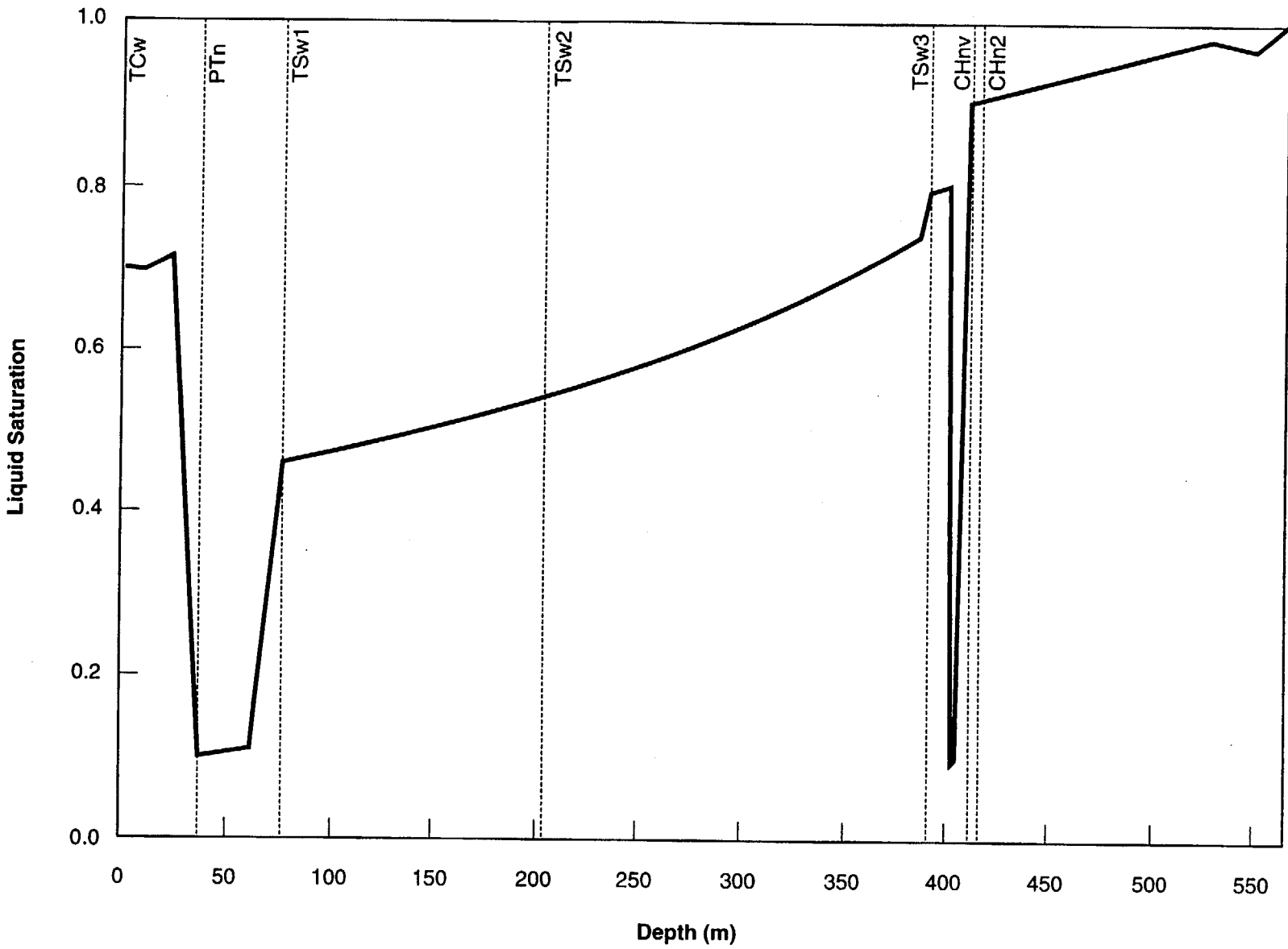


Figure 3.7-2. Ambient Liquid Saturation.

to determine whether sensitivities existed and varying more than one parameter at a time would have made interpretation more difficult. Thus the actual magnitudes calculated may change and only the trends should be considered in these results.

Calculations were done at AMLs of 27.4, 20.5, 13.6, and 5.9 kgU/m<sup>2</sup> (111, 83, 55, and 24 MTU/acre) and the results can be found in M&O, 1994d. For illustration the results from the 27.4 kgU/m<sup>2</sup> are provided in this report. The calculations of the vertical temperature and liquid saturation changes as a function of time for the baseline case can be found in the interim study reference or in Figure 3.2-1 of Section 3.2. However, those calculations were done with YFF(10) fuel. As discussed in Section 3.2, the base case fuel has been changed by the program to OFF. The far-field, mountain-scale calculations run for the different depths used OFF fuel characteristics. The differences in fuels should have little impact on the far-field, long-term hydrothermal behavior (Buscheck and Nitao, 1994).

The differences in temperatures and saturations can best be demonstrated by a comparison of Figures 3.7-3 and 3.7-4 which show the calculated vertical temperatures and liquid saturations for the 27.4 kgU/m<sup>2</sup> case and repository horizon depths of 200 and 430 m respectively. The calculations are shown at times of 1000, 10,000, and about 30,000 years and are shown for three radial locations. The comparisons of the two figures show that the deeper repository stays hotter longer than the shallower repository. The differences at 10,000 years in the repository center can amount to about 30°C. These temperature differences continue to times beyond 10,000 years. These peak temperature predictions are summarized in Table 3.7-1.

The hydrologic behavior is also influenced somewhat by the depth of burial. In particular, the rewetting seems to be enhanced for the deeper repository. This is likely due to the proximity to the water table. The faster rewetting at the 430 m depth is evident at 30,000 years in the center of the repository and at earlier times it can be observed in the outer areas of the repository.

Table 3.7-1. Predicted Peak Temperatures as a Function of Depth of Overburden for three times

Temperature (°C) <sup>1</sup>			
Depth	1000 years	10,000 years	30,000+ years
200 m	170	70	45
Nominal (343 m)	172	88	49
430 m	175	97	60

<sup>1</sup> Temperature predictions are for the center of the repository.

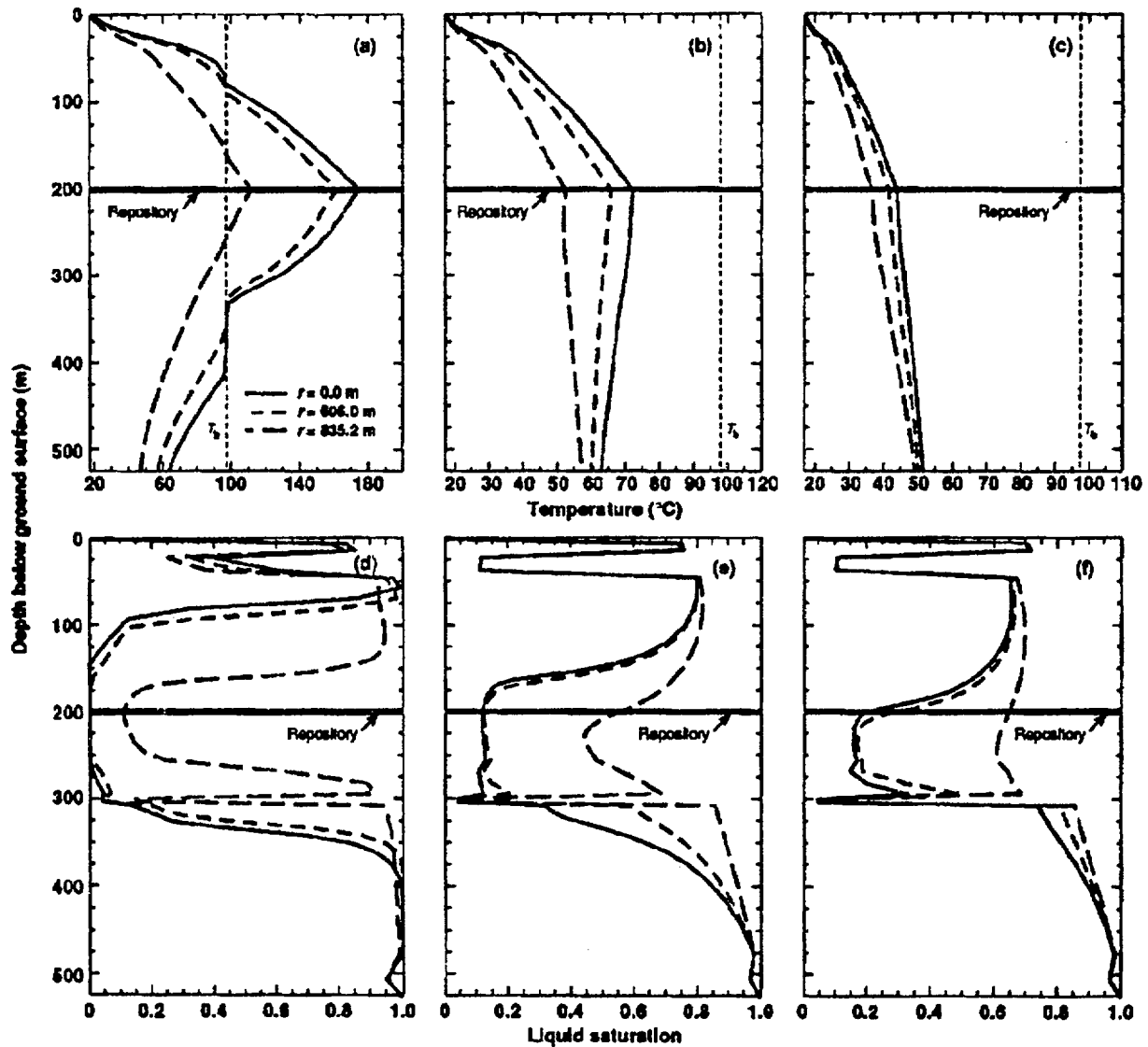


Figure 3.7-3. Vertical Temperature Profiles at Various Radial Distances,  $r$ , from Repository Centerline for  $k_b = 280$  millidarcy, a 200 m Thick Overburden, and an AML of  $27.4 \text{ kgU/m}^2$  at (a)  $t = 1,000 \text{ yr}$ ; (b)  $t = 10,000 \text{ yr}$ ; and (c)  $t = 32,730 \text{ yr}$ . Note different temperature scales. Vertical liquid saturation profiles are also plotted at (d)  $t = 1,000 \text{ yr}$ ; (e)  $t = 10,000 \text{ yr}$ ; and (f)  $t = 32,700 \text{ yr}$ .

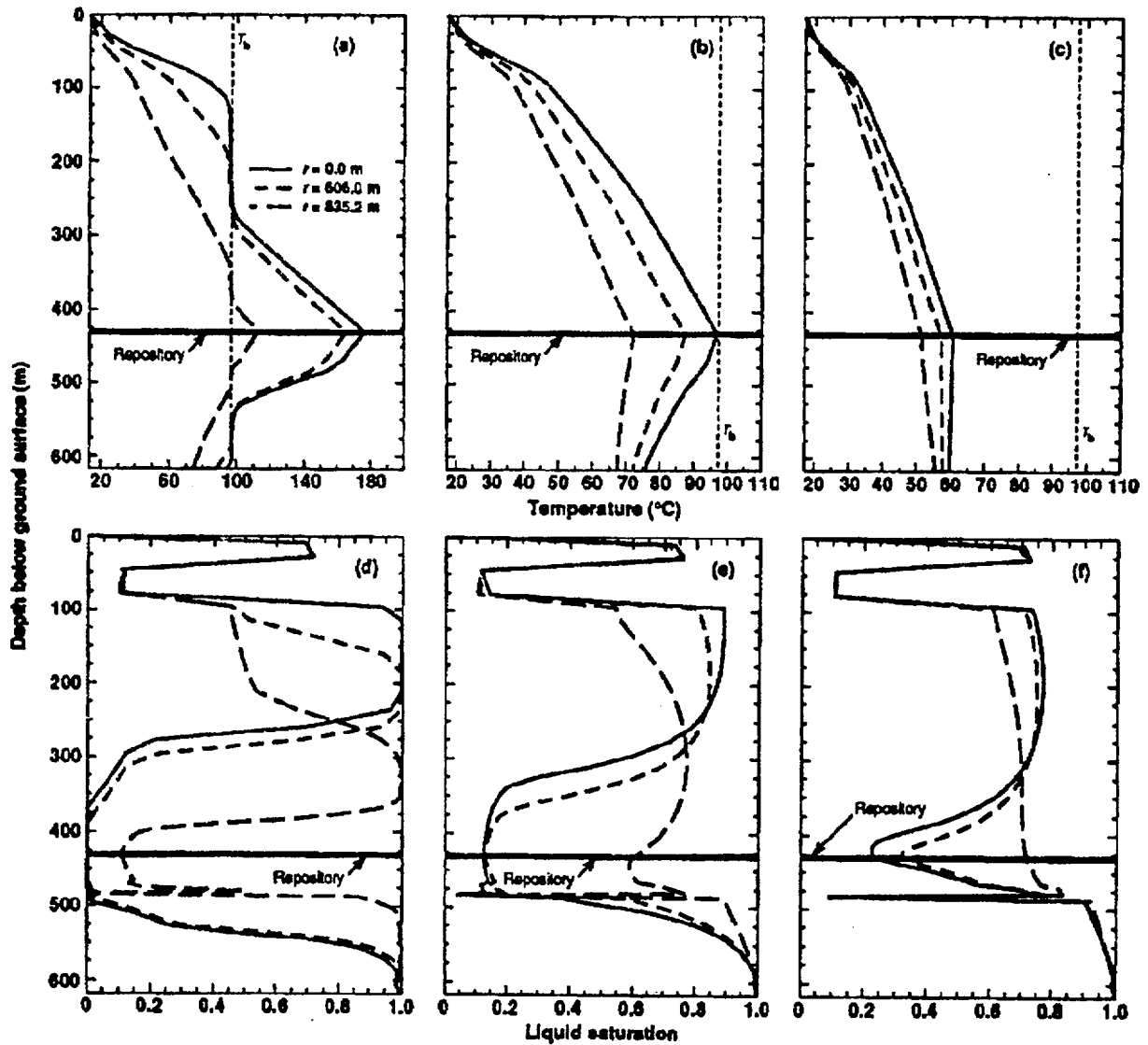


Figure 3.7-4. Vertical Temperature Profiles at Various Radial Distances,  $r$ , from Repository Centerline for  $k_b = 280$  millidarcy, a 430 m Thick Overburden, and an AML of  $27.4 \text{ kgU/m}^2$  at (a)  $t = 1,000 \text{ yr}$ ; (b)  $t = 10,000 \text{ yr}$ ; and (c)  $t = 31,680 \text{ yr}$ . Note different temperature scales. Vertical liquid saturation profiles are also plotted at (d)  $t = 1,000 \text{ yr}$ ; (e)  $t = 10,000 \text{ yr}$ ; and (f)  $t = 31,680 \text{ yr}$ .

In summary, the temperature and liquid saturation conditions in the potential repository were found to depend significantly on the depth of burial of the waste. In particular, the shallower portions of the repository were found to cool significantly faster than the areas with more overburden. The deeper areas, on the other hand, tend to rewet faster due to the proximity to the water table. Although not calculated here, relative humidities at the repository horizon would reflect these differences. Calculations also were done for the lower AMLs and, although not presented here, essentially negligible differences in temperature and liquid saturation were predicted for the 5.9 kgU/m<sup>2</sup> (24 MTU/acre) case. Some care must be taken in using these results since the three-dimensional nature was not considered and, as shown in Section 3.2, the three-dimensional features can affect the temperature and hydrology.

Since the Yucca Mountain Project (YMP) is emphasizing a high thermal loading as the reference design thermal loading, the depth of burial appears to be of importance. All of the range of depths (200 m to 430 m overburden) considered in this section can occur in the primary emplacement area being considered at this time. It is doubtful that tests can be run to evaluate this since these differences occur at very late times, but this effect should be considered in the design analysis and TSPA evaluations.

### **3.8 THERMOMECHANICAL EVALUATIONS**

Drift stability is an important performance issue, particularly for the concept of a waste package in an open drift. Drift stability is both a preclosure and postclosure issue. Specifically, preclosure worker safety and waste package retrievability can be affected by drift stability. Drift stability and the potential for rockfall, which might damage a waste package or the potential formation of cracks and upheaval of rock masses, which may alter the hydrologic performance of the repository, are important postclosure issues. Thermal loading is important since the addition of heat alters rock stress and may affect drift stability. Thus the coupled effects between thermal and mechanical behavior are important to understand. The thermomechanical calculations initiated for the thermal loading study are discussed in this section. The details of the analysis and a more comprehensive set of calculations can be found in the interim report of this study (M&O, 1994d).

When a drift is excavated in a rock mass, the introduction of the boundary surfaces (drift walls) reduces the traction on them from that corresponding to the natural state of stress to zero. Such traction reduction changes the stress state in the host rock around the drift and the displacements in the vicinity of the excavation. Furthermore, rock blocks of a highly fractured rock mass may dislocate from each other. Fractures in the rock mass may be extended or initiated, and existing fractures can be opened or closed by the change of the stress state. Thermally induced stresses in rock can enhance these responses. In a two- or three-dimensional mechanical system, fracture closure can be generated by high thermal stress in one horizontal direction, when the displacement is more confined in this direction than in the vertical direction. Fracture closure in one direction may induce fracture opening in other directions because of the rigid body motion of rock blocks. During rapid cooling of a repository drift, performed for the retrieval of the waste packages, the volume of rock blocks decreases with the decreasing temperature. Since the displacement boundary condition of the system does not change, and the movement of rock blocks is not reversible upon the addition and removal of heat, the fracture size in the rock mass may increase during the temperature reduction stage.

To assess the drift stability, thermomechanical analyses, using the numerical code Discontinuous Deformation Analysis (DDA), were initiated to support the thermal loading study. The opening and closing of fracture apertures in the vicinity of a waste emplacement drift, together with the induced stress state, are used to provide information for assessing the stability of the unsupported drift. Since the DDA code cannot model the initiation of new fractures (cracking) because of the change of stress state, only the dislocation and the opening/closing of existing fractures are simulated. The theoretical detail and the formulations of the DDA code can be found in Shi (1993) and Tsai (1993). Additional discussion of the details of the calculations is found in M&O, 1994d.

The thermomechanical analyses, which examined the mechanical behavior of the rock blocks, were done using inputs of calculations of near-field temperatures as a function of time predicted for each block. The predicted mechanical response of rock blocks caused by temperature changes is the variation of block strains. When the potential energy corresponding to the stress perturbation is taken into account for obtaining the dynamic equilibrium condition of the system, movements (deformations, rotations, and translations) of blocks generated by the thermal loads are induced. Since the material domain of the DDA simulations extends to 20 m above and below the drift, there should be negligible effect of this boundary condition on the rock deformation around the drift.

Input information about the jointed-rock pattern, in-situ stress condition, and the material properties of intact rock and rock joints are adopted from the YMP RIB (DOE, 1994) and a YMP report (Lin et al., 1993). Some modifications to the above-described information are made to obtain a simple model that can be reasonably analyzed using the DDA code. Nonlinear thermal expansion coefficients for the rock blocks are adopted from the preliminary results of a laboratory test performed by SNL (Chocas, 1994). The specimen used for this laboratory test was taken from borehole USW NRG-6 at the Yucca Mountain site. Over the temperature ranges considered, the expansion coefficients do not change much with temperature from the constant value of about 10 ppm/°C used in past calculations.

Four computer runs were conducted using the DDA method to investigate the effects of drift size and thermal load on the stability of the unsupported emplacement drift. Table 3.8-1 shows the identification of these computer runs. For a given thermal load expressed by the value of AML, the drift spacing must be adjusted according to the chosen waste package spacing. Therefore, only three drift layouts are needed for these four computer runs. The AML values listed in Table 3.8-1 were computed using average BWR and PWR fuel and the YFF(10) fuel characteristics (using a conversion of 1.03 kW/MTU) discussed by M&O, 1994c. For example, 27.4 kgU/m<sup>2</sup> (111 MTU/acre) is equivalent to 28.2 W/m<sup>2</sup> (114 kW/acre), and 20.5 kgU/m<sup>2</sup> (83 MTU/acre) is equivalent to 21.0 W/m<sup>2</sup> (85 kW/acre). For the thermomechanical calculations, the hotter YFF(10) fuel provides a more conservative estimate of mechanical response than OFF. However, it should be noted there will be areas where, even for the OFF scenario, localized hot spots could be hotter than the YFF(10) averages as a result of fuel variability. This is a parametric analysis with various drift sizes and spacings that do not necessarily correspond to the current repository subsurface conceptual design.

Table 3.8-1. Computer Run Identification

Run ID	AML (kg U/m <sup>2</sup> )	Drift Diameter (m)	Drift Spacing (m)	Waste Package Spacing (m)	Time (years)
#1	20.5	4.3	27.38	16.0	100
#2	27.4	4.3	20.48	16.0	100
#3	20.5	7.0	23.30	18.8	100
#4	27.4	7.0	23.30	14.0	100

The case run at 27.4 kgU/m<sup>2</sup> (111 MTU/acre) was higher than the 24.7 kgU/m<sup>2</sup> (100 MTU/acre), identified in the FY 1993 Thermal Loading Study (M&O, 1994c) as a potential upper limit for the thermal loading. Minimal thermal mechanical calculations were done in that study. Thus, it was decided to choose the higher AML value of 27.4 kgU/m<sup>2</sup> to determine if a potential problem in rock stability might exist at that level. This was done to ensure that the study would be able to identify AMLs where problems might occur.

As a part of input data for studies reported here, predicted 100-year post-emplacement temperatures were used at the center of each rock block in the deformed mesh generated by the excavation simulation for all runs identified in Table 3.8-1. The thermal profiles as a function of distance into the rock are shown for two of the four cases in Figure 3.8-1.

If the retrieval of waste canisters is required, it will be necessary to cool the air temperature in the drift by ventilation (rapid cooling) to facilitate the retrieval operation. The temperature distribution in the host rock during the retrieval operation is a function of the time history of the drift air temperature. Some limited ventilation studies have been done (Svalstad and Brandshaug [1983], Danko and Mousset-Jones [1993], and an M&O study [1993b]). Based on the work of Svalstad and Brandshaug (1983), it was decided that ventilation would be applied until the temperature of the drift walls reached 43°C. The thermal profiles into the rock for this case are also shown in Figure 3.8-1. The thermal profiles after cooling shown in the figure were produced by applying a boundary condition of 43°C<sup>7</sup> at the drift wall and then calculating the temperature decay for a given period using a conduction model. This simulation was done only to evaluate if forced cooling would cause a significant change in the rock stresses. It was not intended as a completely accurate representation of what cooling would do.

The stress distribution of the initial loading simulation (after excavation) is shown in Figure 3.8-2. These predictions indicate that the stress concentration around the drift after excavation forms a pressure arch, which makes the drift opening structurally stable. Except for

<sup>7</sup> In the ventilation study by Svalstad and Brandshaug (1983), their calculations maintained an air temperature of 26°C with a drift wall temperature of 43°C. This may be significant from a standpoint of worker safety to enter an emplacement drift, although this is unlikely given current designs. The wet bulb globe temperature (WBGT) is a physiological heat stress index adopted by the National Institute of Occupational Safety and Health (NIOSH) which reflects the combination of air temperature, humidity, radiation, and wind speed. A WBGT of no higher than 26°C should be maintained for worker stress control according to 1972 NIOSH regulations.

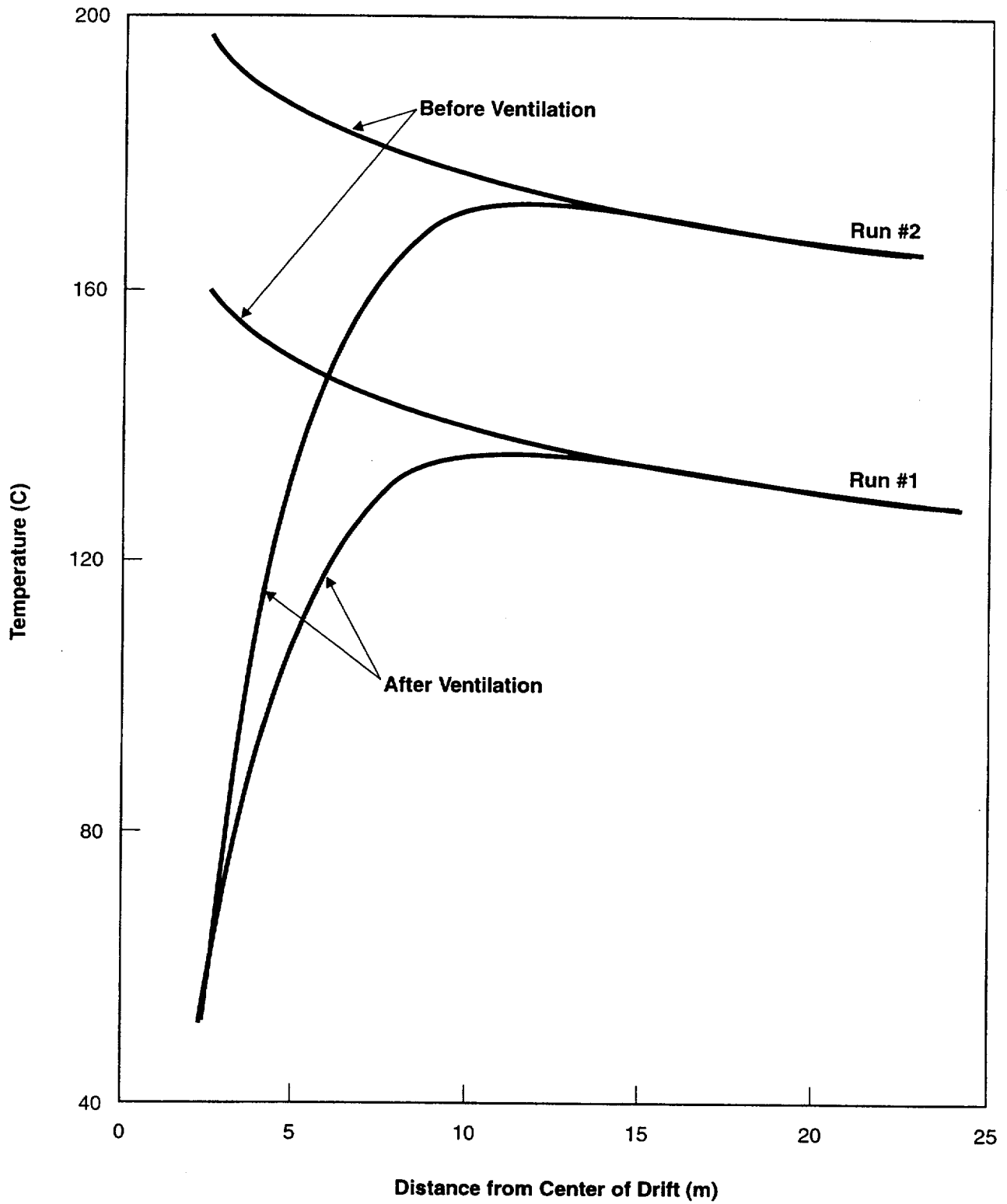
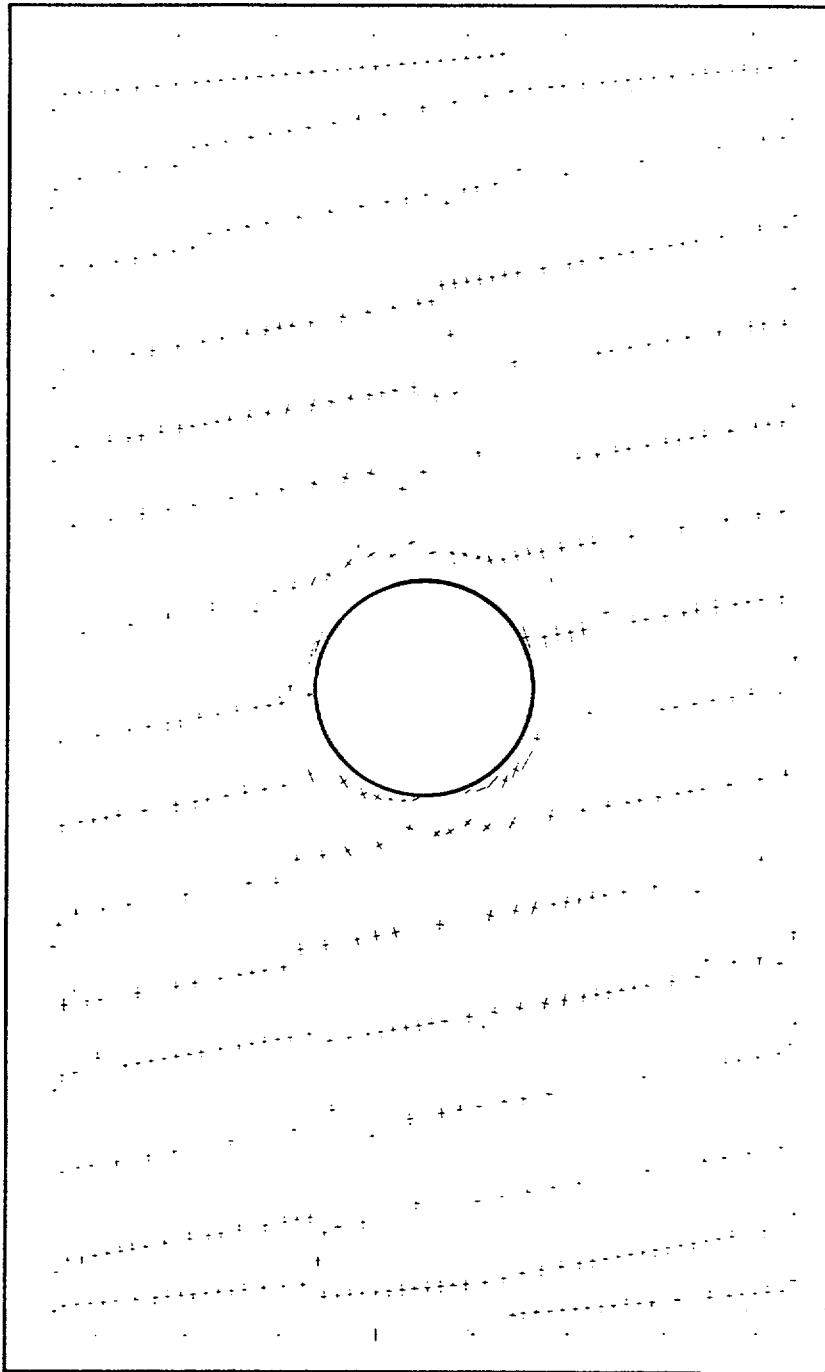


Figure 3.8-1. Temperature Profile for Runs #1 and #2.



Scale: 100MPa 

Figure 3.8-2. Principal Stresses After Excavation for Run #4.

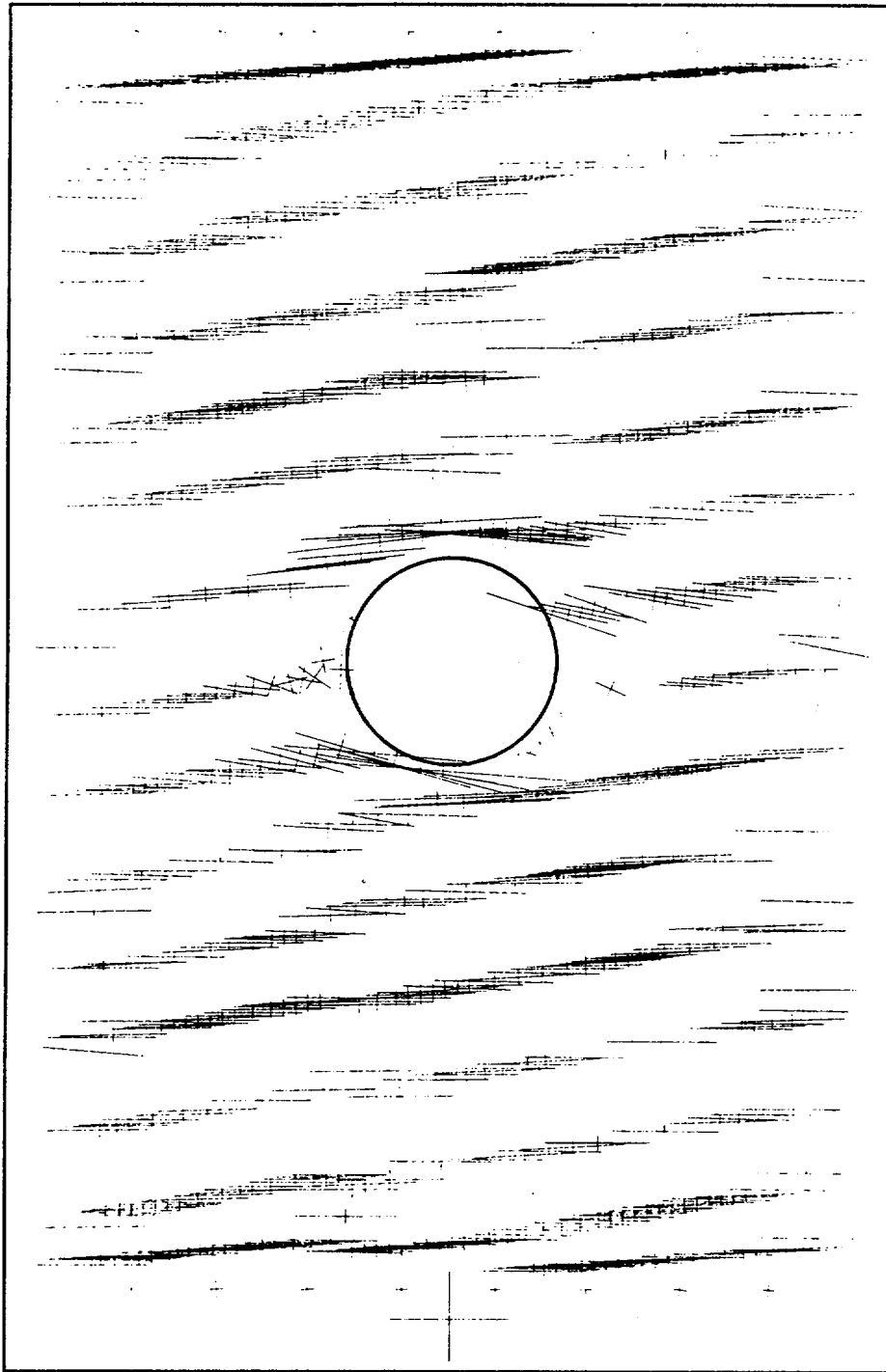
joints formed by a few rock wedges at the upper left and the lower right corners of the drift, the size of joint openings (not shown here but discussed in M&O, 1994d) in the immediate area into the drift wall is on the order of 0.01 mm or less. The vertical and horizontal drift closures after excavation are about 1.6 mm and 0.3 mm, respectively.

Figure 3.8-3 shows the final stress distributions and joint openings after thermal loading. The vertical stresses after thermal loading in all blocks remain close to their initial values (6.5 to 7.4 MPa) due to allowable upward rock mass thermal expansion. The horizontal stresses after thermal loading are significantly increased over the entire mesh because of the fixed lateral displacement boundary condition on both sides of the mesh. In general, the horizontal stresses in the rock mass at a few meters away from the drift are about 55 to 60 MPa. The model with fixed lateral displacement boundary conditions represents the center of the repository only. At the edge of the repository, thermal -induced horizontal stress is lower than at the center of the emplacement area because the heated area is less (no heat source beyond the edge). The model also allows a certain amount of lateral expansion and so lower horizontal stresses can build up. It is conservative in that it does not account for stress relief at fault zones or due to the lower topography to the east and west of the potential repository Primary Area. Accurate determination of the stress distributions at and beyond the edge will require three-dimensional analysis.

The major principal stress may reach 90 MPa in the immediate area around the drift. With this high principal stress in the jointed rock mass immediately around the drift, rock spalling may occur in the drift walls. The large horizontal joint openings (not shown) after thermal loading in the rock mass immediately around the drift wall suggest that some rock wedges at the drift wall may become detached. The openings of horizontal joints are about 0.2 to 0.7 mm (20 to 70 times larger than those produced by excavation) in the area within about 10 m radius from the drift wall. In general, all of the vertical joints remain closed under the thermal loads. In contrast to the 1.6 mm vertical drift closure and 0.3 mm horizontal drift closure generated after excavation, the drift height measured through the center of the drift increases (expands) 13.4 mm, and the drift width measured through the center of the drift closes another 13.3 mm after thermal loading. Thermal loading also raises the top of the modeled rock mass 83.2 mm.

Calculations were done, at 20 m above the drift, for conditions of rapid cooling and the results indicate that the rapid cooling causes the top of the modeled rock mass to subside by 5.8 mm. Except at the corners of the roof and floor, the pressure arch in the rock mass immediately surrounding the drift remains, and the drift is generally stable. However, the large joint openings immediately surrounding the drift suggest that small rockfall may be encountered after the rapid cooling.

Estimates of rock stability were done by Tsai (M&O, 1994d) using rock strength criterion specified in the RIB (DOE, 1994). The estimates of horizontal rock mass strength, based on this criterion, were found to be about 49 MPa. The predicted horizontal stresses after thermal loading in the area a few meters away from the drift were found to be 53 and 55 MPa respectively for Runs #2 and #4 (the two 27.4 kgU/m<sup>2</sup> [111 MTU/acre] cases). This indicates a potential for rock stability problems that must be considered. The 20.5 kgU/m<sup>2</sup> (83 MTU/acre) cases (Runs #1 and #3) have stresses that do not exceed the criteria identified above. However, there are stress conditions (the tangential stress) at this thermal load that exceed the criteria and could result in



Scale: 100MPa 

Figure 3.8-3. Principal Stresses After Thermal Loading for Run #4.

some local rock spalling. Thus, somewhere between 20.5 and 27.4 kgU/m<sup>2</sup> (83 and 111 MTU/acre), rock stability may begin to be a problem and may even be a problem at 20.5 kgU/m<sup>2</sup> in terms of requiring some form of tunnel support. For these higher thermal loads, remediation of these potential stability problems, by the use of stabilizing methods such as rock bolts and/or tunnel liners, should be examined by Subsurface Design. These solutions could affect costs as well as performance.

The calculations do not indicate whether or not potential stability problems would result in a rockfall of any significance. For an emplacement drift, transient dynamic analyses (M&O, 1995g) show that quite a large rock of about 3.4 m diameter with mass of  $4.8 \times 10^4$  kg would be required to damage a 12 PWR size MPC. About half that size rock would be needed to damage a 21 PWR MPC, although calculations were not done for that case.

It should be noted that the DDA code predicts tunnel stability problems because of opening of horizontal joints during heating. Vertical joints will tend to close during heating and the stability problems may not occur as predicted. This code and this kind of scoping analysis only indicates the potential for problems. The calculations have some degree of conservatism in them. Based on measurements, the degree of conservatism needed for design can be established so that an over design is not done.

In summary, thermomechanical issues related to tunnel stability are important considerations at the higher thermal loads. In-situ testing to establish the rock strength will be needed. For example, demonstration of a margin of safety will almost certainly require that an area of tunnel ceiling be heated sufficiently that the temperatures exceed the peak anticipated temperatures. For example, the current drift wall thermal goal is not to exceed 200°C (M&O, a). The designs should be conservative so that tunnel walls will not reach this temperature. Thus, the tunnel should be heated to at least 200°C to provide sufficient thermomechanical data.

It should be noted that the above discussion concerned rock stability only, not hydrologic impacts. The increase or decrease in size of the fractures, depending on location, and the upward expansion (heaving) of the rocks could result in perturbations to the hydrologic system. These aspects need to be investigated further in the in-situ tests and the changes in fracture sizes and number as a result of heating should be measured.

## 4. THERMAL MANAGEMENT EVALUATIONS

Preliminary evaluations of selected thermal management issues were done in the study to assess feasibility and advantages/disadvantages. Thermal management could provide enhanced flexibility, provide for ease or increased safety of operations, and/or may provide for mitigation of risk for the potential repository. More detailed assessment of whether or not to consider a thermal management option in design of the potential repository needs to be done in a systems study where tradeoffs of the various options are considered. This section provides evaluations of several thermal management options including ventilation, use of expansion areas, nonuniform AML, line load variations, repository response to waste stream variability, and aging of spent nuclear fuel using interim storage.

### 4.1 VENTILATION ANALYSIS

Questions have been asked as to whether ventilation could be used to make a high AML repository perform like a low AML repository. From a postclosure standpoint, for a repository which is closed after 100 years, the answer is an emphatic no. However, from a preclosure standpoint for operation and monitoring, ventilation could be used to remove a significant portion of the heat load and mobilized moisture. Some studies (Danko, 1992; Danko and Mousset-Jones, 1992; Yang and Bhattacharya, 1994; and M&O, 1995k) have analyzed ventilation as a thermal management technique to modify the performance of the EBS; however, these studies only considered the effect of dry air flow. However, moisture taken out in the ventilation air can also remove a significant amount of latent heat. This study developed the technique of calculating the amount of heat and moisture removed by coupling a thermohydrology model with a ventilation model. This effort was a joint venture between University of Nevada, Reno, LLNL, and TRW.

Realistic calculations of the psychrometric environment in a potential repository requires an understanding of the amount of heat and moisture that is removed from the emplacement drifts and the near-field rock by ventilation. To do this, the LLNL Nonisothermal Unsaturated-Saturated Flow and Transport (NUFT) code for the hydrothermal calculations in the near-field was coupled with the Mackay Thermal Enhancement and Climate Simulation (MTECS) model (Danko, 1992; Danko and Mousset-Jones, 1992; Danko and Mousset-Jones, 1993; and Danko, 1994). The NUFT code is a suite of multiphase, multicomponent models for numerical simulation of non-isothermal flow and transport in porous media (Nitao, 1995 and Wilgus, 1995). The combination of the two models produces calculations of the hydrothermal behavior of the near-field rock mass, including heat and moisture transport, the behavior at the rock-air interface, and the dilution of water vapor in the drift air flow and subsequent transport out of the system. The coupled codes provide three-dimensional, time-dependent calculations of the heat and moisture transport.

A discussion of the details of coupling the models can be found in the paper by Danko, Buscheck, Nitao, and Saterlie (1995). The work reported in the paper used the VTOUGH code, but the recent work reported in this section was updated using the NUFT code. The boundary conditions discussed in the paper are applicable to either VTOUGH or NUFT.

A set of ventilation calculations was made for a single, 1,232-m drift in the center of a potential repository. The emplacement drifts were 5 m in diameter and the waste packages were emplaced on the floor of the drift with a spacing of 16 m. A cutaway view of the emplacement drift with the waste packages showing the thermal interactions between the containers, the drift wall, and the ventilating air is shown in Figure 4.1-1. Eight cases using different AMLs and different waste package and drift spacings were considered initially in the Danko, Buscheck, Nitao, and Saterlie (1995) work. These eight cases are shown in Table 4.1-1. With the limited time remaining after the coupling work was done and the codes "debugged" only one case, Case E, was run; this case, which has an AML of 20.6 kgU/m<sup>2</sup> (83 MTU/acre), is reported here.

Table 4.1-1. Areal Mass Load, Waste Package and Drift Spacing

	A	C	E	G	I	K	M	O
Areal mass loading (kg U/m <sup>2</sup> ) [MTU/acre]	6.2 [25]	8.9 [36]	20.6 [83]	6.2 [25]	8.9 [36]	20.6 [83]	6.2 [25]	8.9 [36]
Number of waste packages	67	67	67	31	37	56	21	29
Waste package spacing (m)	16	16	16	34.9	29.1	19.1	52.9	36.7
Number of drifts left of center	16	24	55	36	43	66	55	55
Drift spacing (m)	76	52.8	22.9	34.9	29.1	19.1	23	23

The calculations used large waste packages (21 PWR capacity) filled with PWR fuel that had OFF characteristics with an average age of about 26 years (see Section 2 for details of this fuel). The waste packages were 5 m long with a diameter of 1.2 m and they were considered as a smeared heat source within those dimensions. The emplacement drift length was divided into 16 m long calculational segments and the results were calculated from a segment from the first (designated EP#1), first quarter (EP#20), middle (EP#39), third quarter (EP#58), and end (EP#77) of a 1232 m long emplacement drift. Within a particular segment the thermal hydrologic calculations were done for 1 m long segments and only the average of the sixteen temperature and moisture fluxes are reported. Further details of the boundary conditions can be found in Danko, Buscheck, Nitao, and Saterlie (1995).

Three airflow rates of 0 (base case of no ventilation), 1, and 10 m<sup>3</sup>/s were planned for the calculations, but only the base case and the one for 10 m<sup>3</sup>/s were completed. However, a scoping calculation was done to determine how much flow might occur if the drifts were not sealed. It should be noted that 10 m<sup>3</sup>/s corresponds to an airflow of about 0.5 m/s in the drift which is typically borderline between forced and natural convection in underground mines and should be easy to achieve. The air inlet temperature was 26°C and the water vapor pressure in the entering air was 1024 Pa, which implies about a 30 percent relative humidity.

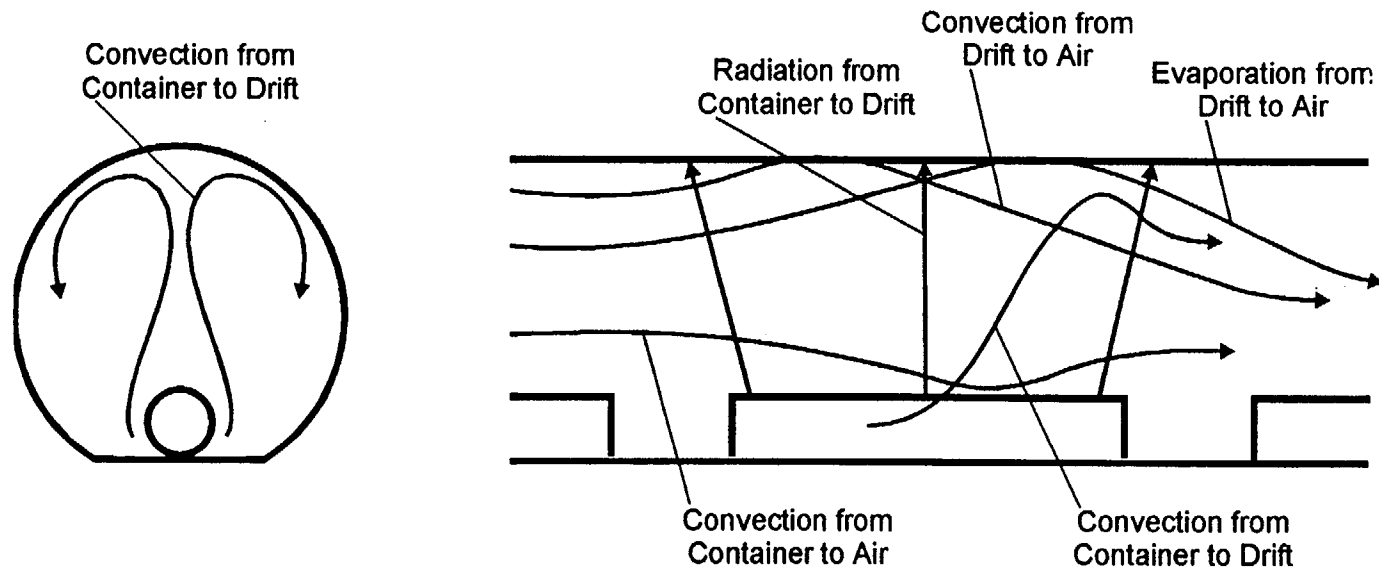


Figure 4.1-1. Container Emplacement With the Thermal Interactions.

The relative humidity at the surface can be drier but this allows for some pickup of moisture as the air is pumped to the emplacement drifts. The 30 percent value also provides a conservative value for the calculations. Calculations were done at various times from the start of emplacement to repository closure at 100 years.

In the following discussion, various examples of the kinds of information available from the calculations are presented. Figure 4.1-2 displays calculations of air temperature as a function of tunnel length for four different times up to 100 years after emplacement. The first curve at 0.5 years shows that the temperature stays relatively constant. At 0.5 years the walls have had little chance to heat up and so the air does not heat up much as it passes through the drift. The variations in temperature of about a degree probably are due to calculational uncertainties. In later years the air temperature shows the expected increase in temperature of 8°C to 10°C as it proceeds down the drift to the exit. The air temperature tends to peak somewhere around 50 years and by 100 years has decreased somewhat. At all times during the preclosure period for this high AML case the ventilation rate was found to keep the air temperature below 40°C compared to the no-ventilation case where air temperatures exceeded 170°C. This would provide an environment where engines could operate since the current requirement for retrieval operations in emplacement drifts is 50°C (M&O, 1995a). Correspondingly, Figure 4.1-3 shows the partial water vapor pressure at four times as a function of distance down the emplacement tunnel. The results show that the vapor saturation increases by as much as about 50 percent at the end of the tunnel as the air picks up moisture being given off as the rock heats up. The vapor pressure tends to peak when the moisture flux from the walls is a maximum (as shown below in Figure 4.1-5) which occurs between 5 and 10 years. As the emplacement tunnel dries out with time the amount of water in the air decreases significantly and at 100 years it is only slightly above zero.

The wall temperature curves are shown as a function of time for five points along the emplacement tunnel in Figure 4.1-4. The temperature steadily increases as the air moves down the tunnel and picks up heat from the waste packages and the walls. The temperature on the walls tends to peak between 10 and 30 years after emplacement but the largest temperatures calculated do not exceed about 42°C. A design evaluation study (McKenzie, 1995) did ventilation calculations with a model that only calculates sensible heat and does not include any effects of moisture. The results are comparable. Calculations in that design study were not done specifically at 20.6 kgU/m<sup>2</sup> (83 MTU/acre) so interpolations were needed between the two AML cases of 18.5 and 24.7 kgU/m<sup>2</sup> (75 and 100 MTU/acre) that were done. The design study indicates that the drift wall temperatures peak between 9 and 20 years which is in reasonable agreement with the coupled model run here. The wall temperatures at the end of the drift, however, were somewhat higher with estimated wall temperatures at 10 years of 67°C compared to 40°C predicted by the coupled model, at 45 years temperatures of 60°C compared to 41°C, and at 100 years temperatures of 45°C compared to the coupled predictions of 38°C. Thus the more realistic coupled model calculates wall temperature anywhere from a few degrees to 20°C cooler than a model that does not contain calculations of moisture. The agreement improves as the tunnel walls dry-out and moisture flux decreases.

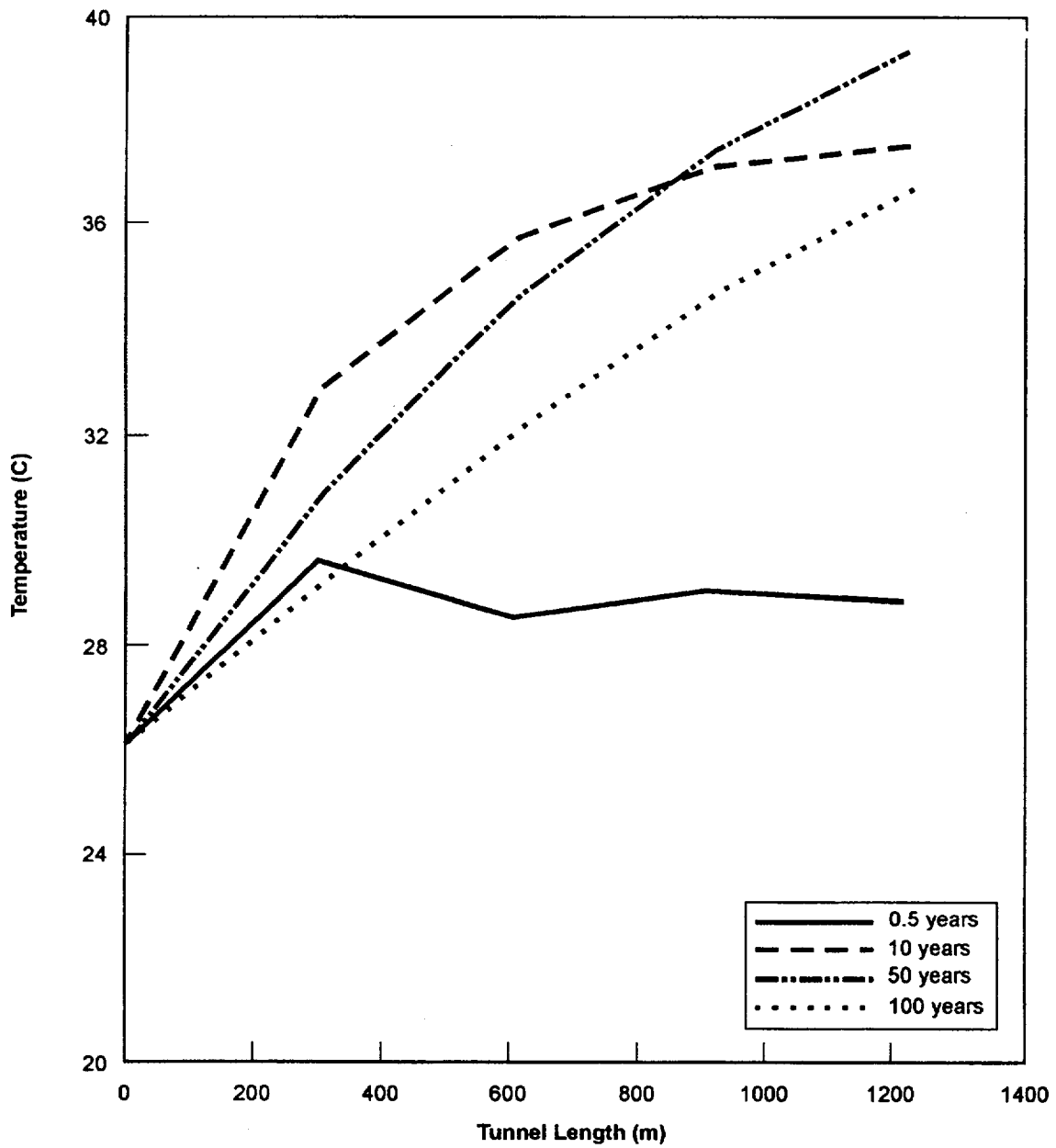


Figure 4.1-2. Air Temperature Profiles at Four Times Over Tunnel Length for a 10 m<sup>3</sup>/s Ventilation Rate at 20.6 kgU/m<sup>2</sup>.

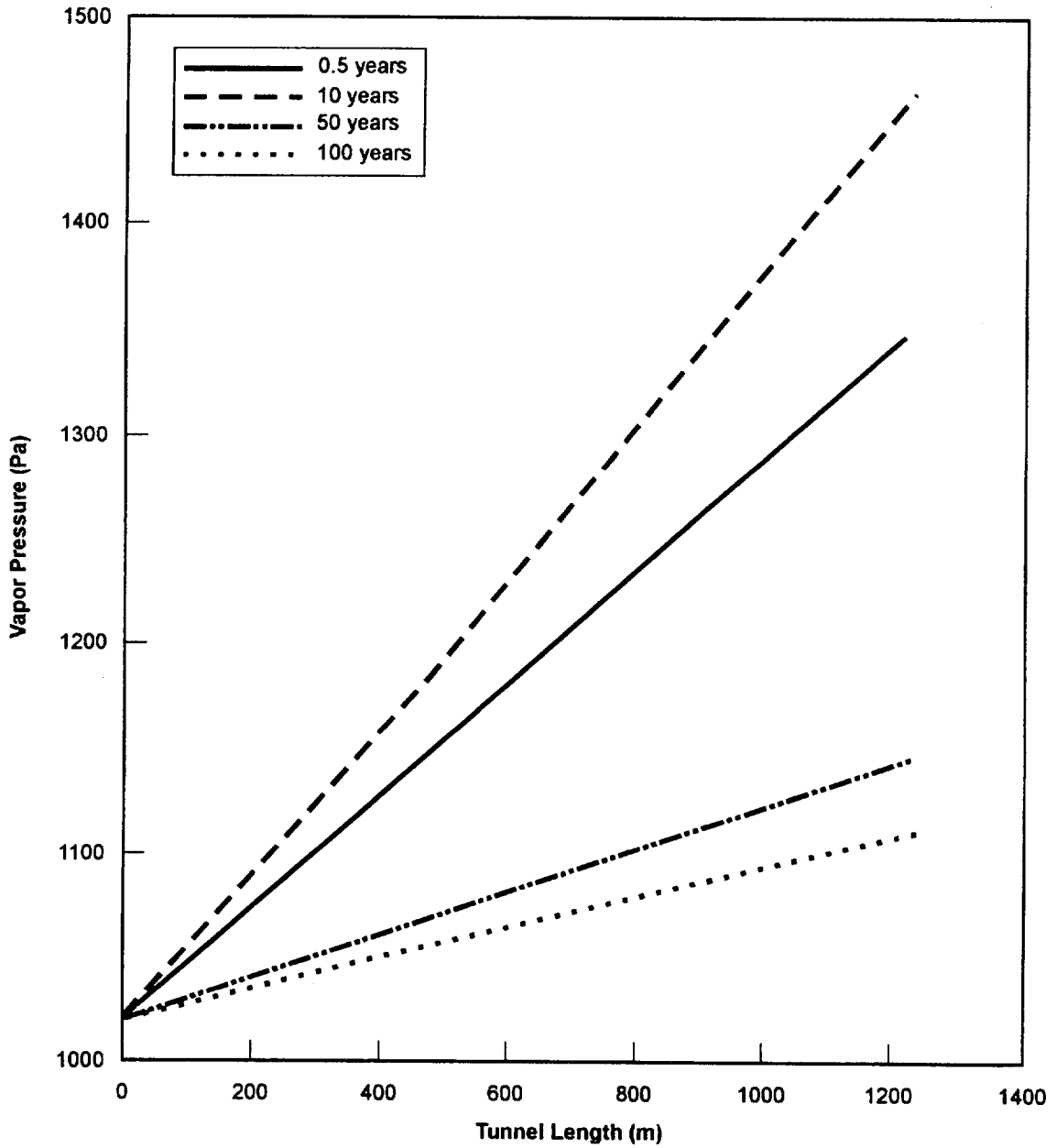


Figure 4.1-3. Partial Vapor Pressure Profile Calculated Over Tunnel Length at Four Times for a 10 m<sup>3</sup>/s Ventilation Rate at 20.6 kgU/m<sup>2</sup>.

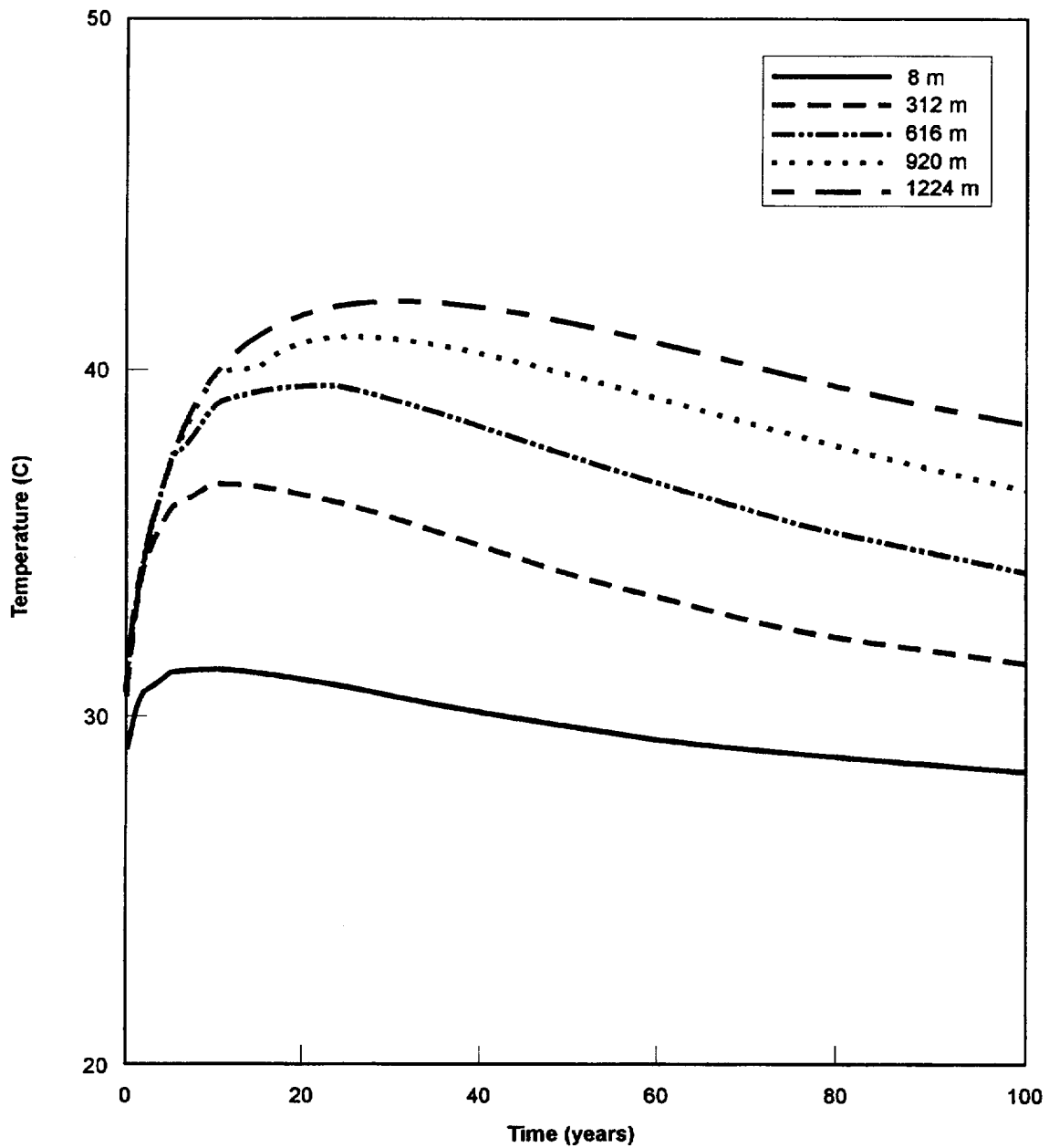


Figure 4.1-4. Maximum Wall Temperatures as a Function of Time at Distances along the Emplacement Drift for a 10 m<sup>3</sup>/s Ventilation Rate at 20.6 kgU/m<sup>2</sup>.

These predictions indicate that during the ventilation time and particularly when moisture is being driven off the rock, that a significant amount of heat in the rock can be removed as latent heat of vaporization. A "back of the envelope" estimate of the fraction of heat that would be removed as latent heat was done using the predicted air temperatures and moisture flux into the tunnel. The estimate indicates that about 130 kW could be removed as sensible heat while about 75 kW could be removed as latent heat during the period when large moisture fluxes occur. Thus roughly as much as about 60 percent additional heat could be removed as latent heat over what is removed as sensible heat.

The coupled code provides calculations of the amount of water that is removed from the walls upon heating and the fraction of this water which goes into the air stream in the drift and is removed from the system. NUFT also calculates the amount of water that is mobilized in the rock and transported away from the repository in the rock matrix but these results are not discussed in this section. Figure 4.1-5 shows the calculated wall moisture flux at two tunnel locations, the first segment (EP#1) and the middle segment (EP#39), as a function of time. The lowest flux is at the tunnel entrance where wall temperatures are lowest and downstream fluxes are substantially higher with all of the subsequent segments in the tunnel providing fairly similar values (similar to values at EP#39). The flux peaks around five years after emplacement and drops significantly with succeeding times as the tunnel walls dry-out. The total moisture removed per unit length of tunnel as a function of time was calculated by integrating the moisture fluxes over time and these are plotted in Figure 4.1-6. This figure shows calculations for the five segments and these values are averages taken over the 16, 1-m lengths in each of the five 16 m long segments. These values were then integrated over the tunnel length to produce an estimate of the total amount of water that is removed from the system by ventilation and this is plotted in Figure 4.1-7. The results show that a significant amount of water, about  $4.4 \times 10^7$  kg, is removed from the rock surrounding a single emplacement drift. However, to put this in perspective, a calculation of possible recharge around the drift over that same 100 years assuming an infiltration rate of 10 mm/year is about  $2.8 \times 10^7$  kg or a little more than half the amount that can be taken out by ventilation. Of course, the recharge could be a factor of 10 smaller if the infiltration rate is only 1 mm/year. If the  $4.4 \times 10^7$  kg were removed uniformly from a volume of tuff rock (estimated pore space of 10 percent and saturation of 80 percent) it would dry-out rock to a radius of about 12 m from the tunnel centerline by 100 years assuming no recharge. In fact, a reduction in saturation from ambient will extend much farther but by the same token it will not be completely dry at distances less than 12 m. However, since this is about half the distance between drifts, the boiling fronts will coalesce and the entire rock between drifts could dry-out significantly.

To put the above calculations in perspective, a scoping calculation of natural ventilation was done to show what might occur if the emplacement drifts are not sealed. A subsurface nuclear waste repository is exothermic and represents a classical thermosiphon arrangement of heat sources at low elevation and a heat sink at higher elevation. Consequently a positive buoyancy pressure difference can be produced in a recirculating air loop. This natural pressure difference, also referred to as the chimney effect, can drive air through the air distribution system, including air filters and the emplacement drifts, without the assistance of electrical fans. The natural ventilation may represent an option to engineer heat and moisture transfer, and improve the overall thermal performance.

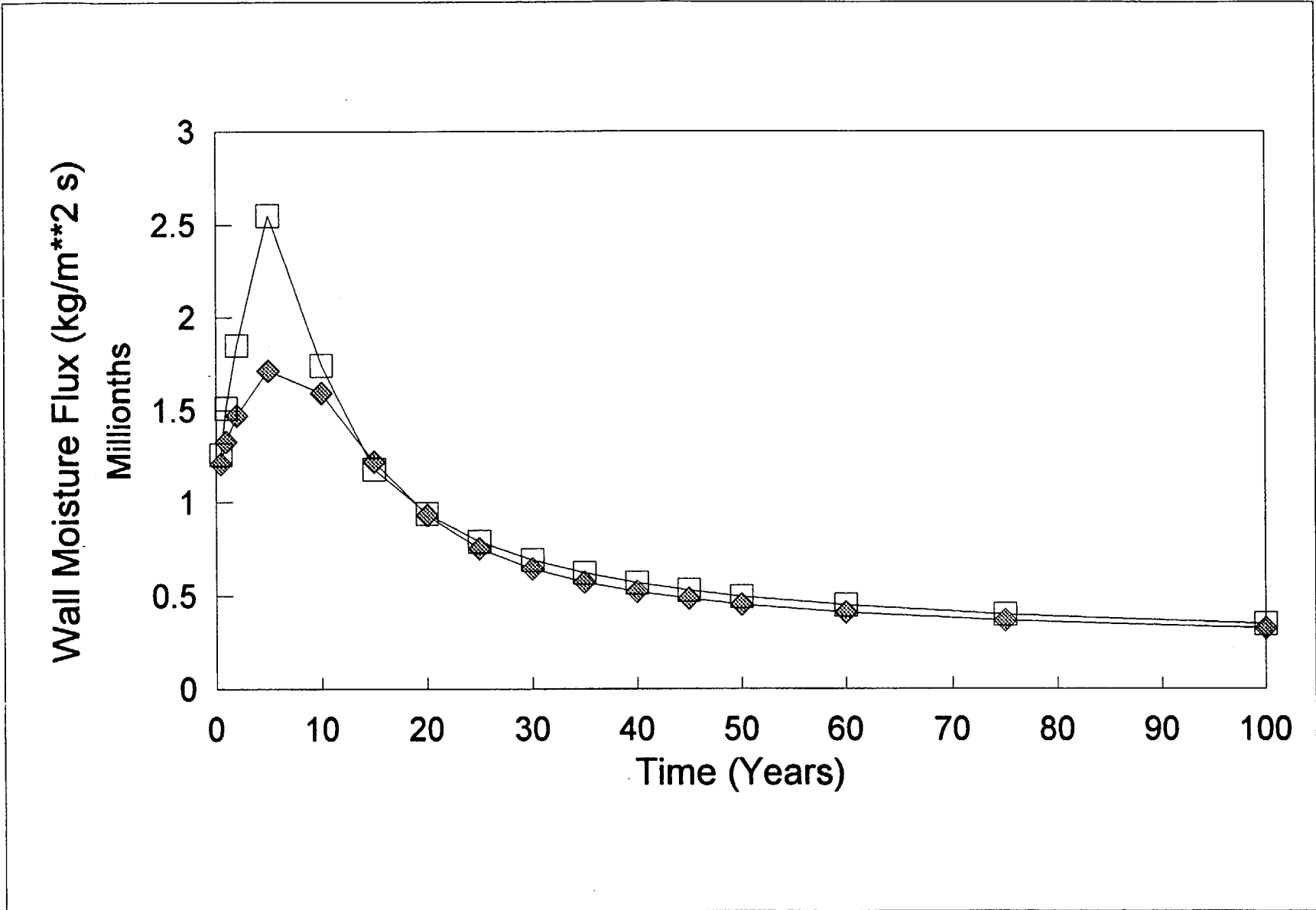


Figure 4.1-5. Wall Moisture Flux Density Versus Time.

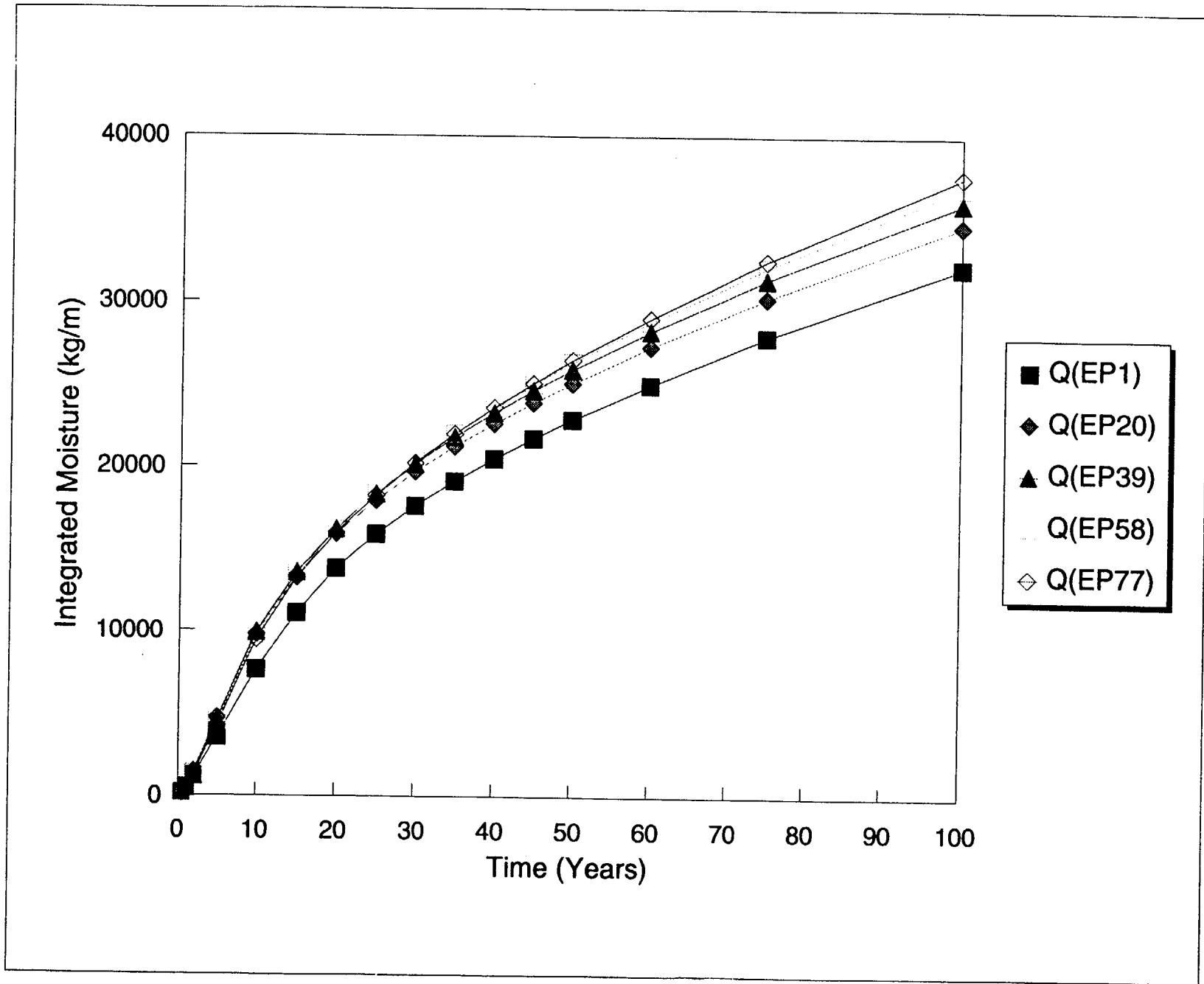


Figure 4.1-6. Total Moisture Removed per Unit Length.

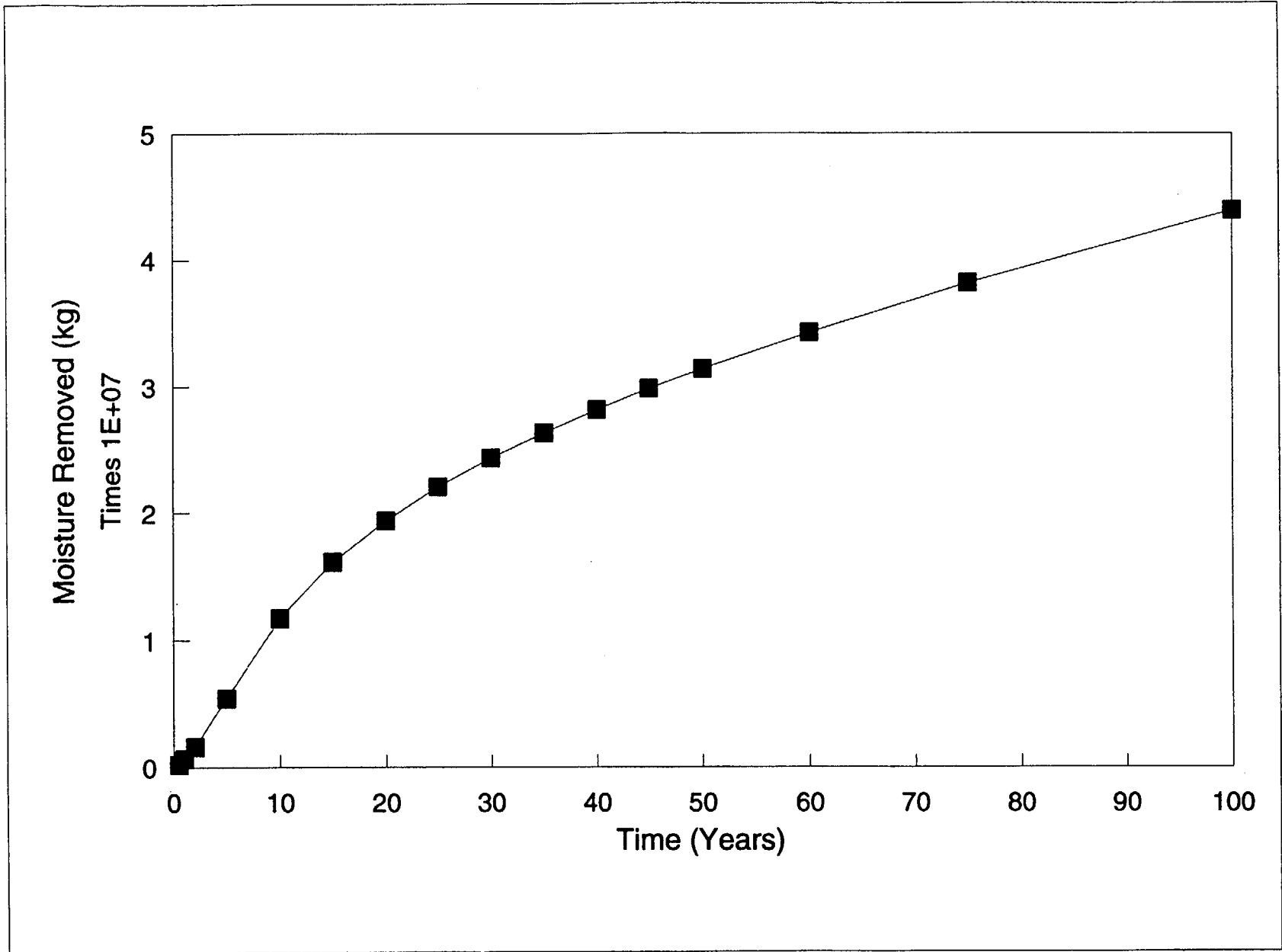


Figure 4.1-7. Cumulative Moisture Removed by Ventilation from a Drift.

The buoyancy pressure difference for a natural ventilation model can be formulated based on the energy balance of an exothermic waste repository. This was done within the context of the following assumptions:

- A dry repository
- Isothermal air columns in the intake and exhaust shafts
- Horizontal emplacement layout at a depth of 300 m below the surface
- 1000 m long emplacement drift
- A constant waste package heat output was assumed, although the heat output was varied over a range of values that are representative of package heat outputs during the first 100 years of repository life
- An input air temperature of 26°C

Any ventilation system, even a passive one, is certainly going to have some type of air filtration. The dominant element of the air flow resistance comes from the pressure loss across the air filters. A conservative rule-of-thumb pressure loss of 1000 N/m<sup>2</sup> is assumed at 1 m<sup>3</sup>/s. In the low-velocity regime, the other components of the total air flow resistance from friction and shock losses are negligible as compared to the filter. Therefore, a quadratic flow resistance characteristic was fitted across the given point for a filter.

The air flow rate was determined as the working point at the intersection of the buoyancy pressure and the flow resistance characteristic curves. Although not shown here, the calculations show that a maximum air flow rate of 0.8 m<sup>3</sup>/s can be expected at 0.5 years after emplacement due to natural ventilation. As the heat decays, this natural ventilation quantity gradually decreases to about 0.6 m<sup>3</sup>/s by the end of 100 years after emplacement. At that time it is anticipated that the natural ventilation would be cut off when the repository is sealed.

The calculations determined that the above air quantity from natural ventilation would produce a peak increase in air temperature in the emplacement drift of about 87°C over the input air temperature. This is certainly more than the maximum increase of 16°C calculated above for the forced ventilation rate of 10 m<sup>3</sup>/s. However, it is considerably less than the increase in air temperature of at least 140°C that was calculated without any ventilation. Thus the potential repository will, if allowed to, act as a thermosiphon resulting in natural ventilation in the emplacement drifts that are not sealed. Such ventilation, while small, still can be used to moderate heat during the preclosure period if such a consideration is needed.

In summary, a significant capability to calculate ventilation effects that includes both heat and moisture transport has been developed. The calculations show that at ventilation rates of 10 m<sup>3</sup>/s emplacement drift temperatures (air and wall) for a high AML loading of 20.6 kgU/m<sup>2</sup> can be kept at or below 40°C during preclosure. The coupled code predicts temperatures that are somewhat lower than those predicted by a ventilation code that does not include moisture effects but in other respects the agreement is good. The calculations showed that a significant amount of water can be removed by ventilation from the host rock surrounding the emplacement drift. Calculations of natural ventilation also showed that some heat can be taken out through the natural air flow that will occur if allowed.

## 4.2 PRELIMINARY ASSESSMENT OF EXPANSION AREAS

The Proposed Thermal Strategy being developed, based on the OCRWM Director's guidance, proposes a working hypothesis that focuses current design activities on a reference design thermal load that will permit emplacement of at least the statutory maximum within the primary repository area. With the current statutory maximum of 70,000 MTU, of which 63,000 MTU is SNF, and an estimated emplacement area of about 4,270,000 m<sup>2</sup> (1055 acre) (M&O, 1994b), this implies that the waste can be emplaced at an AML of 16.4 kgU/m<sup>2</sup> (66 MTU/acre) or higher. However, the proposed strategy will maintain flexibility of alternative AMLs to mitigate risks. For lower AMLs to be viable, more emplacement area than the Primary Area is required to emplace the statutory maximum. Additionally, if a congressional decision is made to increase the statutory maximum, more emplacement area also may be required depending on the thermal load at which it is emplaced. To achieve this it may be necessary to consider some of the proposed expansion areas or other areas for emplacement.

The current Program Plan (DOE, 1994) focuses on characterization of the Primary Area. A number of boreholes also have been drilled outside of the Primary Area. Some additional characterization of the expansion areas would be required to ensure that these areas are in fact similar to the Primary Area. The level of characterization has not yet been determined but could involve examination of borehole data or might require some drifting into these areas. The purpose of this section is to perform a preliminary assessment of the data that is available on the expansion areas. This data includes information about core samples from existing boreholes. The comparisons focused on comparing general variations and trends, not specific percentages.

Four additional optional areas (Optional Areas A through D) have been proposed (M&O, 1994a). These areas, in addition to the Primary Area (Upper and Lower Blocks), are shown in Figure 4.2-1 on an overlay of the Yucca Mountain terrain. The expansion areas are somewhat different than those proposed in the SCP and shown in the Site Atlas. Additionally, suggestions have been made that expansion to areas south of the Primary Area may be an option that should be explored. Early assessments speculated that this area south of the Primary Area might be fractured. This has not been established but more investigation would be warranted. This section discusses what is known about the four expansion areas and the area south of the Primary Area.

Some limited information in the form of borehole and core sample data exists about the optional areas and the area to the south that can be used to provide indications of the similarity or lack of similarity between areas outside of the Primary Area. Figure 4.2-1 shows an overlay of the existing and planned boreholes for Yucca Mountain. As shown on the figure, a few boreholes have been drilled in or near the Optional Areas and some have been drilled south of the Primary Area. LANL analyzed available core data using X-ray diffraction, petrography, and electron microprobes. Additional information on stratigraphy, lithology, and hydrology were used. In general, the comparisons done between the Primary Area and the alternative areas considered an evaluation of the basic stratigraphy to determine whether or not the units were similar, and if differences exist, whether they are likely to result in potentially different performance. Additionally, the thickness of the important units was estimated and the distribution and abundances of specific minerals were compared.

INTENTIONALLY LEFT BLANK

**YUCCA MOUNTAIN  
SITE CHARACTERIZATION PROJECT  
EXISTING and PLANNED  
BOREHOLES with SUBSURFACE LAYOUT**

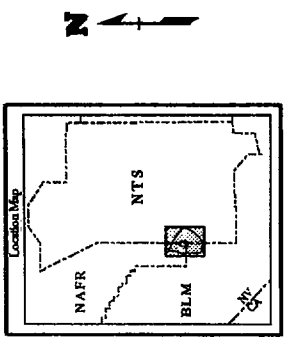
- BOREHOLES**
- Existing
  - Planned
- BOUNDARIES**
- ∩ Potential Repository Outline
  - ∩ Conceptual Controlled Area Boundary
- RAMPS**
- ∩ ESF Ramps
- ROADS**
- ∩ Light Duty, Class 3, Hard Surface
  - ∩ Unimproved, Class 4, Gravel Surface
  - ∩ Trail, Class 5, Four Wheel Drive or Other

**Borehole Outside Map Extent**

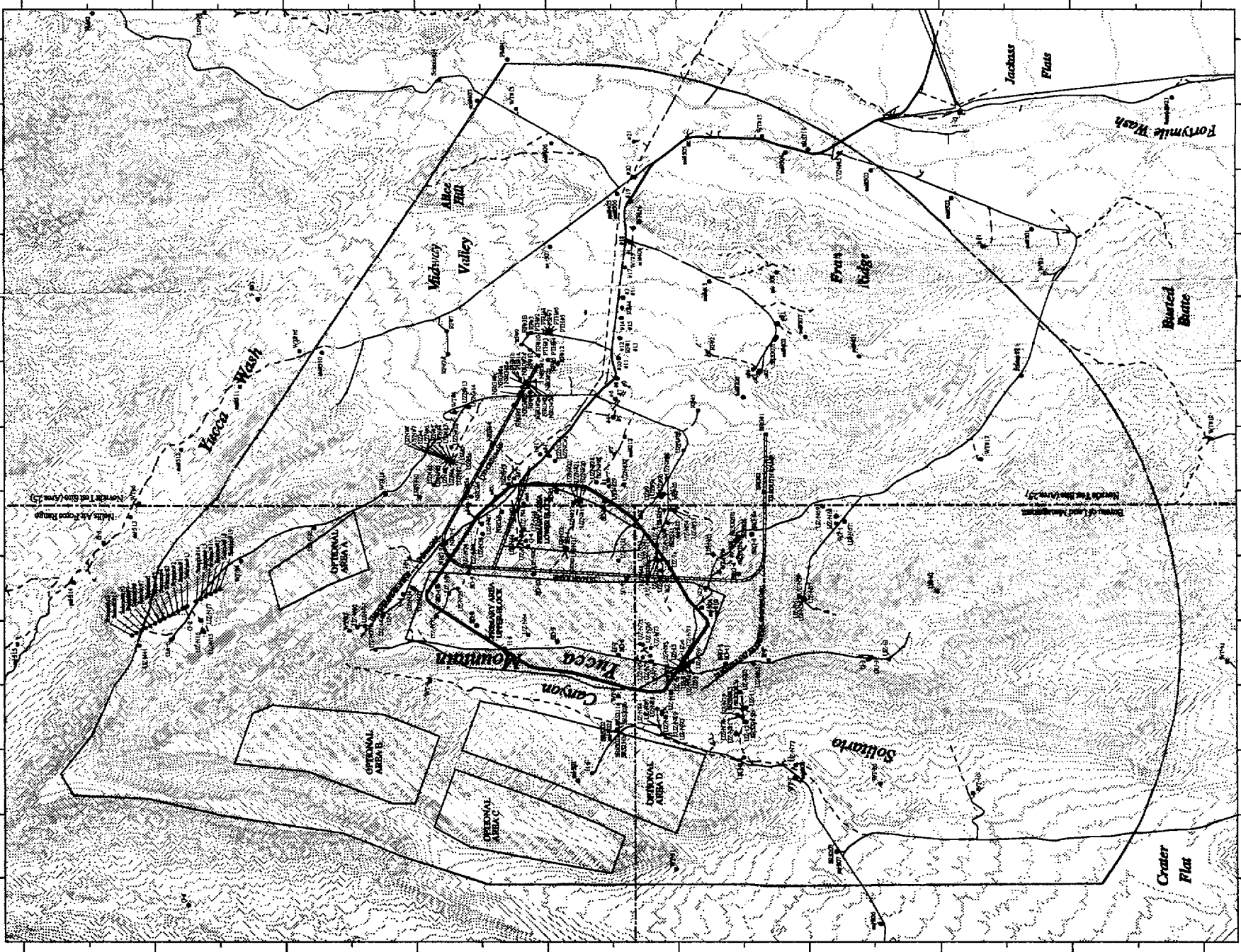
Existing	Planned
U-5 S2400A1	US-59 #1
U-5 S2400A2	US-59 #2
U-5 S2400A3	US-59 V-1
U-5 S2400A4	US-59 V-2
U-5 S2400A5	US-59 V-3
U-5 S2400A6	US-59 V-4
U-5 S2400A7	US-59 W-1
U-5 S2400A8	US-59 W-2
U-5 S2400A9	US-59 W-3
U-5 S2400A10	US-59 W-4
U-5 S2400A11	US-59 W-5
U-5 S2400A12	US-59 W-6
U-5 S2400A13	US-59 W-7
U-5 S2400A14	US-59 W-8
U-5 S2400A15	US-59 W-9
U-5 S2400A16	US-59 W-10
U-5 S2400A17	US-59 W-11
U-5 S2400A18	US-59 W-12
U-5 S2400A19	US-59 W-13
U-5 S2400A20	US-59 W-14
U-5 S2400A21	US-59 W-15
U-5 S2400A22	US-59 W-16
U-5 S2400A23	US-59 W-17
U-5 S2400A24	US-59 W-18
U-5 S2400A25	US-59 W-19
U-5 S2400A26	US-59 W-20
U-5 S2400A27	US-59 W-21
U-5 S2400A28	US-59 W-22
U-5 S2400A29	US-59 W-23
U-5 S2400A30	US-59 W-24
U-5 S2400A31	US-59 W-25
U-5 S2400A32	US-59 W-26
U-5 S2400A33	US-59 W-27
U-5 S2400A34	US-59 W-28
U-5 S2400A35	US-59 W-29
U-5 S2400A36	US-59 W-30
U-5 S2400A37	US-59 W-31
U-5 S2400A38	US-59 W-32
U-5 S2400A39	US-59 W-33
U-5 S2400A40	US-59 W-34
U-5 S2400A41	US-59 W-35
U-5 S2400A42	US-59 W-36
U-5 S2400A43	US-59 W-37
U-5 S2400A44	US-59 W-38
U-5 S2400A45	US-59 W-39
U-5 S2400A46	US-59 W-40
U-5 S2400A47	US-59 W-41
U-5 S2400A48	US-59 W-42
U-5 S2400A49	US-59 W-43
U-5 S2400A50	US-59 W-44
U-5 S2400A51	US-59 W-45
U-5 S2400A52	US-59 W-46
U-5 S2400A53	US-59 W-47
U-5 S2400A54	US-59 W-48
U-5 S2400A55	US-59 W-49
U-5 S2400A56	US-59 W-50
U-5 S2400A57	US-59 W-51
U-5 S2400A58	US-59 W-52
U-5 S2400A59	US-59 W-53
U-5 S2400A60	US-59 W-54
U-5 S2400A61	US-59 W-55
U-5 S2400A62	US-59 W-56
U-5 S2400A63	US-59 W-57
U-5 S2400A64	US-59 W-58
U-5 S2400A65	US-59 W-59
U-5 S2400A66	US-59 W-60
U-5 S2400A67	US-59 W-61
U-5 S2400A68	US-59 W-62
U-5 S2400A69	US-59 W-63
U-5 S2400A70	US-59 W-64
U-5 S2400A71	US-59 W-65
U-5 S2400A72	US-59 W-66
U-5 S2400A73	US-59 W-67
U-5 S2400A74	US-59 W-68
U-5 S2400A75	US-59 W-69
U-5 S2400A76	US-59 W-70
U-5 S2400A77	US-59 W-71
U-5 S2400A78	US-59 W-72
U-5 S2400A79	US-59 W-73
U-5 S2400A80	US-59 W-74
U-5 S2400A81	US-59 W-75
U-5 S2400A82	US-59 W-76
U-5 S2400A83	US-59 W-77
U-5 S2400A84	US-59 W-78
U-5 S2400A85	US-59 W-79
U-5 S2400A86	US-59 W-80
U-5 S2400A87	US-59 W-81
U-5 S2400A88	US-59 W-82
U-5 S2400A89	US-59 W-83
U-5 S2400A90	US-59 W-84
U-5 S2400A91	US-59 W-85
U-5 S2400A92	US-59 W-86
U-5 S2400A93	US-59 W-87
U-5 S2400A94	US-59 W-88
U-5 S2400A95	US-59 W-89
U-5 S2400A96	US-59 W-90
U-5 S2400A97	US-59 W-91
U-5 S2400A98	US-59 W-92
U-5 S2400A99	US-59 W-93
U-5 S2400A100	US-59 W-94
U-5 S2400A101	US-59 W-95
U-5 S2400A102	US-59 W-96
U-5 S2400A103	US-59 W-97
U-5 S2400A104	US-59 W-98
U-5 S2400A105	US-59 W-99
U-5 S2400A106	US-59 W-100



Borehole locations processed by BEACON from data provided by YMP Participants. Borehole information current as of December 1994.  
 Planned borehole locations are provided by M&E/Woodward-Clyde Federal Services and are preliminary at this time.  
 Subsurface layout processed by BEACON from data provided by YMP Participants.  
 Potential Repository Outline processed by BEACON from TUE Design Summary Report for the Repository Studies Facility.  
 Conceptual Controlled Area Boundary processed by BEACON from Nevada National Laboratory project number CAL110.  
 Topographic contours obtained from 1:4000 scale orthorectified aerial photography.  
 Road names obtained from 1:4000 scale orthorectified aerial photography.  
 Topographic contours obtained from 1:4000 scale orthorectified aerial photography.  
 Prepared by: Thomas M. Moore, et al. continuous based on Nevada State Plan Coordinate System, Contour Zone.  
 Map completed June 19, 1995 by BEACON Remote Sensing Laboratory.  
**PRELIMINARY INFORMATION ONLY: YMP-SRS/DO Section 5.2.2 notes that the data provided herein have not received complete technical and quality checks and are for informational purposes only. Do not use for decision making or for any other purpose.**



YMP-95-386.0



**ANSTEC  
APERTURE  
CARD**

Also Available on  
Aperture Card

9605080224-01

INTENTIONALLY LEFT BLANK

This section provides a review of mineralogy-petrology data for optional expansion areas and alternative areas surrounding the Primary Area for a potential high-level nuclear waste repository at Yucca Mountain, Nevada. The evaluation includes four delineated optional areas west and northeast of the Primary Area plus a portion of the mountain immediately south of the Primary Area. Existing data used in this study include published and unpublished qualified and unqualified information.

Information about the Optional Areas was organized into three general categories: (1) stratigraphic variations that affect mineral distributions; (2) properties, abundances and distributions of minerals that could affect repository geochemical or thermal performance; and (3) existence of altered zones that may affect fluid flow paths or rock mechanical properties. No systematic evaluations of stratigraphy, hydrology, or rock mechanics are included because these are beyond the scope of mineralogy-petrology studies. However, individual significant features within these categories have been identified and are described.

The descriptions of optional areas emphasize their differences and similarities to the primary study area. It is important to note, however, that significant variations exist within the Primary Area itself. In some cases, the variability of a property with position is sufficiently known that its magnitude in an Optional Area can be compared in a meaningful way to its variability within the Primary Area.

Information on the Primary Area's stratigraphy and mineralogy-petrology was from boreholes G-1, G-4, H-4, H-5, and UE25A1. Data from these boreholes form the basis for the comparisons of variability between the primary and optional areas.

#### **4.2.1 Zeolite Distribution**

The presence of zeolites in the nonwelded tuff units below the potential repository has long been considered a promising barrier to the transport of radionuclides by groundwater based on the likelihood to increase groundwater travel time in the zeolitic tuffs and the sorptive and retardant properties needed to minimize radionuclide migration (it should be noted that zeolites are not good sorbers for some actinides such as Am, Np, Pu, and U). However, the distribution of clinoptilolite-bearing zeolitized tuffs in the study area is highly variable. In the presence of abundant water, tuffs that were originally nonwelded and glassy underwent diagenetic alteration in which the glass was converted to zeolites. The transition zone from vitric downward to zeolitic tuffs is a gradational, irregular boundary inclined approximately to the east at an angle less than the inclination of the host pyroclastic units. The position of the vitric-zeolitic transition zone relative to the potential repository and to the static water level (SWL), and the location of the zone within the stratigraphic sequence, are significant factors for repository performance. Zeolitic tuffs of the CHn unit have lower porosity and hydraulic conductivity than comparable vitric tuffs (Loeven, 1993), so that variable thicknesses of vitric and zeolitic tuffs below a repository could produce variations in groundwater travel time. Vitric and zeolitic tuffs also differ in their radionuclide sorptive properties (Daniels et al., 1982). The thermal and hydrologic effects of zeolite dehydration in a repository environment are also distinctive compared to vitric tuffs (Carey and Bish, 1995b).

Projections of the distribution of vitric and zeolitic rocks into areas of sparse or no data are based on a conceptual model of zeolitization by Levy (1991). This model relates the distribution of vitric and zeolitic rocks to the timing of pyroclastic deposition, water-level changes, tectonic tilting, and faulting. Additional sources of information on the occurrences of zeolitic rocks are cited as applicable.

#### 4.2.2 Assessment of Optional Areas C and D

The evaluation of Optional Area D is presented first because more data are available and the information can be more easily related to the primary study area. The interpretation of potential features in Area C is directly derived from the evaluation of Area D.

##### Optional Area D

Optional Area D is just west of the Solitario Canyon fault. One deep drill hole, USW H-6, is located within the area. This drill hole was discontinuously cored. Samples from all cores were collected for X-ray diffraction, petrographic, and electron microprobe analyses. A few samples of cuttings also were collected. X-ray diffraction data are contained in Bish and Chipera (1989). Stratigraphic and lithologic information are given in Craig, Reed, and Spengler (1983).

The general stratigraphy of USW H-6 is the same as in the primary study area. The depth from the surface to the potential host rock is about 360 m, within the range of values for the primary area. The SWL is about 155 m below the base of the potential host rock, comparable to values for the eastern part of the Primary Area. No unusual structures or alteration have been identified.

The main vitric-zeolitic transition in H-6 is located in the lower Prow Pass tuff which is typical for the western edge of the primary area (USW H-5) and the area to the south (USW H-3 and G/GU-3). This similarity has been interpreted as an indication that zeolitization of the Prow Pass tuff probably predated much of the offset on the Solitario Canyon Fault (Levy, 1991). Because the stratigraphic section west of the Solitario Canyon Fault is down dropped and the SWL west of the fault is high relative to Yucca Mountain, the top of the H-6 main zeolite zone at about 512 m depth is only 14 m above the static water level at 526 m. Vertical thicknesses of zeolitic tuff between the potential repository and the SWL in the Primary Area vary from about 44 m to 142 m (Vaniman et al., 1984).

A distinctive diagenetic feature identified in drill hole USW H-5 that may exist in H-6 is an isolated zeolitic interval above the main vitric-zeolitic transition (Levy, 1984). The zeolitic interval is about 5 m thick and is located within bedded tuffs near the base of the CH Formation about 100 m below the potential repository horizon. Alteration in the bedded tuffs produced a tightly cemented rock that may act as an aquitard. If this cemented rock existed within the CH bedded tuff throughout Yucca Mountain, it might cause some lateral diversion of recharge water in an eastward direction parallel to the inclined strata. Such a diversion probably would not be a major concern for Yucca Mountain because, in the eastern flank of the mountain, the basal CH bedded tuffs are located well below the main vitric-zeolitic transition. Water that might have followed a short circuit would be delivered back to the main body of the zeolitic CH tuff.

## **Optional Area C**

Optional Area C is adjacent to and west of Area D. No drill holes exist within this area and none are planned. The two areas are separated by a NNE trending fault with an unknown amount of downward offset to the west (Lipman and McKay, 1965). The assessment of this region was made based on projections from Area D information. This results in a significant uncertainty in the findings made since no drill hole data is available for this region and the assessment should not be construed as final without further investigation.

The stratigraphic section and probably the diagenetic zones in Optional Area C are down dropped relative to drill hole H-6 and the SWL is probably at least as high as in H-6 (Waddell, Robison, and Blankennagel, 1984). Given these conditions, the main vitric-zeolitic transition probably coincides with the present SWL. There may be almost no zeolitic tuffs above the SWL. The near-absence of a zeolitic section above the SWL is the extreme of variability for this attribute and would be distinctly different from the primary study area at Yucca Mountain. The potential significance for repository performance is the inferred absence of the hydrologic barrier and sorptive capacity represented by zeolitic tuff.

### **4.2.3 Assessment of Southern Yucca Mountain**

No optional area has been formally delineated for southern Yucca Mountain. The subsurface from the southern boundary of the Primary Area Upper Block to the southern end of Yucca Crest (approximately N758000 to N752500 in Nevada State Coordinates) is known from deep drill holes USW H-3 and G/GU-3. G/GU-3 was continuously cored, whereas the materials from H-3 are cuttings and sidewall samples. At present, much more is known about the stratigraphy, lithology, and diagenetic alteration of G/GU-3.

Most of the pyroclastic units that comprise Yucca Mountain were derived from volcanic centers north of the mountain and generally become thinner to the south. At the G/GU-3 site, the TS Tuff is 299.5 m thick compared to a thickness mostly ranging from 330 m to 350 m in the primary study areas (Scott and Castellanos, 1984). Where the TS Tuff is thinner, the internal stratigraphy and the syngenetic zonation (e.g., the distribution of lithophysal and nonlithophysal zones) are also different. Differences in the thickness and distribution of lithophysal and nonlithophysal zones may require redefinition of the potential repository interval within the TS Tuff. The importance of this consideration is likely to increase southward from G/GU-3.

The CH Formation also becomes thinner to the south. This unit is less than 30 m thick at G/GU-3 (Scott and Castellanos, 1984). The aggregate thickness of nonwelded vitric tuff immediately underlying the welded TS Tuff (nonwelded Topopah), CH Formation, plus nonwelded Prow Pass tuff, (known also as the CHnv functional unit) is about 88 m, not too different than in the western part of the primary study area. Studies of outcrops at northern Busted Butte suggest that at least 26 m but probably no more than about 36 m of nonwelded, mostly vitric tuff--less than half the G/GU-3 value--might be present in an equivalent stratigraphic position about one kilometer (km) south of G/GU-3 (Broxton et al., 1993). It should be noted that the thickness of the CH Formation in the Primary Area is also quite variable with approximate thicknesses of the CH proper ranging from 72 m to approximately 144 m.

Although the entire CHn sequence described above is essentially vitric in G/GU-3, a 60 m thick section of clinoptilolite-bearing tuff does exist above the SWL at this site. The zeolitic rocks are located in the lower part of the Prow Pass Tuff and the underlying Bullfrog Tuff, equivalent to the zeolite distribution in the main zeolite zones of western Yucca Mountain within the primary study area. Some information might be obtained on the distribution of zeolites south of G/GU-3 from study of drill hole WT-11 cuttings.

#### 4.2.4 Summary

In summary, preliminary mineralogy-petrology evaluations have been done to compare alternative areas with the Primary Area. Comparisons were done of the stratigraphic variations and mineral distributions and abundances, which could affect repository performance and fluid flow. Based on these evaluations, it would appear that Optional Area D and the area south of the Primary Area (at least south as far as drill holes G/GU-3) have stratigraphic features, thicknesses, and mineralogic characteristics that fall within the range of parameters that exists in the Primary Area. As such, it is possible that these areas can be relatively easy to characterize possibly with some additional boreholes, which may in some cases be planned (see Figure 4.2-1). Additionally, it would appear that Optional Area C may be significantly different from the Primary Area in that there may not be a vitric-zeolitic transition above the SWL. The fact that Area C may be different from the Primary Area does not necessarily imply that it would be unusable for emplacement of spent nuclear fuel, only that a different conceptual model of this region (for example a different hydrologic model) is likely to be needed. This would likely imply that more characterization of this region, such as possibly even drifting and in-situ tests, would be needed to establish its ability to isolate spent nuclear fuel. No assessment could be done of Optional Areas A and B at this time due to the lack of drill holes.

### 4.3 NONUNIFORM AREAL MASS LOADING

Thermal loading impacts many elements of the "dispose of waste" system, including the temperature and moisture content in the host rock. The waste package performance is dependent on the near-field environment since corrosion is governed by temperature and air moisture content. The design basis thermal load intends, based on currently idealized predictions, to constructively utilize heat to mobilize water, dry-out the near-field host rock, and keep the rock dry for extended periods of time (thousands of years). The occurrence and duration of this dry-out is based on models that require in-situ testing for verification. The predictions of a uniform disk-shaped heat source indicate that dry-out may occur for thermal loads above about 9.9 kgU/m<sup>2</sup> (40 MTU/acre) for waste packages in the inner 75 percent of the disk area. A number of calculations, for example Ryder (1993) and Buscheck, Nitao, and Saterlie (1994), have shown that the outer edges of the potential repository will experience significant edge cooling. In some cases, the temperatures at the edges never exceed the boiling point and minimal change in the liquid saturation of the host rock is predicted. This edge environment could result in a much more aggressive corrosion regime than either a hotter environment in the repository interior or a cooler environment for a lower AML. The purpose of this section is to evaluate the thermal management technique of loading the edges of the potential repository with a higher density of waste packages to increase the temperature in those areas.

To evaluate the use of nonuniform AMLs, hydrothermal calculations were done by LLNL using the V-TOUGH model which is described in earlier sections and in Nitao (1989). Temperature, liquid saturation, and relative humidity changes as a function of time and location were calculated with V-TOUGH assuming a smeared heat source, disk-shaped model of the potential repository. Since much of this work was done in 1994, the waste stream used was based on a YFF(10) selection criteria which had an average age of SNF of about 22.5 years. The calculations were run with nominal binary gas-phase diffusion where the gas-phase tortuosity factor was  $t_{eff}=0.2$ . Some additional calculations were done using a higher or enhanced binary gas-phase diffusion in which the tortuosity factor was  $t_{eff}=4.0$ .

Calculations were run at four AMLs. The local AML was established iteratively to provide a nearly uniform duration of boiling throughout the entire repository. There may still be differences of as much as a factor of two between the duration of boiling in the inner area and the edge but it is not an order of magnitude or more as was occurring with a uniform AML. The method used to establish the AML distribution was to reduce the local AML where the local duration of boiling,  $t_{bp}$ , exceeds the average boiling duration  $\langle t_{bp} \rangle$  and increase the local AML where the duration was below average. The following formula was used to establish the local AML (Buscheck, 1994):

$$AML_{local} = (\langle t_{bp} \rangle / t_{bp})^{0.6} AML_{avg} \quad (4.3-1)$$

The value of 0.6 was chosen as an exponent in Equation (4.3-1) based on the observation that  $t_{bp}$  appears to scale as the square of the AML. While an exponent of 0.5 would appear to be more appropriate, a slightly higher value was chosen to accelerate the process of converging on a distribution of AMLs which would provide a more uniform duration of boiling. In general this methodology tends to decrease the duration of boiling in the center of the potential repository while substantially increasing the duration at the edges.

The first case that was run was a mid-range thermal load that would correspond to a uniformly loaded repository at an AML of 13.7 kgU/m<sup>2</sup> (55.3 MTU/acre). The uniform AML cases for comparison were excerpted from a paper by Buscheck, Nitao, and Saterlie (1994). However, there was some difference in that the referenced uniform AML calculations were based on emplacing 63,000 MTU of SNF while the nonuniform AML cases run later emplaced 73,000 MTU. The first step in the process was to remove about 10,000 MTU from the center and put in the edges. However, since the duration of boiling in the center was degraded, 10,000 MTU were added back in the center 75 percent to provide a boiling duration equal to the base case. A reduction of the size of the potential repository by about 16 percent should have been done but would have required regridding the cases for the model runs and therefore it was decided to do the calculations with 73,000 MTU. As such, only qualitative evaluations will be possible but the trends are clearly established as shown below. Additionally, in an effort to keep the duration of boiling as long as possible, Equation (4.3-1) was used only to establish the loading at the outer 25 percent while a constant AML was retained for the inner 75 percent of the disk. This is probably more practical from an operational standpoint as well. Thus the first case had a uniform AML of 13.7 kgU/m<sup>2</sup> in the inner 75 percent and a nonuniform AML in the outer 25 percent increasing toward the edge with an average distribution of 22.3 kgU/m<sup>2</sup> (90.2 MTU/acre). This produced an average AML for the potential repository of 15.8 kgU/m<sup>2</sup> (64.0 MTU/acre). The second case has an average AML of 20.1 kgU/m<sup>2</sup> (81.3 MTU/acre), which is representative of

a 17.3 kgU/m<sup>2</sup> (70 MTU/acre) case, and was formed using a constant 17.3 kgU/m<sup>2</sup> for the inner 75 percent and a nonuniform outer 25 percent with an average AML of 28.3 kgU/m<sup>2</sup> (115.2 MTU/acre). The third case has an average AML of 24.0 kgU/m<sup>2</sup> (96.9 MTU/acre), which is representative of a 20.7 kgU/m<sup>2</sup> (83.4 MTU/acre) case, and was formed using a constant 20.7 kgU/m<sup>2</sup> for the inner 75 percent and a nonuniform outer 25 percent with an average AML of 34.0 kgU/m<sup>2</sup> (137.4 MTU/acre). The fourth case has an average AML of 31.8 kgU/m<sup>2</sup> (128.4 MTU/acre) which is representative of a 27.4 kgU/m<sup>2</sup> (110.5 MTU/acre) case, and was formed using a constant 27.4 kgU/m<sup>2</sup> for the inner 75 percent and a nonuniform outer 25 percent with an average AML of 44.6 kgU/m<sup>2</sup> (180.1 MTU/acre).

Figures 4.3-1 through 4.3-4 show the calculated vertical temperature profiles and liquid saturation profiles for the four nonuniform AML cases at the thermal loads of 15.4, 20.1, 24.0, and 31.8 kgU/m<sup>2</sup> (62.4, 81.3, 96.9, and 128.4 MTU/acre) respectively. Each panel in the four panel set was for a different time after emplacement. The times were 100, 1000, 10,000 and a time close to 30,000 years. The ambient geothermal temperature gradient and liquid saturation profiles are presented in Section 3.7. To evaluate the benefits of nonuniform AML loading, these curves were compared against uniform AML calculations for similar thermal loads. Those calculations were reported in Buscheck, Nitao, and Saterlie (1994), but for comparison, two of the sets of figures have been extracted from that paper and are provided. Figures 4.3-5 and 4.3-6 show the calculations of vertical temperature and liquid saturation changes at times of 1000, 10,000, and about 33,000 years for the uniform AMLs of 13.7 and 20.7 kgU/m<sup>2</sup> (55.3 and 83.4 MTU/acre) respectively. An examination of Figure 4.3-5a (case 1, which is the uniform AML case) shows that the outer areas (labeled as r=1180.6 m) of the repository are predicted to have temperatures that do not exceed the boiling point at 1000 years at the repository horizon. Additionally, Figure 4.3-5d shows that the liquid saturation profiles have minimal change in the outer area. However, when the corresponding nonuniform AML with an average loading of 15.8 kgU/m<sup>2</sup> (64.0 MTU/acre) plot (Figure 4.3-1b) is examined, the predicted temperatures in the outer area exceed the boiling point and significant liquid saturation reductions are predicted to occur. Correspondingly, at the higher AML of 20.7 kgU/m<sup>2</sup> (83.4 MTU/acre), the predictions for this uniform AML case shown in Figure 4.3-6 indicate that the temperature in the outer area of the repository horizon is barely at the boiling point at 1000 years and there is less dry-out of the rock. Comparing this with the corresponding nonuniform AML case, which had an average loading of 24.0 kgU/m<sup>2</sup> (96.9 MTU/acre), the predictions in Figure 4.3-3b show that at 1000 years the temperature in the outer area (labeled as 961.2 m) is substantially above the boiling point and a substantial reduction in liquid saturation is predicted. The predicted temperatures and liquid saturations in the inner areas for the nonuniform AML case are not significantly different from those predicted for the uniform AML cases as can be seen in the corresponding figures.

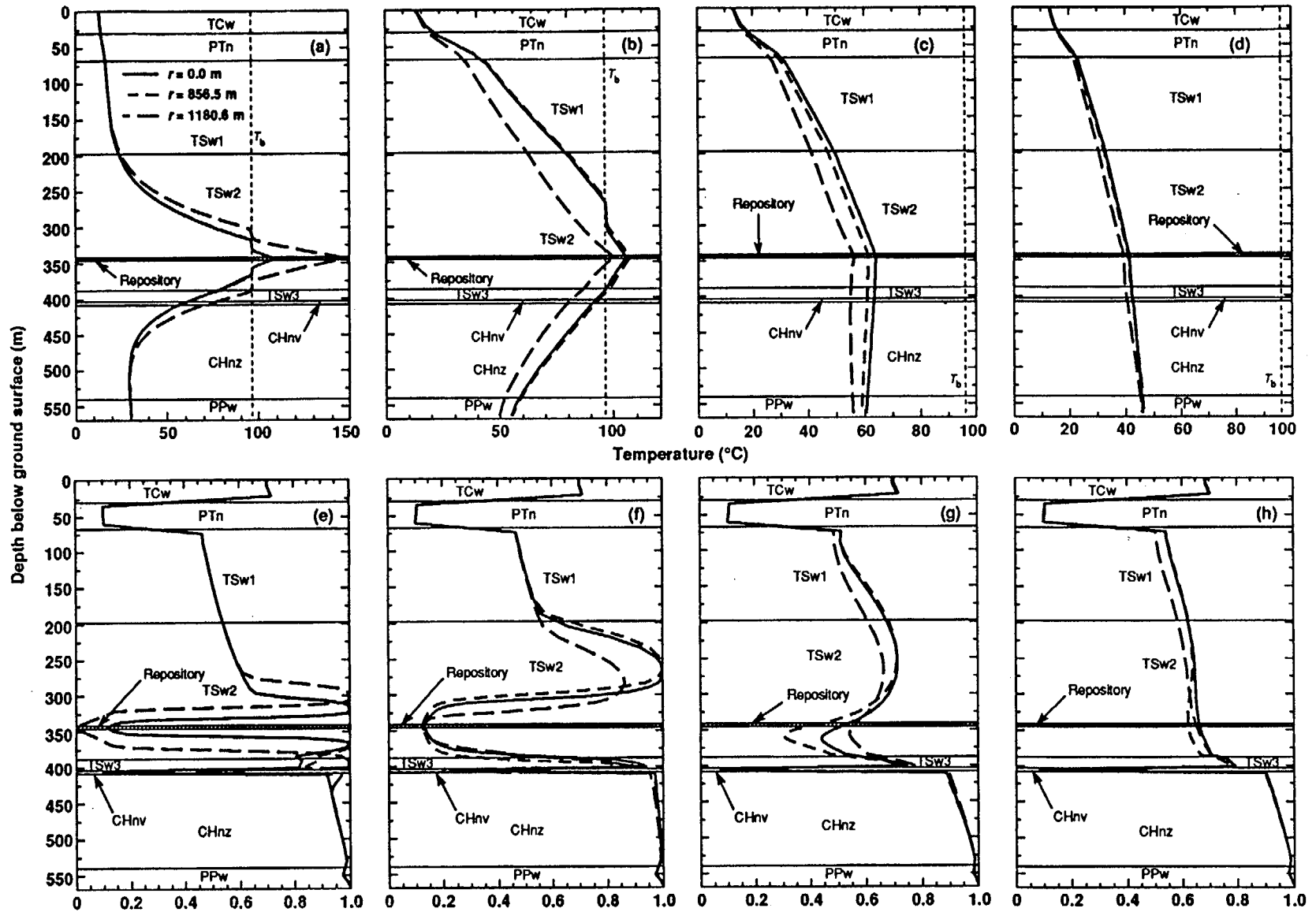


Figure 4.3-1. Vertical temperature profiles at various radial distances,  $r$ , from repository centerline for a nonuniform AML of 64.0 MTU/acre at (a)  $t = 100$  yr, (b)  $t = 1,000$  yr, (c)  $t = 10,000$  yr, and (d)  $t = 33,100$  yr. Note different temperature scales. Vertical liquid saturation profiles are also plotted at (e)  $t = 100$  yr, (f)  $t = 1,000$  yr, and (g)  $t = 10,000$  yr, and (h)  $t = 33,100$  yr. Matrix properties for the TSw1 and TSw2 are based on Klavetter and Peters (1986). Binary gas-phase tortuosity factor  $\tau_{eff} = 0.2$  for all units.

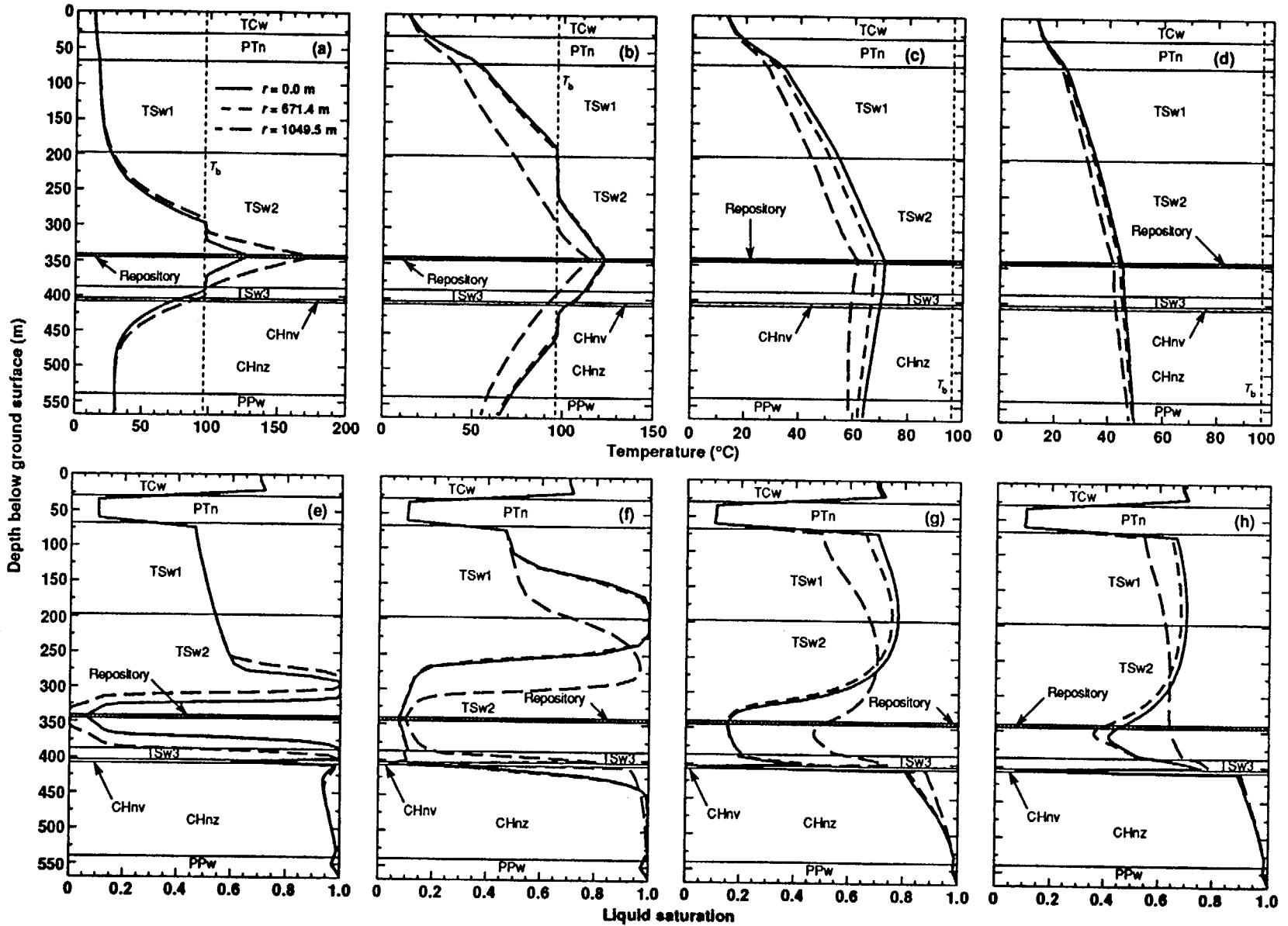


Figure 4.3-2. vertical temperature profiles at various radial distances,  $r$ , from repository centerline for a nonuniform AML of 81.3 MTU/acre at (a)  $t = 100$  yr, (b)  $t = 1,000$  yr, (c)  $t = 10,000$  yr, and (d)  $t = 32,670$ . Note different temperature scales. Vertical liquid saturation profiles are also plotted at (e)  $t = 100$  yr, (f)  $t = 1,000$  yr, and (g)  $t = 10,000$  yr, and (h)  $t = 32,670$ . Matrix properties for the TSw1 and TSw2 are based on Klavetter and Peters (1986). Binary gas-phase tortuosity factor  $\tau_{eff} = 0.2$  for all units.

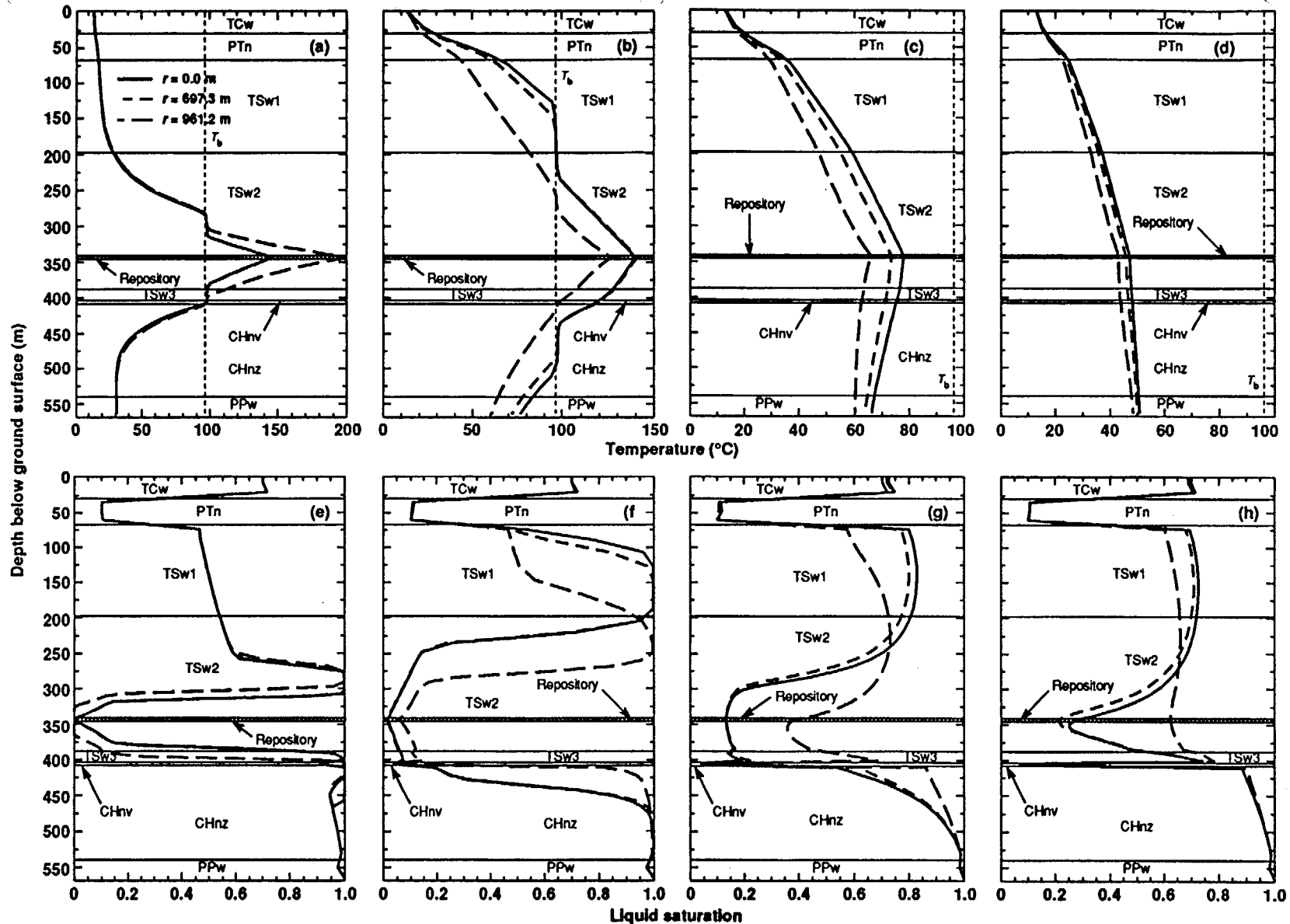


Figure 4.3-3. Vertical temperature profiles at various radial distances,  $r$ , from repository centerline for a nonuniform AML of 96.9 MTU/acre at (a)  $t = 100$  yr, (b)  $t = 1,000$  yr, (c)  $t = 10,000$  yr, and (d)  $t = 33,550$  yr. Note different temperature scales. Vertical liquid saturation profiles are also plotted at (e)  $t = 100$  yr, (f)  $t = 1,000$  yr, and (g)  $t = 10,000$  yr, and (h)  $t = 33,550$  yr. Matrix properties for the TSw1 and TSw2 are based on Klavetter and Peters (1986). Binary gas-phase tortuosity factor  $\tau_{\text{eff}} = 0.2$  for all units.

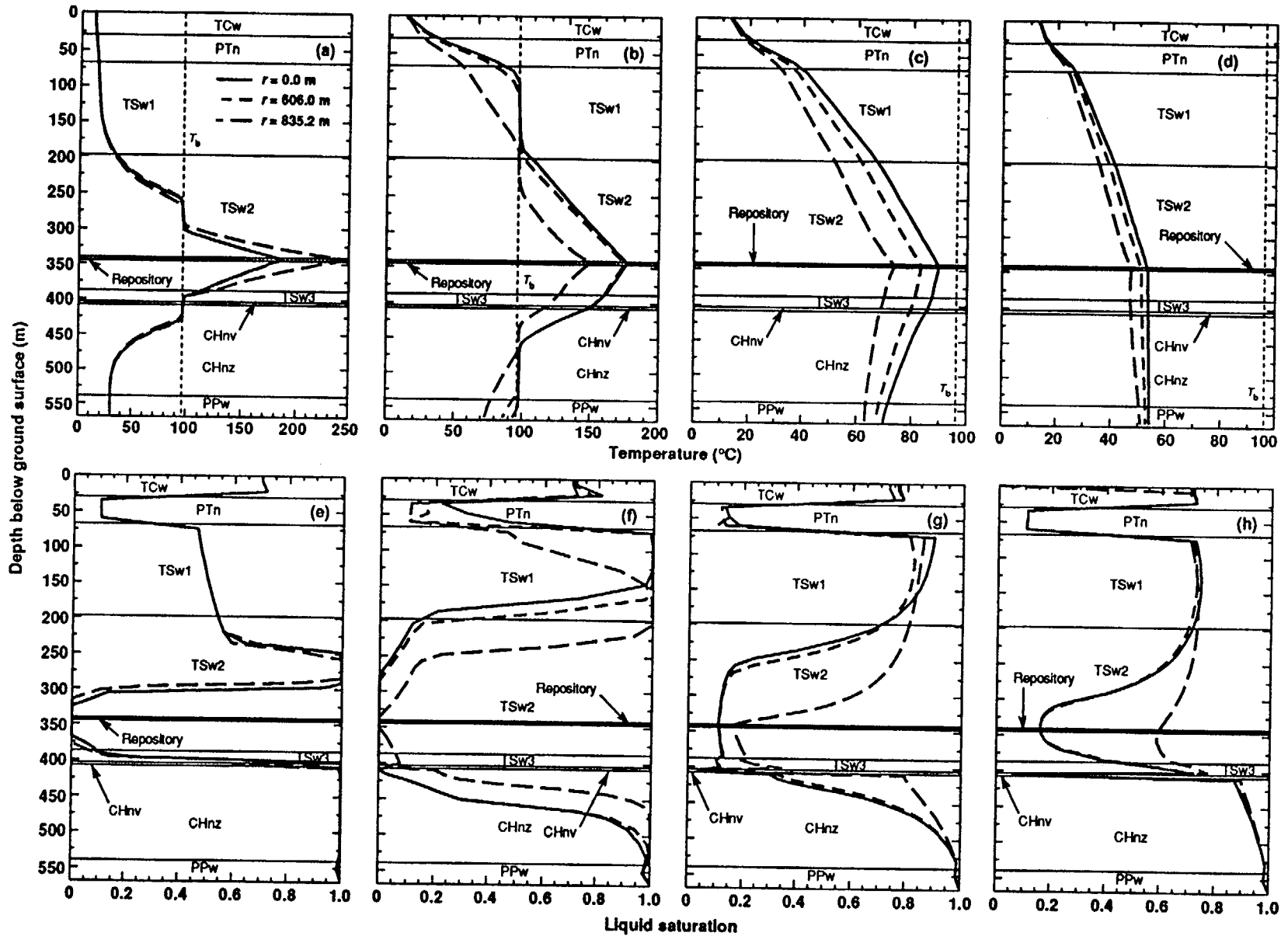


Figure 4.3-4. Vertical temperature profiles at various radial distances,  $r$ , from repository centerline for a nonuniform AML of 128.4 MTU/acre at (a)  $t = 100$  yr, (b)  $t = 1,000$  yr, (c)  $t = 10,000$  yr, and (d)  $t = 30,920$  yr. Note different temperature scales. Vertical liquid saturation profiles are also plotted at (e)  $t = 100$  yr, (f)  $t = 1,000$  yr, and (g)  $t = 10,000$  yr, and (h)  $t = 30,920$  yr. Matrix properties for the TSw1 and TSw2 are based on Klavetter and Powers (1986). Binary gas-phase tortuosity factor  $\tau_{eff} = \frac{\tau_{eff}}{\tau_{eff}}$  for all units.

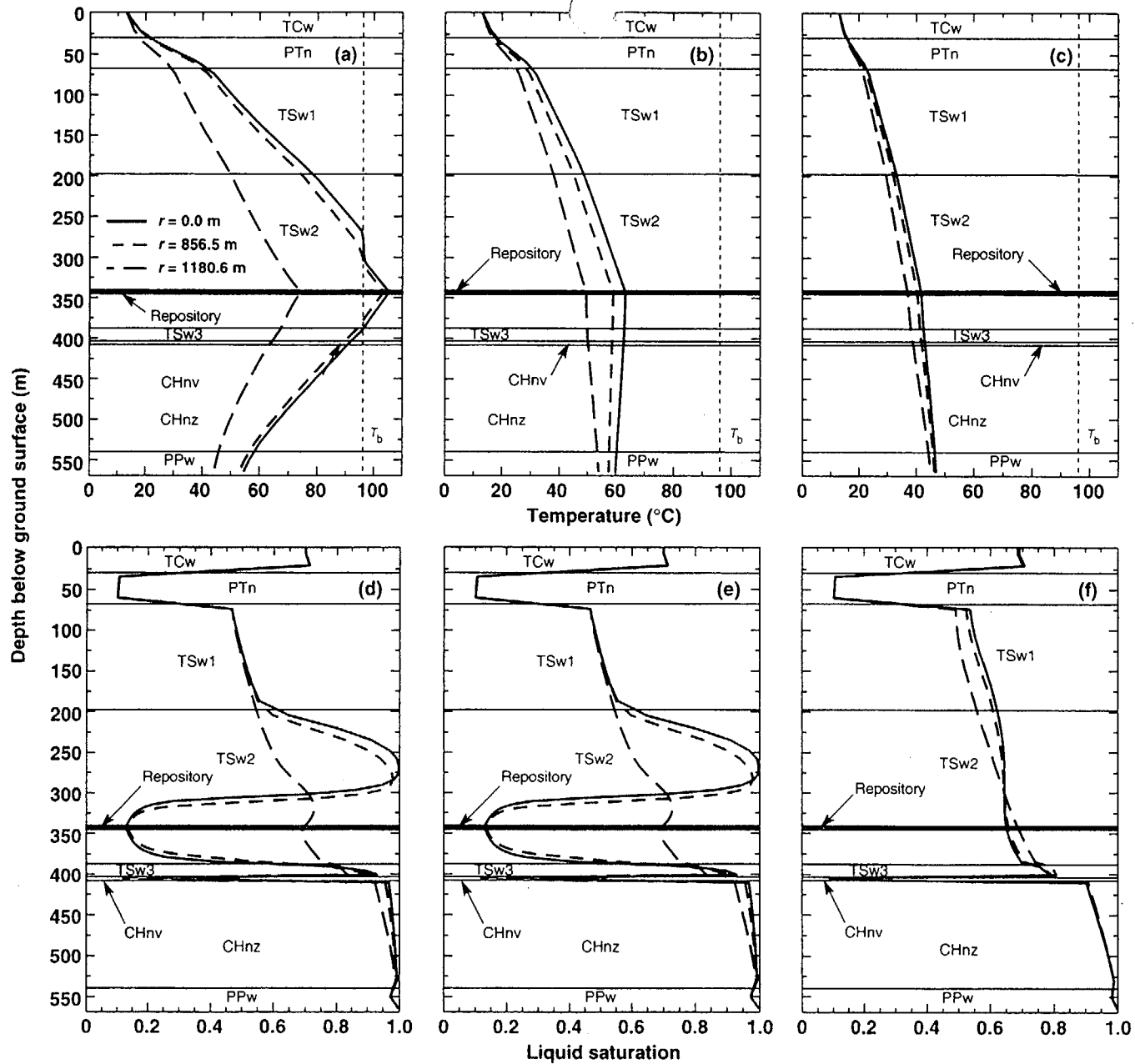


Figure 4.3-5. Vertical temperature profiles at various radial distances,  $r$ , from repository centerline for a uniform AML of 55.3 MTU/acre at (a)  $t=1,000$  yr, (b)  $t=10,000$  yr, and (c)  $t=36,000$  yr. Note different temperature scales. Vertical liquid saturation profiles are also plotted at (d)  $t=1,000$  yr, (e)  $t=10,000$  yr, and (f)  $t=36,000$  yr.

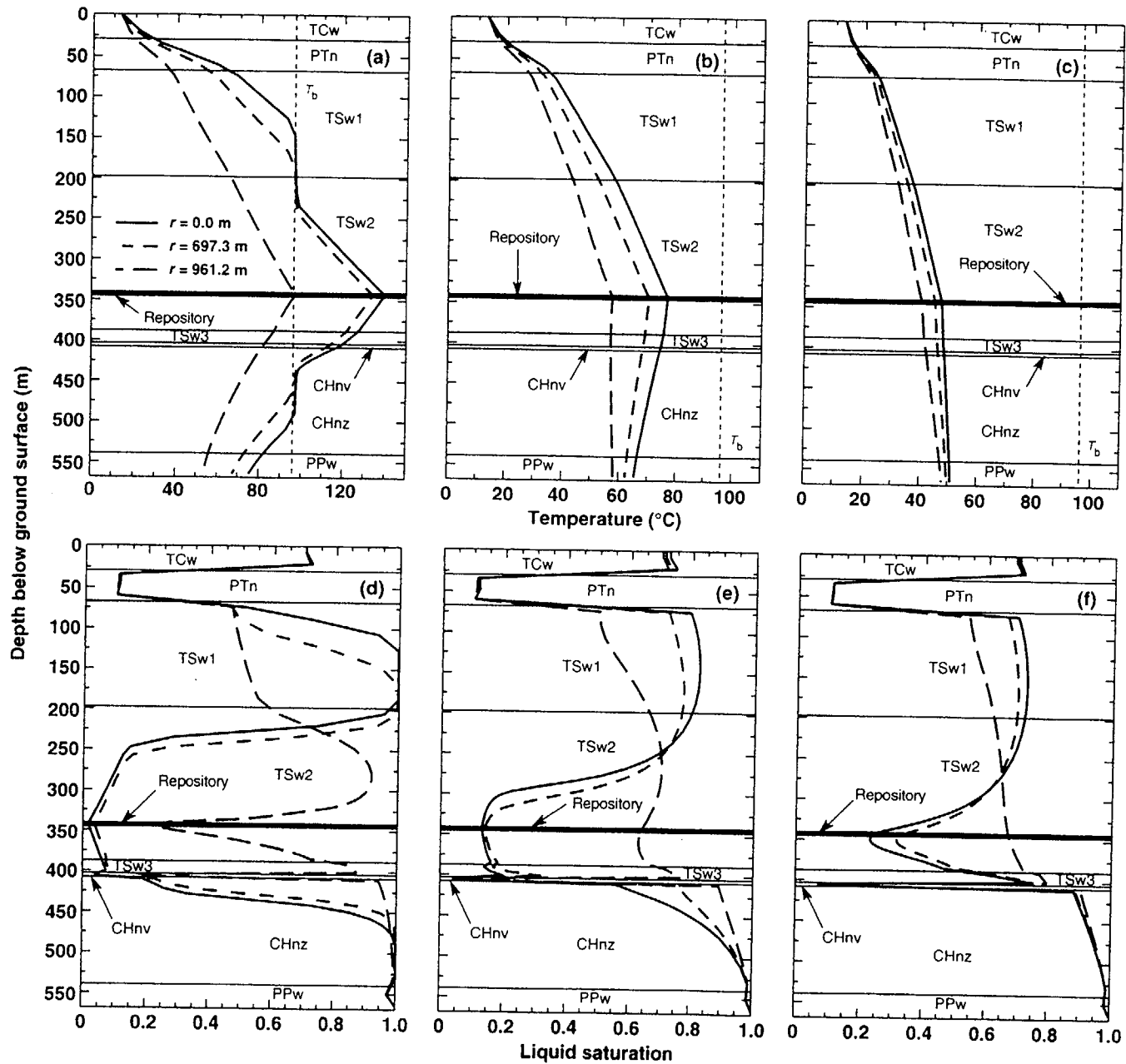


Figure 4.3-6. Vertical temperature profiles at various radial distances,  $r$ , from repository centerline for a uniform AML of 83.4 MTU/acre at (a)  $t=1,000$  yr, (b)  $t=10,000$  yr, and (c)  $t=33,000$  yr. Note different temperature scales. Vertical liquid saturation profiles are also plotted at (d)  $t=1,000$  yr, (e)  $t=10,000$  yr, and (f)  $t=33,000$  yr.

For the mid-range AML of  $13.7 \text{ kgU/m}^2$ , the predictions show that for the outer 10 percent of the disk area, the time that the repository horizon is above boiling is increased from a few hundred years or less in the case of a uniform AML to more than 1,500 years for a nonuniform AML. The liquid saturations, and consequently the relative humidities around the waste packages, are changed very little in the uniform AML case for the outer areas of the potential repository. For the nonuniform AML, there is a substantial reduction in saturation and relative humidities indicating that some drying of the host rock will occur. As one goes to higher AMLs, the duration of boiling in the outer 10 percent of the repository horizon is increased by at least a factor of 1.5 over the uniform AML cases, and the relative humidities are reduced significantly and remain low for longer periods of time. These are calculations that have been done with computer code that should be verified with large-scale, in-situ thermal testing. Additionally, thermohydrological heterogeneity and variability in the heat output of the waste packages will cause local behavior to deviate from average behavior.

The above discussion has centered on postclosure performance. The disposal system also must meet preclosure performance requirements as well. In particular, operability and ability to retrieve must be preserved. To evaluate this, the predicted temperature profiles plotted in Figures 4.3-1 through 4.3-4 for the nonuniform AML cases at 100 years after emplacement were used. Figure 4.3-1a shows that for the  $13.7 \text{ kgU/m}^2$  case at 100 years, the temperature in the outer areas is significantly hotter (about  $150^\circ\text{C}$  compared to  $110^\circ\text{C}$  for the inner areas) than the inner areas. This of course is due to the higher density of emplaced fuel. The temperature plotted is a prediction for that radial distance and temperatures will likely be somewhat hotter at greater distances and somewhat cooler at closer distances. Additionally, the predictions are bulk average rock predictions and the drift wall will have hotter temperatures than shown in these figures. An examination of the other cases shows that for the nonuniform AML case, which has an average loading of  $24.0 \text{ kgU/m}^2$ , the temperature in the outer areas is about  $200^\circ\text{C}$  with the drift wall even hotter. For AMLs above this value (e.g. the  $31.8 \text{ kgU/m}^2$  case in Figure 4.3-4) the temperatures can be significantly above  $200^\circ\text{C}$  in the outer areas of the potential repository during the preclosure period.

Currently, the Program has a thermal goal that the drift wall not exceed  $200^\circ\text{C}$  (M&O, 1993a), which is based on a requirement not to exceed the thermomechanical limit of the rock. Preliminary thermomechanical analyses indicates that if drift wall temperatures exceed about  $200^\circ\text{C}$  that the temperature gradient will be large enough that there is a possibility of significant rock failure. A significant rock fall could potentially damage the waste packages that could result in enhanced corrosion once water vapor returns, which is a postclosure issue and/or may inhibit retrieval, which is a preclosure issue. Operations and retrieval concepts under high temperature conditions have not been fully defined as yet and will likely be very challenging even at elevated temperatures, which are less than  $200^\circ\text{C}$  although ventilation has been considered to reduce temperatures during the time entry into the drift is required. If thermal tests indicate that a not to exceed temperature of something like  $200^\circ\text{C}$  should be established as a requirement, there may still be some steps that can be taken to employ nonuniform AMLs at the higher thermal loadings. One solution might be to wait until just before closure and then load the outer drifts at the higher density. Another option may be to ventilate the emplacement drifts during the preclosure period. Both these cases, though, do not address the postclosure issue of rock fall and could be undertaken only if that is shown not to be a performance issue. Additional discussion of rock fall can be found in the thermomechanical section of the report.

In summary, the calculations show that nonuniform AMLs can be employed to significantly increase the duration of boiling at the edges under conditions of a high thermal load and can produce some rock dry-out which will reduce the relative humidity in the vicinity of the waste package. However, the more uniform duration of boiling in the edges is associated with significantly higher preclosure temperatures. Thermal loads above about 24.0 kgU/m<sup>2</sup> (96.9 MTU/acre), which is representative of a 20.7 kgU/m<sup>2</sup> (83.4 MTU/acre) AML, produce temperatures in the outer areas of the potential repository that exceed the thermal goal of 200°C. Further evaluations are needed to determine the impact on operations and retrieval as well as potential postclosure performance issues. Test results are needed to verify whether or not a not-to-exceed limit of 200°C will be established as a requirement. However, there are potential tradeoffs, such as loading the outer drifts to higher density just prior to closure or ventilation and/or aging could be considered.

#### 4.4 VARIATIONS IN LINE LOADING AS A THERMAL MANAGEMENT TOOL

A number of thermal loading alternatives from a relatively low thermal loading of 6.0 kgU/m<sup>2</sup> (24 MTU/acre) to high thermal loadings of 27.3 kgU/m<sup>2</sup> (111 MTU/acre) or higher have been examined in system studies (M&O, 1994c and M&O, 1994d). The lower thermal loadings, less than about 9.9 kgU/m<sup>2</sup> (40 MTU/acre), are intended to limit the disturbance to the host rock, although in the vicinity of the large waste packages the temperatures will still exceed the boiling point. The high thermal loads are intended to mobilize liquid water, drive it away from the waste packages, and, based on model predictions, will require many thousands of years to rewet back to ambient conditions. The various thermal loads can be achieved in a variety of ways through changing waste package spacing and/or drift spacing. The purpose of this section is to examine some of the aspects associated with adjusting the spacing of the waste packages, adjusting drift spacing, or aging of the waste packages. For example, can waste packages be placed close together in the drifts to locally simulate a high thermal loading but retain large drift separations, which would result in a localized disturbance on a mountain scale?

To examine the influence of waste package spacing and drift spacing on temperature and heat mobilized fluid flow, a number of calculations were conducted at various thermal loads and waste package/drift spacings. A range of thermal loadings from about 1.5 to 29.6 kgU/m<sup>2</sup> (6 to 120 MTU/acre) were used with drift spacings ranging from about 25 to 400 m. For these cases, the waste package spacing varied and is represented by LML (expressed in MTU/m)<sup>8</sup> which ranged from 0.24 to 1.25 MTU/m. Most of the calculations were done using an OFF receipt scenario with approximately 26-year-old fuel at emplacement. Figure 4.4-1 shows a plot of the various ways that an AML might be used with a combination of five different LMLs and the corresponding drift spacings. In addition to the proposed waste package sizes of 12 and 21 PWR capacities, a smaller waste package of only 4 PWR capacity was included so that the lowest LML of 0.24 MTU/m could be attained. It also should be noted that some of the LMLs may be operationally unachievable, however, no intent was made to evaluate these issues in this report.

---

<sup>8</sup> It should be noted that there is some inconsistency in units as in many sections. Specifically, the calculations and plots done by the participants were done in MTU rather than kgU, and rather than replot the curves, the units MTU/m will be used in this section.

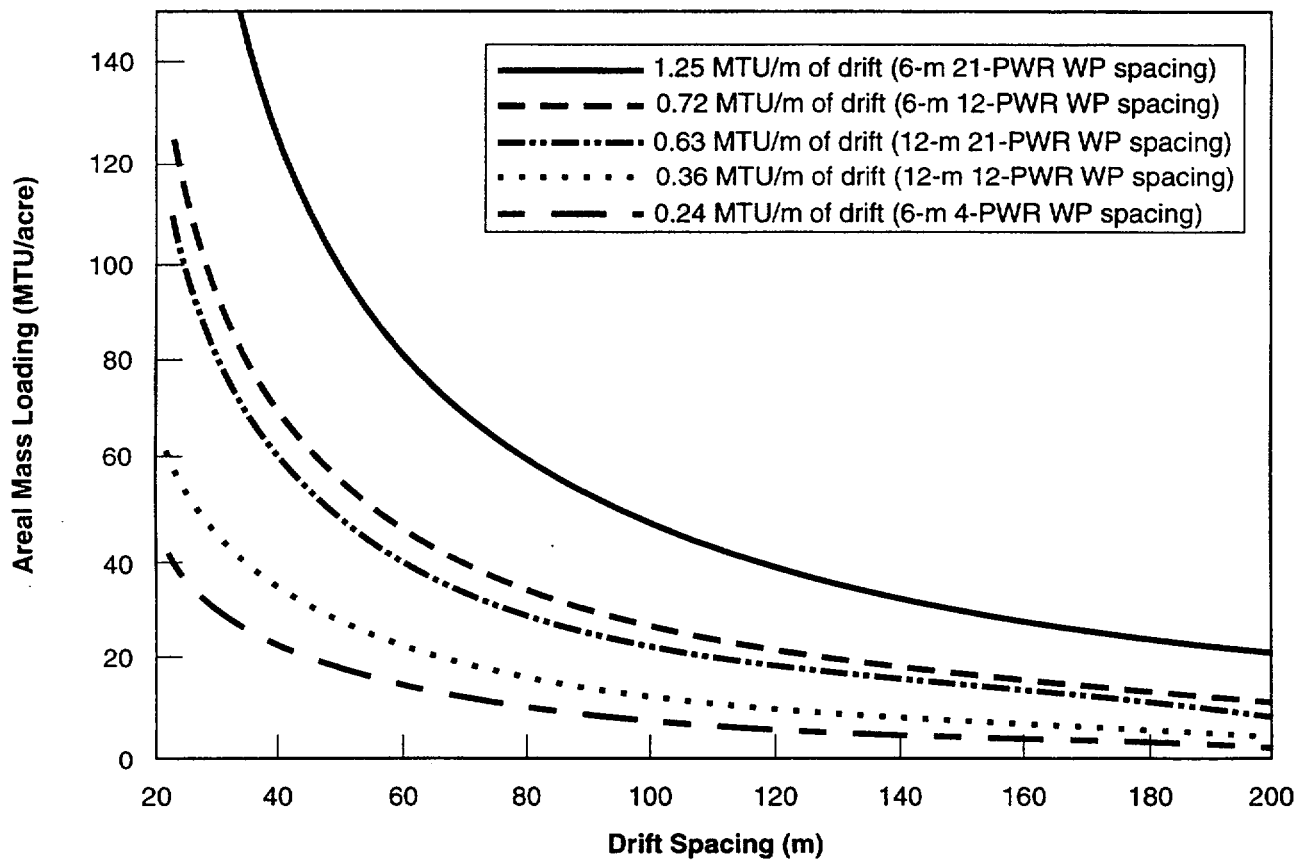


Figure 4.4-1. A Given Repository-Wide Areal Mass Loading Can Be Achieved by Various Combinations of Drift and Waste Package Spacing.

The calculations were done with drift-scale models that represent the details of the waste packages, emplacement drifts, and the pillars separating drifts in a cross-section that is orthogonal to the drift axis. The calculations were done with the V-TOUGH code, although a smeared heat source was not used. The analyses reported here, however, did assume that the heat load along the drift was represented by a line-heat load. This assumption is most applicable when the waste packages are close together, such as in the 6 m spacing. However, if the drifts are not backfilled, thermal radiation between the waste packages and drift wall should be sufficient to allow an axial temperature distribution that is adequately approximated by a line source. For large waste package spacings, equaling the drift spacing, the temperatures may not be as well-represented by the line-heat load. The V-TOUGH code and the inputs used are discussed in previous sections.

Criteria on such things as temperature limits, liquid water movement, relative humidity, or others to apply to achieve the desired performance are not well-defined at this stage. The criteria would likely be different for a high thermal loading than for a low thermal loading. Certain thermal goals have been established for both the near and far field (M&O, 1993a).

Some of these thermal goals may eventually become criteria or requirements once they have been validated based on information gained through in-situ thermal testing. Variations in LML would primarily affect the near-field temperatures and water movement and so near-field criteria need to be ultimately defined for the system. The near-field thermal goals that exist are oriented primarily toward the high thermal loads. Examples of such goals are the following (M&O, 1993a):

1. Keep in-drift wall temperatures  $<200^{\circ}\text{C}$ .
2. Boreholes that do not load container beyond limits imposed under Issue 1.10.
3. Maximize the time the waste package container stays above boiling consistent with the thermal strategy developed.
4. Fuel cladding temperature  $<350^{\circ}\text{C}$ .

The above goals, as indicated, are primarily oriented toward higher thermal loadings. If a low thermal loading option was to be selected, then the goals or criteria established might be different. For example, the presence of liquid water and the temperature of the waste package will be of paramount importance. Corrosion of the waste packages may result if the local relative humidity is high enough and the temperatures are high. Additionally, one may want to restrict the disturbance, in terms of possibly the temperature and/or amount of liquid water that is mobilized, beyond a certain distance from the waste package to avoid geochemical alterations. Therefore, the analyses done in this section will provide some guidance as to how such goals or criteria might be met.

An extensive set of thermal calculations was done for the various AMLs and different LMLs. In addition to these variations, aging of the fuel was simulated as well. For these calculations it was assumed that, instead of emplacing all of the fuel at an average age of about 26 years out of reactor, the fuel was aged longer and the appropriate decay curves used for the older fuel. Cases for fuel ages of 26-, 40-, 60-, 100-, and 200-year-old fuel were considered. Peak waste package temperatures are plotted in Figure 4.4-2a for the five fuel ages for two LMLs of 0.63 and 1.25 MTU/m using the 21 PWR capacity waste packages. Although smooth curves are shown, the calculations were done at only certain AMLs as mentioned above and a smooth curve was fit to the results. As shown in the figure, the peak waste package temperature is a relatively weak function of the AML (except for the lowest LML cases which are not shown here) although it is a strong function of LML. That is, comparing the solid curve in Figure 4.4-2a with the similar curve in Figure 4.4-2b shows a larger LML increases temperatures of the waste packages significantly. The calculations also demonstrate that peak temperature is strongly dependent on fuel age as would be expected.

Estimates of the duration of the boiling period on the drift wall were done for the various AMLs and fuel ages and these are plotted in Figure 4.4-3 for two LMLs. When the temperature drops below the boiling point there may be an opportunity for water to return, however, the matrix may delay the return so these curves are only a crude measure of the potential for corrosion to begin. This calculated bound should not be considered as a high-confidence number, however, because the calculations did not consider other possible phenomenon such as heterogeneities, which could focus flow or water movement to local areas, resulting in earlier cooling and moisture return. Additionally, it should be noted that the calculations provided are for the center of the repository and the edges may have significantly shorter boiling periods as discussed in the previous section. The results show that, at least at the lower LML, the AML should be above some threshold before boiling will occur and this threshold increases with fuel age. The duration of the boiling period is a relatively strong function of AML and fuel age, although fuel age is not as significant a driver at the higher LML.

Figure 4.4-4 indicates the estimates of the maximum vertical extent of the boiling point isotherm above the potential repository for various AMLs and fuel ages. The curves clearly show the threshold of about  $9.9 \text{ kgU/m}^2$  (40 MTU/acre), which the AML must be above for significant (above a few meters distance) boiling to occur. The vertical extent of boiling is clearly a strong function of AML and fuel age above the threshold. However, the figures show that the vertical extent of boiling does not depend much on the LML, except below the threshold of  $9.9 \text{ kgU/m}^2$ , with vertical extent being similar at 1.25 MTU/m as it is for the 0.63 MTU/m case, all other things being equal. To alter the extent of boiling by a large amount only through aging appears to require aging of about 200 years which is impractical. However, aging of 34 years, thus producing an average fuel age of 60 years, could decrease the vertical extent of boiling by 50 to 75 m, which could be sufficient to protect some geologic barrier such as the PTn from alteration.

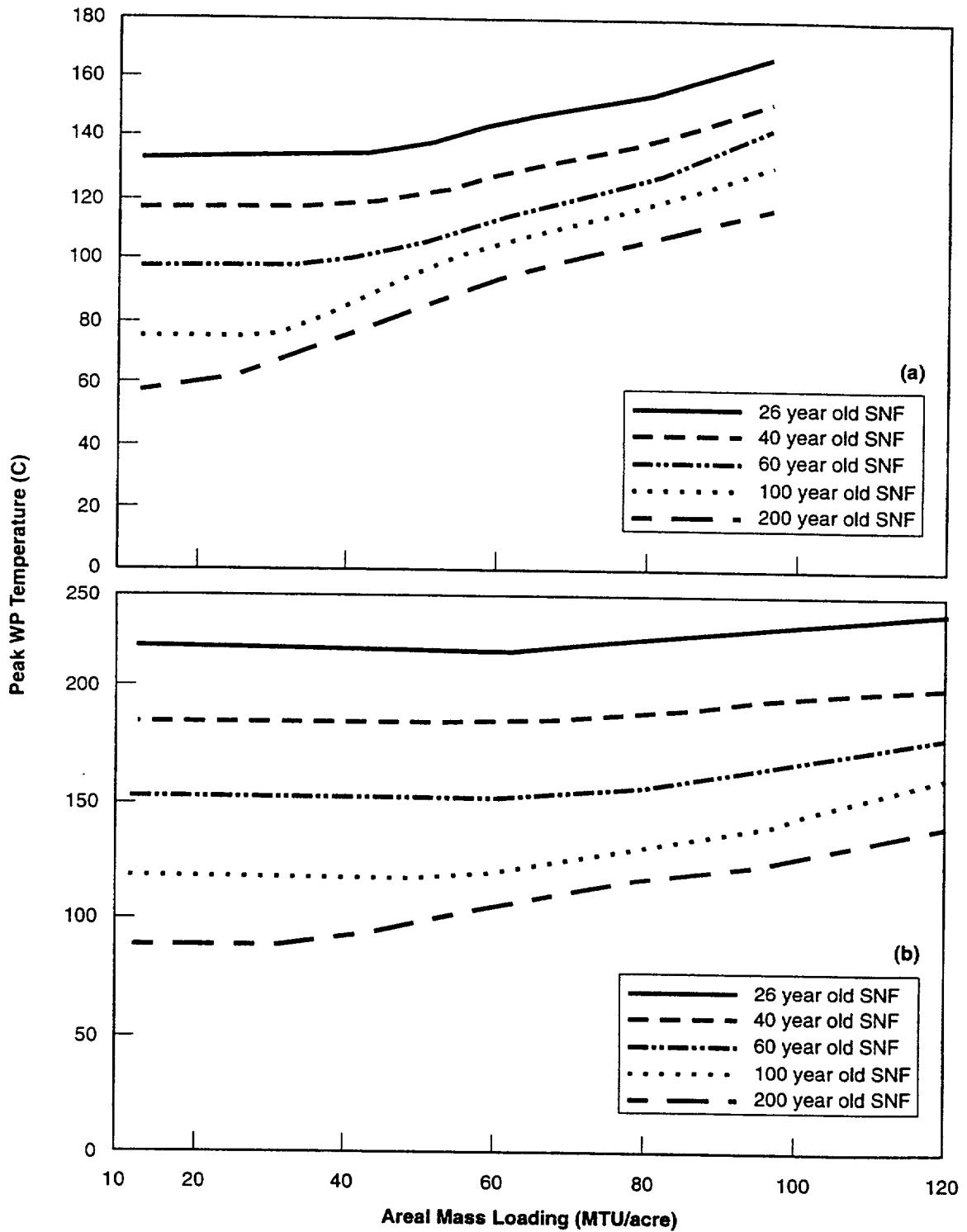


Figure 4.4-2a. Peak Waste Package Temperature for Lineal Mass Loading of 0.63 MTU/m (12-m 21-Pressurized Water Reactor Waste Package Spacing).

Figure 4.4-2b. Peak Waste Package Temperature for Lineal Mass Loading of 1.25 MTU/m (6-m 21-Pressurized Water Reactor Waste Package Spacing).

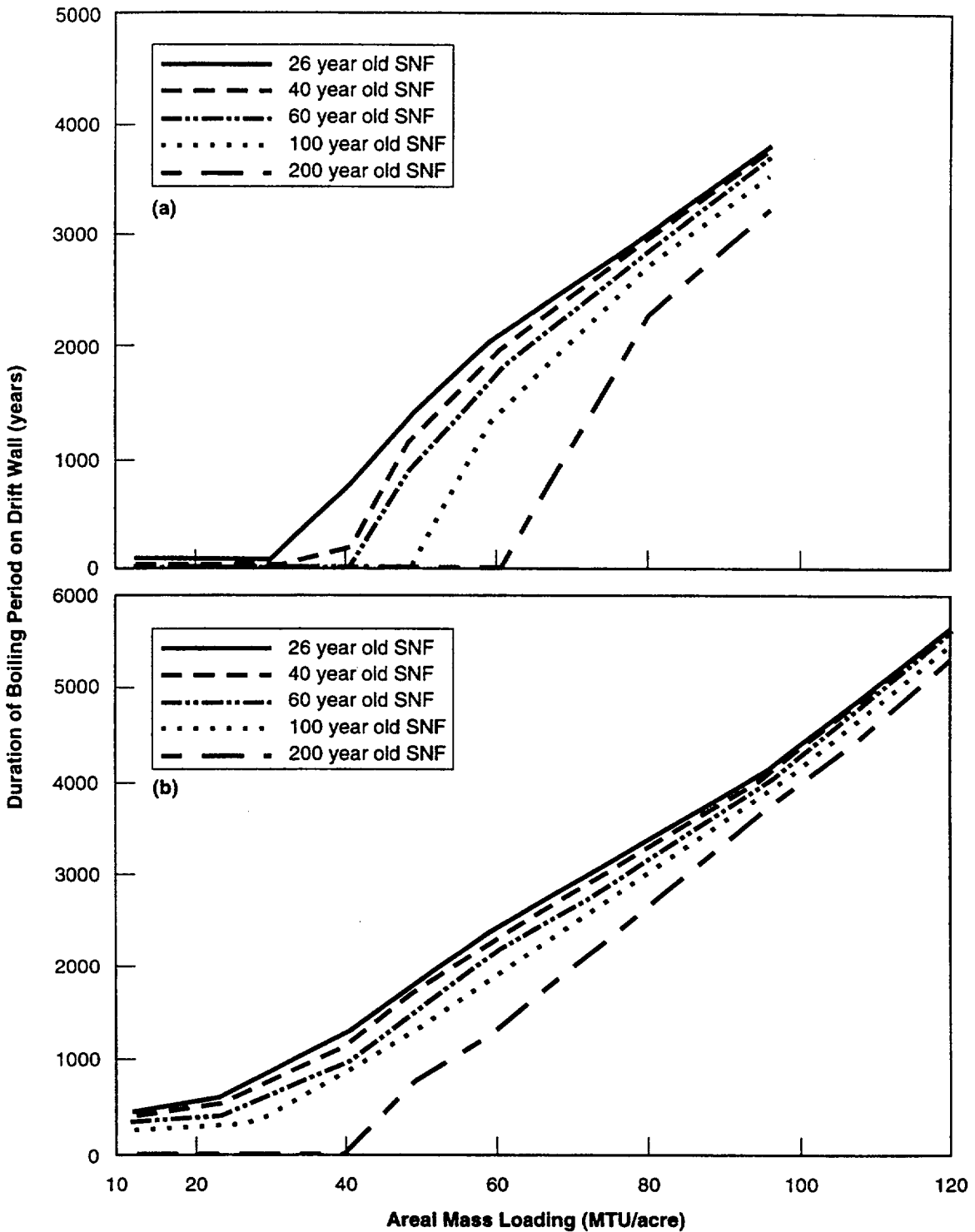


Figure 4.4-3a. Duration of the Boiling Period on the Drift Wall for Lineal Mass Loading of 0.63 MTU/m (12-m 21-Pressurized Water Reactor Waste Package Spacing).

Figure 4.4-3b. Duration of the Boiling Period on the Drift Wall for Lineal Mass Loading of 1.25 MTU/m (6-m 21-Pressurized Water Reactor Waste Package Spacing).

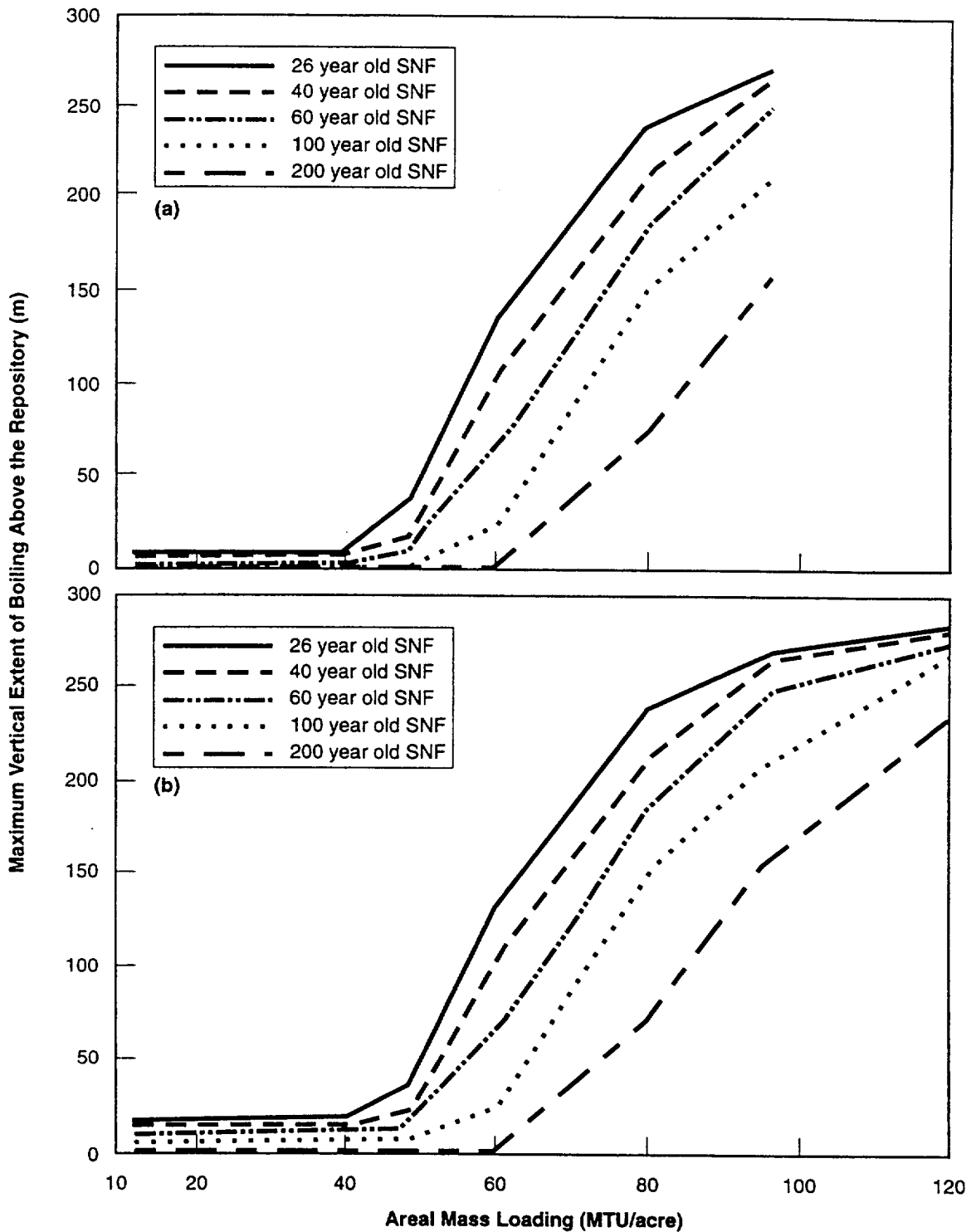


Figure 4.4-4a. Maximum vertical extent of the boiling point isotherm above the repository for Mass Loading of 0.63 MTU/m (12-m 21-Pressurized Water Reactor waste package spacing).

Figure 4.4-4b. Maximum vertical extent of the boiling point isotherm above the repository for Lineal Mass Loading of 1.25 MTU/m (6-m 21-Pressurized Water Reactor waste package spacing).

One of the key questions being addressed in this section was whether or not variations in LML (actually waste package and drift spacing) would significantly change the temperatures in the near field. The calculations show that for moderate to higher AMLs (above the threshold mentioned above), the estimates of duration of boiling on the drift walls and the extent the boiling front propagates into the host rock is relatively insensitive to LML. It would seem that above loadings of about 9.9 kgU/m<sup>2</sup> there does not appear to be an advantage of one LML over another, and therefore, the choice should be made more on which is operationally more efficient or easier. On the other hand, at lower AMLs the choice of an LML to use does appear to make a difference, and a selection of LML will need to be based on satisfying the near-field criteria that must be established.

The calculations showed that aging can alter the waste package peak temperatures, the duration of boiling, and to some degree, the extent that the boiling front propagates into the host rock. The differences are most significant for the waste package peak temperatures. Significant aging (greater than about 40 years) would be required to appreciably affect the duration of boiling on the drift wall and the extent of boiling.

#### **4.5 REPOSITORY THERMAL RESPONSE DUE TO WASTE STREAM VARIABILITY**

The type of spent nuclear fuel (PWR or BWR), the age, and burnup of the fuel all influence the heat output of a waste package and thus, significant variability will exist between waste packages. As a part of the thermal management evaluations conducted in the Thermal Loading System Study, the way in which the waste package heat output variability is handled in the thermal predictions and the effect it has on the temperature predictions was investigated. The approach most commonly taken in studies to date is to use waste stream smearing, which represents the entire waste inventory by a single set of average characteristics. Since more than 200,000 assemblies will ultimately make up the waste stream, errors can be made by representing the waste stream as a single average. Another approach, which has more detail, is to use source term aggregation on an annual basis in which the waste stream is averaged by year and by waste type (PWR or BAR). The analysis discussed in this study examines the next level of resolution to evaluate what differences might result if the actual package to package variability in waste age, burnup, and enrichment were considered. Use of such detail is typically not done in practice because of the large number of packages that must be modeled, but it is important to understand the implications of this resolution of waste stream variations on predictions of host-rock temperatures.

This work was done in support of the System Study by SNL using thermal conduction models. In this effort, the predicted temperatures at 5 meters above the potential repository obtained for a base case that was done using yearly averages in support of subsurface design (YMP, 1993) were compared with predictions made for a case in which three years of emplaced waste were replaced by actual package-to-package heat characteristics. Further details of the effort, beyond the summary of information below, can be found in a Sandia report by Ryder and Dunn (1995).

#### 4.5.1 Modeling Assumptions

The internal details of the waste package are not of a scale that is important for repository scale analyses of host rock thermal response. Thus the waste packages were assumed to be adequately represented by a smeared heat source, which was a 4.91 m long cylinder with a diameter of 1.83 m, which is consistent with a large size MPC.

The waste stream characteristics assumed YFF fuel since this was the fuel used for calculations of the base case that will be discussed below. The YFF scenario characteristics are given in references in M&O (1993d) and M&O (1994). This waste stream assumed flow through and no YFF fuel out-of-reactor is accepted for disposal at the repository. For this investigation, package-by-package information for fuel projected to arrive at the repository for emplacement in years 2028, 2029, and 2030 were considered. The package-by-package details can be found in the more detailed Ryder and Dunn (1995) report. Additionally there was no limit placed on the heat output of the packages. Recently, the Program has assumed a not-to-exceed limit of 14.2 kw on the waste packages for emplacement (DOE, 1995b). A few of the waste package in the years 2028 and 2029 were above this limit.

The base case model used for all the comparisons assumed a constant AML of 19.3 kgU/m<sup>2</sup> (78.2 MTU/acre). Based on the waste stream used, this can be translated into an APD, but APD changes with time as the fuel decays. The calculated instantaneous value of APD at emplacement for the base case was about 24.7 W/m<sup>2</sup> (100 kW/acre). The thermal calculations considered that the 63,000 MTU of SNF were emplaced at the above AML in about 3.24 x 10<sup>6</sup> m<sup>2</sup> (800 acre) in the upper block of the primary area. This required only the first 93 drifts of the upper block to be modeled. The drifts were spaced 30.5 m apart (M&O, 1993c).

The specific thermal model chosen for the study is documented in Wilson, et al. (1994). The waste was assumed to be located in a semi-infinite rock mass that had a thermal conductivity of 2.1 W/m-K and a heat capacitance of 2.14 J/cm<sup>3</sup>-K. These values are consistent with ones reported in the RIB for TSw2. The surface temperature was assumed to remain constant throughout the 1000 year modeled time frame.

#### 4.5.2 Method and Results

The base case in this analysis used source term aggregation on an annual basis to obtain the heat output for each type of waste package. This base case was done in support of North Ramp design activities (YMP, 1994). The yearly average characteristics of each waste package type (PWR or BWR) were then assigned an order for emplacement for a given year using a nonunique, randomized selection process which minimized bias (Ryder and Dunn, 1995). Canister-to-canister spacings in a drift were assigned based on yearly average values of MTUs per canister defined for each type of waste which would provide a uniform AML of 19.3 kgU/m<sup>2</sup>.

Figure 4.5-1 shows the predicted base case temperature contours (Ryder and Dunn, 1995) at 5 m above the potential repository horizon (a plane connecting the waste package centerlines) for 50 years after the initial start of waste emplacement (assumed to be in 2010). The effects of stepped emplacement (emplacement started on the left side and progresses to the right) can clearly be seen in the figure as a growth in temperature perturbations. It also is apparent from the figure that the isothermal contours do not form regular bands that expand uniformly across the repository. Instead hotter and "colder" (implying cooler temperatures than surrounding areas) regions form. This is a result of the assumptions applied to this analysis, which were a large waste package capacity, and a constant AML. The MPC, with its large capacity, will result in a coarser distribution of heat than would a much larger number of smaller packages. The constraint of a constant AML results in the fact that in some areas hotter waste can be emplaced next to "cold" waste as long as the AML remains constant. At much later times, the temperature variations due to these constraints are negligible as shown in Figure 4.5-2 for a calculation at 1000 years. It should also be noted from an examination of the figures, that with a constant AML, significant edge cooling can occur in the potential repository. More was discussed concerning edge cooling in a previous section.

As can be seen in an examination of Figure 4.5-1, even the base case, with annual averages of the waste stream, produces nonuniformity in localized temperatures when constrained to preserve a constant AML. As a result of this, the local area power densities (LAPD) for this base case vary between 9.8 to 30.9 W/m<sup>2</sup> (40 to 125 kW/acre) as discussed in Ryder and Dunn (1995). Most of the variations and lower LAPDs occur in the last few years of emplacement (about 2030 or later) when the older fuel stored at the utilities is shipped.

This effort looked at how the general trends described above were affected by using an increased resolution in the waste stream. For this effort, package-by-package variations for waste packages emplaced during the years 2028, 2029, and 2030 were examined. These years were chosen in part due to the fact that significant variations were noted in the waste stream. The average packages emplaced in those years in the base case were replaced by the detailed package heats. This amounted to about 12 drifts, which were used in the revised calculations, and the area of the potential repository affected is shown in Figure 4.5-3.

Since the model used in generating the Base Case results was linear, it was possible to remove sections of the solution (the thermal contributions for specific emplacement years) and replace them with solutions obtained using different waste streams. Case I uses the majority of the Base Case solution with the exception that the temperature contributions from waste emplaced during the years 2028, 2029, and 2030 are replaced with the more detailed waste stream representation. Individual decay curves were used, based on each package's burnup, enrichment, and age, which explicitly model the power outputs. Package spacings were assigned based on satisfying the requirement to maintain a constant AML of 19.3 kgU/m<sup>2</sup> (78.2 MTU/acre). For this case, even more dramatic differences occur in variations in LAPD than in the Base Case with LAPDs that range from as low as 0.1 to 56.7 W/m<sup>2</sup> (0.5 to 230 kW/acre) (Ryder and Dunn, 1995).



INTENTIONALLY LEFT BLANK



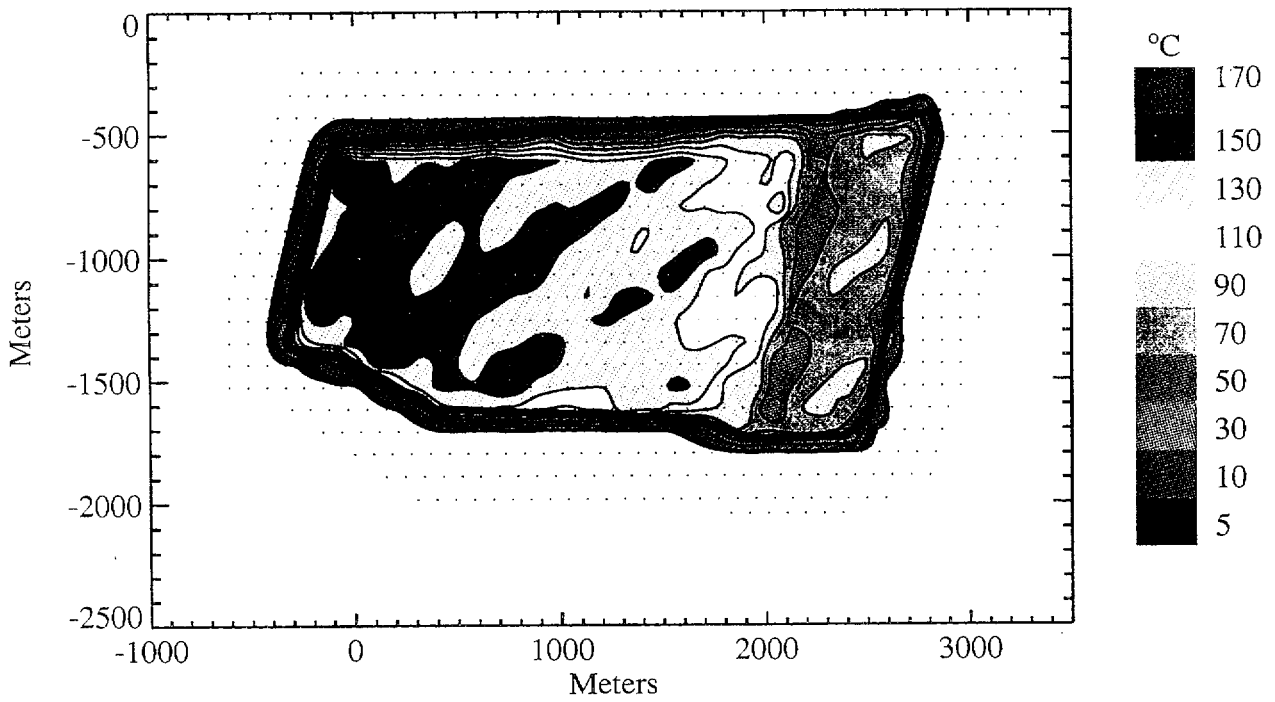


Figure 4.5-1. Contours of Temperature Change 5 m Above the Repository Plane 50 Years After the Start of Waste Emplacement.

INTENTIONALLY LEFT BLANK

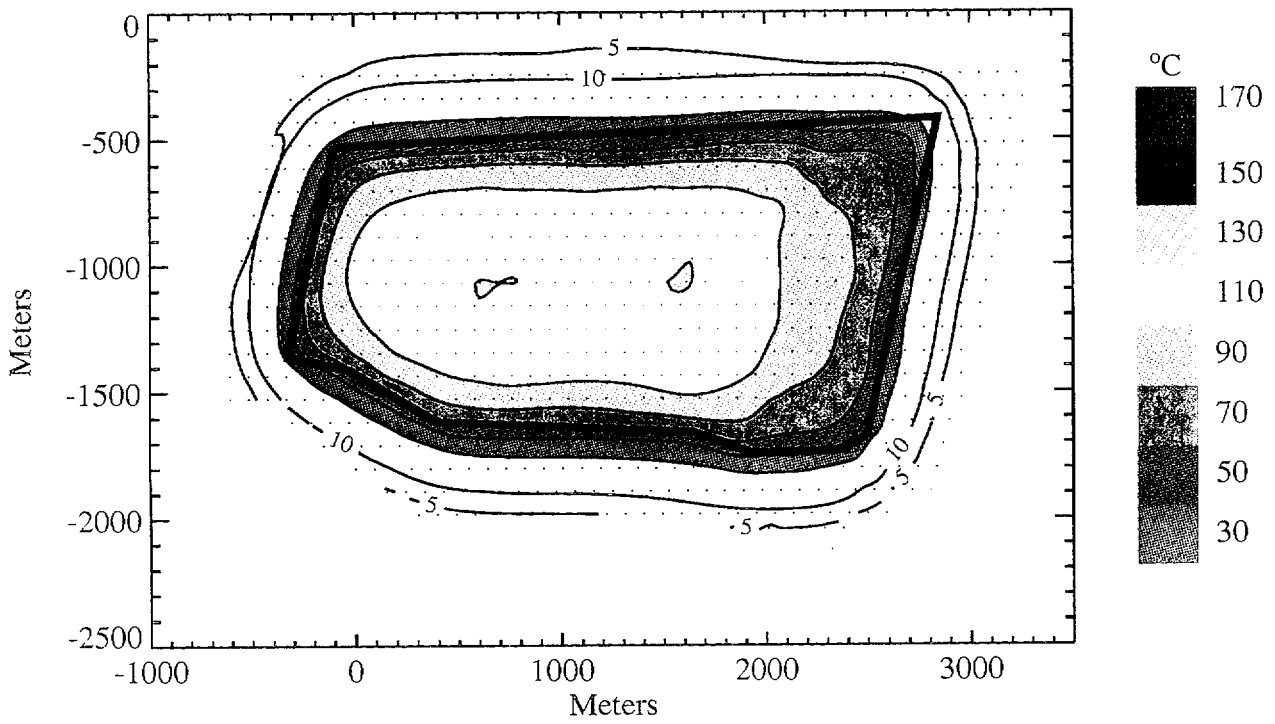


Figure 4.5-2. Contours of Temperature Change 5 m Above the Repository Plane 1,000 Years After the Start of Waste Emplacement.

INTENTIONALLY LEFT BLANK

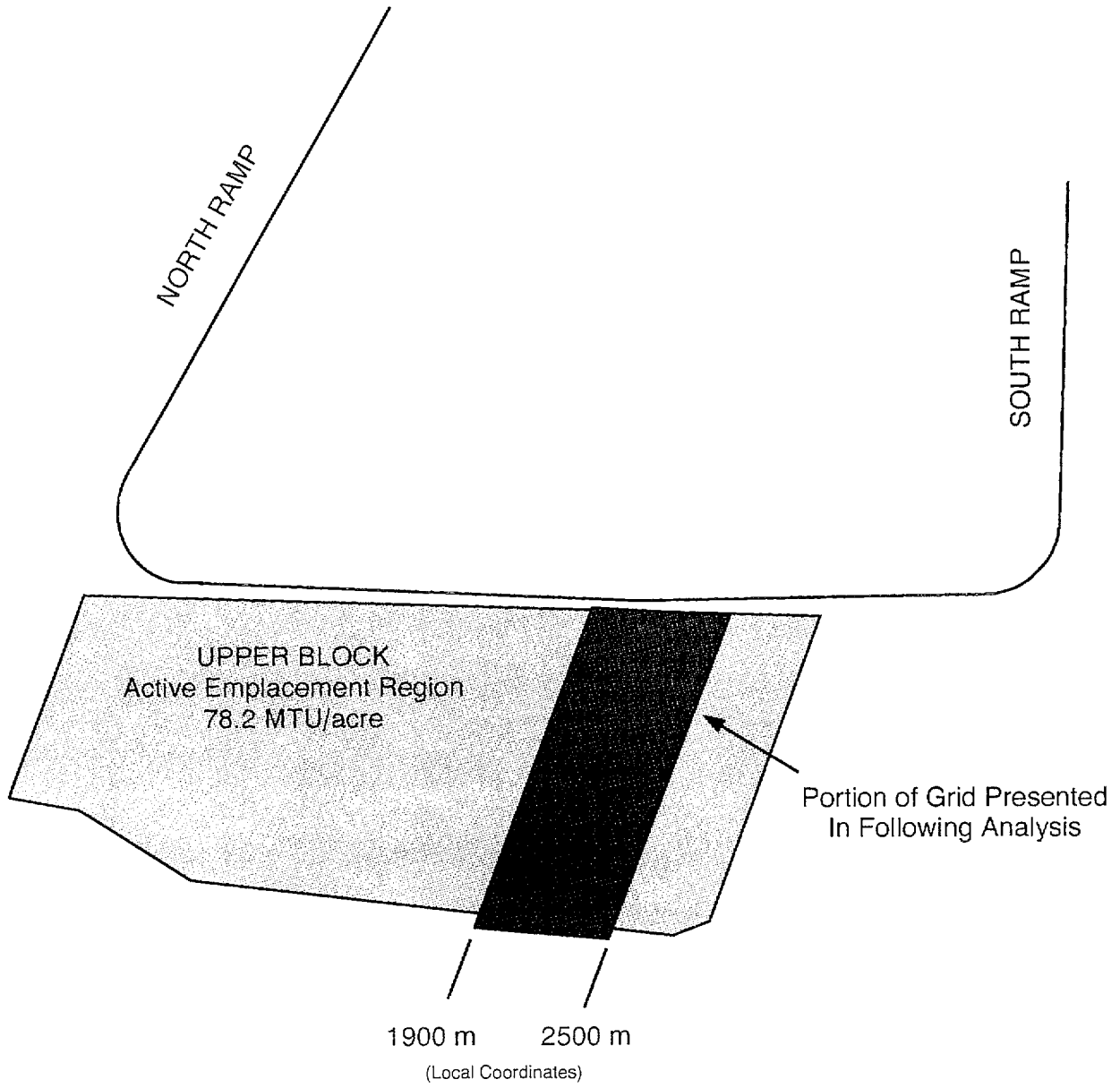


Figure 4.5-3. Location of High Resolution Grid.

INTENTIONALLY LEFT BLANK

The temperature differences between Case I and the Base Case are plotted in Figure 4.5-4 for different times after emplacement. Since the temperature differences at a location were determined by subtracting the temperatures predicted for Case I from the Base Case, positive temperature differences (toward the blue color on the figures) indicate the Base Case predicts higher temperatures while negative values (toward the red color on the figures) indicate the Case I predicts higher values. The maximum numerical temperature differences between the two modeled cases are documented in Table 4.5-1. An examination of the figures shows that the waste package variability in power output produces a number of localized hot and "cold," implying "colder" temperatures than surrounding areas, spots for times up to about 100 years or slightly longer after emplacement. The increased waste stream resolution results in a significant increase in localized temperature differences over the Base Case. In several locations temperature differences of over 100°C were predicted to occur between locations that are in close proximity (about 10 m apart). Beyond about 140 years, the Case I temperature predictions are generally less with the Base Case predicting persistent higher temperatures of about 6 to 22°C over Case I.

Table 4.5-1. Maximum and Minimum Temperature Differences Predicted Between the Base Case and Case I ( $T_{\text{Base}} - T_{\text{Case I}}$ ).

Time (Years)	Minimum (°C)	Maximum (°C)
18	0.00	0.00
19	-53.93	28.74
20	-63.66	35.23
21	-66.74	39.07
22	-67.79	43.61
23	-68.11	46.71
24	-67.75	49.09
25	-67.07	51.05
26	-66.25	52.67
27	-65.31	54.06
28	-64.19	55.20
29	-63.20	56.19
30	-62.38	56.98
40	-53.13	59.76
50	-43.59	58.19
60	-34.97	55.23

Table 4.5-1. Maximum and Minimum Temperature Differences Predicted Between the Base Case and Case I ( $T_{\text{Base}} - T_{\text{Case I}}$ ) (Continued)

Time (Years)	Minimum (°C)	Maximum (°C)
70	-27.67	52.21
80	-21.43	49.30
90	-16.19	46.75
100	-12.68	44.53
120	-11.18	41.01
140	-10.06	38.48
160	-9.22	36.67
180	-8.56	35.32
200	-8.01	34.30
300	-6.07	31.12
400	-4.64	29.05
500	-3.42	27.55
600	-2.36	26.38
700	-1.47	25.37
800	-0.72	24.37
900	-0.11	23.35
1000	0.37	22.24

The early time temperature difference predictions between the two models is a result of the large variations in LAPD that occur. This range of LAPDs produces localized hot and "cold" areas within the potential repository. The reasons that the Base Case produces predictions of higher long-term temperatures appear to be linked to the representativeness of the assumed yearly average used (Ryder and Dunn, 1995). A scatter plot of waste age vs. canister power output for the PWR fuel emplaced in 2029 is shown in Figure 4.5-5. The figure shows that the bimodal distribution of fuel in that year has distinctly different characteristics than the aggregate annual average used in the Base Case. As shown in Figure 4.5-6 for the PWR fuel arriving in 2029, over the long term, the integrated energy obtained using the aggregate annual averages in the Base Case is about 26 percent larger than if individual package energies are used. This could result in underpredictions of the long-term heating, which may result in underprediction of the time that the host rock stays above boiling for the strategy, which relies on heat to dry-out the rock and keep moisture away from the waste packages as long as possible.

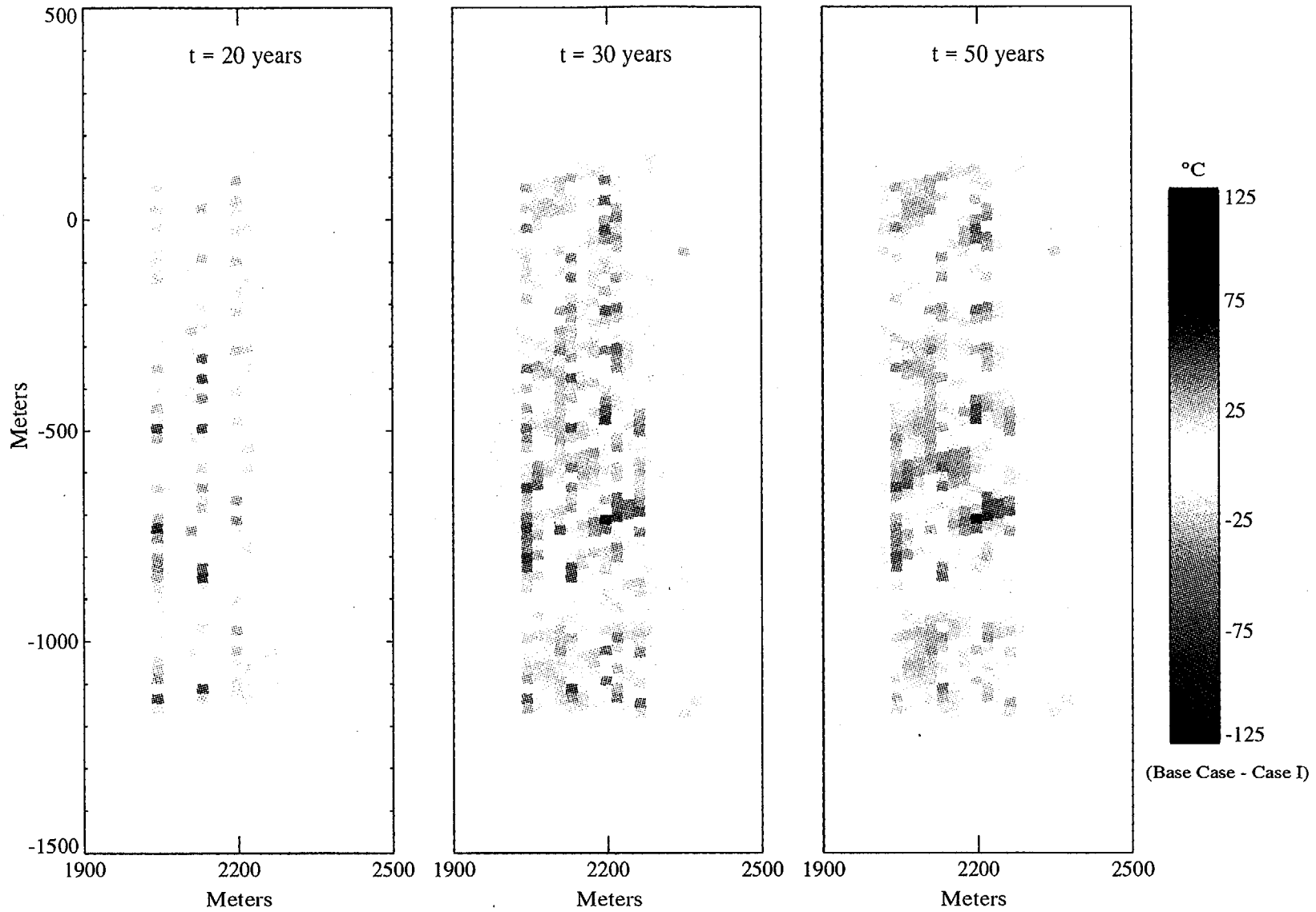


Figure 4.5-4. Temperature Difference History Between the Base Case and the Case I Models.

INTENTIONALLY LEFT BLANK

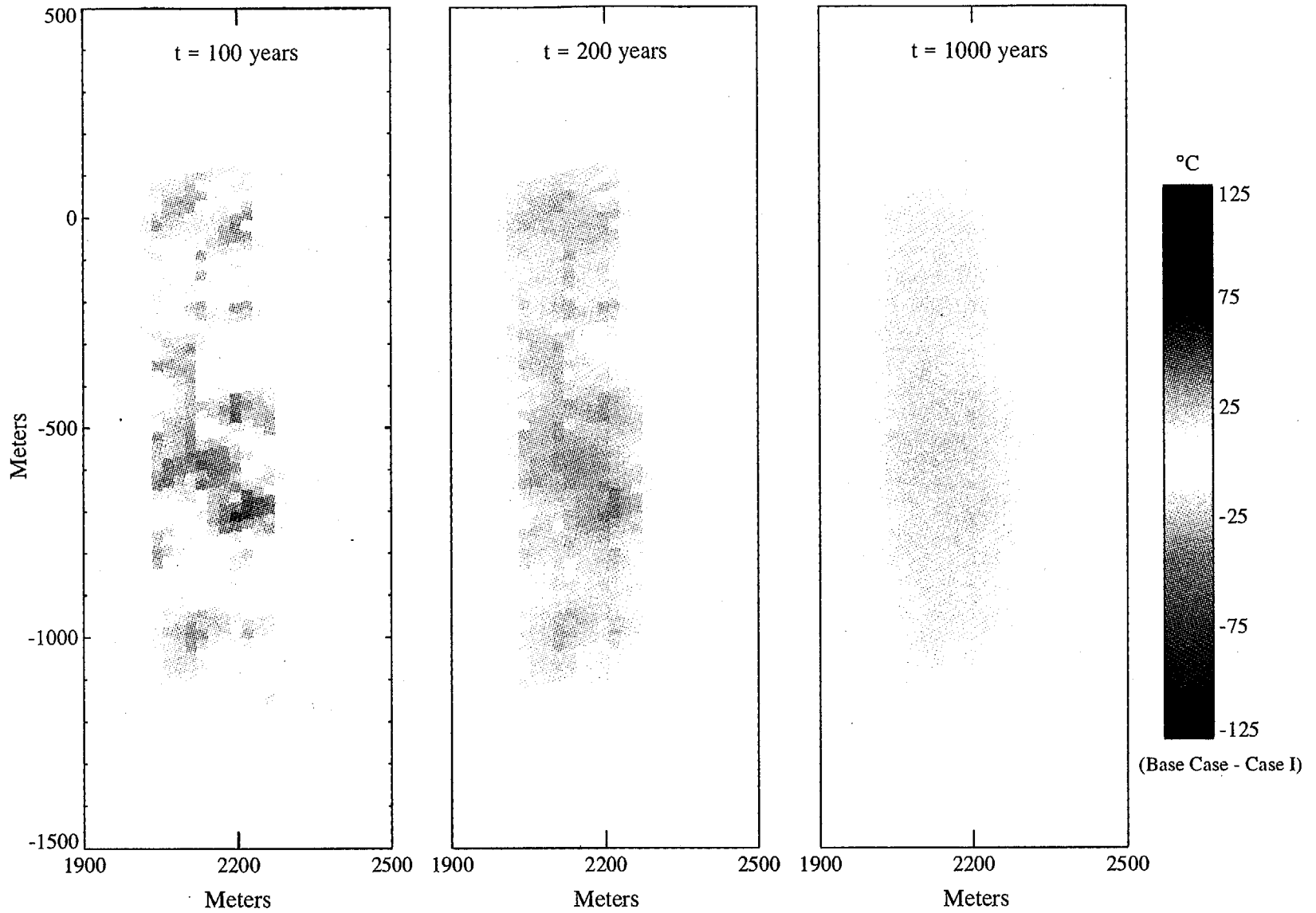


Figure 4.5-4. Temperature Difference History Between the Base Case and the Case I Models (Continued).

INTENTIONALLY LEFT BLANK

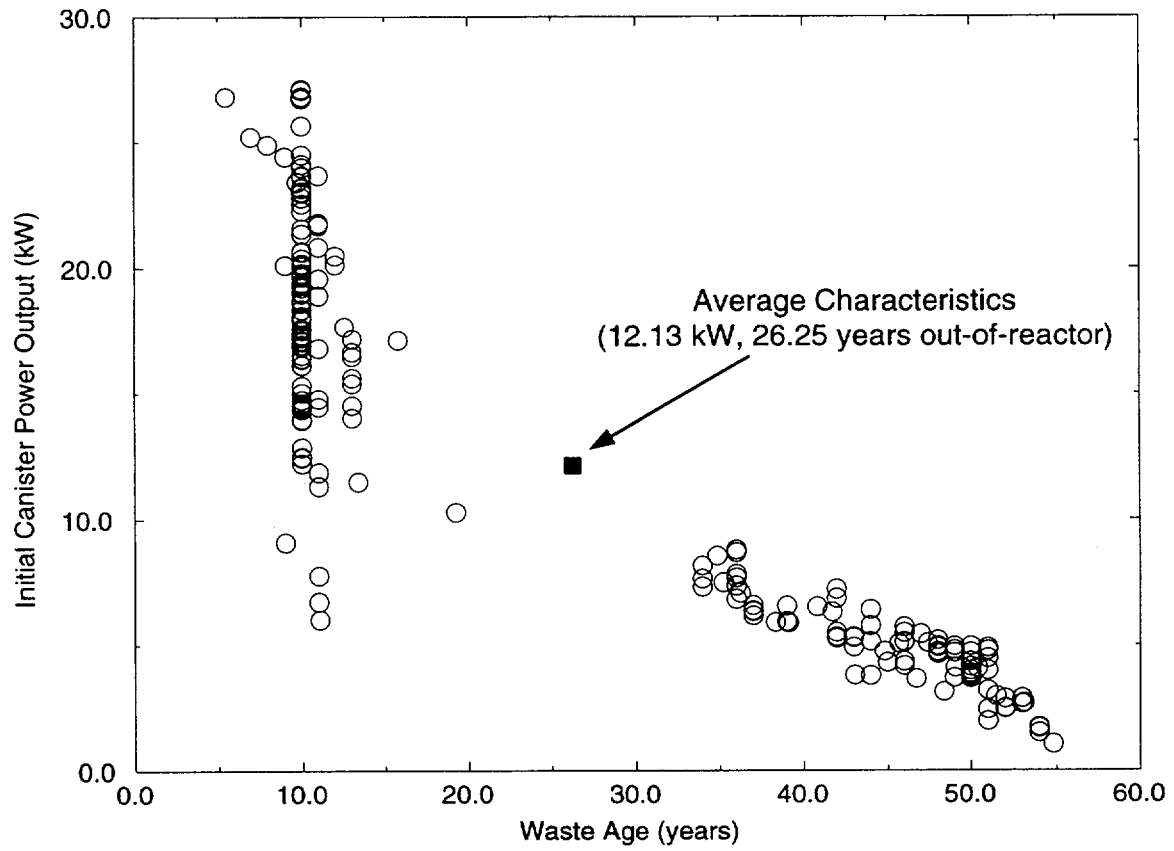


Figure 4.5-5. Logical Grouping for Averaging Waste Stream Characteristics for 2029 Pressurized Water Reactor Waste Packages.

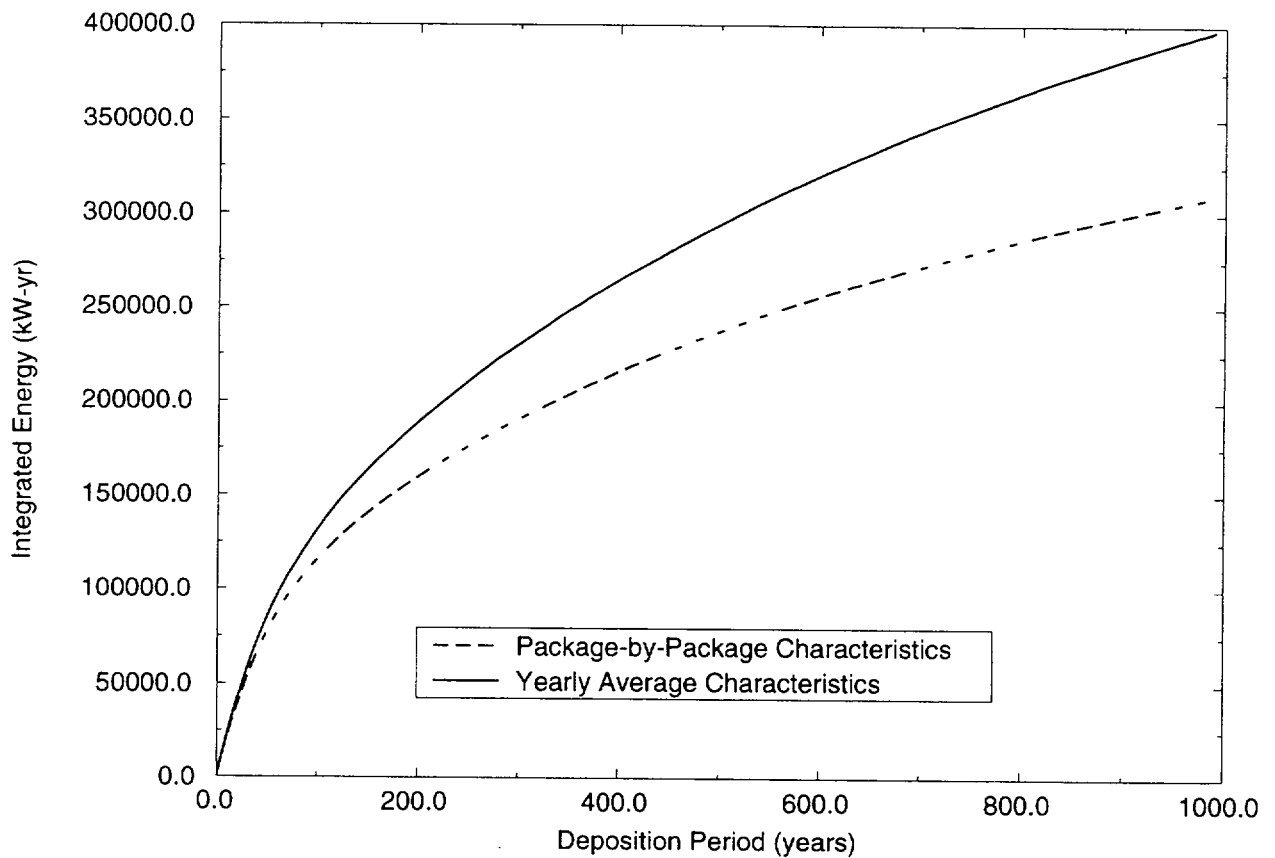


Figure 4.5-6. Integrated Energy Deposition for 2029 Pressurized Water Reactor Waste Packages Calculated Using Both the Yearly Averaged Characteristics and Package-by-Package Characteristics.

To establish a bounding case, the waste packages for the three years of 2028, 2029, and 2030 were specifically ordered with the highest output waste packages placed in the center of a circular ring and the lower output packages around the outer edges. This evaluation, designated as Case II, again constrained the emplacement to be done with a constant AML of 19.3 kgU/m<sup>2</sup> (78.2 MTU/acre). This, of course, is opposite to what was considered in a previous section that describes nonuniform AML loading where higher densities were emplaced toward the edges of the potential repository and is unlikely to occur. This Case II is referenced with respect to the Base Case and the temperature differences are shown in Figure 4.5-7 for three different times. As shown in the figure, the temperature differences between the Base Case and Case II are very large and more ordered than with Case I. The maximum temperature increase at 5 m above the potential repository horizon in this center ring exceeds 250°C at 60 years (Ryder and Dunn, 1995). These temperatures exceed the tridymite and cristobalite inversion temperatures and certainly exceed the current drift wall thermal goal of 200°C established to preserve tunnel stability (M&O, 1993a). Thus these high temperatures could result in impact of ability to retrieve and even possibly postclosure performance because of both the geochemical and mechanical changes. It should be noted that convection and/or heterogeneity would affect these results and neither were included in these calculations.

#### 4.5.3 Section Summary

Waste stream variability and the resolution at which the waste stream is modeled were evaluated and found to be important for thermal predictions. The results showed that localized hot and "cold" areas would occur as a result of the waste stream variations and the constraint of a constant AML. These localized variations in temperature can have design and performance assessment implications, which should be evaluated and considered prior to any final emplacement/operation designs.

Modeling the large MPC waste packages with package-by-package characteristics instead of a single average or an aggregate annual average produces a significant number of localized hot and "cold" areas. In a number of areas predicted temperature differences of as much as 100°C occur in small localized areas (on the order of 10 m). Limiting the energy output of waste packages as assumed in the MGDS Requirements Document (DOE, 1995b) will likely be needed to reduce these temperature variations. Further evaluation should be done to determine whether or not a limit lower than 14.2 kw should be established.

It also was determined that the distribution in package energies is significantly different than would be predicted using average characteristics. This results, for the most part, in less energy being deposited into the host rock for long times for the case where individual package characteristics are considered as opposed to the case where aggregate annual averages are used. For some years, such as 2029, this can result in as much as 25 to 30 percent less integrated energy at 1000 years, but for other years, such as 2030, the differences are much smaller (on the order of four percent at 1000 years). Improved accuracy in predicting integrated energies can be obtained, however, by using representative groupings of waste packages (e.g. using the average of the two distinct groupings shown in Figure 4.5-5). Using these representative average characteristics, the integrated energy output at 1000 years falls within 0.3 percent of that calculated for a package-by-package basis.

INTENTIONALLY LEFT BLANK

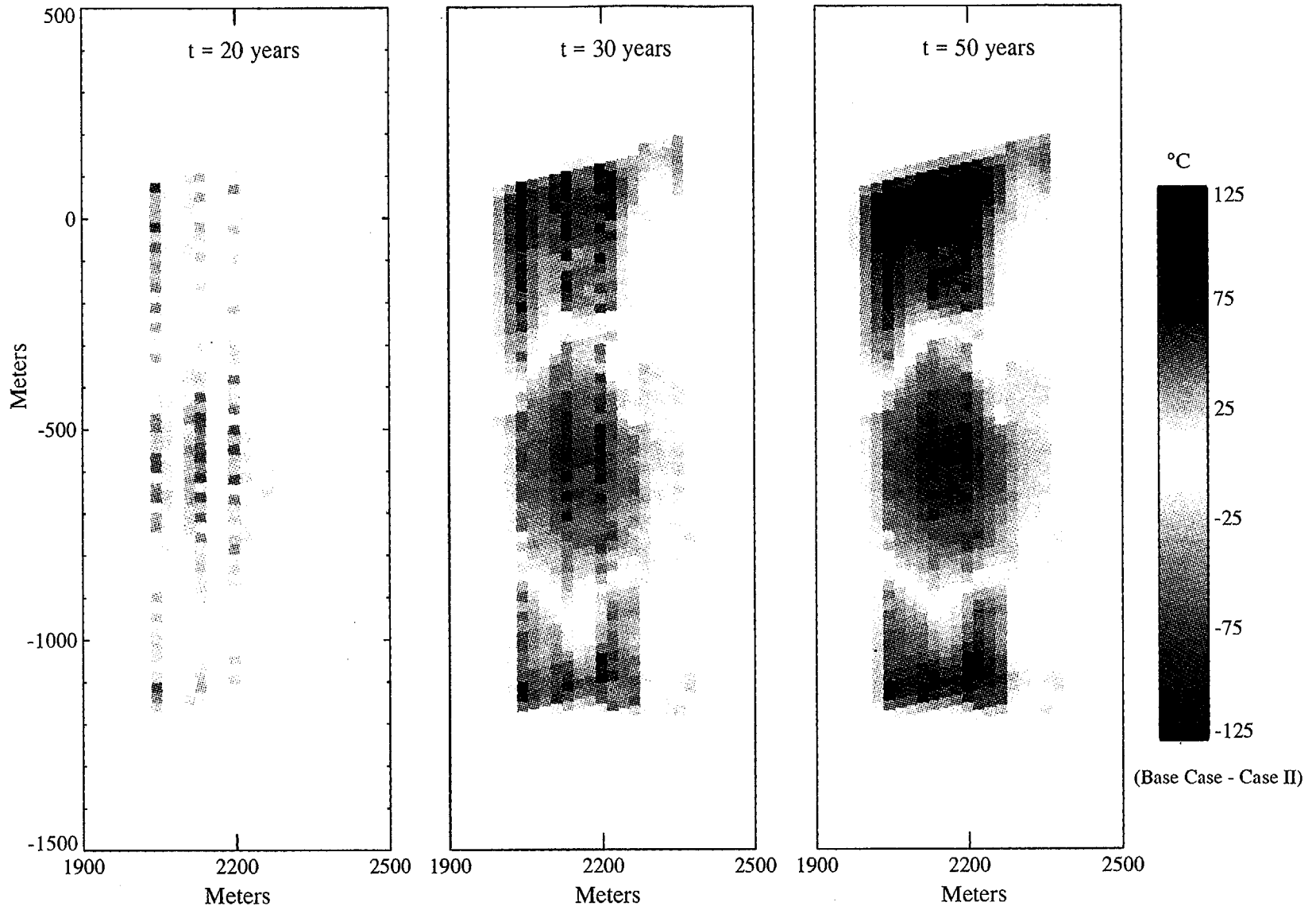


Figure 4.5-7. Temperature Difference History Between the Base Case and the Case II Models.



INTENTIONALLY LEFT BLANK



Finally, using a constant AML in defining waste package layouts needs to be re-examined. Some of the hot spots are of sufficient magnitude to result in tunnel stability questions. Furthermore, the variations in heat could cause moisture movement from regions of hot to "cold" regions which could have postclosure performance implications. However, no matter what method is used to establish locations and spacings of waste packages, either package-by-package characteristics or annual averages, the waste stream variability will result in some variations in temperatures, and the effects of these variations must be considered in the designs.

#### **4.6 AGING OF SPENT NUCLEAR FUEL VIA INTERIM STORAGE**

An initial examination of the system impacts of Centralized Storage with heat-based Inventory Management (IM) for the repository has been performed. This task utilizes aging of SNF via interim storage to reduce the instantaneous heat output of MPCs shipped to the repository to a parametric varied limit. The detailed results of this task will be documented in the Thermal Inventory Management Report (M&O, 1995c), but this section summarizes the major topics to be covered in that report. Under the Program Approach system, waste acceptance begins in 2010 and ramps to a steady-state acceptance rate of 3,000 MTU/year. In scenarios developed for the Total System Life Cycle Cost (TSLCC) estimate (M&O, 1995d), which is used for cost comparisons, all packages are emplaced into a single repository during the year of arrival at the MGDS, with final emplacement occurring in 2043. Under current legislation, the total waste to be emplaced (about 84,000 MTU) exceeds the limit (70,000 MTU) of a single repository, therefore two repositories would be required. For the purposes of simplifying the analysis and conservatively bounding the impacts, the single repository scenario was used in this task. Recent CSF studies, conducted in response to legislative initiatives, have assumed that waste acceptance would begin in 1998, and all incoming packages would be stored above ground on storage pads until MGDS emplacement operations began in 2010. However, for this study, a key distinguishing assumption is that there is no time lag between the start of CSF operations and the start of MGDS emplacement operations. This assumption is based on the CSF being developed solely to support thermal management for the repository i.e., this study does not consider a CSF with a mission to accept and store waste prior to the beginning of repository operations. The CSF was assumed to be located close enough to the potential repository that transportation costs between the two are negligible. All uncanistered SNF was assumed to be shipped directly to the repository; therefore requiring no bare fuel facilities at the CSF. The majority of the balance-of-plant facilities are shared with the repository. A consequence of both the Performance Approach system and the CSF system is that the repository emplacement thermal source term mirrors the waste stream. For this study, a fundamental assumption is that the emplacement heat limit may be considerably less than the transportation heat limit. This assumption decouples the waste stream and the thermal source terms.

The Waste Stream Model (M&O, 1995e) determines on an annual basis the quantity of SNF assemblies accepted by cask type according to: 1) the waste acceptance schedule, 2) individual reactor cask handling capabilities, 3) cask or MPC capacity, and 4) transportation modal split. The WSM also considers SNF selection, OFF or YFF(10), and the historical plus projected SNF discharges. Data from WSM along with cask loading/unloading times, distances, and facility information (number of processing bays, shifts) is used in a model called Interface (M&O, 1995f) to calculate the required transportation fleet size.

Fuel assemblies arriving in truck casks at the MGDS were repackaged into uncanistered fuel (UCF) waste packages (such that the emplacement heat limits were not exceeded) and emplaced in the year of arrival. All MPCs were loaded at the reactor sites (either for dry storage or for shipment) and were loaded to the corresponding MPC storage or transportation heat limit. As the MPCs arrived at the MGDS, they were placed into either storage overpacks at the CSF or disposal overpacks for emplacement, depending on the total package heat output at arrival.

To determine the effect of different emplacement limits, the emplacement limit was decreased parametrically from 14.2 kW to 12, 10, and 8 kW, respectively. Since MPCs are loaded at the reactor (to either the transportation or dry storage limit depending on their immediately planned disposition), the emplacement limit has no effect on the overall number of MPCs. The varying heat limits determine the numbers of MPCs that need to be cooled, the length of cooling necessary, and the waste package emplacement schedule. Emplacement heat limits determine the number of UCF waste packages needed for the bare fuel from incoming truck casks. Assemblies were loaded into a UCF waste package until the emplacement limit was reached, and then the package was closed, even if it was not full (derated), and emplaced.

Each year, the heat output of each incoming MPC is calculated. Transportation from the reactors to the MGDS/CSF branch point is IM Mode 1 (see Figure 4.6-1 for the IM flow model). If the MPC heat does not exceed the emplacement heat limit, the canister is placed into a waste package and emplaced. Waste emplaced in the repository in the year of arrival from the reactors is an IM Mode 2 activity. If the MPC heat exceeds the emplacement heat limit, the canister is given a storage overpack and placed into the CSF for cooling. In the IM model, the movement of waste from the reactors to the CSF is Mode 4. When the current year's arrivals have been evaluated, the CSF cask inventory is evaluated to determine if any previously stored MPCs have cooled sufficiently for emplacement. If so, the canisters are moved to the repository for emplacement under IM Mode 3.

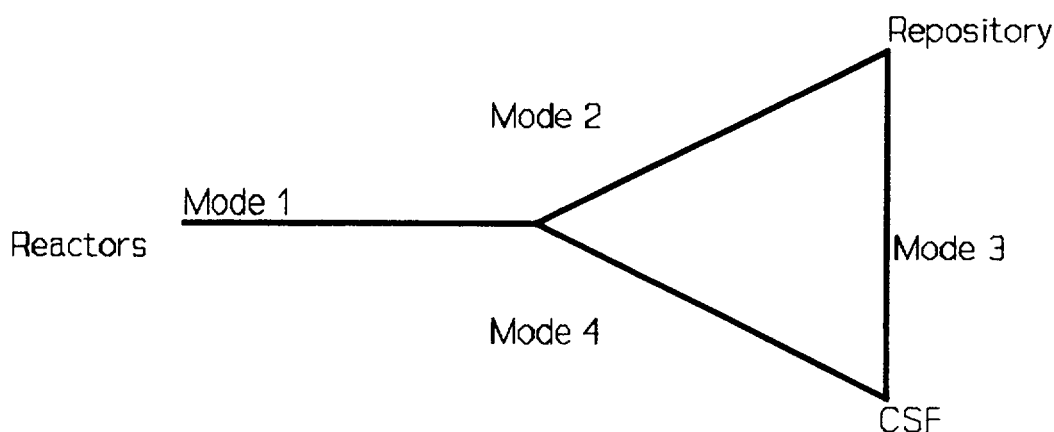


Figure 4.6-1. Inventory Management Flow Model.

Table 4.6-1 provides a short description of each case used for the IM study. The base case waste stream for this study, O14-14, uses the OFF pickup selection, a transportation heat limit of 14.2 kW in order to meet the emplacement heat limit. The O14-14 case is essentially identical to the scenario used for the latest TSLCC study, and except for single repository assumption is identical to the FY 1995 Base Case, as discussed in Section 2.2. The Y14-14 case uses the YFF(10) pickup selection, a transportation heat limit equal to the 14.2 kW emplacement heat limit, and is identical to the FY 1995 Variant except for the single repository assumption.

Costs estimates for those cost elements that would be significantly impacted by alternative transportation and emplacement heat limits as defined by the case description in Table 4.6-1 were developed. Repository design and operational cost elements were not considered in this analysis.

Table 4.6-1. Inventory Management Study Case Description

Pickup Selection	Case Name	Power Limits (kW)	
		Emplacement	Transportation
OFF	O14-14	14.2	14.2
	O15-14	14.2	15.33
	O15-12	12.0	
	O15-10	10.0	
	O15-8	8.0	
YFF(10)	Y14-14	14.2	14.2
	Y15-14	14.2	15.33
	Y15-12	12.0	
	Y15-10	10.0	
	Y15-8	8.0	

Since reduced heat emplacement limits do not affect Waste Generator and Transportation logistics, Table 4.6-2 shows the MPC/Cask savings resulting from loading MPCs to the transportation limit of 15.33 kW rather than the disposal limit of 14.2 kW. This results in the number of derated casks being decreased by 345 (1634-1289) for the OFF scenarios and by 417 (2991-2574) for the YFF(10) scenarios. Typically, derated canisters are nearly full, only a few assembly locations are empty, and by filling these previously empty locations slightly reduces the total number of MPC assemblies needed. An increase in the transportation heat limit from 14.2 kW to 15.33 kW resulted in a reduction of 85 MPCs for the OFF pickup selection and a reduction of 129 MPCs and one PWR Legal Weight Truck (LWT), GA-4, cask for YFF(10).

Table 4.6-2. Multi-Purpose Canister/Cask Savings Resulting from an Increase to 15.33 kW Transportation Limit

Pickup Selection	MPC Assembly					Truck Casks	
	B-LG	P-LG	B-SM	P-SM	B-IN-P	B-LWT	P-LWT
OFF	0	85	0	0	0	0	0
YFF(10)	1	128	0	0	0	0	1

The CSF inventory profile for all cases is shown in Figure 4.6-2. From the figure one can see that as the emplacement heat limits are reduced, the storage requirements increase dramatically. Lower emplacement limits also increase the length of CSF operations. The total storage, representing the sum of MPCs in storage for each year of CSF operation (see Figure 4.6-3), increases in successively greater proportions as the heat limit decreases. As the difference between the transportation and emplacement heat limits increases, the corresponding peak cask storage requirements (a major cost driver) increase proportionally greater. Except for cases O14-14 and Y14-14, the YFF(10) pickup cases result in greater peak storage requirements. Since YFF(10) results in earlier drawdown from dry storage, the cask storage requirements due to dry storage casks are more evenly distributed (by CSF operation year). For all OFF cases, the peak inventory occurs near the end of pickup operations (2038-2040); a direct result of the hotter waste stream occurring at the end of OFF pickup. For the YFF(10) cases, the peak inventory occurs during or before 2033. Table 4.6-3 summarizes the CSF logistics results.

Table 4.6-3. Inventory Management Summary Statistics

Summary/Case	O14-14	O15-14	O15-12	O15-10	O15-8	Y14-14	Y15-14	Y15-12	Y15-10	Y15-8
Total Storage (Cask-Years)	522	1,730	11,038	33,188	85,178	843	3,047	15,919	43,868	100,729
CSF Operations End in Year	2,045	2,044	2,054	2,065	2,080	2,042	2,051	2,060	2,071	2,085
Peak Storage (Casks)	85	132	585	1,379	3,006	70	194	922	2,079	3,632
Peak Storage Occurs in Year	2,038	2,038	2,040	2,040	2,040	2,033	2,021	2,022	2,028	2,033

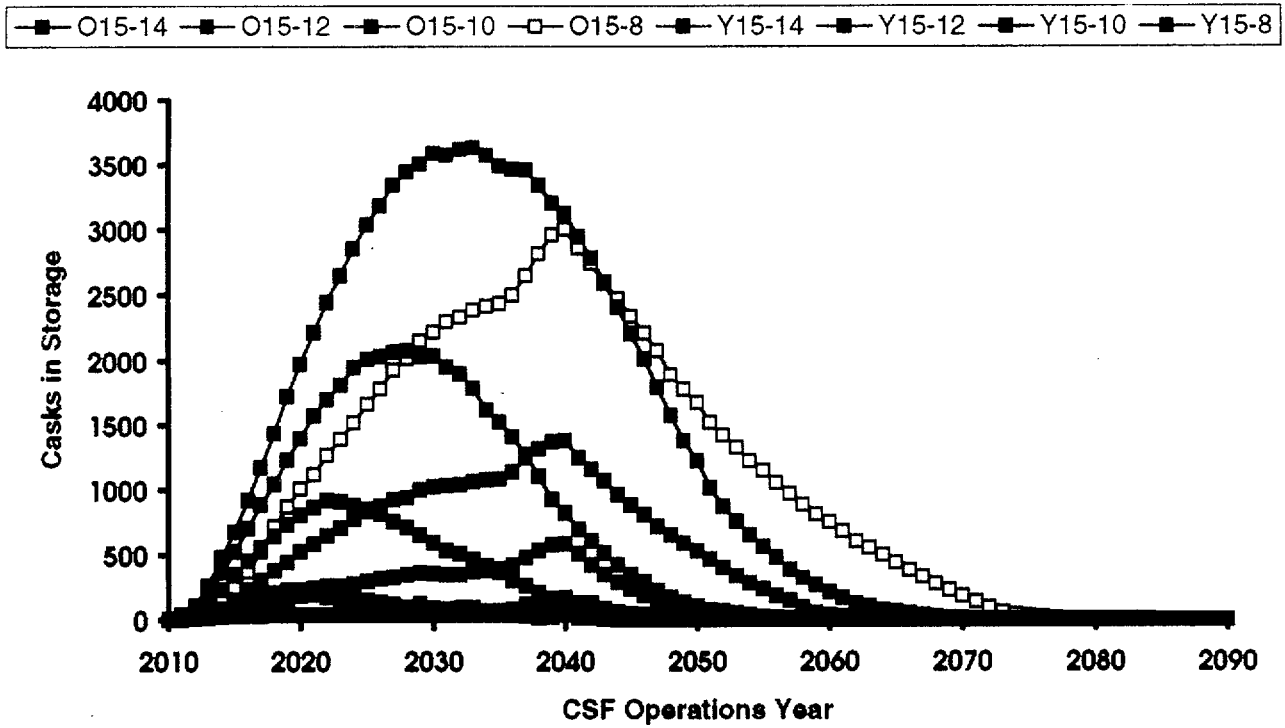


Figure 4.6-2. Centralized Storage Facility Cask Inventory.

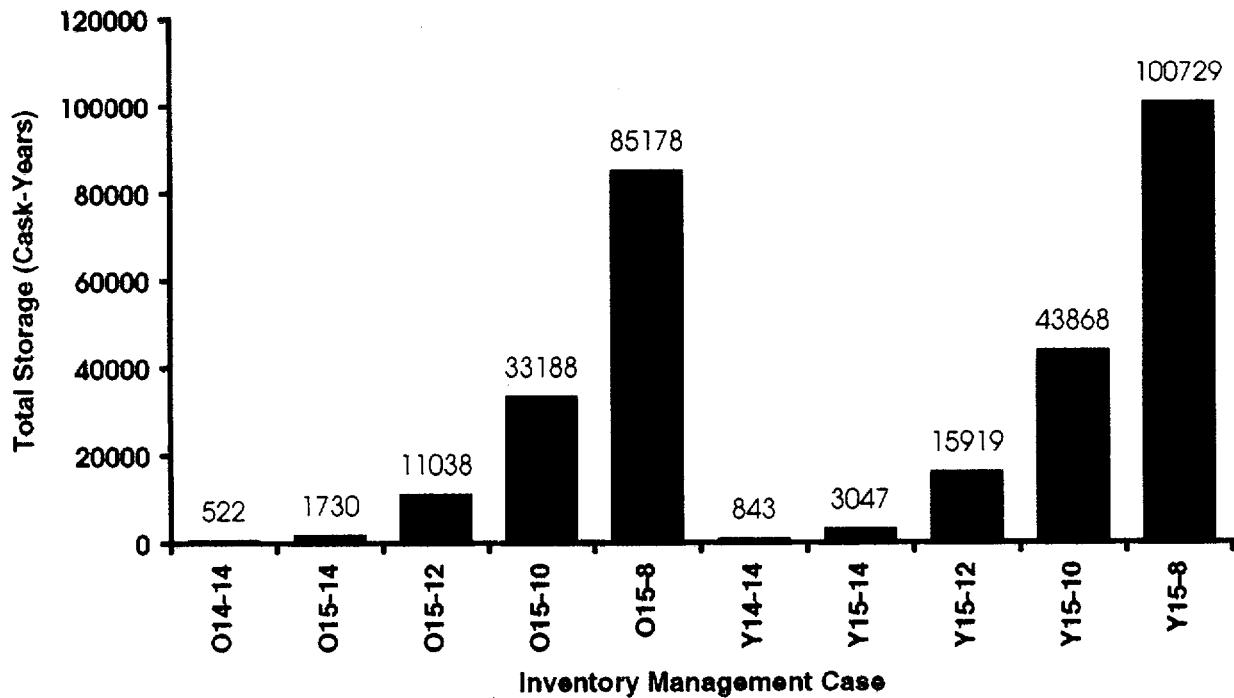


Figure 4.6-3. Centralized Storage Facility Total Storage Requirements.

INTENTIONALLY LEFT BLANK

The storage of MPCs arriving above the emplacement heat limit influences the emplacement throughput and logistics. The cost and design impacts of these changes have not yet been evaluated, but a summary of the MTU and waste package emplacement is provided below in Table 4.6-4. OFF pickup results in a more leveled MTU loading for emplacement heat limits versus YFF(10) pickup. Generally, the MTU emplacement rates trend as the waste package emplacement rates, although for some cases, the peaks occur at different times. The peak MTU emplacement rates exceed 3,000 MTU per year (the current MGDS design requirement), by as much as 40 percent for case Y15-10. This is because the number of MPCs being discharged from the CSF is significantly larger than the number of MPCs being sent to the CSF for aging.

Table 4.6-4. Inventory Management Emplacement Summary Statistics

Summary/Case	O14-14	O15-14	O15-12	O15-10	O15-8	Y14-14	Y15-14	Y15-12	Y15-10	Y15-8
Peak MTU Emplacement Rate (MTU/year)	3,157	3,136	2,978	2,961	2,777	3,113	3,245	3,496	4,288	4,142
Peak MTU Emplacement Occurs in Year	2039	2039	2030	2035	2035	2036	2017	2029	2034	2039
Peak Waste Package Emplacement Rate (Waste Packages/year)	437	431	424	417	399	465	455	493	575	510
Peak Waste Package Emplacement Occurs in Year	2039	2015	2032	2032	2035	2014	2017	2027	2034	2039
Final Year of Emplacement	2045	2044	2054	2065	2080	2042	2052	2061	2071	2085

OFF pickup results in a relatively hot waste stream at the end of operations and thus requires longer cooling times than YFF(10) at the end of the emplacement cycle for casks which are shipped from dry storage at the reactors. The YFF(10) pickup results in more derated casks, especially in the early years, more overall casks, and therefore higher waste package emplacement rates. Concerning the effect of decreasing emplacement heat limits on waste package emplacement rates, the trends are similar for both the OFF and YFF(10) pickup scenarios. As the difference between the transportation limit and the emplacement limits increase, the length of CSF operations also increases. There is relatively little difference between the waste package emplacement rates for a 14.2 and 12 kW limit, however the 10 and 8 kW limits cases require approximately 20 years to ramp up to the waste package emplacement rates of the 14.2 kW limit case with operations extending out to the year 2085 in the worst case.

Table 4.6-5 presents a summary of the heat emplacement results. During the operations phase, OFF pickup results in a slightly cooler repository for cases in which the transportation heat limits exceed the emplacement heat limits. For the cases O14-14 and Y14-14, OFF pickup results in a somewhat lower thermal source term than YFF(10). Changing the emplacement limits from 14.2 kW to 12.0 kW does not contribute a significant lower thermal source term. However, as the emplacement limits are reduced further to 10 kW and 8 kW, the aggregate thermal source term becomes cooler. An emplacement limit of 8 kW results in a total instantaneous heat output at emplacement of about 70 MW compared to 87 MW of the O14-14 case and 96 MW of the Y14-14 case. The actual thermal source term, taking into account the many years of emplacement and the decay heat from waste already emplaced, is expected to yield very benign results for cases O15-10, O15-8, Y15-10, and Y15-8 (relative to O15-14, O15-12, Y15-14, Y15-12) because the extended CSF operations would result in a smaller range of package heat outputs and an extension of the emplacement period. When considering just the preclosure operations period, this difference is significant. Over the long term, the reduction in the total integrated heat is not significant.

Table 4.6-5. Inventory Management Heat Emplacement Summary Statistics

Summary/Case	O14-14	O15-14	O15-12	O15-10	O15-8	Y14-14	Y15-14	Y15-12	Y15-10	Y15-8
Total Heat (Without Decay, MW)	87	87	84	79	71	96	95	90	83	73
Peak Heat at Emplacement in a Year (MW)	4.0	3.9	3.2	2.8	2.3	4.4	4.4	4.3	3.8	2.7
Peak Heat at Emplacement Occurs During Year(s)	2039	2039	2027 2030	2028 2039	2034 2035	2022	2017	2027	2037	2038 2039

Table 4.6-6 shows the total cost increases (except for repository operations cost impacts) for different pickup and emplacement scenarios. The total cost deltas for this study are the sum of the CSF deltas, the transportation deltas, and the waste generator deltas, including dry vertical concrete casks (DVCCs). It is estimated that these costs would increase in the range of \$0.1 to \$0.4 billion dollars for any of the 14.2 and 12 kW emplacement heat limit cases to as much as \$1.8 billion dollars (1995 constant year dollars) for the YFF(10) scenario with the 8 kW emplacement heat limit.

Table 4.6-6. Summary Cost Deltas, All Scenarios versus Program Approach

Case	Subcost Element Deltas (\$M, 1995 Dollars)					Total
	CSF	Transportation		Waste Generator	Reactor DVCCs	
		MPCs	Truck			
O15-14	212	(29)	0	(20)	(24)	139
O15-12	397	(29)	5	(20)	(24)	329
O15-10	714	(29)	14	(20)	(24)	655
O15-8	1,319	(29)	29	(20)	(24)	1,275
Y14-14	60	275	9	(38)	(49)	257
Y15-14	325	192	9	(45)	(56)	425
Y15-12	603	192	19	(45)	(56)	713
Y15-10	1,054	192	32	(45)	(56)	1,177
Y15-8	1,619	192	53	(45)	(56)	1,763

Note: Case O14-14 is the base case, Program Approach.

INTENTIONALLY LEFT BLANK

## 5. SCALING ISSUES

The emplacement of heat-generating SNF in an underground repository results in large-scale propagation of heat and fluid flow. The resulting coupled thermal-hydrologic-mechanical-chemical processes can, depending on thermal load, extend over hundreds to thousands of meters and perturb the ambient conditions for many thousands of years. The large time and distance scale over which these processes operate provides a significant challenge in developing an adequate understanding of these processes. This is needed in order to demonstrate reasonable assurance that the applicable regulatory requirement for a geologic repository will be satisfied. The program must rely on laboratory scale and eventually in-situ drift scale thermal tests combined with analytic modeling for prediction of the behavior of the host rock on the mountain scale. Larger scale, longer duration in-situ thermal tests would be done during performance confirmation if the repository is constructed. In some cases, limited information on longer term and larger scale processes can be obtained from investigations on natural analogs. Understanding the scaling (time and distance) between the different measurements/experiments that will be conducted by the program is essential to develop the necessary reasonable assurance arguments for licensing. This section will provide an overview of the scaling issues and recommend testing and evaluations.

The thermohydrologic conditions that may occur at Yucca Mountain after the emplacement of waste are controlled by two factors. The first is the physics, and the second is geometry. The physics of multiphase fluid and heat processes involves movement of liquid and gaseous phases, the transport of latent and sensible heat, and phase transition of water. As heat is released from the waste packages and transferred to the surrounding host rock, temperatures near the waste packages will exceed the boiling point of water. Formation water will then be vaporized, with associated increases in vapor partial pressure and overall gas pressure. The result will be forced convection of the gas phase with redistribution of liquid water, accompanied by latent heat and diffusive effects. The phase transformation and gas-phase flow will alter the original fluid saturation distribution in both fractures and matrix. As the source of heat output declines, liquid water will be able to re-enter those areas where temperature has fallen below vaporization temperature. The drivers for heat and fluid transport are therefore gravity, pressure gradients, capillarity, and temperature gradients. While the physics for the multiphase flow problem remains the same at all scales, regardless of whether it is on the waste package scale, the emplacement drift scale, the repository scale, or the site scale; the geometry and the formation properties of the natural setting have great variability with scale. The geometry and the formation properties of the natural setting are not only different from one scale to the other, they are also variable from one location to another, even on the same scale. The matter of scaling therefore becomes an important issue because the actual thermohydrological behavior at the repository is controlled by both the scale and space-independent physics and the extremely scale- and space-dependent geometry and formation properties of the natural setting. Since thermal perturbations from the repository are on the scale of thousands of years, and thermal testing can only be carried out on a much shorter time scale and much smaller spatial scale, the matter of how the knowledge gained from this smaller scale testing can be used to predict (with confidence) the repository performance under different thermal loading becomes an important issue. In the following, the anticipated thermohydrological behavior on different scales will first

be described, then the issues of minimizing uncertainty in the prediction of the performance of the repository will be addressed.

Each waste package can be considered as one heating unit. On the waste package scale, as temperature near the heated unit rises above the boiling point of water, the vaporized water will move away from the waste package. In the partially saturated medium of welded tuff, if there is thermodynamic equilibrium between the matrix and the fracture, that is, if the matrix and the fracture have identical liquid pressure, then it is anticipated that the majority of liquid water resides in the tight matrix pores while the fractures are essentially desaturated. In this case, the fractures provide the fast pathways for rapid transport of vapor away from the waste package. At cooler regions away from the heated unit, the vapor condenses. If the condensed water can return to the heated unit at a rate comparable to that of the vapor, then a heat pipe has developed, creating a waste package environment that is wet and cool (below boiling). On the other hand, if there are no fast pathways for the condensed water to return to the waste package, then the temperature around the waste package continues to rise above boiling, creating a hot and dry waste package environment. The driving forces for water to return to the waste package are always present; these are capillary gradient and gravity. Whether liquid water will actually return to the waste package via the connected fractures depends very much on the geometry and formation properties of the natural setting. If fractures can be idealized as pairs of parallel planes with apertures considerably larger than the matrix pores, and if thermodynamic equilibrium is maintained at all times, then liquid water is not expected to flow through the connected fractures until the tuff matrix is almost saturated with the vapor condensate. If the formation around each waste package is characterized by homogeneous properties, then for a given thermal output of the heated unit, numerical modeling using an effective continuum approximation can supply the information on the extent of the dry-out region around each heating unit as well as the time period before refluxing of condensate occurs. Therefore on the average, a dried out zone with an outer condensation zone can occur around each waste package, and the return of liquid back to the waste package is expected only after liquid saturation has built up sufficiently in the condensation zone, and only if the temperature around the waste package has fallen below the vaporization temperature. However, modeling results (Pruess and Tsang, 1994) also indicate that once the assumption of spatial homogeneity of the formation is relaxed, that is, when the fractures are more realistically modeled as a two-dimensional heterogeneous medium, and when the matrix properties are also allowed to vary from location to location, as one would expect in the natural setting, then there can be some locations where the saturation built-up from the condensate will be very much above the average and liquid fracture flow conditions are satisfied. Contrary to the average behavior where water is held in the condensation zone for a period until uniform refluxing conditions are satisfied, small scale heterogeneity in the formation can give rise to intermittent release of water in fast path (connected fractures) at random locations in the dry-out zone and at times before the predicted refluxing time. In other words, spatial variability introduces a wide range of possible behavior on the waste package scale. On the other hand, different thermal loading is not expected to create thermohydrologic conditions around each waste package different from that discussed above, since the unit heat source from the waste package remains the same for all thermal loading.

The different thermal loading in terms of average power density is achieved by varying the area allotted to each unit heat source, in other words, by varying the spacing of the waste packages. On the drift scale, therefore, the thermohydrological conditions are expected to differ not only

for the different thermal loads, but also for the alternative loading configurations. For example, the same thermal load can be achieved by either wider spacing between packages along the drift with moderate spacing between drifts, or by closer spacing between packages along the drift with wider spacing between drifts. For the loading configuration of close heating unit spacing along the drift, one may envision the drift as a single elongated heat source, then the description of thermohydrological behavior previously given for the waste package as a heating unit is applicable there, as long as the waste packages are modeled by the "single" elongated heat source the length of the drift as the heating unit. Here the average dry-out region and the condensation zone will be dictated by the symmetry of the drift rather than that of the waste package. However, for the same reasons that spatial heterogeneity can create a range of non-average behavior on the waste package scale, so here on the drift scale similar non-average behavior may be anticipated. That is, within the dry-out zone surrounding the drift as a single heating unit, one can expect locations where condensate is released onto the drift, at times earlier than the refluxing time predicted from calculations assuming uniform formation properties. In this case, not only heterogeneity of the fracture and rock matrix properties can be important but also variability in the waste stream resulting in variable heat outputs of the packages can be important as shown in previous sections. On the other hand, for the loading configuration of wide spacing of waste package along the drift, each individual waste package rather than the entire drift will act as a heating unit and drive the thermohydrologic processes at early times, giving opportunity for liquid drainage between waste packages before the average behavior of a "dried out region" on the drift scale set in. At later times, the hydrological condition of the two different loading configurations would converge. The thermohydrologic conditions are expected to be qualitatively similar for different thermal loading at these later times. That is, intermittent liquid flow and heat pipe conditions can occur for all different thermal loadings, but perhaps more probable for higher thermal loading since more condensate is generated at higher thermal loading, and thus providing more opportunities for water to flow down connected fractures from stress releases.

Concepts of extended dry-out region and condensation envelope away from the dry-out zone are all results of numerical modeling based on the approximation that the formation is homogeneous and that the matrix and fractures are in steady state thermodynamic equilibrium. Since heterogeneity on all scales is the norm rather than the exception in the natural setting, it is expected that intermittent liquid flow at various locations can occur before the predicted refluxing time obtained from idealized models and/or homogeneous properties. This behavior can occur at all scales. Therefore, a credible conceptual model to describe the thermo-hydrological behavior of the repository on all scales must incorporate the effects of heterogeneity, and especially the heterogeneity of the relevant scale. That is, the important features of heterogeneity, which are to influence the thermohydrological behavior on a particular scale, must be of similar scale, since the effects of the heterogeneity on a much smaller scale will be averaged out. Therefore, an important factor in the strategy of "scaling up" should be the utilization of specific site characterization data at the relevant scale. The thermal testing program is intended to yield data on successively larger scales. The first ESF thermal test includes a shakedown phase in which the heating unit is on the scale of a single waste package, and the main test where the heating unit is on the drift scale. The tests will be rather densely instrumented for spatial and temporal monitoring of the temperature, moisture content, and fluid movement. To supplement the in-situ measurements, thermal process tests in the laboratory will be performed to probe the same thermohydrological processes expected to occur in the field. These laboratory tests need to investigate the following processes: development of heat-pipes, existence of fast paths,

enhanced vapor diffusion, nonequilibrium fracture-matrix coupling, and buoyancy flow. Measurements should be performed on many samples collected from the ESF thermal test bed. The strategy for scaling up from information gained in these tests on a smaller scale to the prediction of the thermo-hydrological behavior of the repository would require close integration of laboratory tests, field tests, conceptual and numerical modeling, as well as input from natural analog studies. A proposed strategy for scaling up is outlined below.

Starting from the laboratory scale ( $<0.5$  m), measurements should be performed on a variety of tuff samples collected from the ESF thermal test bed and boreholes. These samples should capture as wide a range as possible of thermohydrologic behavior that exists. The laboratory observations will be used to confirm or refute the present theoretical understanding of the coupled processes. As an improved understanding of the physics is achieved, this understanding needs to be incorporated in the conceptual models. Additionally, the range of possible formation properties from the laboratory samples will be used to represent the heterogeneity of the site within a stochastic framework. A stochastic approach is needed because the number of samples tested in the laboratory would not be numerous enough to cover the entire test site adequately. The stochastic approach allows the generation of a heterogeneous formation consistent with the range of formation properties obtained from the laboratory testing.

Although laboratory data can provide very controlled boundary conditions and allow for a large number of samples to be tested relatively inexpensively, it does not capture some of the processes that occur at larger scales. Information on the few meter scale is needed as the next step in this strategy. Characterization information on this scale can be obtained in the test region from such tests as gas-injection interference pumping tests, which are on the scale of about 5 to 10 m. A Large Block Test is starting, which should provide some information on the couple of meter scale. An ESF Shakedown test and drift scale test are planned to gather characterization data and experimental behavior on the 5 to 10 m scale. Some of the measurements that are needed are obviously thermohydrological to include an investigation into the existence of heat pipes and fast paths as well as the extent of dry-out and rate of rewetting, thermomechanical, and geochemical. Pretest calculations based on the site-specific conceptual models should be carried out to model the thermohydrological behavior of both the Large Block Test and the Shakedown Test at this waste package scale. In this way, both the physics as well as the geometry of the natural setting are included in the modeling exercise. In turn, the measured results of the tests, particularly the Shakedown phase, should be used to refine the input formation parameters and adjust the model.

In the next phase of the strategy, the conceptual model should be adjusted to be site specific for the drift scale test at the tens of meters scale by the incorporation of the site characterization data on the scale of the heater emplacement drift test ( $\sim 40$  m). This site-specific drift scale model would then be used to model the thermohydrological behavior of the drift scale test. Results from the drift scale test will again be used for further refinement and calibration/verification of the thermal conceptual models. As mentioned earlier, the existence of heat pipes, fast paths, dry-out, rewetting, and other items need to be investigated.

Finally, the site characterization data on the scale of the repository and possibly on the scale of the mountain will be needed to incorporate into the latest revised conceptual model in order to model the thermohydrological behavior on those scales. Testing heating and subsequent water movement on this scale will likely require that the tests be done during the performance

confirmation period. By this approach of iterative information feed and calibration at successive scales (laboratory, waste package, drift, and repository), site characterization data of the relevant scale is incorporated at each step of the scaling process, building confidence that the scaling up from small scale to large scale is not arbitrary. Still, the largest difference in scales occurs in the last step of moving from the drift scale test to the repository scale performance prediction. One can easily see how the credibility of this last scaling may be called into question. It is here that natural analogs can play an important role to supply the information to fill this data gap in the thermal testing program. Additionally, for many of the geochemical processes involving mineralogic changes over long periods of time, the natural analog is necessary to provide data on some of these issues. The natural analog studies should involve (1) the evaluation of known two-phase fractured hydrothermal systems; (2) the identification of the hydrological, geochemical, and geological data that control the development of large-scale heat pipes; (3) the development of an approach to determine the potential for the development of large-scale heat pipes at Yucca Mountain; and (4) geochemical changes in important mineralogical assemblages. It is therefore, by closely integrating the site-specific data from testing on the laboratory scale and field scale, plus indirect information from hydrothermal natural analog studies, together with conceptual and numerical modeling, that the limited data are utilized efficiently to reduce the uncertainty in the prediction of performance on the repository scale.

The above discussion indicated that because of the heterogeneity that exists in the host rock and the limited amount of measurements and testing that can be obtained, a stochastic approach has been suggested. If a homogeneous system were present then a deterministic approach would be adequate and tests/samples from one area would be sufficient to represent the behavior of the host rock under the anticipated conditions. However, when systems have sufficient heterogeneity then a stochastic approach appears to be more appropriate. Drift scale testing might be used as an example of how this might be applied through the following considerations. The current test program plans to conduct just a few thermal tests; an in-situ single heater test (shakedown phase), an in-situ drift scale test, and some performance confirmation tests. In addition to these thermal tests, rock property measurements will be made at a number of areas underground. Statistics should be used to fill in the rock properties throughout the repository horizon and then verified three-dimensional models used to predict performance under thermally perturbed conditions. The verification of these models must rely on the in-situ thermal tests as well as laboratory data and natural analog studies.

In the discussion of the scaling strategy in this section, it is clear that this iterative process, which proceeds to larger and larger scales, will require a significant period of time. The strategy allows information and confidence to be developed over time. The Program objectives laid out in the Program Plan (DOE, 1994) and currently under revision require that certain milestones be achieved. Specifically there is a Technical Site Suitability Determination in 1998, a License Application in 2001, a License Application update around 2008, and a license to close at about 100 years after emplacement begins. The specific milestones and dates are being revised, based on recent program developments, including reduced annual budgets and increased emphasis on interim storage.

This strategy, if implemented in the testing program, will allow laboratory data, the Large Block test, possibly some information from the Shakedown Test, and natural analog data to be used for Technical Site Suitability. Natural analog data and analytic predictions will be the primary

information available on repository or mountain scale at that time. License Application in 2001 can rely not only on the laboratory data, natural analog data, and the few meter scale tests (Large Block, Shakedown, and gas injection), but will be able to use some of the preliminary information from the heater emplacement drift test. However, not until License Application Update will the Program be able to obtain complete in-situ thermal test data on a drift scale. Repository scale or larger (except what is obtained from natural analog studies) information will be obtained in the performance confirmation period. It also should be noted that the above discussion emphasized thermohydrologic issues, but similar information and modeling are needed in the geochemical and thermomechanical areas in order to ultimately achieve a credible understanding of the coupled processes.

## 6. CONCLUSIONS AND RECOMMENDATIONS

An approximately 18-month Thermal Loading System Study was conducted from about April 1994 until September 1995. This effort continues and builds on previous efforts to develop the technical foundation for ultimately making a thermal loading decision. The Thermal Loading System Study had two main objectives that were designed to support the program objective of making a decision. The first objective was to provide input to the design of the testing program. The approach taken was to perform a limited sensitivity analysis on selected parameters to determine which of these parameters would change the response of the rock (thermal, hydrologic, mechanical, and geochemical) as a function of thermal load and the range over which changes in those parameters seemed important. The analysis identified the range of uncertainty existing in these parameters and whether or not changes in these parameters, as a function of heating, might potentially affect performance. The information gained in this effort was developed into recommendations that will be provided to the test program. The second objective was to examine selected management issues that could provide flexibility to the design and evaluate their viability and advantages or disadvantages. The purpose of this report is to provide the details and findings of the 18-month effort. The conclusions and recommendations are arranged according to the (1) thermal testing recommendations and (2) thermal management evaluations.

Developing an accurate estimate of the effects of thermal loading on the repository will be necessary to ensure that regulatory standards for nuclear waste disposal are met. In a regulatory framework, this implies that the Program must be able to demonstrate with reasonable assurance that radionuclide release standards are met in order to have a docketable license application. To do this requires an understanding of the behavior of the host rock and EBS in the potential repository when it is subjected to heat released from the disposed waste. The U.S. Nuclear Regulatory Commission has provided guidance in NUREG-1466 (NRC, 1992a) that says compliance with the criterion stated in 10 CFR 60.133(i) requires an understanding of the coupled TMHC processes that may occur. The TMHC processes and their effect on the natural and EBS performance can vary with different thermal loading. Based on the thermal strategy, the program has made a programmatic decision to focus design activities on a high thermal loading of 19.8 to 24.7 kgU/m<sup>2</sup> (80 to 100 MTU/acre) with viable alternative thermal loads maintained as contingencies. The effectiveness of these barriers (natural and engineered) for the reference thermal loading and various alternative thermal loads must be compared and presented in the licensing argument [10 CFR 60.21(c)(1)(ii)(D)]. Thus the sensitivity studies in this effort were conducted over a range of thermal loads from about 6 to 24.7 kgU/m<sup>2</sup> (24 to 100 MTU/acre) although in some cases calculations at higher thermal loads were done to ensure that a sufficient range was considered to identify any sensitivities that might exist.

### 6.1 SENSITIVITY ANALYSIS AND TESTING RECOMMENDATIONS

The testing strategy that is being developed has evolved from the philosophy of the Site Characterization Plan, which was basically to conduct comprehensive studies over a wide range of issues. To better manage the available resources the approach being adopted now is to focus characterization activities into essentially three areas: those activities needed for evaluating site suitability (to be completed by 1998), those required for supporting License Application in 2001, and those for confirming postclosure performance. As such, the Program is focusing on a few specific in-situ thermal tests which will support a Technical Site Suitability Determination in

1998, License Application in 2001, and License Application update in 2008. However, these dates may change based on potential changes in the Program. The thermal testing program must ensure a well-integrated set of laboratory tests, in-situ thermal tests, and natural analog studies in concert with appropriate analytic models be accomplished to ensure that the thermally affected processes are understood adequately. Currently, many of the parameters that may influence performance as a function of thermal loading are not well known or have significant uncertainty in their values. Additionally, significant uncertainty exists as to how some of these parameters scale (time and distance) as one goes from laboratory to waste package to drift to repository or mountain scale. This study performed a number of sensitivity analyses in an attempt to identify parameters that potentially appeared to influence performance as a function of thermal loading and the range of uncertainty in these parameters. Since total system performance calculations could not be done on the large number of sensitivity analyses conducted to evaluate impact on performance, the study considered that any significant calculated changes in temperature or hydrology (water movement, gas flow, and/or relative humidity) were likely to result in potential impacts to performance. Also important to performance is the spatial variability or heterogeneity in the host rock across the repository. Recommendations were developed from the results of this sensitivity analysis to assist the testing effort develop the measurement details for the tests. The following provides a brief overview of the conclusions and recommendations identified in the study:

1. The investigation found that variations in bulk permeability (fracture plus matrix) will influence the amount of water movement as a function of thermal loading. The current uncertainty in bulk permeability in the TSw2 layer, based on air permeability measurements, extends over at least three orders of magnitude ( $10^{-13}$  to  $10^{-11}$  m<sup>2</sup>) and the heterogeneity in these values is not known. The calculations show that there are significant increases in buoyant gas-phase convection if bulk permeabilities are above  $10^{-13}$  m<sup>2</sup>. Larger increases in the amount of mobilized water occur for bulk permeabilities above  $10^{-12}$  m<sup>2</sup>. If bulk permeabilities are about  $10^{-14}$  m<sup>2</sup> or less, heat transport is essentially by conduction. At larger bulk permeabilities, more heat transport occurs by convection and can produce heat pipes that are efficient carriers of heat. Based on these calculations, it would appear that the formation and the extent of heat pipes developed in in-situ tests could be used to establish the appropriate bulk permeability values. In-situ measurements of bulk permeability need to be done to confirm the range of these values in the host rock. It is suggested that measurements of bulk permeability be done in the host rock considering the current range of uncertainty in this parameter from a few tenths of  $10^{-12}$  to  $10^{-11}$  m<sup>2</sup> or more. Measurements of temperature and the amount and quantity of water that is moved by the heat needs to be established and compared with model predictions to determine the effect of permeability variations. The degree of spatial variability or heterogeneity in the host rock also needs to be established.
2. Calculations were conducted, which spanned the range of rock parameters that might influence water and gas flow, such as liquid saturation of the rock, matrix porosity, matrix permeability, and parameters associated with the van Genuchten equation. Values for many of these parameters have been developed from borehole data and can vary considerably depending on the borehole sample used. The range of these values is tabulated in Section 3.2 of the report. These values represent an estimate of the average range of values that might exist in the TSw unit. The results indicate that for most cases the temperature,

duration of boiling, and relative humidity at the end of the boiling period are not very dependent on the choice of matrix properties selected from the range of values determined in borehole measurements at least within the context of using an ECM. However, the results show that the liquid saturation and consequently relative humidity do depend on the capillary suction pressure curve that is used. There may be some rock that exists in the Topopah Spring member that could have properties sufficiently different to produce liquid saturations different than the reference case. However, using the measurements from these regions to determine what the liquid permeability is without commensurate scaling of the capillary suction curve may produce errors in the predictions. Some emphasis needs to be placed on determining how the capillary suction curve might change in different types of rock in the mountain and how heterogeneous these areas are in the mountain. Additionally, the in-situ tests need to verify the calculations obtained using measurements from small ( $\leq 10$  cm) core samples. Scaling issues are covered in more detail below. Some sensitivity analyses probably are warranted with a nonzero infiltration rate and dual permeability model.

Predictions of temperature and thermohydrologic response of Yucca Mountain to a potential repository with a high thermal loading were done by LBL with a three-dimensional site-scale model. The predictions evaluated the potential effect that the Ghost Dance and Solitario Canyon faults might have on the temperature and liquid saturation. The results determined that the presence of such faults could be important to performance, since these calculations showed the faults provided major pathways for transport of heated gas and heat. High thermal loads in the potential repository could produce many orders of magnitude increase in heat flux and gas flux at the surface, which could have environmental implications that need to be examined. Because the faults could provide more efficient removal of heat, the predicted potential repository temperatures are lower and boiling duration less than predicted with a two-dimensional model without faults. As such, the effect on performance as a result of the presence of such faults needs to be understood. It is recommended that in-situ measurements of the fracture and surrounding rock properties such as permeability, saturation, and porosity be measured. Additionally, the moisture content near the fault should be monitored. These measured parameters should then be used in a site-scale model to evaluate the environment as a function of time to establish duration of boiling, extent of dry-out, relative humidity in the drift, and rewetting time.

3. The above two issues concentrated on parameters that affect the transport of liquid in the host rock. In another issue investigated during the study, the variations in gas-phase diffusion were examined. The parameters associated with binary diffusion in a porous medium were varied over the range of possible values to determine the importance on temperature and relative humidity values as a function of time. The tortuosity parameter representing the "connectivity" of the pores was varied over the factors of 1 to 20 from its nominal value of 0.2. This variation was felt to be suitable to account for not only uncertainty in the value of tortuosity but also porosity and gas saturation which are parameters that govern buoyant-gas diffusion. The results of this sensitivity study indicated that variations in the parameters affecting buoyant gas-phase diffusion may modestly affect the duration of boiling and the time required to rewet to a particular humidity. Higher vapor diffusion (a factor of 10) can result in some decrease (10 to 12 percent) in the duration of boiling. The effect on below boiling (bulk average) thermal loads was not

investigated. Thus, for high thermal loads the in-situ tests should investigate binary gas-phase diffusion since there appears to be a modest sensitivity to duration of boiling, although it does not appear to have a profound impact on the temperature and relative humidity.

4. The issue of heterogeneity in the rock properties and any subsequent effect on temperatures as a result of heating is a concern that needs to be resolved by testing. Additionally high-porosity (large-cavity) lithophysal zones in the TS Member have been hypothesized and some variations have been observed in boreholes and in the rock surfaces exposed by the Tunnel Boring Machine in the initial excavations. The question was asked in this study as to whether such variations in porosity might affect the temperatures and hydrology in the rock as a function of thermal loading. The presence of high-porosity lithophysal zones will produce variations in thermal conductivity values found in regions of more competent rock, and this study examined the impact that such changes might have on the temperature in the potential repository. With information from borehole measurements, geostatistical models were used to construct estimates of porosity and hence thermal conductivity representing the possible spatial variability in the rock mass. The calculations with the geostatistical model found that the rock saturation for welded tuff may vary over a factor of two from about 40 to 80 percent. This could produce differences in thermal conductivity from the mean (1.6 W/m-K) of about 0.25 W/m-K, which would produce minor temperature changes at the repository horizon of about 5°C. Changes of thermal conductivity, in the rock as a result of drying due to heating were found to produce differences of between 0.25 to 0.5 W/m-K in thermal conductivity, which could result in significantly hotter temperatures by as much as 30°C over predictions that consider thermal conductivity to be constant. The spatial correlation length used in the geostatistical model to develop the expected material property values also was found to be important with differences of as much as 1.9 W/m-K in thermal conductivity, which produced as much as 20°C difference in temperature predictions. A hypothesized lithophysal-cavity zone at a depth of about 130 m with significantly higher porosity was shown to have only a modest effect of about 5°C to 10°C on the temperatures at the repository horizon. The sensitivity analysis determined a potential impact of heterogeneities in material properties on repository host rock temperatures. It is recommended that the subsurface investigations (mapping and possibly in-situ thermal testing) examine this issue.
5. Most of the thermohydrologic calculations to date have relied on an effective continuum model (ECM), which averages the rock matrix and fractures (the conductance between fractures and matrix is infinite). This assumption results in transport of liquid and vapor being governed by bulk relative and intrinsic permeabilities. However, in actual fact, the conductance between fractures and rock matrix is not infinite and it may not be justified to determine the liquid and vapor transport with averages of fracture and matrix permeabilities (the bulk permeability). The study investigated the effect that the fracture-matrix coupling has on thermohydrology by using dual permeability calculations. A coupling factor relating the fracture and matrix permeabilities was varied over four orders of magnitude and is clearly indicative of our current uncertainty in this coupling. The results of this investigation into the effects of the fracture-matrix coupling in the host rock and changes in permeabilities have shown a sensitivity to variations in these parameters. The predictions show that the temperatures of the drifts and waste packages could be more

than 20°C cooler than what either predictions with an ECM with small bulk permeabilities on a conduction model would indicate. These results show that not only are variations in the host rock permeability important, but the communication between fractures and matrix is also critical to understand. A large range chosen for the coupling factor and the sensitivities predicted over that range indicate a need for test information. Such information would include measurements of matrix permeability, area of the fracture-matrix interface (a derived model parameter that cannot be directly measured), and fracture separations. Additionally, the spatial variability in these parameters is important as well since variations in temperature could occur across the repository that could result in cooler spots forming in some areas.

6. Geochemical processes will play an important part in waste isolation in Yucca Mountain. These geochemical processes can be affected by the heat introduced into the host rock as a result of the decay of the SNF. The study performed a preliminary evaluation of the effect that heat may have on the water that is bound in the zeolitic mineral assemblages, the majority of which can be found in rock formations below the repository horizon, and the impact that dehydration and/or mineral alteration might have on the porosity of the rock and hence the permeability of that rock. These were preliminary calculations that are based on currently available measurements taken in the laboratory using samples from borehole and mineral separates. A set of calculations was made to provide an estimate of the magnitude of the effect of hydrous minerals on the thermal and hydrologic evolution of Yucca Mountain using the best estimates of mineral abundance. The estimates of the amount of water released show, as expected, a strong dependence on thermal loading. Significant amounts of water are lost from the zeolites at the higher thermal loads (e.g., an increase of up to 20 to 30 percent available for thermally mobilized fluid transport). For example, estimates show that, for clinoptilolite, the total water released per unit volume of rock at the AML of 27.3 kgU/m<sup>2</sup> (111 MTU/acre) is approximately a factor of three larger than the amount released at the AML of 8.9 kgU/m<sup>2</sup> (36 MTU/acre). The amount of water lost from the zeolites, the effect this water has on temperature, and where this water goes once mobilized may be critical to understand for waste isolation. It also was determined that current borehole core sample data indicate that the ambient porosities in the zeolitized regions of host rock varies from about 5 to around 20 percent. The calculations found that an increase in porosity as a result of the water loss is appreciable at the higher thermal loads. A concern is that the resulting rock shrinkage could produce a network of microfractures that may increase permeability and thus enhance water transport. The recrystallization of clinoptilolite to analcime produces a significant increase in porosity (more than 10 percent at the higher thermal loads) and is irreversible. This could exacerbate the production of fractures. It should be noted that if temperatures remain below 100°C, the dehydration of clinoptilolite is reversible, but above 100°C it starts converting to analcime, which retains less water and is irreversible. Investigation of this issue needs to be done to examine the behavior of zeolitized rock before, during, and after heating and to assess its potential impact on waste isolation. Based on the analysis conducted in this report at thermal loads of about 19.8 kgU/m<sup>2</sup> (80 MTU/acre) and above, significant amounts of water and porosity changes occur in the zeolite-bearing rocks. Since these zeolites predominately occur in the CHn unit, in-situ thermal tests conducted in the CHn unit may be warranted to understand these issues at high thermal loads.

7. An assessment was done to study the fact that the potential repository horizon is not at a constant depth in the mountain with respect to the distance to the surface or the water table. The distance to the surface (overburden) and the distance to various stratigraphic units and the water table varies in the Primary Area of the potential repository and in some of the alternate areas under consideration for waste disposal. The nominal overburden considered in the FY 1993 study was 343 meters. However, the overburden can be from as little as 200 m to as much as 400 m within the Primary Area. The predicted hydrothermal behavior of the host rock for various thermal loads was found to change under conditions where the overburden or distance to the water table differs from the nominal case and consequently the performance of the potential repository could change under these conditions. The calculations of the temperature and liquid saturation conditions in the potential repository were found to depend significantly on the depth of burial of the waste. In particular, the shallower portions of the repository were found to cool significantly faster than the areas with more overburden. The deeper areas, on the other hand, tend to rewet faster due to the proximity to the water table. Although not calculated here, relative humidities at the repository horizon would reflect these differences. Calculations also were done for the lower AMLs and, although not presented here, essentially negligible differences in temperature and liquid saturation were predicted for the 5.9 kgU/m<sup>2</sup> (24 MTU/acre) case. Since OCRWM is emphasizing a high thermal loading as the reference design thermal loading, the depth of burial appears to be of importance. It is doubtful that tests can be run to evaluate this since these differences occur at very late times, but this effect should be considered in the design analysis and TSPA evaluations. It is suggested that results of these one-dimensional calculations need to be supplemented with multidimensional simulations including the effects of spatially variable upper boundary location in order to better quantify three-dimensional thermohydrologic mixing and its effect on redistribution of heat and moisture.
  
8. Emplacement drift stability is an important performance issue, particularly for the concept of a large waste package in an open drift. Drift stability is both a preclosure and postclosure issue. Thermal loading is important since the addition of heat alters rock stress and may affect drift stability. To assess the drift stability, thermomechanical analyses, using the numerical code DDA, were done for the study. The predicted horizontal stresses after thermal loading in the area a few meters away from the drift were found to be about 55 MPa for runs at an AML of 27.4 kgU/m<sup>2</sup> (111 MTU/acre). Since these values exceed the predicted rock mass strength of 49 MPa, this indicates a potential for rock stability problems that must be considered. The 20.5 kgU/m<sup>2</sup> (83 MTU/acre) cases were found to have stresses that do not exceed the criteria identified above for most regions except for some of the tangential stresses at the roof. Thus, somewhere between 20.5 and 27.4 kgU/m<sup>2</sup> (83 and 111 MTU/acre) rock stability will be a problem and may even be a problem at 20.5 kgU/m<sup>2</sup> in terms of requiring some form of tunnel support. For these higher thermal loads, remediation of these stability problems if possible, by the use of stabilizing methods such as rock bolts and/or tunnel liners, will be examined by Subsurface Design. These solutions could affect costs as well as performance. Additionally, whatever design solutions considered must be compatible in thermal expansion to that of the rock. In summary, thermomechanical issues related to tunnel stability are important considerations at the higher thermal loads. In-situ testing to establish the rock strength will be needed.

A determination of a margin of safety will almost certainly require that an area of tunnel ceiling be heated sufficiently that failure occurs or at least to temperatures that exceed conservative expectations of maximum temperatures.

It should be noted that the above discussion concerned rock stability only, not hydrologic impacts. The increase or decrease in size of the fractures, depending on location, and the upward expansion (heaving) of the rocks could result in perturbations to the hydrologic system. These aspects need to be investigated further in the in-situ tests and the changes in fracture sizes and number as a result of heating should be measured.

## 6.2 THERMAL MANAGEMENT EVALUATIONS

In the study, the first steps were taken to evaluate whether or not a number of thermal management issues may ultimately need to be considered in the design. Such issues as ventilation, assessment of expansion areas, nonuniform loading of the potential repository, variations in line loads, response due to waste stream variability, and aging of fuel were examined. The following is a brief discussion of the conclusions and the results from those evaluations:

1. Ventilation cannot be used to make a "hot" repository look like a "cold" one from the standpoint of postclosure performance. But ventilation may be used constructively in the preclosure operations to remove both sensible and latent heat and moisture. Realistic calculations of the psychrometric environment in the potential repository requires an understanding of the amount of heat and moisture that is removed from the emplacement drifts and the near-field rock by ventilation. As a result of this study, an LLNL thermohydrologic code was coupled with a University of Nevada at Reno climate (ventilation) code. The combination of the two models produces calculations of the hydrothermal behavior of the near-field rock mass, including heat and moisture transport, the behavior at the rock-air interface, and the dilution of water vapor in the drift and subsequent transport out of the system. The coupled codes yield three-dimensional, time-dependent calculations of the heat and moisture transport and provide a significant advance of calculational capability for the Program. Preliminary results show that both air and rock wall temperatures in a drift can be kept to 40°C or less through ventilation during the preclosure period for an AML case of 20.5 kgU/m<sup>2</sup> (83 MTU/acre). Retrieval operations generally require temperatures less than 50°C and there is a thermal goal established at 50°C for some operations (M&O, 1993a). Also, a significant amount of water can be removed through ventilation.

Calculations of natural ventilation also were done. The results showed that, if allowed to, the potential repository will act as a thermosiphon producing air flow through the emplacement drifts of 0.6 to 0.8 m<sup>3</sup>/s. This will result in modest cooling of the emplacement drift. At most about an 87°C temperature rise would occur compared to about a 140°C rise in temperature for a sealed drift.

2. The Thermal Strategy proposes a working hypothesis that focuses current design activities on a high thermal loading of 19.8 to 24.7 kgU/m<sup>2</sup> (80 to 100 MTU/acre) while maintaining alternative thermal loadings as contingencies. For lower AMLs to be viable, more

emplacement area than the Primary Area is required to emplace near the statutory maximum. Since the current Program Plan (DOE, 1994) focuses on characterization of the Primary Area, some additional characterization of expansion areas outside of the Primary Area would be required to ensure that these areas are in fact similar to the Primary Area. The level of characterization has not been determined but could involve examination of borehole data or might have to involve some drifting into these areas. This study performed a preliminary assessment of the data that is currently available on the expansion areas. This data included existing information from core samples from boreholes that have been drilled.

Preliminary mineralogy-petrology evaluations were done to compare alternative areas with the Primary Area. Comparisons were done of the stratigraphic variations and mineral distributions and abundances that could affect repository performance and fluid flow. Based on these evaluations, it would appear that both Optional Area D and the area south of the Primary Area (at least south as far as drill holes G/GU-3) have stratigraphic features, thicknesses, and mineralogic characteristics that fall within the range of parameters that exists in the Primary Area. As such, it is possible that these areas can be relatively easy to characterize possibly with some additional boreholes, which may in some cases be planned (see Figure 4.2-1). Additionally, it would appear that Optional Area C may be significantly different from the Primary Area in that there may not be a vitric-zeolitic transition above the SWL. The fact that Area C may be different from the Primary Area does not necessarily imply that it would be unusable for emplacement of SNF, only that a different conceptual model of this region (for example a different hydrologic model) is likely to be needed. This would likely imply that more characterization of this region, such as possibly drifting and in-situ tests, would be needed to establish its ability to isolate SNF. No assessment could be done of Optional Areas A and B at this time due to the lack of drill holes.

3. Predictions with idealized models have indicated that heat may be constructively utilized to mobilize water, dry-out the near-field host rock, and keep the rock dry for extended periods of time (thousands of years). However, a number of calculations have shown that the outer edges of the potential repository suffer significant edge cooling. This environment at the edges could result in a much more aggressive corrosion regime than either a hotter environment or a cooler environment. The study evaluated the thermal management technique of loading the edges of the potential repository with a higher density of waste packages to increase the temperature in those areas particularly to achieve improved postclosure performance by increasing the duration of boiling in the outer areas. The calculations showed that nonuniform AMLs can be employed to significantly increase the duration of boiling at the edges under conditions of a high thermal load and can produce some rock dry-out, which will reduce the relative humidity in the vicinity of the waste package. However, this produces significantly higher preclosure temperatures. Nonuniform thermal loads above about  $24.0 \text{ kgU/m}^2$  (96.9 MTU/acre), which is representative of a  $20.7 \text{ kgU/m}^2$  (83.4 MTU/acre) uniform AML, produce drift wall temperatures in the outer areas of the potential repository exceeding the emplacement drift wall thermal goal of  $200^\circ\text{C}$ . Calculations in this study showed that this could result in degradation of tunnel stability. Further evaluations are needed to determine the impact on operations and retrieval as well as potential postclosure performance issues. Test results are needed to verify if a

requirement should be established not-to-exceed 200°C. Potential tradeoffs might be investigated, such as loading the outer drifts to higher density just prior to closure or ventilation and/or aging.

4. Various thermal loads, from low to high, can be achieved through a combination of waste package and drift spacing. For example, can waste packages be placed close together in the drifts to locally simulate a high thermal loading but retain large drift separations, which would result in a localized disturbance on a mountain scale? The influence of waste package spacing and drift spacing on temperature and heat mobilized fluid flow were examined in this study to address this question. A wide range of thermal loadings from about 1.5 to 29.6 kgU/m<sup>2</sup> (6 to 120 MTU/acre) and waste package spacing variations as represented by LMLs (LML expressed in MTU/m), which ranged from 0.24 to 1.25 MTU/m were used. The calculations show that for moderate to higher LMLs, the estimates of duration of boiling on the drift walls and the extent the boiling front propagates into the host rock is relatively insensitive to LML for AMLs above the threshold of about 9.9 kgU/m<sup>2</sup> (40 MTU/acre). This threshold is where significant (more than a few meters) of boiling in the host rock begins to occur. It would appear that above loadings of about 9.9 kgU/m<sup>2</sup> there may not be an advantage of one LML over another, and therefore, the choice should be made more on which is operationally more efficient or easier. On the other hand, at lower AMLs, the choice of an LML to use does appear to make a difference and a selection of LML should be based on satisfying the near-field criteria that must be established.

The calculations showed that aging can alter the waste package peak temperatures, the duration of boiling, and the extent that the boiling front propagates into the host rock. The differences are most significant for the waste package peak temperatures. Significant aging (greater than about 40 years) would be required to appreciably affect the duration of boiling on the drift wall and the extent of boiling.

5. The type of SNF (PWR or BWR), the age, and burnup of the fuel all influence the heat output of a waste package and thus, significant variability will exist between waste packages. As a part of the thermal management evaluations conducted in the Thermal Loading Study, the way in which the waste package heat variability is handled in the thermal predictions, and the effect it has on the temperature predictions was investigated. The results of the evaluations showed that the waste stream variability and the resolution at which the waste stream is modeled are important for thermal predictions. The results showed that localized hot and "cold" areas would occur as a result of the waste stream variations and the constraint of a constant AML. In some cases (100 years after emplacement or earlier) predicted temperature differences of as much as 100°C could occur in localized areas (on the order of 10 m) for emplacement of the large MPC waste packages. These localized variations in temperature can have design and performance assessment implications, for example tunnel stability, which should be evaluated and considered prior to any final emplacement/operation designs. The evaluations found that the distribution in package energies are significantly different than would be predicted using average characteristics. Specifically, if individual package characteristics are used for a set of packages received in a given year the integrated energy deposited over 1000 years could result in as much 20 to 30 percent less integrated energy than if average characteristics are

used. Improved accuracy could be obtained in predicting integrated energies if representative groupings of waste packages are used. In all cases it would appear that the waste stream variability should be considered in the design analyses.

6. The thermal analysis conducted in the study has shown the potential for developing "hot" and "cold" spots in the repository as a result of the fuel variability arriving at the repository in any given year. The potential benefits in performance indicate a need to produce a more even heat distribution in the emplacement drifts. To do this would require adjusting waste package spacings, selecting waste packages for emplacement by heat output from a "pool" of waste packages, and/or a combination of the two. To have the capability of selecting waste packages from more than a single year might require interim storage such as a CSF. As such, the thermal management option of using aging of the SNF in a CSF with heat-based IM to retain MGDS design flexibility was studied. The study focused the assessment on three primary areas; 1) system logistics and cost from reactors to the MGDS; 2) Interim Storage/IM logistics and cost; and 3) thermal source term variance. It did not, however, take the next step to evaluate whether or not a selection strategy could be developed that would provide more uniform emplacement temperatures in the potential repository.

The evaluations examined differences between OFF and YFF(10) fuel and performed a parametric evaluation of the impacts of changing emplacement limits over a range of package heats from 14.2 to 8 kW. Several conclusions were reached in the study. It was determined that increasing the limit at which casks are loaded for transportation to 15.3 kW from 14.2 kW (the program has tentatively planned to the lower limit since that is the current emplacement limit) would provide a savings in the fact that fewer casks would need to be derated (345 fewer for OFF and 417 fewer for YFF). However, these costs do not outweigh the additional cost of developing and operating the CSF. Concerning the effect of decreasing emplacement heat limits on waste package emplacement rates, the trends are similar for both the OFF and YFF(10) pickup scenarios. There is relatively little difference between the waste package emplacement rates for a 14.2 and 12 kW limit, however the 10 and 8 kW limit cases require approximately 20 years to ramp up to the waste package emplacement rates of the 14.2 kW limit case with operations extending out to the year 2085 in the worst case. Lower emplacement limits clearly increase the length of CSF and repository operations. It was determined that the peak inventory of a CSF would occur near the end of the pickup operations in 2038 to 2040 for OFF (due to the hotter waste stream at the end of the pickup) and occurs during or before 2033 for YFF(10). Changing the emplacement limits from 14.2 kW to 12.0 kW does not contribute a significant lower thermal source term. However, as the emplacement limits are reduced further to 10 kW and 8 kW, the aggregate thermal source term becomes cooler. When considering just the preclosure operations period this difference is significant. Over the long-term, the reduction in heat is not significant.

Costs of a CSF were evaluated and included the cost of the CSF, transportation cost deltas from the base case, and waste generator cost deltas. The results indicated that cost increases over the TSLCC estimate were in the range of \$0.1 to \$0.4 billion dollars for any of the 14.2 and 12 kW emplacement heat limit cases to as much as \$1.8 billion dollars (1995 constant year dollars) for the YFF(10) scenario with the 8 kW emplacement heat limit. The evaluations indicated some of the potential advantages and cost impacts of a

CSF if emplacement heat limits are changed. Tradeoffs between cost impacts and ability to provide a more uniform heat distribution need to be done in a system study to determine whether or not such a storage facility is in fact viable and what the size of such a facility must be.

### 6.3 SUMMARY

This Thermal Loading System Study focused on two main areas: 1) to perform sensitivity studies on a variety of parameters to make recommendations that will support the testing program design; and 2) to evaluate selected thermal management issues. In the first area the study examined a variety of parameters to determine if changes in those parameters as a function of thermal loading might possibly impact performance from the standpoint of producing significant changes in temperature, hydrology, etc. Examined in the study were such parameters or issues as bulk permeability, variations in rock properties (such as rock liquid saturation, matrix porosity, matrix permeability, etc.), variations in gas-phase diffusion, effect of heterogeneity in rock properties (thermal conductivity), dual permeability (fracture-matrix coupling) effects, geochemistry changes, repository elevation variations, and thermomechanical effects. The assessment first determined, where possible, what the current range of uncertainty is in the values for these parameters. Calculations were made using various models over the known or anticipated range of parameter values to determine the effect on predictions of temperature, hydrology, or mechanical response. The results showed that in a number of cases variations in the parameters did appear to result in potential changes in performance although a few of the parameters showed little sensitivity. Recommendations for testing were provided for those parameters that were deemed to be significant.

As a part of the study, some discussion was provided of the important issue of scaling and the implications on testing. The program must rely on laboratory scale and eventually in-situ drift scale thermal tests combined with analytic modeling for prediction of the behavior of the host rock on the mountain scale. In some cases, limited information on longer term and larger scale processes can be obtained from investigations of natural analogs. Understanding the scaling (time and distance) between the different measurements/experiments that will be conducted by the program is essential to develop the necessary reasonable assurance arguments for licensing. Based on the scaling discussion, it is recommended that an iterative information feed and calibration at successive scales (laboratory, waste package, drift, and repository characterization data), of the relevant scale is incorporated at each step of the scaling process, thus building confidence that the scaling up from small scale to large scale is not arbitrary. Predictions of long-term performance will require that these data be used in an aggressive modeling effort which will result in verified models for the Program. At each step in the process (laboratory, drift scale, etc.), a stochastic approach is recommended by the study. In this stochastic approach, available data from a particular scale should be used to represent the heterogeneity of the site within this framework. A stochastic approach is needed because the number of samples tested at any particular scale would not be numerous enough to cover the entire test site. Although not discussed in any detail in the study, the reliance on numerical modeling to provide performance predictions requires that the development and verification of such computer codes are of key importance in the testing program. Additionally, the in-situ tests need to investigate the appropriateness of using parameters derived from small core samples to represent much larger (ten to hundred meter) scale conditions.

Numerous sensitivity studies were conducted in this effort. The sensitivity studies were successful in identifying parameters or issues which appeared to be important to performance from the standpoint of producing significant changes in predictions of temperature or hydrology. In some areas the sensitivity studies provided a significant advance in that they used as much data as was available for inputs to the analytic models and assessments. A synopsis of the study findings and recommendations is the following:

- Bulk permeability of the host rock for some regimes is important to moisture movement and needs to be measured in the in-situ tests. The existence and extent of heat pipes could be used to verify permeabilities.
- Duration of boiling and relative humidity at the end of boiling do not appear to be sensitive to such rock parameters as liquid saturation, porosity, and van Genuchten parameters. However, rewetting appears to be sensitive to spatial variability in rock matrix properties and the capillary suction pressure in the rock. The rewetting times and rates should be further investigated and measurements made to determine the capillary suction pressure.
- The Ghost Dance and Solitario Canyon faults may provide major pathways for transport of heated gas and heat with potential to cool the repository sooner than expected. Measurements of rock properties around these faults should be done and used in a three-dimensional site-scale model to determine potential impact.
- Some investigation of binary gas-phase diffusion is warranted at high thermal loadings but it does not appear to have a profound impact on temperatures and liquid saturations (about 10 to 12 percent in duration of boiling for a factor of 10 change).
- Both drying of the host rock surrounding the repository and potential zones of high-porosity (large cavity) lithophysal zones will result in variations in thermal conductivity which could produce significant increases (up to 30°C) in repository temperature. Address this through subsurface mapping and in-situ testing.
- Fracture matrix coupling increases over those anticipated could result in possibly cooler temperatures (about 20°C) than existing predictions. Measurements of matrix permeability, derivations of fracture-matrix interface area, and fracture separations as well as the spatial variability in these parameters should be done.
- High thermal loading can produce temperatures in such regions as CH, which will dehydrate the zeolites, releasing significant quantities of liquid water, and may produce irreversible crystallization of clinoptilolite to analcime, which could produce appreciable increases in porosity. Zeolitized rock should be examined before, during, and after heating to determine the amount of liquid water released and the results used in TSPA to determine if a potential impact on waste isolation may occur. If the analysis indicates such a potential, then in-situ thermal testing in CH may be warranted for a high thermal loading.

- Significant variations may result from differences in repository overburden (it varies from 200 to 400 m in the Primary Area). It is recommended that multidimensional calculations be done to supplement these one-dimensional evaluations and the results considered in the design analysis and future TSPA evaluations.
- Thermomechanical evaluations indicated potential drift stability problems between 19.8 to 27.4 kgU/m<sup>2</sup> (80 to 111 MTU/acre). Although the thermomechanical model needs to be verified, it is recommended that an area of the tunnel be heated to at least 200°C, which exceeds expected peak temperatures.
- Scaling (time and distance) was found to be important since OCRWM must rely on laboratory scale and in-situ drift scale thermal tests as well as natural analog studies to provide predictions of long term performance. Because of the heterogeneity in the host rock and the limited tests and measurements that will be available, a stochastic approach is recommended. In-situ tests need to verify that scaling up from smaller to larger measurements is understandable.
- The study recommends that model verification should be a key emphasis in the testing program.
- The study used the available data to the maximum extent possible but found that interpolations over large distances were required with resulting large uncertainties. While this is a significant advance over what has been done in the past (essentially only analysis) there is clearly a need for considerably more data/measurements.

The study also performed some investigations of selected thermal management issues to assess feasibility and advantages/disadvantages. The various thermal management issues addressed in the study may appear in some cases to have contradictory results but for the most part may be trying to achieve different objectives. For example, ventilation tries to reduce temperatures in the potential repository and would be used primarily to achieve preclosure goals. Another thermal management option could involve selectively increasing the AML at the repository edges to increase the heat in those regions. This option is primarily oriented to achieve postclosure goals and increasing the AML would not likely occur until the end of the preclosure period. The following is a synopsis of the study conclusions and recommendations:

- The effort succeeded in coupling a thermohydrologic code (NUFT) with a psychrometric environmental (ventilation) code which was a significant advance in that it provides three-dimensional, time-dependent calculations of heat and moisture transport with ventilation. Preliminary calculations show that drift temperatures can easily be kept at or below 40°C for preclosure and a significant amount of water can be removed by ventilation. The coupled code predicts somewhat lower temperatures than a ventilation code that does not include moisture. Additionally, natural ventilation, if allowed to occur, will produce some cooling.
- The study did an assessment of stratigraphic variations and mineral distributions and abundances from borehole data in potential expansion areas which may be required to maintain viable alternative thermal loading options. The evaluations indicated that

Optional Area D (M&O, 1994a) and the area south of the Primary Area (at least south as far as drill holes G/GU-3) appear to have stratigraphic features, thicknesses, and mineralogic characteristics which fall within the range of parameters that exists in the Primary Area. As such, it is possible that these areas can be relatively easy to characterize. Optional Area C may be significantly different from the Primary Area and due to lack of data no assessment could be done of Optional Areas A and B.

- Loading the edges of the potential repository to a higher AML than the internal areas can increase the duration of boiling at the edges for the high thermal load case. However, a higher AML at the edges will result in conditions that exceed some preclosure thermal goals. Potential tradeoffs such as ventilation and aging should be looked at to possibly mitigate some of these effects.
- Variations in Lineal Mass Loadings (LMLs) by changing waste package spacing and drift spacing without changing the overall AML were examined. Boiling duration and boiling front propagation were found to be relatively insensitive to LML above about 9.9 kgU/m<sup>2</sup> (40 MTU/acre). Thus for AMLs above this value the choice of an LML should be based on operational efficiency. At lower AMLs the choice of LML does make a difference and should be based on satisfying near-field criteria that are yet to be established. It is recommended that potential near-field thermal goals be investigated and identified.
- Waste stream variability could produce substantial variations in temperature of as much as about 100°C in a localized area of as little as 10 m. These localized "hot" or "cooler" regions could result in thermomechanical problems or transport of water to the cooler regions. It is recommended that waste stream variability be considered in the design analyses and efforts be taken to mitigate the variability. Future calculations should use better resolution package heats rather than simple averages.
- Aging of spent nuclear fuel in an interim or Centralized Storage Facility (CSF) was examined. Lower emplacement limits below 14.2 kW for each package increase the length (time) of CSF and repository operations but does not contribute a significantly lower thermal source term unless limits are reduced to 10 kW or below. For preclosure operations aging can provide advantages but from the standpoint of postclosure the differences are not significant. CSF costs were between \$0.1 to \$0.4 billion dollars (1995 constant year dollars) for any of the 14.2 to 12 kW emplacement limit scenarios. If the limit is reduced to 8 kW then the costs of aging large MPCs could increase to \$1.8 billion dollars. Tradeoffs between cost impacts and ability to provide a more uniform heat distribution should be examined in a future system study.

The study provided conclusions and recommendations on the two areas: (1) thermal testing recommendations and (2) thermal management evaluations. These recommendations should be given to the test planners to assist them in development of the tests. Additionally, the thermal management evaluations should be given to the design organizations for their consideration to assist in developing their designs.

## 7. REFERENCES, STANDARDS, AND REGULATIONS

Bird, R. B.; Stewart, W. E.; and Lightfoot, E. N., 1960. *Transport Phenomenon*. New York, New York: John Wiley and Sons. p. 505.

Bish, D. L. and Chipera, S., 1989. *Revised Mineralogic Summary of Yucca Mountain, Nevada*. LA-11497-MS (1989). Los Alamos, New Mexico: Los Alamos National Laboratory.

Bish, D. L., 1984. "Effects of Exchangeable Cation Composition on the Thermal Expansion/Contraction of Clinoptilolite." *Clays and Clay Minerals*, 32. pp. 444-452.

Brandshaug, T., 1991. *A Thermomechanical Far-Field Model of Yucca Mountain*. SAND85-7101. Albuquerque, New Mexico: Sandia National Laboratories. p. 120.

Broxton, D. S.; Chipera, S. J.; Byers, Jr. F.; and Rautman, C., 1993. *Geologic Evaluation of Six Nonwelded Tuff Sites in the Vicinity of Yucca Mountain, Nevada for a Surface-Based Test Facility for the Yucca Mountain Project*. LA-12542-MS. Los Alamos, New Mexico: Los Alamos National Laboratory.

Buscheck, T. A.; Nitao, J. J.; and Saterlie, S. F., 1994. "Evaluation of Thermohydrological Performance in Support of the Thermal Loading Systems Study." *Proceedings of the International High-Level Radioactive Waste Management Conference*. Las Vegas, Nevada. May 22-26, 1994. pp. 592-610.

Buscheck, T. A., 1994. *Lawrence Livermore National Laboratory Yucca Mountain Project Status Report for February 1994*. Livermore, California: Lawrence Livermore National Laboratory. p. 20.

Buscheck, T. A. and Nitao, J. J., 1994. "The Impact of Buoyant Gas-Phase Flow and Heterogeneity on Thermo-Hydrological Behavior at Yucca Mountain." *Proceedings of the International High-Level Radioactive Waste Management Conference*. Las Vegas, Nevada. May 22-26, 1994. pp. 2,450-2,474.

Buscheck, T. A. and Nitao, J. J., 1993. "The Analysis of Repository-Heat-Driven Hydrothermal Flow at Yucca Mountain." *Proceedings of the International High-Level Radioactive Waste Management Conference*. Las Vegas, Nevada. April 26-30, 1993. pp. 847-867.

Carey, J. W. and Bish, D. L., 1995a. "Equilibrium in the Clinoptilolite-H<sub>2</sub>O System." *American Mineralogist*. (In preparation.)

Carey, J. W. and Bish, D. L., 1995b. "Partial and Molar Enthalpy of Hydration of Clinoptilolite." *Proceedings of the Clay Minerals Society 32nd Annual Meeting Program and Abstracts*. Baltimore, Maryland. June 1995. p. 26.

Chocas, C., 1994. Personal communication to S. F. Saterlie. Las Vegas, Nevada.

Code of Federal Regulations, Title 10, Part 60, 1993. *Disposal of High-Level Radioactive Wastes in Geologic Repositories*. Washington, D.C.: U.S. Nuclear Regulatory Commission.

Craig, R.; Reed, R.; and Spengler, R., 1983. *Geohydrologic Data for Test Well USW H-6, Yucca Mountain Area, Nye County, Nevada*. USGS-OFR-83-856. Denver, Colorado: U.S. Geological Survey.

Daniels, W.; Wolfsberg, K.; Rundberg, R.; Ogard, A.; Kerrisk, J. et al., 1982. *Summary Report on the Geochemistry of Yucca Mountain and Environs*. LLA-9328-MS (1982). Los Alamos, New Mexico: Los Alamos National Laboratory.

Danko, G. and Mousett-Jones, P., 1992. "Coupled Heat and Moisture Transport Model for Underground Climate Prediction." *Proceedings of the International High-Level Radioactive Waste Management Conference*. Las Vegas, Nevada. April 1992. pp. 790-798.

Danko, G., 1992. *Modeling of the Ventilation for Emplacement Drift Re-Entry and Rock Drying*. University of Nevada, Reno, Research Report. Reno, Nevada. June 1992.

Danko, G. and Mousset-Jones, P., 1993. "Modeling of the Ventilation for Emplacement Drift Re-entry and Rock Drying." *Proceedings of the International High-Level Radioactive Waste Management Conference*. Las Vegas, Nevada. April 1993. pp. 590-599.

Danko, G. 1994. *Ventilation and Cooling Enhancement for High-Level Waste Repositories*. University of Nevada, Reno, Interim Research Report. Reno, Nevada. December 1994.

Danko, G.; Buscheck, T. A.; Nitao, J. J.; and Saterlie, S. F., 1995. "Analysis of Near-Field Thermal and Psychrometric Waste Package Environment Using Ventilation." *Proceedings of the International High-Level Radioactive Waste Management Conference*. Las Vegas, Nevada. April 30-May 5, 1995. pp. 323-330.

Deutsche, C.V. and Journel, A. G., 1992. *GSLIB Geostatistical Software Library and User's Guide*. New York, New York: Oxford University Press.

DOE [U.S. Department of Energy], 1994. *Civilian Radioactive Waste Management Program Plan*. Three volumes. DOE/RW-0458. Washington, D.C.: Office of Civilian Radioactive Waste Management System.

DOE, 1995a. *Conceptual Description of the Civilian Radioactive Waste Management System*. DOE/RW-0470, Rev. 1. Washington, D.C.: Office of Civilian Radioactive Waste Management System.

DOE, 1995b. *Mined Geologic Disposal System Requirements Document*. DOE/RW-0404, Rev. 1. Washington, D.C.: Office of Civilian Radioactive Waste Management System.

DOE, 1995c. *Multi-Purpose Canister (MPC) Subsystem Design Requirements Document*. DOE/RW-0466. Washington, D.C.: Office of Civilian Radioactive Waste Management System.

DOE, 1995d. *Analysis of the Total System Life Cycle Cost of the Civilian Radioactive Waste Management Program*. DOE/RW-0479. Washington, D.C.: Office of Civilian Radioactive Waste Management System.

Flint A. L.; Flint, L. E.; and Hevesi, J. A., 1993. "The Influence of Long-Term Climate Change on Net Infiltration at Yucca Mountain, Nevada." *Proceedings of the International High-Level Radioactive Waste Management Conference*. Las Vegas, Nevada. April 26-30, 1993.

Fridrich, C. J.; Dudley, Jr. W. W.; and Stuckless, J. S., 1994. "Hydrogeologic Analysis of the Saturated-Zone Ground-Water System Under Yucca Mountain, Nevada." *Journal of Hydrology*, 154. pp. 133-168.

Journel, A. G., 1983. "Nonparametric Estimation of Spatial Distributions." *Mathematical Geology*, 15. pp. 445-468.

Journel, A. G. and Huijbregts, C. J., 1978. *Mining Geostatistics*. New York, New York: Academic Press. p. 600.

Klavetter, E. A. and Peters, R. R. 1986. *Estimation of Hydrologic Properties of an Unsaturated Fractured Rock Mass*. SAND84-2642. Albuquerque, New Mexico: Sandia National Laboratories.

Langkopf, B., 1987. "Problem Definition Memo for COVE3a Benchmarking Problem." March 26, 1987. Albuquerque, New Mexico: Sandia National Laboratories.

Levy, S., 1984. *Petrology of Samples from Drill Holes USW H-3, H-4 and H-5, Yucca Mountain, Nevada*. LA-9706-MS. Los Alamos, New Mexico: Los Alamos National Laboratory.

Levy, S., 1991. "Mineralogic Alteration History and Paleohydrology at Yucca Mountain, Nevada." *Proceedings of the International Conference on High-Level Radioactive Waste Management*. Las Vegas, Nevada. pp. 477-485.

Lin, M; Hardy, M. P.; and Bauer, S. F., 1993. *Rock Mass Mechanical Property Estimations for the Yucca Mountain Site Characterization Project*. SAND92-0450. Albuquerque, New Mexico: Sandia National Laboratories.

Lipman, P. and McKay, E., 1965. *Geologic Map of the Topopah Spring SW Quadrangle, Nye County, Nevada*. Map GQ-439. Denver, Colorado: U.S. Geological Survey.

Loeven, C., 1993. *A Summary and Discussion of Hydrologic Data from the Calico Hills Nonwelded Hydrogeologic Unit at Yucca Mountain, Nevada*. LA-12376-MS. Los Alamos, New Mexico: Los Alamos National Laboratory.

M&O [Civilian Radioactive Waste Management System Management and Operating Contractor], 1993a. *Site Characterization Plan Thermal Goals Re-evaluation*. B00000000-01717-5705-00005, Rev. 00. Las Vegas, Nevada.

M&O, 1993b. *Repository Underground Ventilation System Design Concepts*. B00000000-0717-5705-00003, Rev. 00. Las Vegas, Nevada.

M&O, 1993c. *Repository Subsurface Layout Options and ESF Interface*. B00000000-01717-5705-00007, Rev. 00. Las Vegas, Nevada.

M&O, 1993d. "Data Transmittal for Phase 2 Thermal Loading Study." TRW Interoffice Correspondence to Saterlie, S. F. and Ryder, E. VA.SEJK.10/93.125. Vienna, Virginia. October 22, 1993.

M&O, 1994. "Second Data Transmittal for FY 1994 Thermal Loading Studies." Interoffice Correspondence from King, J. to E. Ryder. VA.SA.JK.05/94.048. Vienna, Virginia. May 4, 1994.

M&O, 1994a. *Generic Subsurface Layouts for Various Repository Thermal Loadings*. BC0000000-01717-5705-00002, Rev. 00. Las Vegas, Nevada.

M&O, 1994b. *Initial Summary Report for Repository/Waste Package Advanced Conceptual Design*. B00000000-01717-5705-00015, Rev. 00. Volume II. Las Vegas, Nevada.

M&O, 1994c. Saterlie, S. F. and Thomson B. *FY 1993 Thermal Loading Systems Study Final Report*. B00000000-0717-5705-00013, Rev. 01. Las Vegas, Nevada.

M&O, 1994d. Saterlie S. F. *Thermal Loading System Study Interim Report*. B00000000-01717-5705-00016, Rev. 00. Las Vegas, Nevada.

M&O, 1995a. *Controlled Design Assumptions Document*. B00000000-01717-4600-00032, Rev. 01. Las Vegas, Nevada.

M&O, 1995b. *Recommended Layout Concepts Report*. BCAA00000-01717-5705-00001, Rev. 00. Las Vegas, Nevada.

M&O, 1995c. *Thermal Inventory Management Report*. B00000000-01717-5705-00026, Rev. 00. Vienna, Virginia.

M&O, 1995e. *User's Guide, Waste Stream Model (WSM) Version 3.3*. A00000000-01717-2002-020021, Rev. 04. Vienna, Virginia.

M&O, 1995f. *User's Guide, Interface Code Version 3.1, Revision 4.*  
A00000000-01717-2002-2009, Rev. 04. Vienna, Virginia.

M&O., 1995g. "Rock Fall Analysis Results." TRW Interoffice Correspondence.  
LV.WP.ZC.10/95.349. October 20, 1995. Las Vegas, Nevada.

M&O, 1995h. "System Logistics and Waste Stream Data for MGDS CDA Update." TRW  
Interoffice Correspondence to B. Thomson. VA.SA.JK.03/95.038. March 28, 1995. Vienna,  
Virginia.

M&O, 1995i. "FY 1995 CDA Update Waste Stream Follow-On Data." TRW Interoffice  
Correspondence to Thomson, B. VA.SA.JD.04/95.046. April 7, 1995. Vienna, Virginia.

M&O, 1995j. "Heat Routine Functional Requirements (Revised)." TRW Interoffice  
Correspondence to Hadfield, D. VA.SA.JK.11/94.134. Vienna, Virginia. February 21, 1995.

M&O, 1995k. *Heating and Cooling Scoping Analysis Report.*  
BC0000000-01717-5705-00007, Rev. 00. CRWMS M&O. Las Vegas, Nevada. April 5, 1995.

McKenzie III, D. G., 1995. *Waste Emplacement Management Evaluation Report.*  
BC0000000-01717-5705-00011, Rev. 00. Las Vegas, Nevada.

Nitao, J. J., 1989. *V-TOUGH - An Enhanced Version of the TOUGH Code for the Thermal  
and Hydrologic Simulation of Large-Scale Problems in Nuclear Waste Isolation.*  
UCID-21954. Livermore, California: Lawrence Livermore National Laboratory.

Nitao, J., 1995. *Reference Manual for the NUFT Flow and Transport Code, Version 1.0.*  
UCRL-ID-113520. Livermore, California: Lawrence Livermore National Laboratory.

NRC (Nuclear Regulatory Commission), 1992a. *Staff Technical Position on Geologic  
Repository Operations Area Underground, Facility Design-Thermal Loads.* NUREG 1466.  
Washington, D.C.

NRC, 1992b. *Repository Operational Criteria.* NUREG/CR-5428. Washington, D.C.

Ortiz, T. S.; Williams, R. L.; Nimmick, F. B.; Whittet, B. C.; and South, D. L., 1985. *A  
Three-Dimensional Model of Reference Thermal/Mechanical and Hydrologic Stratigraphy at  
Yucca Mountain, Southern Nevada.* SAND84-1076. Albuquerque, New Mexico: Sandia  
National Laboratories.

Pruess, K. and Tsang, Y. 1994. *Thermal Modeling for a Potential High-Level Nuclear Waste  
Repository at Yucca Mountain, Nevada.* LBL-35381. Berkeley, California: Lawrence Berkeley  
Laboratory. March 1994.

Pruess, K., 1991. *TOUGH2 - A General Purpose Numerical Simulator for Multiphase Fluid  
and Heat Flow.* LBL-29400. Berkeley, California: Lawrence Berkeley Laboratory.

Pruess, K., 1987. *TOUGH User's Guide, NUREG/CR-4645*. Berkeley, California: Lawrence Berkeley Laboratory.

Rautman, C. A. and Longenbaugh, R. S., 1995. "Effect of Modeling Assumptions on Thermal Profiles for a Cross Section of Yucca Mountain, Nevada." SLTR95-005. Albuquerque, New Mexico: Sandia National Laboratories.

Rautman, C. A., 1995. "Preliminary Geostatistical Modeling of Thermal Conductivity for a Cross Section of Yucca Mountain, Nevada." SAND94-2283. Albuquerque, New Mexico: Sandia National Laboratories.

Rautman, C. A.; Flint, L. E.; Flint, A. L.; and Istok, J. D., 1995. *Physical and Hydrologic Properties of Outcrop Samples from a Nonwelded to Welded Tuff Transition, Yucca Mountain, Nevada*. Water Resources Investigations Report 95-4061. Denver, Colorado: U.S. Geological Survey

Ryder, E. and Dunn, E., 1995. *Repository Thermal Response: A Preliminary Evaluation of the Effects of Modeled Waste Stream Resolution, June 8, 1995*. SAND95-0917. Albuquerque, New Mexico: Sandia National Laboratories.

Ryder, E. E., 1993. "Comparison of Predicted Far-Field Temperatures for Discrete and Smeared Heat Sources." *Proceedings of the International High-Level Radioactive Waste Management Conference*. Las Vegas, Nevada. April 26-30, 1993. pp. 841-846.

Scott, R. and Castellanos, M., 1984. *Stratigraphic and Structural Relations of Volcanic Rocks in Drill Holes USW GU-3 and USW G-3, Yucca Mountain, Nye County, Nevada*. Open-File Report 84-491. Denver, Colorado: U.S. Geological Survey.

Shi, G., 1993. "Block System Modeling by Discontinuous Deformation Analysis." *International Journal of Computational Mechanics in Engineering*. South Hampton, United Kingdom.

Smyth, J. R. 1982. "Zeolite Stability Constraints on Radioactive Waste Isolation in Zeolite-Bearing Volcanic Rocks." *Journal of Geology*, 90. pp. 195-201.

SNL [Sandia National Laboratories] 1987a. *Nevada Nuclear Waste Storage Investigations Project, Site Characterization Plan Conceptual Design Report*. SAND84-2641. Albuquerque, New Mexico: Sandia National Laboratories.

Spengler, R. W.; Muller, D. C.; and Livermore, R. B., 1979. *Preliminary Report on the Geology and Geophysics of Drill Hole UE25a-1, Yucca Mountain, Nevada Test Site*. Open-File Report 79-1244. Denver, Colorado: U.S. Geological Survey.

Svalstad, D. K. and Brandshaug, T. 1983. *Forced Ventilation Analysis of a Commercial High-Level Nuclear Waste Repository in Tuff*. SAND81-7206. Albuquerque, New Mexico: Sandia National Laboratories.

Tsai, F., 1993. *Dynamic Interaction of Discrete Continuum - The Theory of Non-Overlapping Continuum*. Doctoral Dissertation. Berkeley, California: Department of Engineering-Material Science and Mineral Engineering, University of California at Berkeley.

Tsang, Y. W. and Pruess, K., 1990. *Further Modeling Studies of Gas Movement and Moisture Migration at Yucca Mountain, Nevada*. LBL-29127. Berkeley, California: Lawrence Berkeley Laboratory.

Vaniman, D.; Bish, D.; Broxton, F.; Byers, G.; Heiken, B.; Carlos, E.; Semarge, F.; Caporuscio, F.; and Gooley, R., 1984. *Variations in Authigenic Mineralogy and Sorptive Zeolite Abundance at Yucca Mountain, Nevada, Based on Studies of Drill Cores USW GU-3 and G-3*. LA-9707-MS. Los Alamos, New Mexico: Los Alamos National Laboratory.

van Genuchten, R., 1978. "Calculating the Unsaturated Hydraulic Conductivity with a New Closed-Form Analytical Model." *Water Resources Bulletin*. Princeton, New Jersey: Princeton University Press.

Vargaftik, N. B., 1975. *Tables on the Thermophysical Properties of Liquids and Gases, 2nd Edition*. New York, New York: John Wiley and Sons.

Waddell, R.; Robison, J.; and Blankennagel, R., 1984. *Hydrology of Yucca Mountain and Vicinity, Nevada-California - Investigative Results Through Mid-1983*. Water-Resources Investigations Report 84-4267. Denver, Colorado: U.S. Geological Survey.

Wilgus, C., 1995. *Individual Software Plan for the Qualification of NUFT*. ISP-NF-13, Rev. 0. Livermore, California: Lawrence Livermore National Laboratory.

Wilson, M. L.; Barnard, R. W.; Barr, G. E.; Dockery, H. A.; Dunn, E.; Eaton, R. R.; Gansemer, J. D.; Gauthier, J. J.; Guerin, D. C.; Halsey, W. G.; Lamont, A. D.; Lewis, L. C.; Lu, N.; Martinez, M. J.; Meijer, A.; Morris, D. E.; Nilson, R.; Rautman, C. A.; Robey, T. H.; Ross, B.; Ryder, E. E.; Schenker, A. R.; Shannon, S. A.; Skinner, L. H.; and Triay, I. R., 1994. *Total System Performance Assessment for Yucca Mountain - SNL Second Iteration (TSPA-1993)*. SAND93-2675. Albuquerque, New Mexico: Sandia National Laboratories.

Wittwer, C.; Chen, G.; Bodvarsson, G.; Chornack, M.; Flint, A.; Flint, L.; Kwickles, E.; and Spengler, R., 1995. *Preliminary Development of the LBL/USGS Three-Dimensional Site-Scale Model of Yucca Mountain, Nevada*. LBL-37356. Berkeley, California: Lawrence Berkeley Laboratory. June 1995.

Wu, Y. S.; Chen, G.; and Bodvarsson, G., 1995. *Preliminary Analysis of Effects of Thermal Loading on Gas and Heat Flow within the Framework of the LBL/USGS Three-Dimensional Site-Scale Model*. LBL-37729. Berkeley, California: Lawrence Berkeley Laboratory.

Yang, H. and Bhattacharya, K. K., 1994. "Ventilation Considerations for Repository Subsurface Advanced Conceptual Design." *Proceedings of the International High-level Radioactive Waste Management Conference*. Las Vegas, Nevada. May 1994. pp. 530-537.

YMP, 1994. *Design Support Analyses: North Ramp Design Package 2C, Rev. 1*, Technical Data Information Form, DTN: SNT01122093001.002, TDIF#303124, April 1994.

YMP, 1995. *The Yucca Mountain Site Characterization Project Reference Information Base, Rev. 3/ICN 1*. YMP/93-02. Las Vegas, Nevada.

## 8. ACRONYMS

### ACRONYM LIST AND EQUATION SYMBOLS

AML	Areal Mass Loading of spent nuclear waste (kgU/m <sup>2</sup> or MTU/acre)
APD	Areal Power Density (w/m <sup>2</sup> or kW/acre)
BWR	Boiling Water Reactor
C	degrees Celsius
CDA	Controlled Design Assumptions
CFR	Code of Federal Regulations
CH	Calico Hills member (rock unit)
CHn	Calico Hills nonwelded
CHnv	Nonwelded vitric tuff
cm	centimeters
CRWMS	Civilian Radioactive Waste Management System
CSF	Centralized Storage Facility
DDA	Discontinuous Deformation Analysis
DOE	U.S. Department of Energy
DRD	Design Requirement Document
DVCC	dry vertical concrete cask
EBS	Engineered Barrier System
ECM	effective continuum model
ESF	Exploratory Studies Facility
ft	Feet
FY	Fiscal Year
hr	Hours
IM	Inventory Management
K	degrees Kelvin
kg	Kilogram
km	Kilometer
kW	Kilowatt
LAML	Local Areal Mass Loading. This is the areal mass loading in the emplacement area and does not include any areas needed for access to work areas.
LANL	Los Alamos National Laboratory
LAPD	Local Area Power Densities (w/m <sup>2</sup> )
lb	Pound (1 lb = 16 oz = 0.454 kg)
LBL	Lawrence Berkeley Laboratory

LML	Lineal Mass Loading
LLNL	Lawrence Livermore National Laboratory
LWT	Legal Weight Truck
m	meters
MESC	Multi-Element Sealed Canister
M&O	Management and Operating Contractor
MGDS	Mined Geologic Disposal System
mm	millimeters
MPA	Mission Plan Amendment
MPC	Multi-Purpose Canister
MRS	Monitored Retrievable Storage
MTU	Metric Tons of Initial Uranium Equivalent
NAS	National Academy of Sciences
NRC	U. S. Nuclear Regulatory Commission
NUREG	Nuclear Regulatory Document
NWPA	Nuclear Waste Policy Act of 1982, as amended
NWPAA	Nuclear Waste Policy Act, Amendment of 1987
OCRWM	Office of Civilian Radioactive Waste Management (DOE)
OFF	Oldest Fuel First
P	Pressure
PA	Performance Assessment
PCCB	Program Change Control Board
PPA	Proposed Program Approach
PTn	Paintbrush Tuff, Non-welded vitric tuff
PWR	Pressurized Water Reactor
RHI	Relative Humidity Indicator
RIB	Reference Information Base
r	radial distance
SCP	Site Characterization Plan
SCPB	Site Characterization Program Baseline
Sg	Gas Saturation
SNF	Spent Nuclear Fuel
SNL	Sandia National Laboratories
SWL	Static Water Level
t	Time; unless stated otherwise refers to time after emplacement
T	Temperature, also repository horizon temperature at repository center
T-M-H-C	Thermal-Mechanical-Hydrological-Chemical
TOUGH2	(Revision) Transport of Unsaturated Groundwater and Heat Computer Code
TS	Topopah Springs
TSLCC	Total System Life-Cycle Cost

TSPA	Total System Performance Assessment
TSw	Topopah Spring Member
TSw1	Topopah Spring Member, densely welded devitrified lithophysal-rich tuff
TSw2	Topopah Spring Member; densely welded devitrified lithophysal-poor tuff
TSw3	Topopah Spring Member; vitrophyre tuff
U	Uranium
UCF	uncanistered fuel
UO	The undifferentiated overburden layer that comprises the surface of Yucca Mountain
USGS	U.S. Geological Survey
VTOUGH	Vectorized Transport of Unsaturated Groundwater and Heat Computer Code
Wb	Wet bulb
YFF	Youngest Fuel First
YFF(10)	Youngest Fuel First at least 10 years out of reactor
YM	Yucca Mountain
YMP	Yucca Mountain Site Characterization Project
YMSCO	Yucca Mountain Site Characterization Office
Yr	Year
$\infty$	Thermal diffusivity of rock
$\beta$	Specifies properties relevant to binary diffusion
$\rho$	Density ( $\text{g}/\text{cm}^3$ ) of rock or air depending on context
$\rho C$	Volumetric specific heat of rock at repository horizon ( $\text{W}\cdot\text{yr}/\text{m}^3 \cdot ^\circ\text{C}$ )
$\phi$	Porosity of rock
$\tau$	Time used in ventilation analysis, also a tortuosity factor
$\theta$	A constant value of 1.8 that the temperature is raised to in the calculation of diffusion
$\mu\text{m}$	Micro meter

INTENTIONALLY LEFT BLANK

MOL.19960123.0161